UV-LED advanced oxidation processes for the efficient removal of organic micropollutants from water

Bertagna Silva, Danilo

University of Zagreb

FACULTY OF CHEMICAL ENGINEERING AND TECHNOLOGY

Universitat de Girona

FACULTY OF SCIENCES

Danilo Bertagna Silva

UV-LED ADVANCED OXIDATION PROCESSES FOR THE EFFICIENT REMOVAL OF ORGANIC MICROPOLLUTANTS FROM WATER

INTERNATIONAL DUAL DOCTORATE

Zagreb, 2022

SVEUČILIŠTE U ZAGREBU
FAKULTET KEMIJSKOG INŽENJERSTVA I TEHNOLOGIJE

Kandidat **Danilo Bertagna Silva**

predao je dana: 6. svibnja 2022. doktorski rad izrađen pod mentorstvom prof. dr. sc. Sandre Babić, Sveučilište u Zagrebu, Fakultet kemijskog inženjerstva i tehnologije i dr. sc. Gianluigija Buttiglierija, Catalan Institute for Water Research.

Povjerenstvo za ocjenu doktorskog rada u sastavu:

prof. dr. sc. Dragana Mutavdžić Pavlović, Fakultet kemijskog inženjerstva i tehnologije Sveučilišta u Zagrebu
doc. dr. sc. Marin Kovačić, Fakultet kemijskog inženjerstva i tehnologije Sveučilišta u Zagrebu
prof. dr. sc. Mira Petrović, Catalan Institute for Water Research (ICRA), Spain
dr. sc. Maria Jose Martin Sanchez, University of Girona, Spain
prof. dr. sc. Davor Ljubas, Fakultet strojarstva i brodogradnje Sveučilišta u Zagrebu

pozitivno je ocijenilo doktorski rad doktoranda Danila Bertagne Silva, a Fakultetsko vijeće Fakulteta kemijskog inženjerstva i tehnologije Sveučilišta u Zagrebu na sjednici održanoj dana 11. srpnja 2022. prihvatilo je ocjenu i odobrilo obranu doktorskog rada pred povjerenstvom u istom sastavu.

Obrana doktorskog rada održana je dana 21. srpnja 2022.

D e k a n
prof. dr. sc. Ante Jukić

University of Zagreb

FACULTY OF CHEMICAL ENGINEERING AND TECHNOLOGY

Universitat de Girona

FACULTY OF SCIENCES

Danilo Bertagna Silva

UV-LED ADVANCED OXIDATION PROCESSES FOR THE EFFICIENT REMOVAL OF ORGANIC MICROPOLLUTANTS FROM WATER

INTERNATIONAL DUAL DOCTORATE

Supervisors:

Prof. Sandra Babić, PhD

Gianluigi Buttiglieri, PhD

Zagreb, 2022

University of Zagreb

FAKULTET KEMIJSKOG
INŽENJERSTVA
I TEHNOLOGIJE

Universitat de Girona

FACULTY OF
SCIENCES

Danilo Bertagna Silva

UV-LED NAPREDNI OKSIDACIJSKI PROCESI ZA UČINKOVITO UKLANJANJE ORGANSKIH MIKROZAGAĐIVALA IZ VODE

MEĐUNARODNI DVOJNI DOKTORAT

Mentori:

Prof. dr. sc. Sandra Babić

Dr. sc. Gianluigi Buttiglieri

Zagreb, 2022.

University of Zagreb

FACULTY OF CHEMICAL ENGINEERING AND TECHNOLOGIES

Universitat de Girona

FACULTAD DE CIENCIAS

Danilo Bertagna Silva

PROCESOS DE OXIDACIÓN AVANZADA EN UV-LED PARA LA ELIMINACIÓN EFICIENTE DE MICROCONTAMINANTES ORGÁNICOS DEL AGUA

DOCTORADO DUAL INTERNACIONAL

Supervisores:

Prof.ª Dr.ª Sandra Babić

Dr. Gianluigi Buttiglieri

Zagreb, 2022

- Bibliographic page
- UDK: 544.526.5:628.316.12:547(043.3)=111
- Scientific area: Natural sciences
- Scientific fild: Chemistry
- Scientific branch: Applied chemistry
- Institutions:

  University of Zagreb, Faculty of Chemical Engineering and Technology

  University of Girona, Girona, Spain

  Catalan Institute for Water Research, Girona, Spain
- Supervisors: Prof. Sandra Babić, PhD and Gianluigi Buttiglieri, PhD
- Number of pages: 179 (with Apendix)
- Number of figures: 68
- Number of tables: 19
- Number of appendices: 11
- Number of references: 226
- Date of defence: 21 July 2022
- Defence Committee:

  Prof. Dragana Mutavdžić Pavlović, PhD, University of Zagreb, Faculty of Chemical Engineering and Technology

  Asst. prof. Marin Kovačić, PhD, University of Zagreb, Faculty of Chemical Engineering

  and Technology

  Prof. Mira Petrović, PhD, Catalan Institute for Water Research (ICRA), Spain

  Prof. Maria Jose Martin Sanchez, PhD, University of Girona, Spain

  Prof. Davor Ljubas, PhD, University of Zagreb, Faculty of Mechanical Engineering and Naval Architecture
- The thesis is stored at:

  National and University Library in Zagreb, Hrvatske bratske zajednice bb; Library of

  Faculty of Chemical Engineering and Technology, University of Zagreb, Marulićev trg 20.

The topic of this thesis

UV-LED ADVANCED OXIDATION PROCESSES FOR THE EFFICIENT REMOVAL OF ORGANIC MICROPOLLUTANTS FROM WATER

was accepted at the 251st session of the Faculty of Chemical Engineering and Technology, University of Zagreb Faculty Council, held on 20 December 2021, and approved at the session of the University of Zagreb Senate held on 29 March 2020.

ACKNOWLEDGEMENTS

First and foremost I would like to thank the European Commission for funding the Nowelties project and everyone involved in its creation and development. I will always be grateful to my supervisors Prof. Dr. Sandra Babić and Dr. Gianluigi Buttiglieri for giving me this opportunity; I deeply appreciate their kindness, trust, patience and tireless support during these atypical years - despite pandemics and earthquakes.

I want to thank everybody who worked with me in the University of Zagreb and contributed directly or indirectly: Kristina Tolić Čop, Dr. Martina Biošić, Slavica Kos and Tanja Ivančić. My acknowledgements to Dr. Dario Dabić for all the good advices, Alan Badrov for the comradeship, Bruna Babić for the *Vibrio fischeri* experiments, Goran Smoljanić for the total organic carbon analysis, Tomislav Babić for assembling the Arduino-LED device, Prof. Dr. Hrvoje Kušić for the Design Expert software and Prof. Dr. Lidija Ćurković for the TiO_2 nanofilm.

In ICRA I would like to thank Dr. Maria José Farré and Dr. Elisabeth Cuervo Lumbaque for their assistance with the elusive Orbitrap and Esther Mendoza for preparing the pharmaceuticals' standard stock solutions.

I am very lucky to have as my colleagues the other 13 early-stage researchers from the Nowelties project who supported each other no matter what. Special thanks to Marina Gutiérrez Pulpeiro for putting up with me every day, even during my moodiest moments.

My gratitude to my old friends and the wonderful people I met during this fantastic journey and made it all worth it: Ana Paula Salomé, Rafaella Pontes, Léo Schürmann de Azevedo, Florencia Lentijo, Rodrigo Cardoso Ramos, Walewska Duran, Jye Ming Ong, Marija Klepo, Tea Dodig, Lorena Zvonarić, Iva Tutiš, Kaja Ocvirek-Krušić, Maja Kezić, Petra Čačič, Gabriela Levy, Dajana Pejaković and, last but certainly not least, Karmen Babić-Praljak.

Zagreb će uvijek biti u mom srcu.

Obrigado mamãe e titia por tudo.

Danilo

Nowelties

European Joint Doctorate

This work is supported by the European Union's Horizon 2020 research and innovation program under Marie Sklodowska-Curie grant agreement № 81288 – Nowelties ITN-EJD project.

ABSTRACT

The recent developments of ultraviolet light-emitting diodes (UV-LEDs) open up new horizons for advanced oxidation processes (AOPs) for water treatment such as photocatalysis. In this work, the performance of UV-LED-based AOPs for the removal of organic micropollutants (OMPs) in water was investigated in a multitude of scenarios. Initially, the light profiles of a lab-scale photoreactor were simulated using different UV-LED arrays to investigate light intensity and homogeneity. A design of experiments (DoE) was made to access which variables have more significance for the apparent kinetic rate (k_{app}) and electrical energy per order consumption (E_{EO}) of the antibiotic ciprofloxacin, and the optimal photoreactor design was defined. The simultaneous and individual degradation of 5 OMPs (all in the EU Watch List of Contaminants of Emerging Concern of 2020) was studied in sub sequential DoEs investigating the significance of numerous parameters (concerning both the photoreactor design and matrix composition) on relevant process outputs. The influence of simultaneous wavelength use on E_{EO} values was investigated. Finally, a transformation product (TP) analysis was carried out to identify which molecules are generated for different scenarios, and their possible correlation with toxicity levels.

Results show that a higher light homogeneity inside a cylindrical photoreactor is not necessarily achieved with more LEDs around it. The DoEs gave accurate models to predict outputs. LEDs' controlled periodic illumination was able to increase k_{app} values for photocatalytic experiments, but this was not followed by a benefit in E_{EO}. Disparate responses of different OMPs to each situation suggest that the optimized treatment of choice will depend on matrix composition, target pollutant reactivity and required standards of the final effluent. The use of UV-C for photocatalysis is not recommended due to screening effects. The E_{EO} values of photocatalysis remain unfeasible for practical purposes. The use of simultaneous wavelength did not lead to a decrease on E_{EO} values. Nevertheless, improvements can be foreseen due to the unique features of UV-LEDs and their exponential performance enhancements in the last few years, which should have a direct impact on process costs. Transformation products for different reaction scenarios were identified, but their correlations with toxicity remain unclear due to possible synergistic effects and undetected TPs.

Key words: Advanced oxidation processes; photocatalysis; photoreactor design; contaminants of emerging concern; ultraviolet light-emitting diodes; water treatment.

PROŠIRENI SAŽETAK NA HRVATSKOM

Klimatske promjene uzrokuju stres na izvorima čiste vode. Sve veći zahtjevi našeg društva u pogledu standarda kvalitete voda potiču razvoj održivih tehnologija za pročišćavanje voda koje će omogućiti razgradnju novih zagađivala (engl. *contaminants of emerging concern*, CEC), kao što su organska mikrozagađivala (engl. *organic micropollutants*, OMP). Iako se ovi spojevi nalaze u malim koncentracijama u vodnom okolišu, postoji mogućnost njihove bioakumulacije u okolišu. Akutna i kronična izloženost OMP-ima može uzrokovati štetne, a opet nepredvidive učinke na zdravlje ljudi i drugih živih organizama. Konvencionalni postupci obrade voda nisu u mogućnosti ukloniti te tvari na zadovoljavajući način, budući da su mnoge od njih antropogenog podrijetla (npr. farmaceutski proizvodi i pesticidi) sa sporim putevima biološke razgradnje.

Napredni oksidacijski procesi (engl. *advanced oxidation process*, AOP) moguće su rješenje ovog problema, s obzirom da se tijekom tih procesa generiraju visoko reaktivni radikali, poput hidroksilnih radikala, sposobnih razgraditi OMP-e. AOP-i često zahtijevaju znatnu količinu električne energije ili dodatnih kemikalija. Zbog toga većina njih još uvijek nije praktično primjenjiva. Među AOP-ima, fotokataliza uz TiO_2 kao fotokatalizator, privlači veliku znanstvenu pozornost u posljednjih nekoliko desetljeća jer može generirati reaktivne radikale djelovanjem Sunčevog zračenja. Time se omogućava učinkovita obrada vode potaknuta obnovljivom energijom. Ipak, fotokataliza se još uvijek svrstava među energetski najzahtjevnije AOP-e zbog svoje niske fotonske učinkovitosti.

Brzi razvoj svjetlećih dioda koje emitiraju ultraljubičasto zračenje (engl. *ultraviolet light-emitting diode*, UV-LED) stvorio je nove mogućnosti za AOP-e koji se temelje na djelovanju zračenja, kao što je fotokataliza. Jedinstvene značajke UV-LED-a kao što su kontrolirano periodično osvjetljenje (engl. *controlled periodic illumination*, CPI), karakter točkastog izvora i veliki izbor valnih duljina omogućuju znatno fleksibilniji dizajn reaktora u usporedbi s tradicionalnim UV živinim svjetiljkama.

U ovoj je disertaciji istražena izvedba UV-LED AOP-a za uklanjanje OMP-a u vodi u nekoliko različitih scenarija. U prvom koraku dizajn fotoreaktora planiran je primjenom softvera koji omogućava simulaciju optičkih profila i raspodjelu svjetlosti unutar cilindričnog

laboratorijskog reaktora (150 mL). Simulirani su intenzitet i homogenost svjetla za različite položaje i brojeve UV-LED traka postavljenih oko reaktora. Također je istražen učinak udaljenosti između LED dioda i stijenki reaktora na profil zračenja. Rezultati su pokazali da, iako se veći svjetlosni fluks i intenzitet zračenja postižu u slučaju kada više LED-dioda okružuje reaktor, homogenija raspodjela svjetlosti nije nužno postignuta s više LED-dioda.

Na temelju simulacije korištena su dva identična fotoreaktora izrađena od kvarca. U jednom je na njegove unutarnje stijenke sol-gel postupkom nanesen nanofilm TiO_2 za fotokatalitičke eksperimente, dok je drugi reaktor korišten za eksperimente fotolize. Pripremljen je dizajn eksperimenata (DoE) (*categorical full factorial design*) kako bi se istražio utjecaj 4 varijable na prividnu konstantu brzine reakcije (k_{app}) i potrošnju električne energije (E_{EO}). Eksperimenti su provedeni s antibiotikom ciprofloksacinom. Promatrane varijable bile su: broj LED-dioda oko reaktora, njihova udaljenost od stijenke reaktora, korištenje CPI i prisutnost TiO_2 nanofilma. Temeljem eksperimentalnih rezultata određen je točan model predviđanja utjecaja promatranih varijabli na konstantu brzine reakcije. Rezultati su pokazali da, iako je korištenje većeg broja LED-dioda i primjena CPI povećalo k_{app} vrijednosti, nije postignut statistički značajan utjecaj na smanjenje vrijednosti E_{EO}. Jedino je prisutnost fotokatalizatora i kraće udaljenosti između LED-dioda i stijenke reaktora utjecalo na smanjenje E_{EO}-vrijednosti. Potvrđeno je da je CPI učinkovito samo u prisutnosti fotokatalizatora, dok ne utječe na razgradnji tijekom fotolize. Odabran je optimalan dizajn s 3 LED-trake oko reaktora udaljene 10 mm od stijenke s obzirom na postignute visoke k_{app} i niske E_{EO}-vrijednosti. Ovaj dizajn reaktora odgovara simulaciji kojom je postignuta najhomogenija raspodjela svjetlosti unutar reaktora.

Koristeći optimalni dizajn reaktora, istražena je razgradnja 5 OMP-a (ciprofloksacin, trimetoprim, sulfametoksazol, venlafaksin i o-desmetilvenlafaksin - svi se nalaze na trenutno važećem popisu za praćenje), pojedinačno i istovremeno, pri različitim eksperimentalnim uvjetima. S obzirom na različita fizikalno-kemijska svojstva ispitivanih spojeva, postignuti su različiti stupnjevi razgradnje za različite spojeve i različite eksperimentalne uvjete. Dodatak vodikovog peroksida ubrzao je razgradnju pri svim uvjetima, što je i očekivano s obzirom da doprinosi stvaranju više reaktivnih vrsta.

Drugi DoE (*full-factorial categorical design*) napravljen je s ciljem proučavanja utjecaja odabranih varijabli na k_{app}-vrijednosti za svaki od 5 ispitivanih OMP-a, smanjenje ukupnog

organskog ugljika (TOC) i toksičnosti (određena praćenjem inhibicije bioluminiscencije *Vibrio fischeri*). Odabrane varijable bile su: prisutnost fotokatalizatora, valna duljina svjetlosti, CPI i matrica uzorka vode. Više k_{app}-vrijednosti dobivene su za UV-A fotokatalizu ili UV-C fotolizu, ovisno o spoju. Iako se kraćim valnim duljinama poput UV-C postiže bolja fotolitička razgradnja, tijekom fotokatalitičke razgradnje fotokatalizator apsorbira to zračenje prije nego dođe do zagađivala stvarajući učinak zasjenjenja (*screening*). Za neke od proučavanih OMP-ova, ubrzanje razgradnje uslijed djelovanja reaktivnih vrsta generiranih na fotokatalizatoru nije kompenziralo učinak zasjenjenja (*screening*) te su postignute niže k_{app}-vrijednosti. Kada je vodovodna voda korištena kao matrica, smanjenje TOC-a je značajno opalo, čime se naglašava važnost predobrade prije AOP-a. Općenito, glavni čimbenik za smanjenje toksičnosti otpadnih voda je uporaba UV-C zračenja u odnosu na UV-A. Veća inhibicija luminiscencije uočena je za UV-A fotokatalizu zbog stvaranja toksičnih produkta razgradnje. Također, određeni su matematički modeli za predviđanje pojedinačnih i kombiniranih utjecaja ispitivanih varijabli na smanjenje TOC-a i toksičnosti.

Nadalje, analiziran je utjecaj početne pH-vrijednosti na istovremenu razgradnju 5 OMP-a UV-A fotokatalizom. Općenito, više pH-vrijednosti pogoduju stvaranju reaktivnih vrsta i ubrzavaju razgradnju. Ipak, ionsko stanje svakog ciljanog OMP-a, njegova reaktivnost s generiranim reaktivnim vrstama i afinitet prema TiO_2 također utječu na proces razgradnje. Provedena su ispitivanja koja su uključila tvari koje inhibiraju reaktivne vrste (*scavengers*) kako bi se utvrdili putevi fotokatalitičke razgradnje za svaki od ispitivanih OMP-ova.

Treći DoE (*response-surface Box-Behnken design*) napravljen je kako bi se provjerio utjecaj tvari uobičajeno prisutnih u realnim uzorcima voda (bikarbonati, nitrati i huminske kiseline) na k_{app}-vrijednost 5 ispitivanih OMP-a UV-A fotokatalizom. I ovdje je uočen različit utjecaj na razgradnju različitih spojeva zbog višestrukih kemijskih interakcija u sustavu. Štoviše, proučavane varijable mogu doprinijeti ili spriječiti razgradnju, ovisno o ciljanom OMP i drugim eksperimentalnim uvjetima.

Istražena je istodobna primjena dviju valnih duljina (UV-A i UV-C u kombinaciji) zbog mogućnosti poboljšanja uslijed izlaganja OMP-a različitim valnim duljinama. Međutim, nije postignuto značajno smanjenje E_{EO} -vrijednosti, vjerojatno zato što su odabrane valne duljine bile previše udaljene da bi izazvale sinergijski učinak.

Konačno, provedena je analiza uzoraka vode nakon razgradnje primjenom vezanog sustava tekućinske kromatografije (LC) i spektrometrije masa visoke razlučivosti (Orbitrap). Uspješno su identificirani razgradni produkti 3 ciljana OMP-a nastali UV-A fotokatalitičkom razgradnjom. Uspoređeni su razgradni produkti nastali u MQ i vodovodnoj vodi nakon UV-A fotokatalize i UV-C fotolize. Za svaki proces identificirani su različiti razgradni produkti. Nakon UV-A fotokatalize identificirani su isti razgradni produkti za MQ i za vodovodnu vodu, iako u različitim količinama. Molekula niti jednog od detektiranih razgradnih produkata nije bila znatno manja u odnosu na početnu molekulu, što može objasniti povećanje toksičnosti i ukazuje na postojanost ispitivanih OMP-a.

Različit stupnjevi razgradnje ispitivanih OMP-a u svakom od ispitanih scenarija sugeriraju da će optimalni postupak obrade ovisiti o sastavu matrice, reaktivnosti ciljanog OMP-a i ciljanom standardu kvalitete konačnog efluenta. E_{EO}-vrijednosti TiO_2 fotokatalize uz korištenje UV-LED izvora zračenja su i dalje visoke za praktičnu primjenu. Međutim, u skoroj budućnosti može se očekivati značajno smanjenje potrošnje energije zbog eksponencijalnog poboljšanja svojstava UV-LED izvora zračenja postignutog u posljednjih nekoliko godina. Fotokataliza može biti vrlo učinkovita i pogodna za primjenu u malom mjerilu izravno na mjestu upotrebe u slučajevima kada se zahtijevaju efluenti visoke kvalitete. Pozornost treba obratiti na potencijalne razgradne produkte koji mogu utjecati na povećanje toksičnosti efluenta.

Ključne riječi: napredni oksidacijski procesi; fotokataliza; dizajn fotoreaktora; UV-LED; nova zagađivala; razgradni produkti; obrada vode.

RESUMEN EXTENDIDO EN CASTELLANO

El cambio climático causa estrés en las fuentes de agua. Las crecientes demandas de estándares de calidad de nuestra sociedad han estado impulsando el desarrollo de tecnologías sostenibles de tratamiento de agua capaces de degradar compuestos de preocupación emergentes recalcitrantes (en inglés: *contaminants of emerging concern*, CECs), tales como los microcontaminantes orgánicos (en inglés: *organic micropollutants*, OMPs). Aunque estos compuestos se encuentran en pequeñas concentraciones en los cuerpos de agua, sí no son removidos adecuadamente, se pueden bioacumular en el medio ambiente. La exposición aguda y crónica a los OMPs puede causar efectos nocivos e impredecibles para la salud de las personas y otros organismos vivos. Los sistemas de potabilización y tratamientos de aguas residuales no son capaces de remover estas sustancias satisfactoriamente, debido a que muchos de ellos son de origen antropogénico (p. ej. productos farmacéuticos y pesticidas) con baja degradabilidad.

Los procesos de oxidación avanzada (en inglés, *advanced oxidation process*, AOPs) son una posible solución a este problema, debido a que pueden generar especies altamente reactivas de oxígeno (en inglés*: radical oxygen species*, ROS) capaces de degradar los OMPs. Los AOPs a menudo requieren una cantidad considerable de electricidad o productos químicos adicionales. Debido a esto, la mayoría de estos procesos aún son inviables para propósitos prácticos. Entre todas los AOPs, la fotocatálisis basada en el TiO_2 ha llamado mucho la atención de la comunidad científica en las últimas décadas, debido a que puede generar ROSs a partir de la luz solar, prometiendo ser un tratamiento de agua eficiente impulsado por energía renovable. Sin embargo, la fotocatálisis aún se encuentra entre los AOPs que más demandan energía debido a su baja eficiencia fotónica.

El rápido desarrollo de los diodos emisores de luz ultravioleta (en ingles: *ultraviolet light-emitting diodes*, UV-LEDsLEDs) abre nuevas posibilidades para los AOPs basados en la luz, tales como la fotocatálisis. Las características únicas de los LEDs de UV tales como iluminación periódica controlada (en inglés: *controlled periodic illumination*, CPI), el carácter de fuente puntual y la adaptación de la longitud de onda, permiten un diseño de reactor mucho más flexible en comparación con las lámparas UV de mercurio tradicionales.

En esta disertación, el desempeño de los AOPs basados en los UV-LEDs para la remoción de OMPs presentes en el agua fueron investigados en una multitud de escenarios. Inicialmente, un diseño de reactor fue realizado con un software capaz de simular los perfiles ópticos y la distribución de luz dentro de un reactor cilíndrico a escala de laboratorio (150 mL). La intensidad y homogeneidad de la luz fue estudiada para configuraciones conteniendo diferentes cantidades de líneas de LEDs UV alrededor del reactor. Los efectos en los perfiles de luz también fueron investigados para variaciones en la distancia entre los LEDs y las paredes del reactor. Los resultados muestran que, aunque se obtienen mayores flujos de luz e irradiación cuando más LEDs se aplican al reactor, no necesariamente se alcanza una distribución más homogénea de la luz cuando más LEDs son usados.

Basado en la simulación, dos fotoreactores idénticos hechos de cuarzo fueron usados. En uno de ellos, una nano pelicula de TiO_2 fue aplicada en las paredes internas del reactor, usando el método sol-gel, para experimentos fotocatalíticos, mientras el otro reactor fue usado para estudiar la fotólisis. Un diseño de experimentos (en inglés: *design of experiments*, DoE) categórica factorial completo fue hecho para investigar el impacto de 4 variables en la tasa de la constante cinética aparente (k_{app}) y en la energía eléctrica por orden de consumo (E_{EO}) para el antibiótico ciprofloxacino, seleccionado con compuesto objetivo. Las variables escogidas fueron el número de LEDs alrededor del reactor; su distancia de las paredes del reactor; el uso de la CPI y la presencia de la nano película de TiO_2. Un modelo de predicción preciso fue obtenido. Los resultados mostraron que mientras más LEDs e CPI incrementaron los valores de k_{app}, la tendencia energética no fue estadísticamente suficiente para convertir esta ganancia en una menor E_{EO}. Solo la presencia de la nano película y menores distancias entre los LEDs y las paredes del reactor fueron capaces de reducir los valores de E_{EO}. Fue confirmado que la CPI solo puede ser efectiva en la presencia de un catalizador, sin ninguna contribución en la degradación durante la fotólisis solamente. Un deseno optimo con 3 líneas de LEDs alrededor del reactor, a una distancia de 10 mm del reactor, fue seleccionado debido a su mayor valor de k_{app} y menor valor de E_{EO}. Esta elección coincide con la simulación que tuvo la más alta homogeneidad de luz.

Usando el DoE, las degradacines individuales y simultáneas de 5 OMPs (ciprofloxacino, trimetoprima, sulfametoxazol, venlafaxina y o-desmetilvenlafaxina – todos actualmente en la lista de observacion de la UE de CECs) fueron investigadas en varias condiciones. Cada compuesto

respondió diferentemente a cada tratamiento. La adición de peróxido de hidrógeno mejoró la degradación en todos los escenarios, debido a que contribuye a la formación de más ROS.

Un segundo DoE categórico factorial completo fue hecho para estudiar el impacto en el k_{app} individual para cada uno de los 5 contaminantes objetivo, la disminución del carbono orgánico total (en inglés: *total organic carbon*, TOC) y la toxicidad (representada por inhibición bioluminiscente en *Vibrio fischeri*) del efluente. Las variables escogidas fueron la presencia de la nanopelícula, la longitud de onda, CPI y diferentes matrices. Mayores valores de k_{app} fueron obtenidos para UV-A fotocatálisis o para UV-C fotólisis, dependiendo del compuesto. Aunque longitudes de onda más cortas como UV-C son capaces generar reacciones fotolíticas, la presencia de la nano película absorbe estos rayos antes de que ellos puedan llegar al contaminante. Para alguno de los OMPs estudiados, el incremento en la degradación producida por los ROS generados en la nano película no compensó la obstrucción de fotólisis por UV-C, causando un efecto de apantallamiento que redujo los valores de k_{app}. Al emplear agua del grifo como matriz, la reducción del TOC cayó considerablemente, destacando la importancia de un efluente limpio y los pretratamientos en el desempeño de los AOPs. En general, el principal factor para reducir la toxicidad de los efluentes fue el uso de luz UV-C en vez de UV-A. Se observó una mayor inhibición para la fotocatálisis UV-A debido a la formación de productos de transformación tóxicos (en inglés: *transformation products*, TPs) en todos los casos. De nuevo, los modelos matemáticos desarrollados fueron capaces de predecir con precisión todos los resultados basados en los efectos individuales y combinados de las variables escogidas.

El impacto del pH inicial en la degradación simultanea de los 5 OMPs por fotocatálisis UV-A fue también analizado. Generalmente, a pH altos se favorece la formación de ROS y se incrementa la degradación. Sin embargo, el estado iónico de cada contaminante, su reactividad respecto a los ROS y su afinidad superficial hacia el TiO_2 también influencia el proceso. Un estudio involucrando inhibidores de ROS fue realizado para estimar que rutas fotocatalíticas son prevalentes para cada uno de los OMPs.

Se ejecutó un tercer DoE (superficie de respuesta – diseño de Box-Behnken) para verificar el impacto de sustancias comúnmente encontradas en matrices reales (bicarbonatos, nitratos y ácido húmicos) en los valores de k_{app} de los 5 OMPs por fotocatálisis UV-A. De nuevo, fue evidente que cada contaminante responde diferentemente a cada condición debido a las múltiples

interacciones químicas en el sistema. Adicionalmente, las variables estudiadas pueden contribuir o impedir la degradación, dependiendo del contaminante objetivo y de otras condiciones de reacción.

El uso simultáneo de UV-A y UV-C fue investigado debido a las posibilidades de mejora generadas por el acoplamiento de las longitudes de onda. Sin embargo, una reducción insignificante de los valores de E_{EO} fue obtenida, posiblemente porque las longitudes de ondas escogidas fueron muy separadas en el espectro, para causar algún tipo de efecto sinérgico o interferencia positiva.

Finalmente, un análisis realizado en un LC-.MS de alta resolución (Orbitrap) fue capaz de identificar los TPs de 3 de los contaminantes durante sus degradaciones mediante fotocatálisis UV-A. Se intentó correlacionar la formación de los TPs con los niveles de toxicidad de los efluentes. Las comparaciones fueron hechas entre los TPs obtenidos en dos matrices (MQ y agua de grifo) y bajo distintos tratamientos (fotocatálisis UV-A y fotólisis UV-C). Diferentes TPs fueron obtenidos para cada tratamiento. Mediante fotocatálisis UV-A, se observaron los mismos TPs en MQ y agua de grifo, aunque en diferentes cantidades. Ningún TP detectado fue considerablemente mas pequeño que su respectivo compuestos original.

Las respuestas dispares de los OMPs para cada escenario sugieren que el tratamiento óptimo a elegir dependerá de la composición de la matriz, reactividad del contaminante objetivo y de los requerimientos del efluente final. Los valores de E_{EO} de los LEDs UV para la fotocatálisis basada en el TiO_2 continúan siendo inviables a efectos prácticos. Sin embargo, una reducción considerable de los costos se puede prever debido al mejoramiento exponencial del desempeño de los LEDs UV en los últimos años. La fotocatálisis puede encontrar su nicho en el punto de uso, en aplicaciones a pequeña escala para objetivos específicos que requieran un efluente de más alta calidad. Se debería prestar atención a los TPs y correlaciones entre ellos y se puede especular la toxicidad del efluente. Sin embargo, para escenarios reales, deberían buscarse soluciones más simples debido al elevado número de variables que pueden influenciar la toxicidad en los cuerpos de agua, y las dificultades de su identificación

Palabras clave: procesos de oxidación avanzada; fotocatálisis; diseño de fotorreactores; contaminantes de preocupación emergente; diodos emisores de luz ultravioleta; tratamiento de aguas.

RESUM AMPLIAT EN CATALÀ

El canvi climàtic pot afectar també les fonts d'aigua neta i, per aquesta raó, les creixents exigències dels estàndards de qualitat de la nostra societat han impulsat el desenvolupament de tecnologies sostenibles de tractament d'aigua capaces també de degradar els anomenats contaminants emergents (en anglès: *contaminants of emergin concern*. CECs) com els microcontaminants orgànics (en anglès: *organic micropollutants*, OMPs). Tot i que aquests compostos es troben a baixa concentració a les masses d'aigua, si no es degraden adequadament, es poden bioacumular al medi ambient. L'exposició aguda i crònica als OMP pot causar efectes nocius i, a més, imprevisibles per a la salut humana i altres organismes vius. Els tractaments convencionals d'aigües i aigües residuals no son capaços de degradar aquestes substàncies de manera satisfactòria, ja que moltes d'elles són d'origen antròpic (per exemple, productes farmacèutics i pesticides) i sovint amb una biodegradació lenta.

Els processos avançats d'oxidació (en anglè: *advanced oxidation processes*, AOPs) són una possible solució a aquest problema, ja que poden generar espècies radicals d'oxigen (en anglès: *radical oxygent species*, ROS) altament reactives, capaces de degradar els OMP. Els AOP sovint exigeixen una quantitat considerable d'electricitat o productes químics addicionals. Per això, la majoria d'ells encara són inviables per a finalitats pràctiques. Entre els AOP, la fotocatàlisi basada en TiO_2 ha cridat molt l'atenció científica en les últimes dècades, ja que pot generar ROS a partir de la llum solar, prometent un tractament eficient de l'aigua alimentat amb energies renovables. No obstant això, la fotocatàlisi encara no es troba entre les AOP més eficients en termes d'energia a causa de la seva baixa eficiència fotònica.

El ràpid desenvolupament dels díodes emissors de llum ultraviolada (en anglès: *ultraviolet light-emitting diodes*, UV-LEDs) obre noves possibilitats per als AOP basats en la llum, com ara la fotocatàlisi. Les característiques úniques dels LED UV, com la il·luminació periòdica controlada (CPI), el caràcter de font puntual i l'adaptació de la longitud d'ona, permeten dissenys de reactors molt més flexibles en comparació amb les làmpades de mercuri UV tradicionals.

En aquesta tesi, es va investigar el rendiment dels AOP basats en UV-LED per a l'eliminació d'OMP a les aigües en una multitud d'escenaris. Inicialment, es va realitzar un

disseny d'un fotoreactor amb un programa informàtic capaç de simular els perfils òptics i la distribució de la llum dins d'un reactor cilíndric a escala de laboratori (150 ml). Es va estudiar la intensitat i l'homogeneïtat de la llum per a matrius que contenien diferents quantitats de tires UV-LED al voltant del reactor. També es van investigar els efectes sobre el perfil de llum per a diferents distàncies entre els LEDs i les parets del reactor. Els resultats mostren que, tot i que s'obtenen fluxos de llum i irradiància més forts quan més LED envolten el reactor, no necessàriament s'aconsegueix una distribució de la llum més homogènia amb més LED.

A partir dels resultats obtinguts amb la simulació, es van utilitzar dos fotoreactors idèntics de quars. En un d'ells, es va afegir un nanofilm de TiO_2 a les seves parets interiors per a experiments fotocatalítics mitjançant el mètode sol-gel, mentre que l'altre reactor es va utilitzar per estudiar la fotòlisi. Es va fer un disseny categòric complet d'experiments (en anglès: *design of experiments*, DoE) per investigar l'impacte de 4 variables sobre la constant cinètica aparent (k_{app}) i l'energia elèctrica per consum de comanda (E_{EO}) per a l'antibiòtic ciprofloxacina, seleccionat com a compost objectiu. Les variables escollides van ser el nombre de LEDs al voltant del reactor; la seva distància des de les parets del reactor; l'ús de CPI i la presència del nanofilm de TiO_2. Es va obtenir un model de predicció precís i els resultats van mostrar que, mentre que l'adopció de més LED i CPI va augmentar els valors de k_{app}, la compensació energètica no va ser estadísticament suficient per convertir aquest guany en un E_{EO} més baix. Només la presència del nanofilm i les distàncies més curtes entre els LED i les parets del reactor van ser capaços de reduir els valors d'E_{EO}. Es va confirmar que el CPI només pot ser efectiu en presència d'un catalitzador, no contribuint a la degradació només en cas que hi hagi la fotòlisi. Es va seleccionar un disseny òptim amb 3 tires LEDs al voltant del reactor a 10 mm de distància de les parets a causa dels seus alts valors de k_{app} i baixos de E_{EO}. Aquesta elecció va coincidir amb la simulació que tenia la major homogeneïtat de la llum.

Utilitzant el disseny òptim, es va investigar la degradació individual i simultània de 5 OMPs (ciprofloxacina, trimetoprim, sulfametoxazol, venlafaxina i o-desmetilvenlafaxina, tots actualment a la llista de vigilància de CEC de la UE) en diverses condicions. Cada compost va respondre de manera diferent als tractaments. L'addició de peròxid d'hidrogen va millorar la degradació en tots els escenaris, ja que contribueix a la formació de més ROS.

Es va fer un segon DoE categòric complet per estudiar l'impacte sobre el k_{app} individual per a cadascú dels 5 contaminants objectiu, la reducció del carboni orgànic total (en anglès*: total orgnaic carbon*, TOC) de l'efluent i la toxicitat (representada per la inhibició de la bioluminescència sobre el *Vibrio fischeri*). Les variables escollides van ser la presència del nanofilm, la longitud d'ona de la llum, el CPI i les diferents matrius. Es van obtenir valors de k_{app} més alts per a la fotocatàlisi UV-A o la fotòlisi UV-C, depenent del compost. Tot i que les longituds d'ona més curtes com la UV-C són més capaces de reaccions fotolítiques, la presència del nanofilm absorbeix aquests raigs abans que puguin arribar al contaminant. Per a alguns dels OMP estudiats, l'augment de la degradació provocat per les ROS generades al nanofilm no va compensar la menor prestació de la fotòlisi UV-C, provocant un efecte de cribratge que disminueix els valors de k_{app}. Quan es va utilitzar l'aigua de l'aixeta com a matriu, la reducció del TOC va baixar considerablement, destacant la importància d'un efluent net i dels tractaments previs en el rendiment dels AOP. En general, el principal factor per reduir la toxicitat dels efluents va ser l'ús de llum UV-C en lloc d' UV-A. Es va observar una inhibició més alta de la fotocatàlisi UV-A a causa de la formació de productes de transformació tòxics (en anglès: *transformation products*, TPs) en tots els casos. De nou, es van obtenir models matemàtics precisos per predir tots els resultats basats en els efectes individuals i combinats de les variables escollides.

Es va analitzar l'impacte del pH inicial sobre la degradació simultània dels 5 OMP mitjançant fotocatàlisi UV-A. En general, els pH més alts afavoreixen la formació de ROS i augmenten la degradació. No obstant això, l'estat iònic de cada contaminant objectiu, la seva reactivitat amb els ROS i l'afinitat superficial amb TiO_2 també influeixen en el procés. Es va fer un estudi que implicava compostos que bloquegen l'activitat dels ROS per estimar quines rutes fotocatalítiques prenen preferiblement cadascú dels OMP.

Es va fer un tercer DoE (response-surface Box-Behnken) per verificar l'impacte de les substàncies que es troben habitualment en matrius reals (bicarbonats, nitrats i àcids húmics) sobre el valor k_{app} dels 5 OMP mitjançant fotocatàlisi UV-A. De nou, va ser evident que cada compost respondrà de manera diferent a cada condició a causa de les múltiples interaccions químiques del sistema. A més, les variables estudiades poden contribuir o dificultar la degradació, depenent del contaminant objectiu i de les altres condicions de la reacció.

Es va investigar l'ús simultani d' UV-A i UV-C per verificar les possibilitats de millora que comporta l'acoblament de longituds d'ona. No obstant això, no es va obtenir cap reducció significativa dels valors d'E_{EO}, possiblement perquè les longituds d'ona escollides estaven massa separades a l'espectre per provocar cap efecte de sinergia o interferència positiva.

Finalment, amb una anàlisi realitzada en un LC-MS d'alta resolució (Orbitrap) es van poder identificar els TP de 3 contaminants objectiu durant la seva degradació individual per fotocatàlisi UV-A. Es va intentar correlacionar la formació dels TPs amb els nivells de toxicitat dels efluents. Es van fer comparacions entre els TPs obtinguts en dues matrius (MQ i aigua de l'aixeta) sota diferents tractaments (fotocatàlisi UV-A i fotòlisi UV-C). Es van obtenir diferents TP per a cada tractament. Per a la fotocatàlisi UV-A, es van observar els mateixos TP tant per a MQ com per a l'aigua de l'aixeta, encara que en quantitats diferents. Cap TP detectat va ser considerablement més petit en massa que els seus respectius compostos pares.

Les respostes dispars dels OMP a cada escenari suggereixen que la selecció del tractament òptim dependrà de la composició de la matriu, la reactivitat del contaminant objectiu i els estàndards requerits de l'efluent final. Els valors E_{EO} de TiO_2 / fotocatàlisi basats en UV-LED segueixen sent inviables per a finalitats pràctiques. No obstant això, es pot preveure una reducció considerable dels costos a causa de les millores exponencials de rendiment dels UV-LED en els últims anys. La fotocatàlisi pot trobar el seu nínxol en aplicacions a petita escala i puntuals per complir objectius específics que exigeixen un efluent de major qualitat. Cal prestar atenció als TPs i es poden fer correlacions entre ells i la toxicitat de l'efluent, però en escenaris reals cal cercar solucions més senzilles a causa de la quantitat incomptable de variables que poden influir sobre la toxicitat a les masses d'aigua i les dificultats per identificar analíticament els productes de transformació de manera adequada.

Paraules clau: processos d'oxidació avançats; fotocatàlisi; disseny de fotoreactors; contaminants de preocupació emergent; díodes emissors de llum ultraviolada; tractament d'aigües.

LIST OF ACRONYMS

#LED	Number of LED strips around the reactor
ANOVA	Analysis of variance
AOP	Advanced oxidation process
AOX	Ammonium oxalate
BG	Band gap
CEC	Contaminant of emerging concern
CB	Conduction band
CIP	Ciprofloxacin
CPI	Controlled periodic illumination
DCy	Duty cycle
DoE	Design of experiments
D_w	Distance between LED strips and reactor's walls
DV	O-desmethylvenlafatine
ESI	Electronspray ionization
HA	Humic acid
HCD	High-energy collision dissociation
HPLC	High performance liquic chromatography
ISOP	Isopropanol
LC	Liquid chromatography
LED	Light-emitting diode
MQ	MilliQ
MS	Mass spectrometry
NOM	Natural organic matter
OMP	Organic micropollutant
PC	Photocatalysis
PNEC	Predicted no-effect concentration
PWM	Pulse-width modulation
ROS	Radical oxygen species

SMX	Sulfamethoxazole
SW	Simultaneous wavelength
TEA	Triethanolamine
TMP	Trimethoprim
TOC	Total organic carbon
TP	Transformation products
UE	European union
UV	Ultraviolet
VB	Valence band
VEN	Venlafaxine
WPE	Wall-plug efficiency
WWTP	Wastewater treatment plant

TABLE OF CONTENTS

1. INTRODUCTION

In the current scenario of water scarcity [1] and raising awareness about the harm caused by contaminants of emerging concern [2], it is fundamental to develop new and sustainable water treatment technologies that are capable of degrading these anthropogenic substances to avoid their bioaccumulation and persistence in the environment [3]. Besides mitigating the toxic impact on aquatic organisms caused by wastewater disposal and reducing the appearance of antibiotic-resistant super bacteria [4], the removal of these contaminants would increase water quality for reuse in agriculture and human consumption.

Advanced oxidation processes (AOPs) have shown a great capacity to degrade **organic micropollutants (OMPs)**, but even technologies that attract a large amount of scientific attention in the past decades such as photocatalysis are still far away from real large-scale applications due to their high energy demands [5,6]. For economic feasibility, the source of light is a critical aspect of AOPs. When solar light is not available (usually because there is not enough reliable sunshine), artificial illumination is required. The most common artificial illumination used in AOPs is low or medium pressure mercury lamps. However, conventional **ultraviolet (UV)** lamps present several problems. These include overheating because of unstable power consumption, low photonic efficiency resulting in high energy consumption, short lifetime, and environmentally unfriendly properties since mercury is a hazardous pollutant. Recently, other sources of UV-light are receiving more attention. **Light emitting diodes (LEDs)** offer potential advantages over traditional UV-lamps such as a better efficiency in converting electricity into light (high quantum yields), lower power requirements and longer lifetimes. They contain a semiconducting material that emits light in a narrow spectrum. In addition, they are less harmful to the environment because they are mercury-free [7].

This work aimed to investigate the degradation of OMPs by photocatalytic processes under different scenarios to assess the impact of variables related to the water matrix and photoreactor design, as well as detect transformation products. The objective was to develop, investigate and optimize innovative technologies based on UV-LED processes for a lab-scale treatment of waters containing OMPs by maximizing their degradation rates, reducing the effluent's eco-toxicity and minimizing energy demands. Moreover, it is fundamental to further understand the mechanism of OMPs degradation and transformation products [8].

The hypothesis of research is that UV-LED based processes have a great potential as sustainable alternatives for water treatment to reduce energy demands. The process efficiency will largely depend on variables such as OMPs' structure and concentration, matrix composition and photoreactor design; and the latter can greatly benefit from new possibilities brought by UV-LEDs. Additionally, an in-depth knowledge of photocatalytic degradation mechanisms can contribute to optimized processes and lower energy consumption levels. Degradation routes will largely depend on the aforementioned variables of the degradation process. The toxicity of the treated effluent will depend on the transformation products formed during OMPs degradation and their concentration. The main objective of this work was to design a lab-scale UV-LED photoreactor and investigate, qualitatively and quantitatively, the many variables which may affect the treatment of OMPs in water by AOPs.

The OMPs studied were part of the 2020's Watch List of Contaminants of Emerging Concern of the European Union [9]. The list contains substances which are ubiquitously found on European surface waters and have been already demonstrated to be potentially toxic to people and/or aquatic organisms. The chosen OMPs were **ciprofloxacin (CIP), trimethoprim (TMP), sulfamethoxazole (SMX), venlafaxine (VEN) and o-desmethylvenlafaxine (DV).** Data on the degradation of these substances is of significant importance for future decisions and contribute to obtaining cleaner and safe water.

The light distribution inside the photoreactor for different LED arrays was investigated using a software for simulation of optical profiles. Reliable models for the prediction of OMPs degradation under the studied ranges of investigated variables were obtained using design of experiments (DoE) strategies for multiple process variables: different LED arrays and their emission wavelength, controlled periodic illumination, presence of TiO_2 nanofilm and water matrix composition. An exhaustive investigation of the multiple causes that may affect OMPs' kinetic rates, effluent's total organic carbon abatement and toxicity variations was made – quantitatively and qualitatively. Finally, an LC-MS analysis was made to investigate transformation products and their possible correlations with toxicity, matrix and choice of treatment.

2. GENERAL PART

2.1. Contaminants of emerging concern in aquatic environment

The rising technological progress of our society and high-quality standard demands of the developed world brought an uncountable amount of new chemicals to our life [10, 11]. Every day, directly or indirectly, we are in contact with thousands of artificially generated substances which are released in the environment after performing their end-goal [8, 12]. As decades pass and society's rhythm of consumption increases, awareness about a new type of water pollution has been growing: the one caused by **contaminants of emerging concern (CEC)** [4, 12]. The main issue about these substances is their persistence in the environment, since most of CECs have very low biodegradation rates due to their anthropogenic character [3, 13]. CECs can be found in the air, ground, animal tissues and all sources of water (e.g. groundwater, rivers, sewages, lakes, oceans) [3, 14–17].

Global warming has been affecting the stability of rain across the world, causing local and/or temporary droughts even in developed countries [18, 19]. The increase of urban and overall population levels requires a high amount of water for crops irrigation, and in a global context which asks for sustainable alternatives, the reuse of water could contribute to reducing carbon footprint and environmental impact. To assure that reused water is safe, the detection and the degradation of CECs in waterbodies - as well as an appropriate assessment of their toxic effects - should be carried out.

Among the substances classified as CECs there are pesticides, pharmaceuticals, industrial chemicals, food additives, microplastics, antibiotic-resistant genes, synthetic hormones and flame-retardants. Many of them are also considered OMPs: organic carbon-based compounds and can be detected in waterbodies in the range of micrograms (μg) or nanograms (ng) per litre [20]. Despite this concentration range, a vast literature shows that, even in such a small amount, CECs (or OMPs) can be harmful to aquatic life and, potentially, to humans [21–23]. These pollutants may cause behavioural changes, endocrine-disruptive effects and other adverse effects in aquatic organisms. The behaviour, fitness and cognition of fish populations have been affected by these substances. Indeed, spatial behaviors such as activity, exploration, and avoidance are key behavioral traits that are often affected by pollution. Fish's boldness and appetite can also significantly change [24]. Regarding human health, end ocrine disruptors may increase the

chances of development of endocrine disorders, like reproductive dysfunction, neurodevelopmental dysfunctions in children, endocrine-related cancers and bone disorders [3, 25]. Nevertheless, chronic toxic effects are still yet highly unpredictable given that there is no widely agreed system to assess the strength of associations between chemical exposure and adverse health outcomes. Synergistic and antagonistic effects taking place when hundreds (or thousands) of CECs are present simultaneously in water make the assessment of the effluent's toxicity highly unpredictable [8, 26].

Another issue concerning specifically antibiotics in the environment is the increase of the population of antibiotic-resistant bacteria. If antibiotics are released in the environment, natural selection will favour the reproduction of microorganisms capable of thriving in these hostile environments. This will invariably pressure the pharmaceutical industry towards the development of more and more antibiotics to deal with ever-more resistant pathogens. Antibiotic-resistant bacteria pose a serious threat to our health and have been the topic of many studies [12, 27, 28].

2.1.1 Metabolites and transformation products

Additionally to CECs, their metabolites and transformation products pose a health threat to people and the environment [8, 29, 30]. When a pharmaceutical is ingested, it goes through chemical reactions to have its desired effect in our body. After ingestion, the compound transforms (partially or totally) into intermediate or final products of our metabolism, called **metabolites**, which are then eliminated via excretion (e.g. urine, faeces, sweating). Although different from the original compound (also commonly called "**parent compound**"), metabolites can still be chemically active and pose a health risk for living organisms and/or the environment just like any other pollutant [31]. The transformation of pharmaceuticals varies considerably: some of them can be largely metabolized before excreted, while others are only moderately or non-metabolized at all. Because of that, pharmaceuticals are usually excreted as a mixture of the parent compound and the metabolite [8, 32, 33]. A study found that the concentration of the metabolite desmethy-venlafaxine was higher than its respective parent compound, venlafaxine, in wastewater. [34].

Transformation products (TPs) is an umbrella term to define compounds that are formed by sub-sequential reactions of the parent compound. These reactions may take place inside living organisms (e.g. biodegradation, formation of metabolites) and in the environment (e.g. solar photolysis and hydrolysis) [35]. The persistence of most CECs allows parent compounds and their TPs to have long half-lives in the environment, moving from water to soil; from fat tissues to air and vice-versa [17, 36, 37]. TPs can also be formed in a more controlled environment, typically during water or wastewater treatment processes. TPs can be the result of any reaction which does not completely mineralize the target pollutant to water and carbon dioxide. TPs can cause, in some cases, more harm to living organisms than their respective parent compounds (e.g. degradation of ciprofloxacin [38, 39]), so attention must be paid to the risk of generating them. Many reports have shown, in fact, an increase in the toxicity after chemical oxidation treatment due to the formation of highly toxic TPs [8, 40, 41]. On the other hand, some larger pollutants quickly lose their toxic features after the first degradation steps, making following treatment efforts counterproductive [42].

The awareness of the environmental and health threat posed by pharmaceuticals and their metabolites and TPs was only possible due to the recent development and optimization of analytical techniques which allowed the detection and quantification of these substances in the environment (see **section 2.**7) [13, 43].

2.2. Target pollutants

All of the target pollutants included in this research are in the current (2022) EU watch list of CECs. The full list is [9] :

- Metaflumizone
- Amoxicillin
- Ciprofloxacin
- Sulfamethoxazole

- Trimethoprim

- Venlafaxine

- O-desmethylvenlafaxine

- Azole compounds

- Clotrimazole

- Fluconazole

- Imazalil

- Ipconazole

- Metconazole

- Miconazole

- Penconazole

- Prochloraz

- Tebuconazole

- Tetraconazole

- Dimoxystrobin

- Famoxadone

2.2.1 Ciprofloxacin

Ciprofloxacin (CIP, molecular formula $C_{17}H_{18}FN_3O_3$) is a commonly prescribed antibiotic and usually well tolerated. It is used to treat bacterial infections in the urinary tract, sexually transmitted diseases, typhoid fever, gastrointestinal infections, salmonellosis, pneumonia and others [44]. Its predicted no-effect concentration (PNEC) in fresh water is 0.089 µg L^{-1} [45].

CIP molecule is from the class of fluoroquinolones. **Figure 1** shows CIP's structural formula. It bears a cyclopropyl, carboxylic acid and a piperazine ring in its structure. This results in different ionisable functional groups. Being so, its photolytic and photocatalytic degradation pathway will largely depend on the solution's initial pH value [46]. Its molecular weight is 331.3 g mol^{-1} and its pK_a values are 6.1 and 8.8 [47].

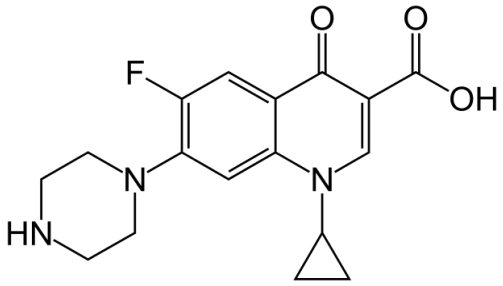

Figure 1. Ciprofloxacin structural formula

2.2.2 Sulfamethoxazole

Sulfamethoxazole (SMX, molecular formula $C_{10}H_{11}N_3O_3S$) is an antibiotic used for bacterial infections such as urinary tract infections, bronchitis, and prostatitis. It is effective against both gram negative and positive bacteria such as *Listeria monocytogenes* and *E. coli* [48]. It is commonly used together with trimethoprim to treat a variety of infections of the urinary tract, respiratory system, and gastrointestinal tract.

SMX molecule is a sulphonamide containing an isoxazole and a phenylamine ring. **Figure 2** shows SMX's structural formula. Its molecular weight is 253.3 g mol^{-1} and its pK_a values are 1.6 and 5.7 [49, 50]. Its PNEC in fresh water is 0.60 µg L^{-1} [45].

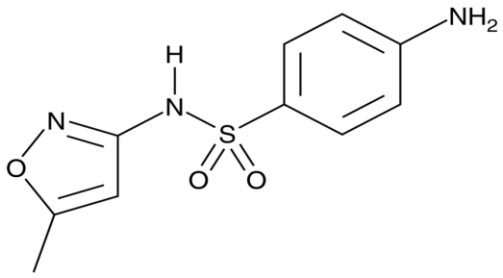

Figure 2. Sulfamethoxazole structural formula

2.2.3 Trimethoprim

Trimethoprim (TMP, molecular formula $C_{14}H_{18}N_4O_3$) is an antibiotic used mainly in the treatment of bladder infections. Other uses are middle ear infections and diarrhoea [51]. It is commonly used combined with SMX for mild-to-moderate bacterial infections and as prophylaxis against opportunistic infections in people with HIV/AIDS [52]. Its PNEC in fresh water is 100.0 μg L^{-1} [45].

TMP molecule consists of a 2-4 diamine pyrimidine ring and a 1-2-3 trimethoxybenzene moiety connected by a methylene bridge. **Figure 3** shows its structural formula. TMP is poorly metabolized in human bodies, so 80% of its dose is excreted through faeces and urine [52]. Its molecular weight is 290.3 g mol^{-1} and its pK_a is 7.1 [47].

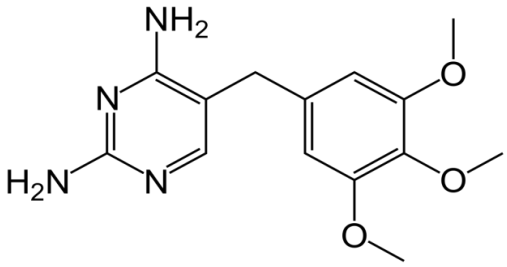

Figure 3. Trimethoprim structural formula

2.2.4 Venlafaxine

Venlafaxine (VEN, molecular formula $C_{17}H_{27}NO_2$) is an antidepressant whose consumption rate has increased in the last few years. It is used to treat major depressive, anxiety and panic disorders, social phobia and chronic pains [53]. Its PNEC in fresh water is 0.038 µg L^{-1} [45].

VEN molecule is a tertiary amino compound connected to hydroxycyclohexyl and methoxyphenyl groups, working as a serotonin and norepinephrine reuptake inhibitor. **Figure 4** shows its structural formula. VEN molecular weight is 277.4 g mol^{-1} and its pK_a is 9.1 [54]. Most of VEN is metabolized by the human body, and its main excreted metabolite is O-desmethylvenlafaxine [8].

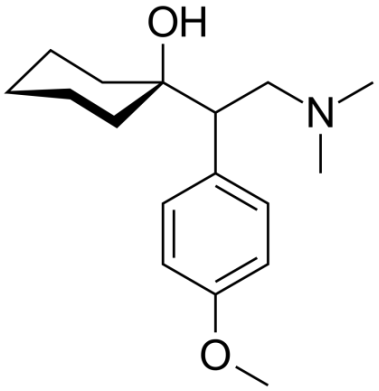

Figure 4. Venlafaxine structural formula

2.2.5 O-Desmethylvenlafaxine

O-Desmethylvenlafaxine, also known as desvenlafaxine (DV, molecular formula $C_{16}H_{25}NO_2$), is the main metabolite of VEN excreted by the human body. DV itself is also used as an antidepressant, although often considered less effective than its parent compound [55]. A study [8] detected DV concentration 5 times higher than its parent compound in wastewater treatment plants.

DV is obtained via de-methylation of the VEN molecule next to its aromatic ring. **Figure 5** shows its structural formula. DV molecular weight is 263.4 g mol^{-1} and its pK_a is 9.1[56]. Its PNEC in fresh water is 7.11 µg L^{-1} [45].

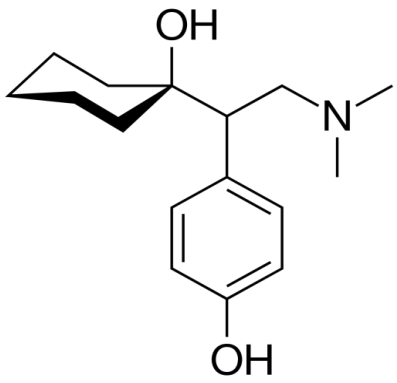

Figure 5. O-desmethylvenlafaxine structural formula

2.3 Overview of CEC regulations

New regulations aiming at the detection and reduction of CEC in waterbodies are the result of a process of increasing public awareness concerned with their potential health and environmental hazards. The European Union has the **Water Framework Directive** 2000/60/EC (WFD) [57] as the fundamental legislation regarding EU waters. The WFD provides local authorities a legislative basis for the maintenance and recovery of water quality to achieve good ecological and chemical status for all surface waters and good chemical status for groundwater. Its amendment **Environmental Quality Standards Directive** (2008/105/EC) [58] established an initial list of priority pollutants and set their environmental quality standards in surface waters based on their toxicity, environmental persistence, and increased risk for human health and environment.

Other directives, such as the **Urban Waste Water Treatment Directive** [59] (UWWTD) (91/271 CEE), Integrated Pollution Prevention and Control Directive (IPPCD) (008/1/EC) and the **Industrial Emissions Directive** (IED) (2010/75/EU) [60] establish rules and guidelines for water quality. The annex II of the latter lists the following water polluting substances:

• Organohalogenated compounds and substances which may form such compounds in the aquatic environment

• Organophosphorus compounds

• Organotin compounds

• Substances and mixtures which have been proved to possess carcinogenic or mutagenic properties or properties which may affect reproduction in or via the aquatic environment

• Persistent hydrocarbons and persistent and bio accumulative organic toxic substances

• Cyanides

• Metals and their compounds

• Arsenic and its compounds

• Biocides and plant protection products

• Materials in suspension

• Substances which contribute to eutrophication (in particular, nitrates and phosphates)

• Substances which have an unfavorable influence on the oxygen balance (and can be measured using parameters such as biological and chemical oxygen demand).

The **EU watch list of contaminants of emerging concern** aim to obtain high-quality union-wide monitoring data on potential water pollutants for the purpose of determining the risk they pose and thus whether Environmental Quality Standards (EQS) should be set for them at EU level [61]. As a consequence, a substance can be removed from the list if sufficient data is collected. The list helps prioritize which compounds need to be further studied to better understand their degradation pathways and toxic effects. The monitoring of the substances on the watch list should generate high-quality data on their concentrations in the aquatic environment, and environmental quality standards would then also be set which member states would have to meet. The first watch list was established in 2015 by the decision EU 2015/495 [61] and included natural and synthetic hormones, anti-inflammatories, antibiotics, pesticides, UV-filters and food

oxidants found ubiquitously in European surface waters. Updates of the watch list were made in 2018 by the decision EU 2018/840 [62] and again in 2020 by the decision EU 2020/1161 [9]. All the target pollutants tested in this work were added in the last version of the watch list except CIP, which was added in 2018 and the EU Commission concluded more data is necessary.

Despite these efforts, the sheer number of OMPs in water is uncountable and substances included in the watch list correspond to an infinitesimal amount of total pollutants [63, 64]. Being so, existing legislation should rise to its challenge and set removal of pollutants in effluents to non-toxic levels as basic requirements for good water quality. Anyhow, new technologies and processes adopted by wastewater treatment plants focusing on the removal of this class of pollutant should be environmentally sustainable and low-cost [6].

Unfortunately, in most of the developing world little attention is paid to these harmful substances in water and no specific regulation is yet discussed. To countries such as Brazil, which has about 50% of its population without access to sewage networks [65], OMPs and CECs might seem like a minor issue: half of Brazilian domestic waste does not even go through basic biodegradation processes such as the one described in **section 2.4**. However, scientists have been warning about contamination of water and soil by OMPs, especially by pesticides [66, 67]. Harmful substances which are prohibited in developed countries, such as glyphosate, are allowed and ubiquitous in Brazilian soil [68]. Regarding environmental legislation of effluent composition, only basic standards of pH, suspended solids, organic matter and nutrients (such as nitrates and phosphates) need to be attained. Even when treatment happens, the governmental inspection is lacklustre in most cases [65, 69].

2.4. Water and wastewater treatment

Although access to water is a recognized basic human right by the United Nations, data by the World Health Organization indicates that about 1/3 of the world's population (2.2 billion people), lack access to safe drinking water [70]. Most of these areas are in the developing world, present endemic poverty and have limited sanitation standards and structures. However, even in developed countries of Europe, Oceania and North America, local or seasonal draughts happen

rather commonly [19]. Water and wastewater treatment have been present in society for centuries, given the primordial importance of clean water sources for the establishment and development of early settlements which will then give birth to large cities [71].

The most typical wastewater treatment process worldwide involves the **conventional activated sludge** [72] as biodegradation step**.** A typical wastewater treatment plant **(WWTP)** compromise 4 stages: in the first stage, a screening of coarse particles (rocks, twigs, dirt and other large objects) is done. This is followed by stage 2, in which suspended solids are separated in a sedimentation tank. This stage can be optimized by the addition of appropriate coagulants that will accelerate particle separation. In stage 3, a biological floc of aerobic microorganisms (bacteria and protozoa) consumes the organic matter in the presence of added oxygen. The system has to be controlled so that its temperature, pH, water flux and oxygen levels remain optimal for microbiological activity. The presence of heavy metals and/or other compounds can also hinder degradation because bacteria tend to be very sensitive to environmental conditions. The produced biomass is then separated from the water again in sedimentation tanks, with part of it recycled back to the system (**figure 6**). In the final stage, the water effluent can go through disinfection by UV light, chlorine, and/or other tertiary/advanced treatment steps prior to environmental discharge. The solid sludge may be anaerobiccally digested until it is stable and dry before being discharged in a landfill or reused in croplands or pasture. The conventional activated sludge process may also have extra phases to remove nutrients such as phosphorus or nitrogen in the form of ammonia (NH_4^+), nitrite (NO_2^-) and nitrate (NO_3^-) using different microorganisms, chemicals and system conditions. **Figure 7** shows a picture of a WWTP viewed from above.

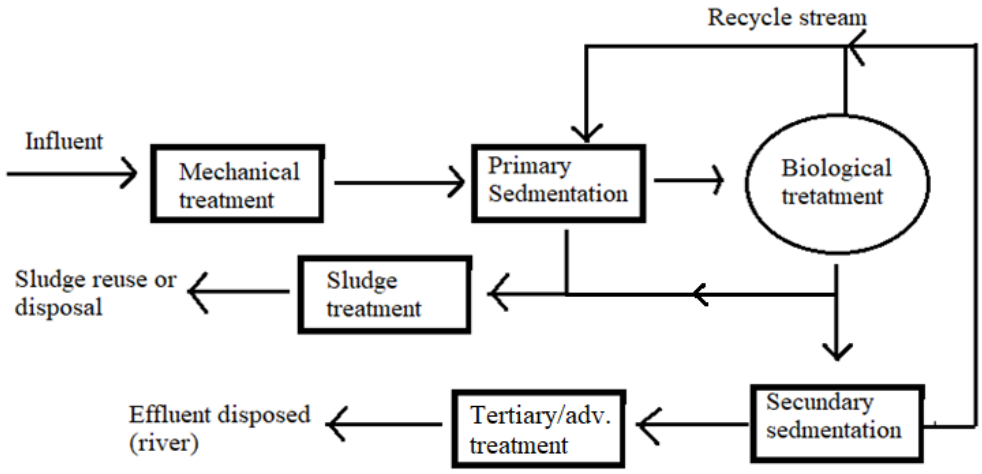

Figure 6. Wastewater treatment plant's general scheme

Figure 7. Wastewater treatment plant viewed from above, showing typical bioreactors (rectangles) and sedimentation tanks (circles) [73]

Drinking water comes from clean sources (e.g. river/groundwater). Its treatment generally includes all the previous steps (except the secundary treatment) and the addition of filtration through synthetic membranes or carbon filters for the removal of smaller molecules and pathogens. The use of ozone (O_3) as a powerful oxidant can be found in more developed regions

[74, 75]. Quality standards for composition, appearance, taste and odour of water become more rigorous so it can be distributed through public water supply systems and reach the general public's tap. In the EU and many other countries it is not allowed to reuse treated wastewater directly as drinking water [58].

2.5. Advanced oxidation processes

Advanced oxidation processes (AOPs) have shown a great potential to degrade OMPs via chemical oxidation [76, 77]. The term AOP encompasses distinct processes which have but one thing in common: the generation of **reactive oxygen species** (ROS), which are capable of starting extremely quick chain reactions to degrade persistent contaminants. The most notable of ROS is the hydroxyl radical ($^{\bullet}OH$), which has an oxidative potential of 2.80 V (other compounds such as oxygen, hydrogen peroxide, ozone and sulfate radical have oxidative potentials of 1.23 V, 1.78 V,2.08 V and 2.60 V, respectively) [78]. Starting points of radical degradation in organic molecules typically are C-H, N-H and O-H simple bonds; C=C double bonds or aromatic rings [79]. Even in the case that radicals are unable to fully mineralize pollutants, AOPs might break down large non-biodegradable molecules into smaller pieces that can be digested by microorganisms, increasing the effluent's biological oxygen demand [77].

The hydroxyl radical is a highly reactive species that is able to instantaneously and unselectively react with its surroundings. Because of that, it has to be generated *in-situ* and its concentration is difficult to measure [80]. Other radical species commonly present in AOP systems are the superoxide radical ($^{\bullet}O_2^-$), the carbonate radical ($^{\bullet}CO_3^-$) and nitric oxide radical ($^{\bullet}NO$), each one of them capable of different rates of degradation, depending on the target pollutant [81, 82]. A common issue that hinders AOPs' performance is the presence of radical scavengers in the effluent. These substances may quickly react with the hydroxyl radical instead of the target pollutants, and form much less-reactive species, such as the carbonate radical [83]. Carbonates and bicarbonate ions, commonly found in drinking water, are widely known radical scavengers (equation 1) [84].

$$^{\bullet}OH + HCO_3^- \rightarrow CO_3^{\bullet -} + H_2O \quad (1)$$

Despite varying in reaction pathways for radical formation, most AOPs have in common a high economic cost, mainly in the forms of electricity consumption and/or the need of additional chemicals. This is the case specially when UV light-based AOPs are used [6] Feasible short and mid-term solutions for this issue is option of employing solar light as a cost-free energy source [85]. Other possibility is the use of hybrid systems in which an AOP is used as an initial step to increase the effluent's overall biodegradation [86]. AOPs' high costs combined with the lack of regulation of CECs in waterbodies are the main hurdle against a world-wide adoption of advanced oxidation processes on a larger scale. Many studies highlight the importance of AOP's process optimization and a better understanding of the parameters which affect radical-based reactions as necessary in pursuit of better water quality [11, 72, 87-89].

An appropriate way of comparing different AOPs process was developed by J. Bolton and co-workers [80], who created the concept of **electrical energy consumption per order (E_{EO})**, defined as the amount of energy (in kWh) necessary to remove 90% of a target pollutant in 1 m^3 of effluent. In a comprehensive literature review [6], diverse AOPs were investigated and ordered from the most E_{EO} consuming process to the least one. **Figure 8** shows their results, indicating AOPs with (1) small E_{EO} values of < 1 kWh m^{-3} (O_3, O_3/H_2O_2, O_3/UV, UV/H_2O_2, UV/persulfate, UV/chlorine), (2) processes with median E_{EO} values in the range of 1 and 100 kWh m^{-3} (Photo-Fenton, plasma, and electrolytic AOPs) and (3) UV-based photocatalysis, ultrasound, and microwave-based AOPs (median E_{EO} values of > 100 kWh m^{-3}), which are considered as not (yet) energy efficient AOPs. The results had a very high variability because other factors can significantly affect E_{EO} values, such as the process' scale, type of matrix, chosen target compound and type of lamp (for UV-based processes). For an accurate and holistic investigation of AOPs, particularly in large scale projects, it is important to analyse other parameters not considered in an E_{EO}-only analysis, such as the life cycle assessment of each scenario [76, 89, 90]. Although the research by [6] presented electron bean technology's E_{EO} < 1 in **figure 8**, newer studies performed by [91] demonstrated that this method demands much more energy (E_{EO} ≶ 130000 kWh m^{-3}).

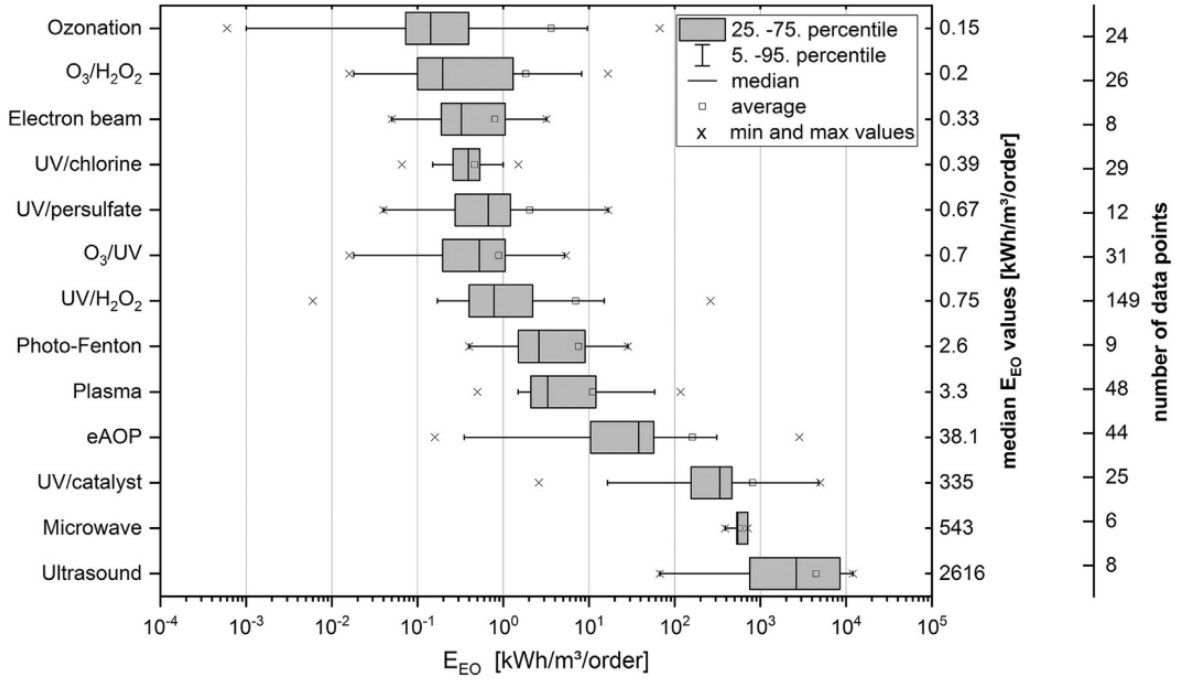

Figure 8. Average E_{EO} values for advanced oxidation processes. Reprinted from [6]. Copyright 2022, with permission from Elsevier

Most common AOPs:

1) Ozonation: Apart from being a strong oxidizing agent by itself, ozone can form hydroxyl radicals in non-acidic environments if the effluent has a low organic charge (equations 2 and 3) [92]. In highly polluted effluents, ozone will react with organic matter prior to its decomposition and no radicals will be formed. Ozonation is a well-established process adopted widely across the world for drinking water treatment [72]. In the case of wastewater treatment, it can be used as a final step (polish, disinfection) or coupled to aerobic/anaerobic digestion, since it can increase the system's biodegradability.

$$O_3 + OH^- \rightarrow HO_2^- + O_2 \quad (2)$$

$$HO_2^- + O_3 \rightarrow {}^{\bullet}OH + {}^{\bullet}O_2^- + O_2 \quad (3)$$

Ozone decomposes quickly and cannot be kept in tanks, having to be produced *in-situ* by electric discharge. It is a highly selective oxidant and leaves no traces (unlike chlorine) [93].

2) UV/Peroxide: hydrogen peroxide undergoes photolysis forming hydroxyl radicals when illuminated by UV rays according to equation 4 [94]:

$$H_2O_2 \xrightarrow{UV} 2\ {}^{\bullet}OH \quad (4)$$

UV/peroxide AOP systems have obtained very high degradation rates for a series of CECs and some large-scale plants have been adopted them, demonstrating the considerable potential of this technology [5]. Its main costs come from chemicals (addition of hydrogen peroxide) and electricity (UV lamps). Nevertheless, the presence of organic matter and scavengers may drastically decrease the system's performance. An excess of peroxide can also compromise the degradation, as demonstrated by equations 5 and 6 [94].

$${}^{\bullet}OH + H_2O_2 \rightarrow {}^{\bullet}HO_2 + H_2O \quad (5)$$

$${}^{\bullet}HO_2 + {}^{\bullet}OH \rightarrow H_2O + O_2 \quad (6)$$

3) **Ozonation with UV and/or peroxide:** the ozone molecule also undergoes photolysis in the presence of UV light, forming hydrogen peroxide according to equation 7 [92]. The next step is equation 4, which also requires UV for the formation of hydroxyl radicals. Finally, equation 8 shows that a direct reaction between ozone and peroxide in the absence of light can also form radicals. The absorptivity of ozone (at 254 nm) is much higher than that of hydrogen peroxide (3000 M^{-1} cm^{-1} for ozone and 18 M^{-1} cm^{-1} for peroxide) [95]; so equation 5 is more likely to occur than equation 4. Thus, a system with a combination of ozone, UV and/or peroxide can degrade target pollutants and form ROS from many different pathways.

$$O_3 + H_2O \xrightarrow{UV} H_2O_2 + O_2 \quad (7)$$

$$O_3 + H_2O_2 \rightarrow 3O_2 + 2\ {}^{\bullet}OH \quad (8)$$

4) **Fenton process**: the cation Fe^{2+} reacts in the presence of hydrogen peroxide forming hydroxyl radicals according to equation 9. The cation Fe^{3+} can be turned back into Fe^{2+} by equation 10 [96]. An acidic environment favours the formation of hydroxyl radicals. The Fenton process is considered one of the most efficient ones in treating effluents containing high amounts of CEC in wastewater [96]. However, it has some serious drawbacks such as the high

consumption of chemicals (acids to keep the pH low and hydrogen peroxide). The process also forms a considerable amount of ferric sludge [97].

$$Fe^{2+} + H_2O_2 \rightarrow {}^{\bullet}OH + OH^- + Fe^{3+} \quad (9)$$

$$Fe^{3+} + H_2O_2 \rightarrow Fe^{2+} + H^+ + {}^{\bullet}O_2H \quad (10)$$

5) Photo-Fenton: in the presence of UV light, the Fe^{3+} cation can turn back into Fe^{2+} and produce even more radicals according to equation 11 [96].

$$Fe^{3+} + H_2O \xrightarrow{UV} Fe^{2+} + H^+ + {}^{\bullet}OH \quad (11)$$

6) Photocatalysis: discussed in-depth in **section 2.5.1.** and **2.6**.

2.5.1. TiO_2 photocatalysis

Photocatalysis is the acceleration of a photochemical reaction in the presence of a photo-active catalyst. Its history dates back to 1911, when Alexander Eibner coined the term to describe the bleaching of the Prussian blue dye by illuminating it in the presence of zinc oxide (ZnO) [98]. For the next 6 decades few developments happened in the field. However, due to the oil crisis of the 70s which led to skyrocketing prices of this commodity, large-scale incentives in finding alternative energy sources to overcome petroleum dependency were initiated by scientists [98].

In this context, Fushijima and Honda (1972) [99] published their research describing the photolytic splitting of water using **titanium dioxide** (TiO_2) illuminated by a near-UV light source. Initially, this work opened the possibilities of producing pure and clean hydrogen gas (H_2) from sources such as water and sunlight. Nowadays, photocatalysis is understood as a widely known technology, which holds the promise of many environmentally friendly solutions for the demands of our society [5, 100, 101]. TiO_2 is an abundant, cheap, non-toxic and stable solid material commonly found in minerals. Rutile, brookite and anatase are TiO_2's crystal types [98]. Its main application is as a white pigment for paints, paper and plastics. TiO_2 nanoparticles are used in the cosmetic industry as a sunscreen agent due to its UV light-absorbing features [98].

TiO_2-based photocatalysis is an AOP that has been constantly drawing scientific attention for the past 40 years. Its main advantage is the possibility of generating ROS by irradiating titanium's dioxide surface with light. This would eliminate the need of adding any other chemical to the mix. By doping TiO_2 with other materials it is possible to change its range of photoactivity, so it can generate more ROS under natural sunlight [102, 103].

2.5.1.1. Mechanism of reaction

TiO_2 is a semi-conductor material, which means its electrical conductivity falls between conductors (e.g. copper) and insulators (e.g. glass). The conductivity of a material depends on the number of charge carriers and their mobility. **Figure 9** shows a scheme of the energy level of different types of materials. It can be seen that metals (conductors) have their Fermi level at the same energy level as their valence band. The grey band represents an overlap between CB and VB at the fermi level, which represents the thermodynamic work required to add one electron to the body [104]. In the case of conductors, the valence and the conduction band are the same. Being so, electrons can easily move from a low energy level to a high one and generate current. For insulators, the energy gap between the valence band and the Fermi level is too large to be surmounted, so electrons stay at the material's valence band and cannot reach the conduction band [98]. However, for semi-conductors this gap is narrower, and electrons may reach the conduction band if they are energetically excited by some external source. By altering the semi-conductors composition using doping techniques, it is possible to decrease this energy gap between bands and increase conductivity [105].

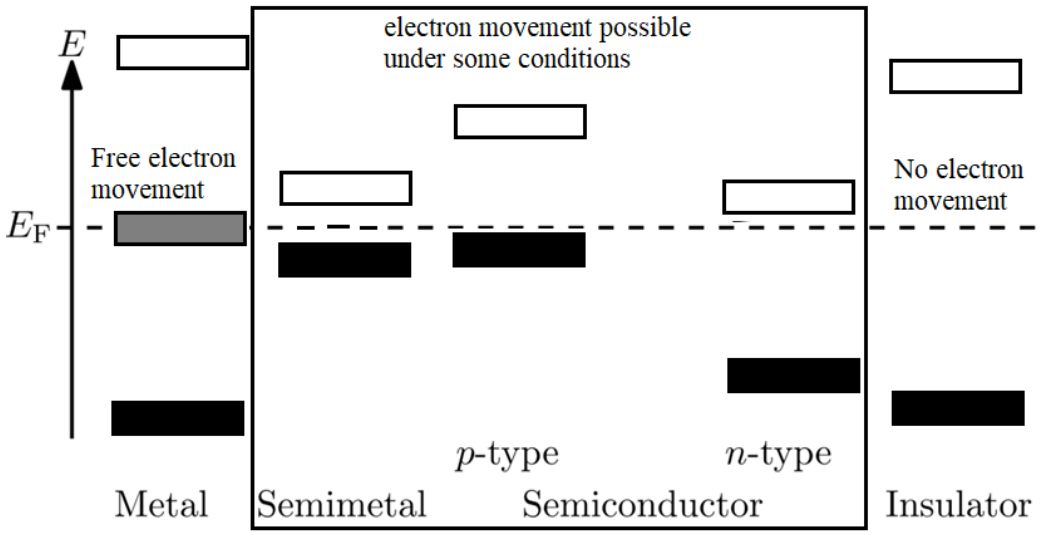

Figure 9. Band diagrams for different materials. Black rectangles show full bands, grey rectangles partially-full bands, white rectangles empty bands.

Photons are a typical external source to activate semi-conductors. The energy E of a photon is defined by the Planck-Einstein relation (equation 12), in which h is the Planck's constant and ν is the frequency of the photon.

$$E = h\nu \tag{12}$$

The frequency ν of the photon traveling at the speed of light (c =3·10^8 m s^{-1}) is defined by its wavelength number $1/\lambda$ in equation 13.

$$\nu = \frac{c}{\lambda \bar{\nu}} \tag{13}$$

Replacing equation 12 in equation 13 we have equation 14, showing that the energy of a photon is inversely proportional to its wavelength λ.

$$E = \frac{hc}{\lambda} \tag{14}$$

For TiO_2, the band gap between valence and conduction bands is between 2.8 and 3.2 eV [98], which corresponds to a maximum wavelength of approximately 390 nm. When a photon of this energy or higher reaches the catalyst surface, the photocatalytic mechanism is initiated. **Figure 10** shows a scheme of this mechanism. The promotion of an electron to a higher energy state generates an electron/hole pair (h^+/e^-) on the catalyst surface [105]. In the absence of a suitable scavenger for these charges, they will quickly recombine back to their original state, on a lower energy level. The separation of the pair is only stable for a few nanoseconds [98]. However, recombination can be avoided if the pair is transferred from the semiconductor to adsorbed species with electron donor or acceptor properties. If this stage is successful, these charges coming from h^+/e^- can start redox reactions which will cause pollutant degradation. Carrier charge recombination can be avoided by a series of actions, such as carefully tailoring the material's properties and reducing TiO_2 surface defects.

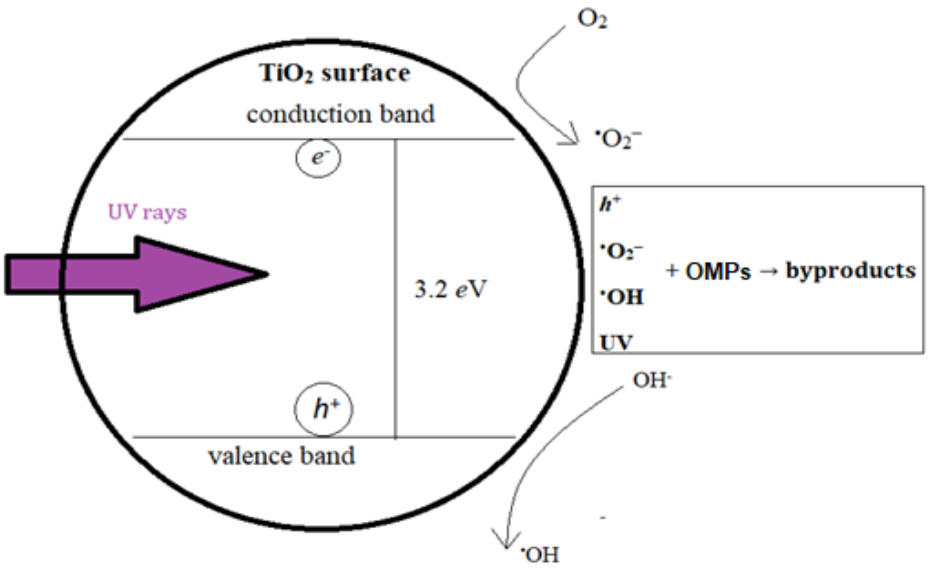

Figure 10. Scheme of photocatalysis mechanisms of pollutant degradation. Rearranged according to [102]

Figure 11 shows possible charge carrier pathways in heterogeneous photocatalysis. In step 1 and 2, the negative and positive charges leave the bulk of the catalyst to reach its surface. Steps 3 and 4 show the recombination that can happen before or after this movement towards the semiconductor's surface. Finally, steps 5 and 6 show the reaction of the h^+/e^- pair with substances in the water matrix.

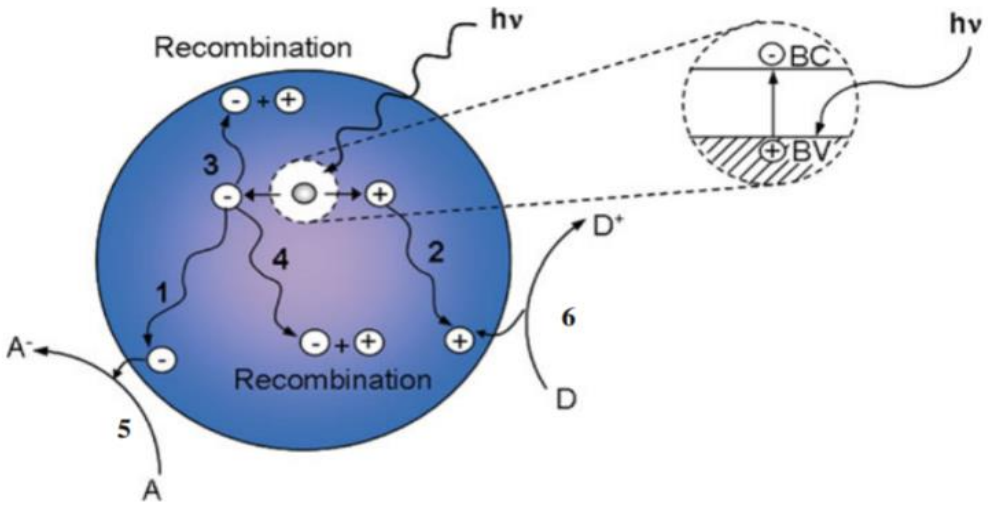

Figure 11. Possible charge carrier pathways in heterogeneous photocatalysis. BC: conduction band, BV: valence band. Reprinted from [98]. Copyright 2022, with permission from Springer

Oxygen (O_2) is commonly dissolved in water and can act as an electron aceptor. Less frequently, other highly oxidative molecules such as H_2O_2 and O_3 can also play that role. Common h^+ aceptors are the hydroxide ion (OH^-), potential target pollutants and even water molecules themselves. Equations 15-22 describe the mechanisms of photocatalysis [98]:

$$TiO_2 \xrightarrow{UV} h^+_{vb} + e^-_{cb} \quad (15)$$

$$e^-_{cb} + O_2 \rightarrow {}^{\bullet}O_2^- \quad (16)$$

$$e^-_{cb} + H_2O_2 \rightarrow OH^- + {}^{\bullet}OH \quad (17)$$

$$h^+_{vb} + H_2O \rightarrow {}^{\bullet}OH + H^+ \quad (18)$$

$$h^+_{vb} + OH^- \rightarrow {}^{\bullet}OH \quad (19)$$

$${}^{\bullet}O_2^- + \text{pollutants} \rightarrow \text{TPs} \quad (20)$$

$$h^+_{vb} + \text{pollutants} \rightarrow \text{TPs} \quad (21)$$

$${}^{\bullet}OH + \text{pollutants} \rightarrow \text{TPs} \quad (22)$$

The mechanism of reaction can be separated in 5 steps. In step 1), the target pollutant moves from the bulk of the solution to the catalyst's vicinities. Step 2) is the adsorption of the target pollutant on the catalyst's surface. Step 3) is the reaction between the target pollutant and the oxidative species generated by the catalyst. Step 4) comprises the desorption of the TPs from

the catalyst and the final step 5) is the movement of these TPs from the catalyst's vicinities back to the bulk of the solution [81, 101].

2.5.1.2. Influential parameters

1) Matrix composition and pH

As it can be seen from the presence of ions H^+ and OH^- in equations 17-19, the pH of water plays a significant role in the generation of radicals. The composition of water or wastewater affects its pH. Equation 19 particularly shows how a more basic environment can increase the formation of hydroxyl radicals, increasing the degradation. These findings have been confirmed by literature [106–109].

Another way in which pH can affect the photocatalysis is by altering the electrostatic affinity between the TiO_2's surface and the pollutant molecule. Since the catalyst is solid and the reaction environment is liquid, TiO_2 photocatalysis for water treatment is a *heterogeneous* case of photocatalysis, in which catalyst and reaction medium have different phases. TiO_2 has a point of zero charge at pH = 6.2 [110], meaning that at pH-values below and above 6.2 the reaction described by equations 23 and 24 [111] take place at the catalyst surface, respectively.

$$TiOH + H^+ \rightleftharpoons TiOH_2{}^+ \quad (23)$$

$$TiOH + OH^- \rightleftharpoons TiO^- + H_2O \quad (24)$$

If the ionic state of a target pollutant at the reaction's pH has the opposite charge than the catalyst, the adsorption will be favoured. If the charges are the same, the adsorption will be hindered [50, 112]. In water solutions, the $\mathbf{pK_a}$ of molecules defines which ionic state is more predominant for a given matrix pH.

The chemical composition of the matrix drastically influences the performance of the photocatalysis. Matrices such as wastewater or river water contain an uncountable number of substances, and to detect and quantify them all would be an impractical task. Nevertheless, the

presence of known inorganic ions has shown to affect the availability of radicals due to their scavenging character [81, 113].

The presence of **natural organic matter (NOM)** can also severely hinder photocatalysis by 1) acting as a radical scavenger [83]; 2) increasing the system's turbidity, which would decrease the number of photons reaching the catalyst [92]; 3) by adsorption at the catalyst's surface and reducing the number of the available sites for target pollutant's reaction [114]. However, in some cases NOM and inorganic ions (e.g. NO_3^-) can increase photodegradation by photosensitization. In this phenomenon, illumination of some molecules presenting unsaturation (π-bonds, e.g. humic acids) can generate radical species that will contribute to pollutant degradation [83, 84].

The **initial concentration (γ_0, in mg L^{-1})** of the target pollutant itself in the matrix is also an important parameter of influence. If γ_0 is too high, the OMPs and their respective TPs formed during treatment greatly surpass the amount of available oxidative species, leading to saturation of the catalyst surface, affecting the photonic efficiency and, ultimately, the reaction rate [115]. Since photocatalysis depends on the adsorption phenomenon, its reaction rate k_{pc} fits the Langmuir-Hinshelwood (L-H) model described by equation 25, in which θ represents the fraction of catalytic sites occupied by the target pollutant, K is the adsorption rate constant of the pollutant, γ is the pollutant's concentration and r is the reaction constant at the catalyst's surface between the pollutant and the oxidative species. This is the simplest model consistent with Langmuir's equilibrium isotherm. The L-H rate model has a dependence upon concentration and is widely applied in determining rates of photocatalytic reactions [116, 117].

$$k_{\mathrm{pc}} = r\theta = \frac{rK\gamma}{1 + K\gamma} \tag{25}$$

It has been shown that photocatalysis often fits well into a pseudo-first order kinetic model [118] regarding pollutant concentration according to equation 26:

$$k_{\mathrm{pc}} = \frac{-\mathrm{d}\gamma}{\mathrm{dt}} \tag{26}$$

By integrating equation 26 we obtain equation 27, in which *t* represents the time of reaction.

$$\mathrm{Ln}\frac{\gamma_{(t)}}{\gamma_0} = k_{pc}t \tag{27}$$

2) TiO_2 concentration, mode of utilization and alteration

The concentration of TiO_2 in its powder form influences photocatalytic degradation rates decisively. Adding more catalyst to the system increases the availability of catalytic sites and allows more hydroxyl radical production and pollutant degradation. However, care must be taken, because if the TiO_2 concentration goes beyond a threshold, additional catalyst will only reduce the process' performance [119, 120]. Too much TiO_2 in solution will cause its particles to agglomerate, which will reduce the reaction surface area. Additionally, the opacity of the solution will increase, which will cause a phenomenon called *screening effect* [119], in which catalyst particles block the light's pathway through water. The optimal concentration of TiO_2 will vary from case to case and will depend on the reactor's geometry and process conditions [121].

Apart from slurry solutions, TiO_2 can also be utilized in another mode: immobilized on surfaces as a thin film. The main advantage of doing this is that it does not require a separation step between the water and the catalyst and allows a continuous-flow operation; both of which would greatly reduce process costs. However, degradation using immobilized TiO_2 generally performs slower than slurry solutions, since the first has a smaller surface area compared to the latter [119, 122]. Mass transport limitations also play a significant role when an immobilized catalyst is used, since TiO_2 reaction sites are not equally distributed in the reaction medium. Another challenge of immobilized TiO_2 is how to keep a homogenous and optimized lighting inside the photoreactor [123]. The performances of immobilized vs. suspended catalysts have different amounts of degradation sites, require different illumination designs and rely on different mass transport mechanisms. For this reason, it is difficult to theoretically compare them directly and more experimental data to support design and modelling are required in this context [121].

Among the main problems regarding TiO_2 photocatalysis, charge carrier recombination and low activity under solar light both rank high. As it was mentioned in **section 2.5.1.1**, TiO_2

can only be photo activated if illuminated with photons of wavelength <400 nm, falling in the near-UV range. Solar light contains only about 3-5% of its spectrum in the UV range [124], so its photo activity is far from ideal in this scenario. There are ways to alter TiO_2's structure and/or surface to increase its photoactivity under solar light. The most common strategies are doping and semi-conductor coupling. When the catalyst goes through doping, different atoms are introduced in the TiO_2 lattice, changing the energy levels of conduction and/or valence bands. If done rightly, this reduces the energy gap in the catalyst and allows a larger number of photons of lower energy (e.g. visible light) to generate (h^+/e^-) pairs, thus increasing degradation [102, 105]. Semi-conductor coupling takes advantage of another semi-conductor with a smaller energy gap TiO_2 (e.g. CdS, Fe_2O_3, V_2O_5 and ZnO) [105]. In this case, the additional semi-conductor acts as a bridge linking the energy gap between the valence and the conduction bands of TiO_2, partially alleviating charge recombination.

3) Light intensity and wavelength

Evidently, light plays a significant part in photocatalytic processes. The photo-dependence character of photocatalysis' kinetics can be described in 3 stages (**figure 12**). At low light intensities (typically described as radiant flux (W) or irradiance (W m^{-2})), the rate of photocatalysis k_{pc} increases linearly with intensity (order of reaction = 1). For intermediate light intensities, k_{pc} order increases with the square root of intensity (order = 0.5). When light is too intense, k_{pc} can become independent of light intensity (complete saturation of catalytic sites and transport limitations, order = 0) [125]. This means that increasing the energetic consumption of light intensity without paying attention to other parameters could result in efficiency losses. The optimal photonic efficiency will correspond to the area where reaction rate is linearly dependent on the light intensity. This threshold will depend on each photoreactor design and other process characteristics, such as the catalyst being used and the matrix composition [126].

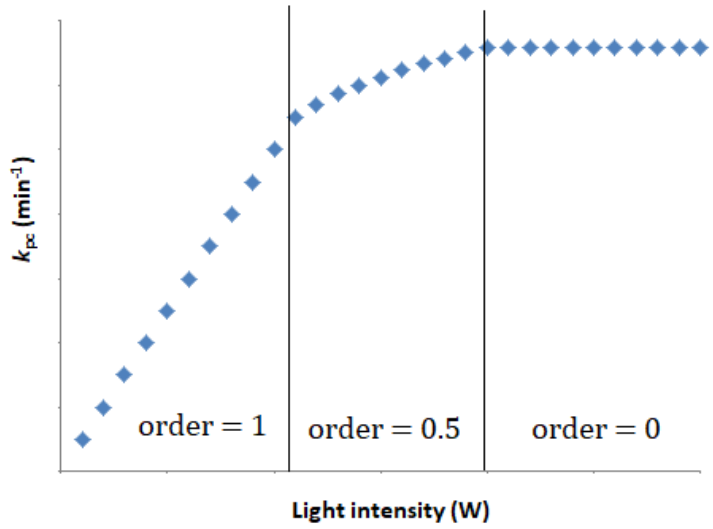

Figure 12. Light intensity correlation with kinetic order

Light's wavelength λ is also a key variable for photocatalysis. As it was explained in this section, photons of a sufficient energy should reach the catalyst's surface for its activation. Photocatalysis can happen under solar light or using artificial UV light sources. The choice of a light source has a direct impact not only on the kinetic rate k_{pc}, but also on the process' photoreactor design, economic costs and environmental impact [127, 128]. Photons of different wavelengths do not behave equally. They have different reactivity with target pollutants; generate divergent amounts of ROS species [129]; demand different amounts of energy consumption from light sources and have contrasting properties like refraction and absorption. Photons of shorter wavelengths (e.g. UV-C) can react faster with OMPs and photoactivate TiO_2. However, they can get easily absorbed by various substances in the water matrix before reaching the target pollutant or catalyst [130].

2.6. Ultraviolet light, photolysis and disinfection

UV light is the electromagnetic radiation of wavelength 100 nm < λ < 400 nm. **Table 1** shows the classification of radiation according to its wavelength.

Table 1. Radiation classification according to wavelength [131]

Light type	Wavelength range (nm)
X-rays	0-100
UV-Vacuum	100-200
UV-C	200-280
UV-B	280-320
UV-A	320-390
Visible	390-780
Infrared	>780

Figure 13 shows the solar irradiance spectrum and its energy distribution. Only a small fraction of sunlight is represented by UV light. Most of these rays (UV-Vacuum, UV-C and UV-B) are absorbed by the ozone layer in our planet's stratosphere (see equation 5). This layer acts as a protective shield to life, since UV rays contain a lot of energy and are capable of damaging the DNA of skin cells, which would produce genetic defects or mutations and can lead to skin cancer and eye damage [132].

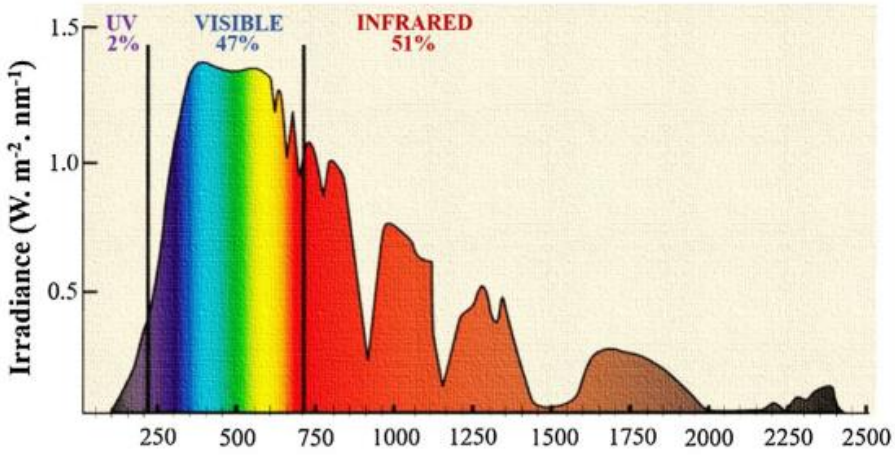

Figure 13. Solar irradiance reaching the surface of the Earth spectrum and its energy distribution in the city of Sao Paulo (Brazil, in 2021) Reprinted from [131]. Copyright 2022, with permission from Elsevier

Nevertheless, UV light can be artificially generated and it has many beneficial practical appliances in our society. It can be used in the photography industry and astronomy to obtain better images [133]; in forensics as an investigative tool to reveal body fluids or bruises [134]; in chemistry, UV/Vis spectroscopy is a widely adopted analytical technique that determines

chemical structure of samples, and UV detectors are commonly used for chromatographs [103] (see **section 2.7.1**).

Photolysis is a chemical reaction in which a molecule is broken down by photons of sufficient energy. The rate of photolysis of an OMP depends upon numerous chemical and environmental factors including the light adsorption properties, the reactivity of the chemical, and the intensity of the radiation.

In a situation in which the matrix and photoreactor parameters are constant, photolysis can be simplified as a pseudo-first order equation 28, in which k_p represents the pseudo first order constant rate of reaction for photolysis [92]:

$$\frac{-\mathrm{d}\gamma}{\mathrm{dt}} = k_p\gamma \tag{28}$$

Photolysis commonly takes place as one of the possible last stages of wastewater treatment plants in a process called **disinfection**. UV light is used to attack the DNA of pathogens such as bacteria, virus and protozoa still present in water. In the presence of UV light (generally UV-C), these microorganisms are destroyed [74]. Disinfection doses found on treatment plants vary between 30 and 1000 mJ cm^{-2}, depending on the pathogens' resistance [135]. Each substance's (or microorganism's) reactivity towards light is different and will depend not only on the UV dose and its light absorptivity but also the water matrix: factors like turbidity, organic charge and suspended solids play a major role on k_p values [106, 136].

In wastewater treatment plants, disinfection is typically carried out using mercury (Hg) UV lamps. When voltage is applied, the mercury in the lamp will evaporate and emit UV light depending on the pressure it might reach. Typically, these lamps also contain some inert gas such as argon, which is ionized when the lamp is turned on and also contributes for light emission. These types of lamps contain trace amounts of toxic mercury, which is harmful for the environment. They have a rigid cylindrical shape and have a relatively short life span (<12,000 hr). They utilize a high voltage discharge to ionize a mercury/gas mixture in the lamp creating plasma that emits UV light. Mercury lamps have fixed emission patterns determined by the inherent properties of mercury, which are either monochromatic or polychromatic depending on

the gas pressure (low or medium, respectively). They are built from fragile quartz material, need a warm-up time (because the Hg inside the lamp takes a few minutes to evaporate) and emit radiation in a radially uniform pattern [7, 87].

The Minamata Convention on Mercury, signed by over 100 countries, which compromises a gradual phasing out of mercury use by 2020 (with a five years tolerance), displays the public awareness of the environmental issue associated with this substance and sets the ground for the current replacement of Hg UV lamps [137].

2.6.1. Light-emitting diodes

Over the last few decades, light-emitting diodes (LEDs) have become common objects of our daily lives. The first visible LED was developed in 1962, and since then, this technology has been replacing the old incandescent bulbs [7]. LEDs have much higher wall-plug efficiency (WPE), which represents the ratio of conversion of electricity to optical power. This reduces considerably their environmental impact and costs. Apart from that, LEDs have a much longer life-time than traditional incandescent lamps [138].

The mechanism of LEDs relies on the conversion of direct current (DC) into light [7]. This current passes through the diode, which is a semiconductor with a p-n junction. This junction is formed when a p-type semiconductor is put in contact with an n-type. The p-type can be formed by adding an impurity with fewer electrons in its valence band, which would cause the formation of a positive charge carrier h^+. The n-type is formed by substituting an element with an additional electron, which will generate a negative charge e^-. At the n-p junction, the carrier charges will diffuse along the diode's interface, leaving behind residual opposite charges. This creates a region around the interface that is free of charge carriers, called the depletion region. The subsequent electric field generated in this region creates a potential difference between p and n sides, opposing further carrier movement. When an external voltage is applied, this equilibrium is disrupted and current starts to flow at the n-p junction, making electrons and holes recombine. As electrons go back to the valence band, energy is released in the form of light. The emitted wavelength will depend on the band gap at the n-p junction, which is an intrinsic characteristic of

the materials of the LEDs. Examples of commonly used materials are gallium arsenide (GaAs) and gallium phosphide (GaP). The electricity-to-light conversion process of LEDs is inversely analogous to the mechanism through which semiconductors generate hydroxyl radicals from light [7] (see **section 2.5.1**). **Figure 14** shows a scheme of the electricity-to-light mechanism of LEDs.

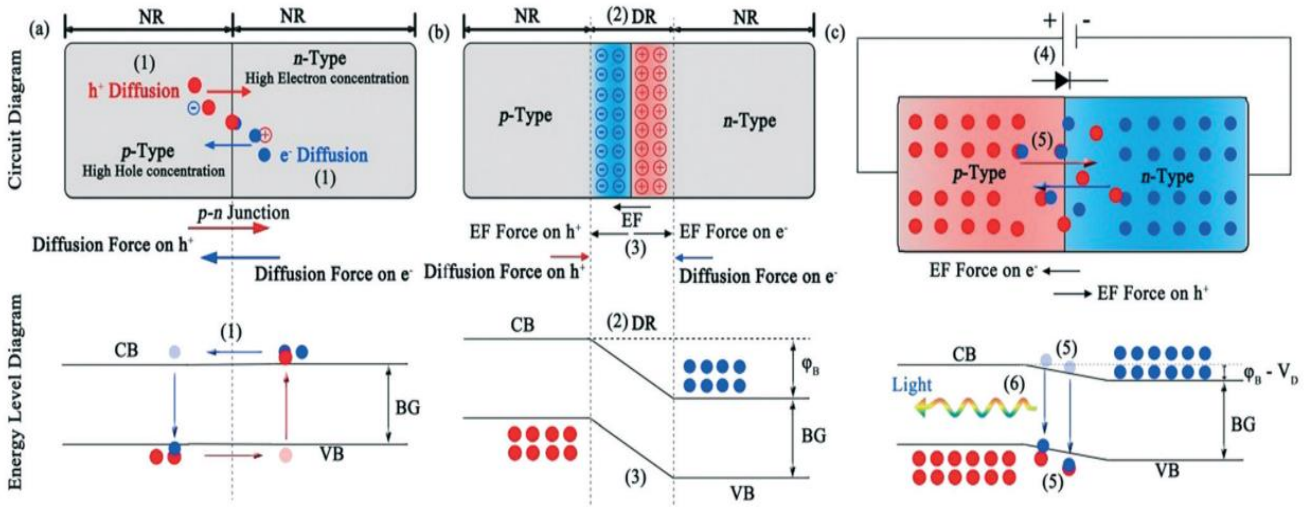

Figure 14. Circuit and energy level diagram schematics of an LED p–n junction in: (a) initial movement of mobile carriers, (b) equilibrium with no voltage applied, and (c) emitting light from the p–n junction when voltage is applied. The process of photon generation: (1) h^+ in the p-type neutral region (NR) and e^- in the n-type NR diffuse toward the interface, (2) forming a depletion region (DR) devoid of mobile charge carriers, (3) creating an electric field (EF) that opposes the further exchange of charge carriers at equilibrium; (4) when a p–n junction is biased in the forward direction, (5) this equilibrium is disrupted and current flows across the interface as electrons are injected from the n region into the p region; (6) when electrons in the n-region conduction band (CB) combine with holes in the p-region valence band (VB), excess energy equivalent to the band gap (BG) is released in the form of light. Reprinted from [7]. Copyright 2022, with permission from the Royal Society of Chemistry

The LED chip contains the n-p junction materials on top of a substrate, between a cathode and an anode which will allow current to flow through the diode. A lens is also positioned, as shown by **figure 15**.

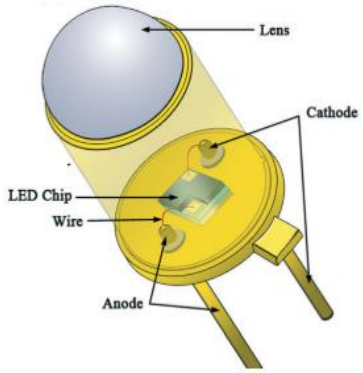

Figure 15. LED chip in detail. Reprinted from [7]. Copyright 2022, with permission from the Royal Society of Chemistry

UV-LEDs (ultraviolet light-emitting diodes) can be obtained by combining semiconductors that will create a band gap corresponding to the UV range. UV-LEDs have a smaller WPE and slower development than visible LEDs [87]. Since the semiconductor's bandgap capable of emitting UV light is larger than the one capable of emitting visible light, higher voltages are necessary to surmount the equilibrium at the depletion region described on **figure 14**. Excessive heat can be generated as a result of high voltage demand, which lowers the WPE and may also damage the device, reducing its time of life and/or affecting its emission's wavelength [7]. Additionally, due to the higher absorptivity of UV rays in comparison to visible LEDs, packaging and lens materials cannot be the same in order to increase the optical energy output. **Figure 16** shows recent (2020) [139] data on UV-LEDs' external quantum efficiency and its dependence on wavelength. A clear trend describing how shorter wavelengths have lower electrical-to-optical ratio efficiencies can be observed.

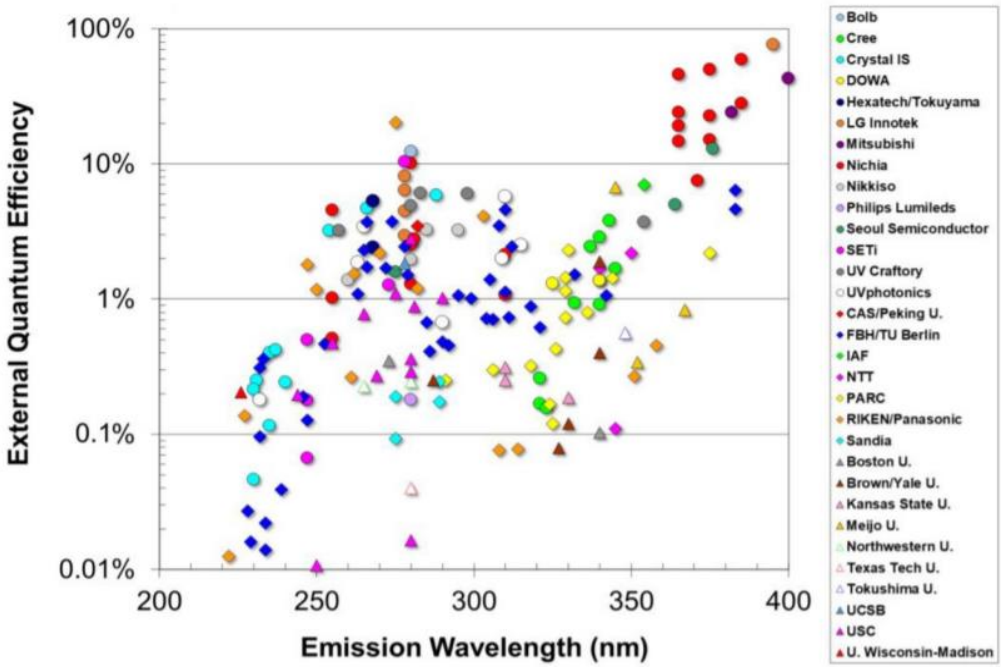

Figure 16. Correlation between UV-LEDs' external quantum efficiency and emitted wavelength for different manufacturers [139]

2.7. Analytical methods for pollutant identification and quatification

The awareness of the environmental and health threat posed by OMPs in general, including pharmaceuticals and their TPs, was possible due to the development of techniques which allowed the detection and quantification of these substances in the environment.

2.7.1. High performance liquid chromatography

High-Performance Liquid Chromatography (HPLC) was developed in the 60s and 70s to reduce the size of chromatographic columns by the adoption of higher operation pressures and smaller stationary phase particle size. **Figure 17** shows a scheme of an HPLC system, in which the mobile phase is pressurized before reaching the column, and a detector (most commonly UV)

identifies a change in a property of the mobile phase (presence of the analyte) and sends the signal to a software that collects the data and draws a chromatogram.

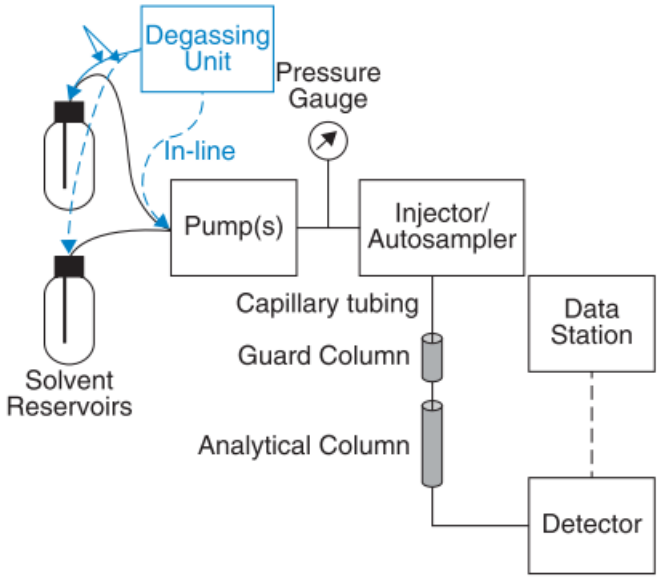

Figure 17. Scheme of an HPLC system. Reprinted from [140]. Copyright 2022, with permission from Wiley & Sons

An HPLC column is generally made of high-purity silica particles with diameter < 10 µm. In reverse-phase chromatography, the mobile phase is typically a mix of ultra-pure water with organic solvents such as methanol or acetonitrile. The sample is injected together with the mobile phase and moves through the pores of the column, where different attraction and repulsion forces will make each individual compound of the mixture elute at different velocities. In the pursuance of an ideal separation, a chromatographic method should be developed specifying all the aforementioned variables [140]. Analytes' sizes and polarities are key aspects of method development. A mobile phase whose composition is mainly water will elute polar (hydrophilic) analytes faster than non-polar (hydrophobic) ones. If the elution of an analyte is happening too fast, common efficient responses are the reduction of the mobile phase's flow or a change in its composition. If the mixture contains few compounds that are easily separated, a simple chromatographic method in which the composition of the mobile phase does not change during elution (isocratic elution) can be sufficient. To separate multiple compounds from a mixture adequately, complex chromatographic methods may be necessary in which the composition of mobile phase changes with time (gradient elution). When dealing with matrices such as

wastewater, some pre-treatment (e.g. filtering, solid phase extraction) is necessary in order to remove interferences and allow detection of analytes at trace levels [140].

2.7.2 Mass spectrometry

Mass spectrometry (MS) is the most widely adopted analytical method for the detection and identification of OMPs and their TPs present in water [140]. MS is used to measure mass-to-charge ratio of ions (*m/z*) and provide data on the analytes' molecular structure. This technique can be coupled with liquid or gas chromatography (LC-MS and GC-MS, respectively). Both methods are powerful tools of identification and quantification of compounds, and recent advances in their technology allowed the possibility of identification of molecules of large molar masses (>10000 g/mol) [15]. Combining the separation power of chromatography (see **section 2.7.1**) with the mass analysis capabilities of MS provides unique solutions to a wide range of problems, resulting in one of the most powerful analytical techniques of today.

The principle of MS lies on the breaking of the analyte's molecules, which will generate different ions (or fragments for tandem MS, explained further in this section) of different *m/z*. Due to that, these fragments will respond differently to electromagnetic fields generated by the equipment, and can be detected accordingly [140]. A typical MS experiment consists of five parts: 1) analyte injection, 2) analyte ionization, 3) separation of ions, 4) ion detection and 5) data processing and interpretation. Following the sample injection, in the ionization step the analyte molecules are transformed into ions in a gas phase. They go through the analyser at a high vacuum ($<10^{-5}$ mbar) where their trajectory will be affected by electromagnetic fields depending on each *m/z* value. The fragments are detected and the results can be visualised in a mass spectrum by quantifying the flow of charged particles on a "stick diagram" or "centroid" showing the relative current produced by ions of different *m/z* ratios. Since each molecule has a unique spectrum according to how its ions fragmentise, it is possible to compare the results with a database and/or a control sample and identify the analyte. A scheme with the main components of MS is shown on **figure 18**, and the example of a mass spectrum (CIP) on **figure 19**.

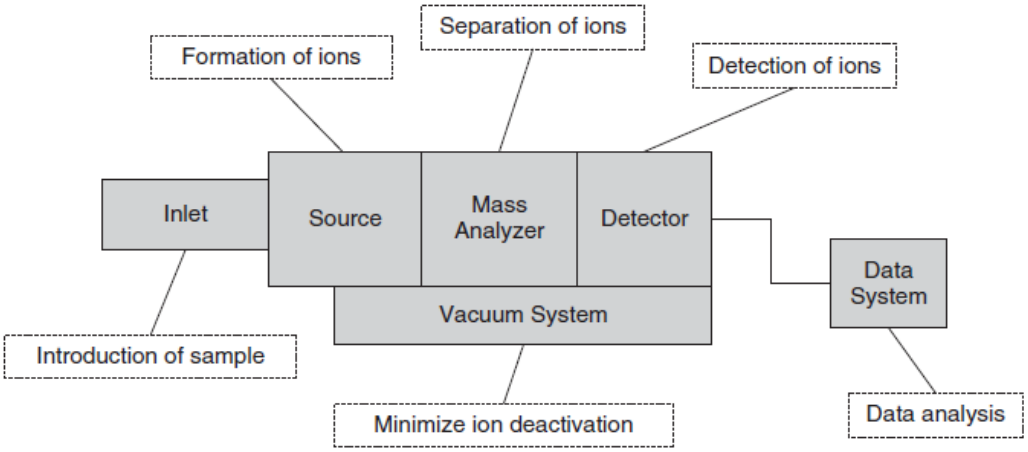

Figure 18. Scheme of main components of MS. Reprinted from [140]. Copyright 2022, with permission from Wiley & Sons

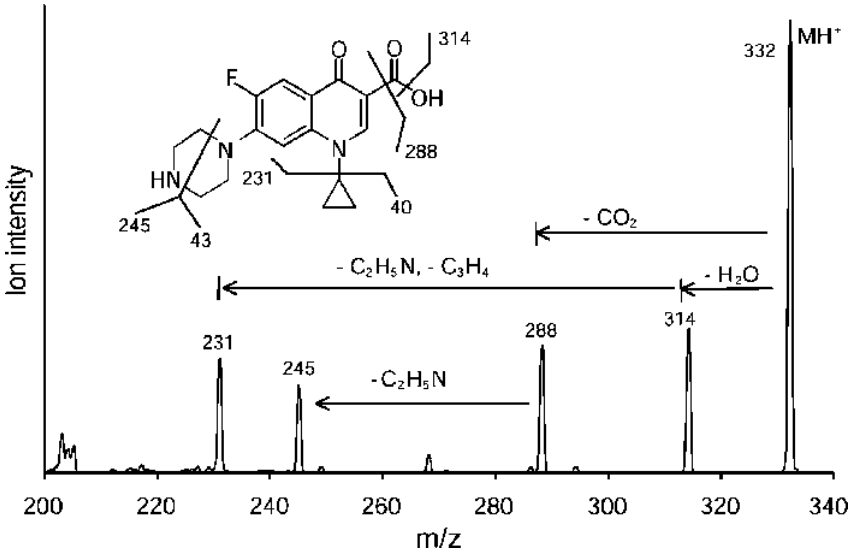

Figure 19. Mass spectrum of ciprofloxacin [141]

The ionization step should generate gas-phase analyte ions either in high vacuum or atmospheric pressure to enable analysis [25, 142]. There are over 50 different ionization techniques [143] and they can be classified depending on the physical state of the analyte. Electron ionization is commonly used for gaseous analytes. It is based on the impact of the analyte with high-energy electrons emitted by an electrically heated filament under high-vacuum conditions and accelerated by an electric field [142]. For the analysis of biomacromolecules, the matrix-assisted laser desorption ionization (MALDI) is the most common ionization method. The

sample is mixed with an appropriate solution that, upon drying, will cause a co-crystallization of all the components in mixture. These crystals are then laser-bombarded at their wavelength of maximum absorption, generating gas-phase ions that can be analysed [144].

Analytes for water and wastewater analysis are in liquid state. Under this condition, the production of ions can be achieved with minimal fragmentation and no energy surplus by soft ionization method. Electrons spray ionization (ESI) is the most used method the analysis of non-volatile and polar compounds, like pharmaceuticals [145]. In this method, the LC mobile phase containing the analyte(s) is nebulized at atmospheric pressure by N_2 sprayed by a pneumatically-assisted capillary in the presence of a strong electric field. Under these conditions, small highly charged droplets are generated and analyte ions present in them will be transported to the gas phase. This phase (which contains N_2, mobile phase solvents and the analytes) will be put through a vacuum interface, where desolvation and collisional cooling will generate protonated and/or deprotonated ionic species, further sent towards the analyser [144–146]. **Figure 20** describes this process.

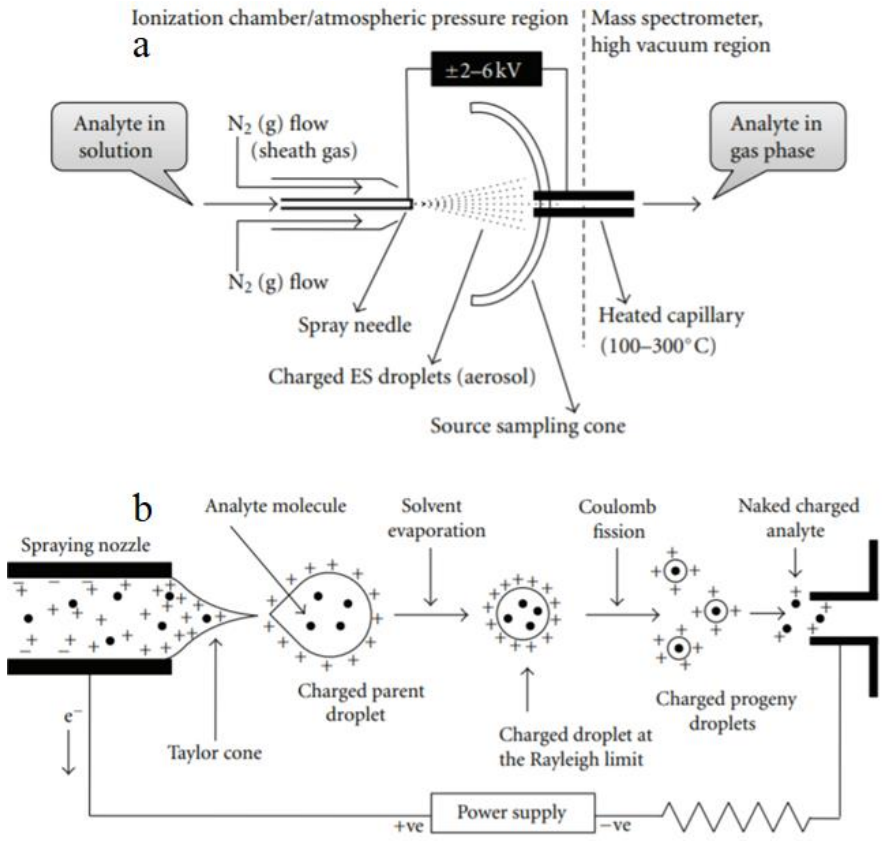

Figure 20. Eletronspray ionization scheme: (a) gas spraying, (b) ionization and fragmentation [146]

Key features and capabilities of the equipment will depend on the analyser being used. The mass resolution is defined as *m/z* divided by the peak's full-width half-maximum (FWHM). Higher resolutions increase the capacity of the equipment to distinguish between peaks of small *m/z* difference, allowing a higher mass accuracy [140]. Mass analysers are classified as either unit-mass-resolution (e.g. quadrupole, ion-trap) or high-resolution (HRMS) (e.g. orbitrap, time-of-flight) instruments. For high resolution instruments, the typical error on mass values is below 3 ppm, whereas for unit-mass resolution equipment this error is around 100 ppm [140]. The resolution power is defined as the inverse of the resolution value. High resolution equipment offers better results for analytes of higher molecular weight, have lower detection limits (higher sensitivity) and provide better results for more complex matrices. From a highly accurate *m/z* value, software tools and databases can be used to calculate possible chemical formulas for the analytes.

The general mode of data acquisition of MS is the **full-scan mode**, which continuously acquires mass spectra between minimum and maximum values of *m/z*. Additionally, some analysers can acquire data in **selected-ion mode**, being programmed to inspect a specific (preselected) *m/z* value for transmission in the detector during the analysis time. Compared to the full-scan mode, this will provide a much larger measurement time for the selected *m/z*, increasing the signal-to-noise ratio. This mode is particularly useful for quantitative analysis of targeted substances that are previously known [13, 142, 147, 148]. These modes are related to the choice of screening procedure for determination of molecules. They depend on the availability of a known standard. In the case this standard is available target screening is made via direct comparison of spectra. If standards are not available, but are predictable, suspect screening on an exact mass range is done and structure can be confirmed with MS databases and other prediction tools. In case the sample is completely unknown, non-target analysis could give the most prominent peaks and proceed with an attempt of identification like in the suspect screening case. **Figure 21** shows a flowchart of the screening procedure in the MS for TP analysis [149].

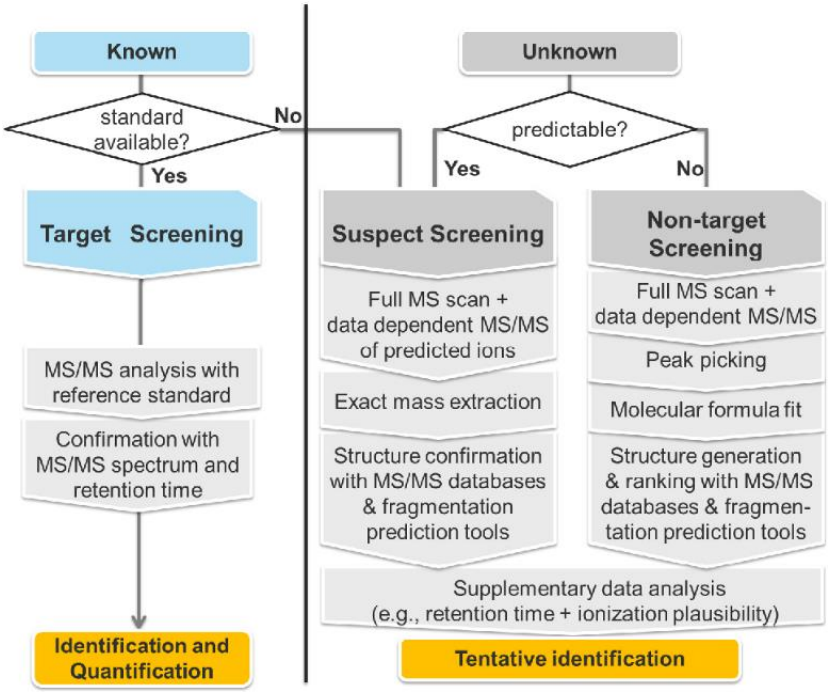

Figure 21. Flowchart of screening procedure in the MS for TP analysis. Reprinted from [149]. Copyright 2022 with permission from Elsevier.

The most common analyser is the **quadrupole**, in which four cylindrical metal rods are positioned parallel in a radial way (**figure 22**). Opposite rods are charged by a direct-current potential, at which an alternating-current (AC) potential in the radiofrequency region (RF) is superimposed. At a given current and radiofrequency value, only the ions of a particular *m/z* range are able to reach the detector, while others with unstable trajectories do not pass the mass filter. By changing current and RF in time, usually at a fixed ratio, ions with different *m/z* values can be transmitted to the detector one after another.

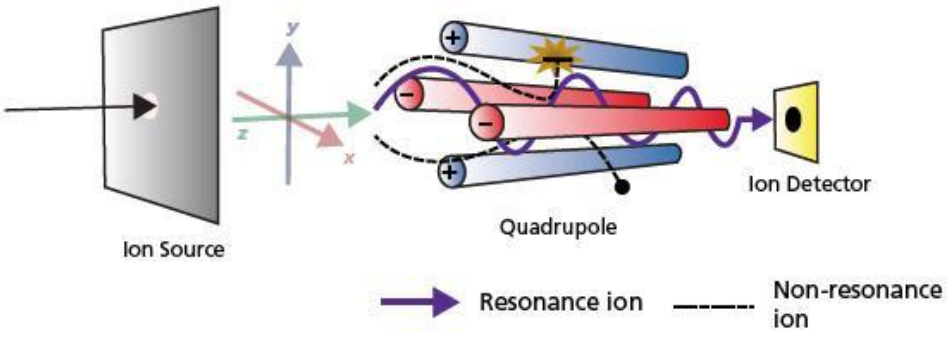

Figure 22. Quadrupole analyser scheme [150]

In tandem MS, two or more analysers are combined in series. By doing that, it is possible to investigate the fragmentation of selected ions, which is fundamental for the study of OMPs' degradation routes and TPs' detection and quantification [146]. In tandem MS, selected ions are further fragmented (after the first analyser) in a gas chamber positioned before the next analyser. The fragments collide with hot gases (generally He, Ar or N_2). For very fast collisions (10^{-15} s), the translational energy given to the fragments in this process is turned into internal energy, followed by ionic decomposition into smaller fragments. High-energy collisional dissociation, practiced mostly in higher-resolution analysers such as orbitrap and time-of-flight, allows the formation of even smaller fragments, which generates more informative and complex results [142].

The **Orbitrap** is a high-resolution tandem MS analyser**.** The ionic fragments rotate around an inner cylindrical electrode and perform axial oscillations due to an electrostatic field. Although the field does not allow a stable equilibrium of ionic particles, its trajectory and decay can be detected by surrounding electrodes [151]. The mass spectrum is generated by the detection of high frequency image currents. Fragments with the same *m/z* will rotate under the same

frequencies, with the *m/z* value being inversely proportional to the square of the frequency. Higher resolution power is obtained when longer measurement times are taken. In order to obtain the appropriate ionic fragment trajectory around the electrode, it is important to correctly deliver the fragments into the analyser. To do that, the orbitrap is generally preceded by a curved high-pressure quadrupole analyser capable of trapping ions (C-trap) which controls the number and *m/z* of ions entering the system; and a high-energy collision dissociation (HCD) cell, which generates even smaller fragments of the analyte's ions by increasing the collision energy (66 eV) [152], allowing the obtainment of more informative and complex data [15, 144, 147]. **Figure 23** shows a scheme of an orbitrap analyser.

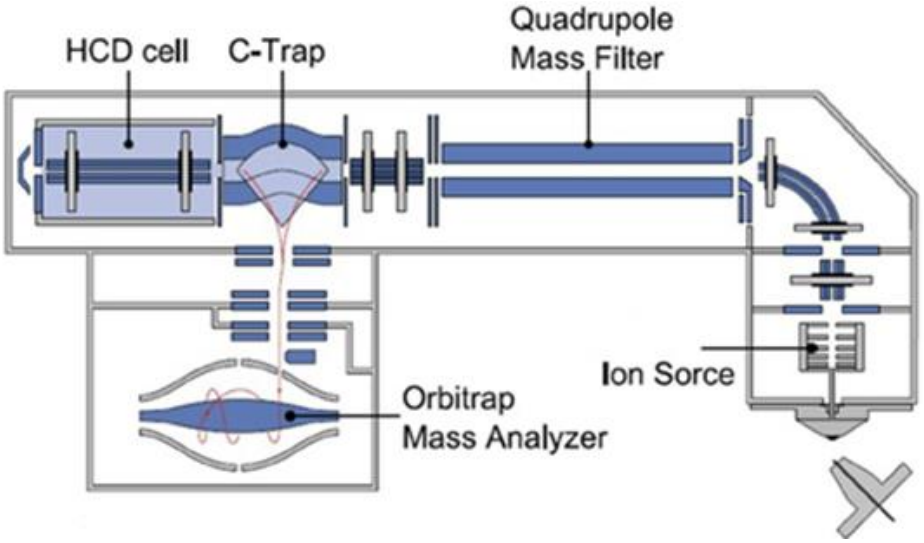

Figure 23. Scheme of an Orbitrap analyser [153]

2.8 Design of experiments

Design of experiments (DoE) is a statistically-robust approach that aims to empirically describe a phenomenon based on its dependent and independent variables. From a quadratic perspective, equation 29 [154] can describe a phenomenon with *n* independent variables (X_i) in which A_i are real numbers and *Y* is the dependent variable.

$$Y = \mathrm{A}_0 + \sum_{\mathrm{i}=1}^{\mathrm{n}} \mathrm{A}_\mathrm{i} X_i + \sum_{\mathrm{i}=1}^{\mathrm{n}} \sum_{\mathrm{j}=1}^{\mathrm{n}} \mathrm{A}_{\mathrm{ij}} X_\mathrm{i} X_\mathrm{j} + \sum_{\mathrm{i}=1}^{\mathrm{n}} \mathrm{A}_{\mathrm{ii}} {X_\mathrm{i}}^2 \quad (29)$$

In which X_i are coded variables between -1 (lower level) and +1 (higher level) obtained by simple linear regression. The independent variables and their range of study are arbitrarily chosen based on what the authors want to investigate. A **full factorial design** allows the simultaneous determination of the impact of multiple independent variables on a dependent one. A full factorial design requires experimental data of all possible combinations of independent variables in all their levels. For 3 variables and two levels (lower and higher), this demands $2^3 = 8$ experiments. **Figure 24** shows the list of necessary experiments of this design and its geometrical representation.

(a)

Experiment	Coded independent variables		
	A	B	C
1	1	1	1
2	1	1	-1
3	1	-1	1
4	1	-1	-1
5	-1	1	1
6	-1	1	-1
7	-1	-1	1
8	-1	-1	-1

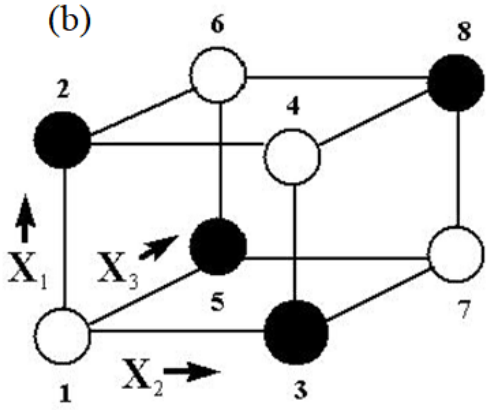

Figure 24. (a) List of necessary experiments for 2^3 full factorial design and (b) its geometrical representation

Each one of the obtained A_i coefficients represents the intensity of the effect of each independent variable (or their combination), as well as if the latter will increase (positive effect) or decrease (negative effect) the dependent output. A positive effect for combined variables means that either the simultaneous increase or decrease of both variables will increase the outcome of the dependent variable (because the result of multiplying two positive or two negative numbers is positive), while increasing one of the independent variable's coded values and reducing the other will result in a decrease of the outcome of the dependent variable (because the product of a positive and a negative number is negative). The Pareto chart shows all effects side by side. The effects beyond the *t*-value limit are considered significant by an **analysis of**

variance (ANOVA) with 95% of confidence and are included into the final model. The eeffects beyond the Bonferroni limit are strongly statistically significant, corrected for multiple testing [155].

When a more powerful method is necessary, the **Box-Behnken design** is an effective **response-surface methodology** design that considers non-linear (quadratic) models that are valid not only at the chosen range limits (as the full-factorial design) but also for the whole interval of the studied range. The number of necessary experiments to obtain an accurate model can be greatly reduced by a correct approach of DoE. A deeper discussion of the Box-Behken design and its application in chemometrics can be found in [156].

2.9 State-of-the-art and current challenges of TiO_2/UV-LED photocatalysis

TiO_2-based photocatalysis for water treatment generated a vast literature, with its efficacy in degrading OMPs being constantly demonstrated [110,154,157]. However, this academic interest is highly contrasted by the lack of real applications of this technology till this day. Loeb et al. [5] describe how the "hype" of photocatalysis in academia is caused by an overemphasis on material design and mechanistic evaluations that investigate the multiple process variables in bench-scale, often overestimating its potential and underestimating its limitations. According to the same authors, this led to a growing scepticism regarding photocatalysis and some question if this AOP will ever become a mainstream water treatment technology.

The main hurdle of photocatalysis is its low photonic efficiency. Energy can be lost in 5 different steps [5]:

1) in UV light sources, due to electrical-to-optical energy conversion (wall-plug efficiency);
2) absorption of photons prior to their reaching the catalyst's surface (e.g. non-optimal photoreactor design, screening effects, light absorption by other substances present in water);
3) catalytic sites being occupied by other compounds (e.g. organic matter, different OMPs) or reaching their light saturation limit;
4) charge carriers recombination;

5) ROS species attacking other substances prior to target compounds (e.g. radical scavengers, TPs, organic matter, other ROS).

Apart from that, both of the catalyst's mode of utilization (slurry vs immobilized, see **section 2.5.1.2**) have significant economic drawbacks (need of a separation step for the first, low catalyst surface area for the latter). The high sensitivity of photocatalysis to matrix composition and the many other variables that may influence the process also hampers the process adoption at large scale for a wide variety of scenarios [5, 6].

Nevertheless, the fast technological development of UV-LEDs and their unique features open up new horizons of possibilities for TiO_2-based photocatalysis for water treatment. The advantages of UV-LEDs against mercury lamps are many: UV-LEDs are mercury-free and built from durable ceramic materials, do not need warm-up period and have simple direct current power requirements - being able to operate on lower voltages than Hg lamps. UV-LEDs' dimensions can be approximated as point-source since they are on a scale of few millimetres. Their radiation patterns and wavelengths can be adjusted by fine-tuning their lens and p-n junction's composition according to process demands [7, 87].

There is a lack of data regarding TiO_2/UV-LED photocatalysis application in real scenarios [121]. Aside from the already mentioned intrinsic issues of photocatalysis itself, the factors that contribute to this lack are: 1) UV-LED is still an early-stage technology with limitations regarding its wall-plug efficiency, particularly for lower wavelengths (UV-C range) [87]; 2) the slow pace of adoption of stricter water quality regulations that demands the removal of CECs; 3) the lack of research taking advantage of unique LED features and exploring innovative photoreactor designs for water treatment due to the convenience of previously-established *know-how* based on UV mercury lamps [7]; and 4) analytical difficulties and instrument limitations when measuring degradation of OMPs in their real range of concentration in waterbodies (between ng/L and µg/L) for real matrices (e.g. tap water, river water, wastewater) [25, 158, 159].

Because of that, most of the UV-LED degradation studies found in literature in the past decade take place in small petri dishes (volume of reaction < 100 mL) illuminated from above [84, 121, 160], with no particular attention being paid to photoreactor design optimization. UV-LED photocatalysis's research is generally performed in very clean matrices (e.g. ultra-pure water) with a much-higher initial concentration of OMPs (mg/L) than the range commonly found

in nature. Another problem is the lack of research investigating simultaneous degradation of multiple substances in a mixture [121]. Although the author of this dissertation recognizes the value and contribution of these previous works, - especially considering this technology's early stages - it is paramount to investigate more complex scenarios to further understand the photocatalytic degradation of OMPs.

Controlled periodic illumination (CPI) is a unique feature of LEDs that allows them to be quickly turned on and off continuously (also known as "light flickering"). This is possible due to LEDs' lack of warm-up time. CPI can improve photocatalytic degradation by decreasing charge carrier recombination. The mechanism of CPI relies on the fact that the initial step of photocatalysis (generation of electron/hole pair, equation 15) is much faster than its sub sequential reactions (equations 16-22). The formation of the electron-hole pair is in the order of femtoseconds (10^{-15} s), while the other steps take nanoseconds to happen [161]. The initial (and faster) step is the only one that needs light to happen. Once the electron-hole pair is generated, ROS-based reactions can be performed in complete darkness. Being so, if the light is turned off while degradation happens, energy is saved.

To perform CPI, a control board containing a pulse-width modulation program is attached to the system. This program will control the electric current reaching the LEDs. For simplicity, the function often is the Heavisde step, but other designs are possible (e.g. linear or sinewaves) [162]. **Figure 25** shows an example of this function for different **duty cycles** (DCy). DCy is a value, between 0 and 1, defined as the time light is turned on divided by the whole period of the cycle, as described by equation 30. The period of the cycle will depend on each control board, but generally is in the order of milliseconds, and its value can also influence on kinetic rates [163].

$$\text{Duty cycle } (DCy) = \frac{t_{\text{lights on}}}{t_{\text{lights on}} + t_{\text{lights off}}} \tag{30}$$

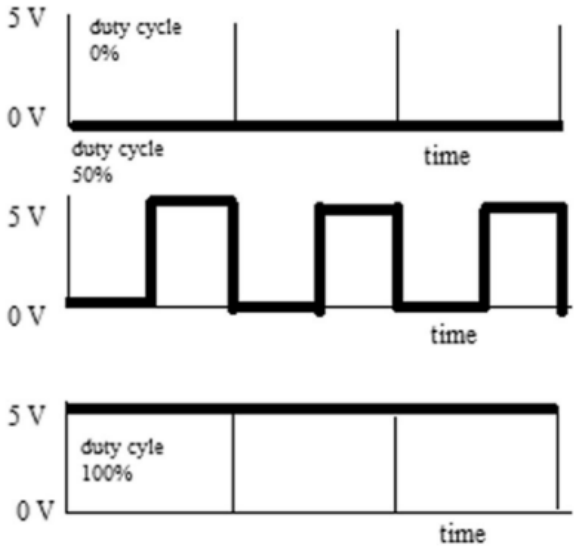

Figure 25. Pulse width modulation functions for duty cycles = 0, 0.5 and 1. Reprinted from [121]. Copyright 2022, with permission from Springer.

It is possible to classify the reaction steps in 3 different stages [164]:

1) *Light period:* from the moment light is turned on until it is turned off;
2) *Dark period I:* from the moment light is turned off until the last of the ROS species reacts with target pollutants or other matrix compounds;
3) *Dark period II:* from the end of dark period I until light is turned on again. No reaction happens.

To optimize CPI, it is important to adjust the DCy so that the dark period II's duration is as close to zero as possible [163]. CPI prevents the continuous introduction of photons, which would result in an excess of carrier charges and ROS at the catalyst vicinities. Although these are required for the desired photocatalytic reactions, their accumulation favours undesirable recombination and scavenging reactions resulting in lower degradation efficiency [161, 163].

Some examples of studies investigating the contributions of CPI to UV-LED photocatalysis [161, 163, 164] were performed in ultra-pure water and showing the benefit brought by this technique. To this author's knowledge prior to this dissertation, no studies were performed investigating CPI in realistic matrices.

Besides CPI, the greatest contribution of the advent of UV-LEDs to photocatalysis is the photoreactor design flexibility they allow. Due to their point-source character, LEDs can be

arranged in a multitude of arrays. This was unpractical using mercury lamps due to their traditional cylindrical shape. **Figure 26** shows two possibilities for UV-LED photoreactor design. The one above is based on Hg lamp design, while the one below is only possible using LEDs. However, as previously mentioned in this section, few studies investigate the impact of the photoreactor design on the degradation rate of OMPs [165–169].

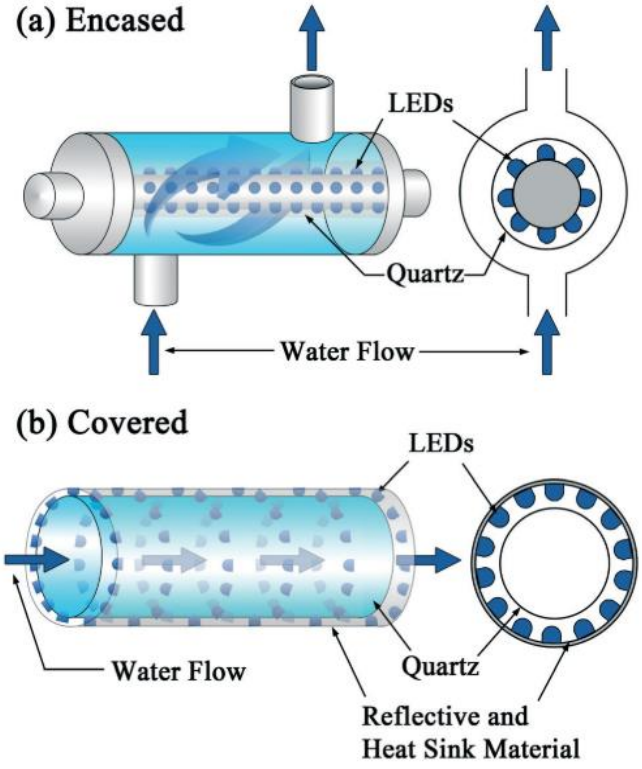

Figure 26. Two different possibilities of UV-LED photoreactor design for a cylindrical continuous-flow reactor. Reprinted from [7]. Copyright 2022, with permission from the Royal Society of Chemistry

The light distribution in LED-based reactors can be highly inhomogeneous if the position of the LEDs in the reactor is not carefully designed. The presence of dark and/or overly-lit areas (see **figure 12**) can result in non-optimal kinetic rates [125, 169, 170]. Ideally, light distribution around the reactor should be homogenous [169, 170]. The distance between the light source and the catalyst surface affects the incident radiation intensity and the catalyst area distribution. Shorter distances increase the radiation intensity (and, consequently, reaction rates) but decrease homogeneity. The studies [127] and [170] showed that the use of more LEDs increases both the light intensity and the homogeneity but requires more electricity.

Another advantage brought by LEDs to photoreactor design is the possibility to combine different wavelengths; since individual light sources can be specifically tailored, each reactor sector could be illuminated with a different wavelength. Shorter wavelengths (UV-C) have higher energy to break pollutants' molecules by photolysis, but longer wavelengths (UV-A) have higher penetrability in matrices due to their lower absorbance coefficient [129, 130]. It is speculated that their combined use in different sectors can have beneficial effects [110].

Additionally, simultaneous emission of different wavelengths allows **wavelength coupling** to happen. This is a wave interference phenomenon that takes place when emission sources of nearby wavelengths are used together, amplifying the intensity of waves of values in-between. Some studies have demonstrated the efficiency of wavelength coupling for disinfection [171, 172].

Regarding energy consumption, a literature review made by the author demonstrated that - in the few cases in which comparisons of E_{EO} values can be drawn between UV-LEDs and traditional mercury lamps - their performances are similar [121]. Projections for the future of UV-LEDs' are optimistic and envisage WPE values of 10 to 20 times higher than current ones for the next 4 years, especially for lower wavelengths (UV-C) [173]. Those improvements have a direct impact on the technology's feasibility and overall costs.

Despite that, it was shown previously (**figure 8**) how photocatalysis ranks low among AOPs on energy performance due to its low photonic efficiency. Other processes such as ozonation and UV/H_2O_2 have a much better performance in most scenarios. However, instead of being abandoned, photocatalysis' development should target niche-specific goals [5]. Unlike other AOPs, it can form h^+ species (equation 21) that are capable of alternative routes of degradation. Photocatalysis' capacity of running on solar light only and its lack of need for additional chemicals could also prove to be useful in isolated regions where transportation of chemicals such as O_2 and H_2O_2 is unmanageable and electrical energy is not promply available [5].

Lab-scale planar and cylindrical photoreactor geometries are the vast majority of the available designs due to by the early stage of this technology, but also for the need for short distances between the catalyst surface and the bulk of the solution for mass transport reasons. Long cylindrical reactors with small diameters allow the light to permeate at high intensity and

homogeneity levels across the entire reaction volume. UV-LED photocatalysis could be better operated in small-scale point-of-use applications. LEDs, in fact, are more suitable than traditional UV lamps since the latter tend to be larger, less flexible and require a higher voltage driver [7, 87, 166].

As it was explained through this general part, there is large number of variables influencing pollutant kinetic rates, energy consumption and effluent's toxicity for photolytic and photocatalytic water treatment. Design of experiments can be a powerful tool towards finding optimal conditions for this process. Chemometrics optimization strategies, such as full-factorial design and response surface methodologies, can be adopted to reduce the number of necessary experiments in the lab and provide empirical models to predict important process-related outcomes [174, 175].

The multiple reaction routes of photocatalysis (**figure 10**) open various pathways that allow the formation of many TPs, including substances which are more toxic than their respective parent compounds. This is another major concern involving photocatalysis and advanced oxidation processes in general. A vast literature focuses on the determination of these TPs [176–179], the variables that affect their formation [30, 180–182] and their potential toxicity [33, 183–186]. However, more data is still necessary due to the large number of substances in real water matrices.

A possible application of UV-LED photocatalysis in the near future could be in domestic residences as final treatment step of reclaimed water reuse, or even for drinking water purpose [5, 7]. In fact, as water would have already gone through previous treatments, the presence of NOM would be small, and the photocatalytic degradation of persistent OMPs would be particularly efficient [121].

3. EXPERIMENTAL PART

3.1 Materials

3.1.1 Chemicals

Table 2 shows the list of chemicals used for the present work.

Table 2. List of Chemicals

Substance	CAS number	Purity	Supplied by
Target OMPs			
Ciprofloxacin	85721-33-1	>98%	Sigma-Aldrich, St. Louis, MO, USA
Sulfamethoxazole	723-46-6	>98%	Sigma-Aldrich, St. Louis, MO, USA
Trimethoprim	738-70-5	>98%	Sigma-Aldrich, St. Louis, MO, USA
Venlafaxine	99300-78-4	>98%	Tokyo Chem. Industry Co., Tokyo, Japan
O-Desmethylvenlafaxine	93413-62-8	>98%	Tokyo Chem. Industry Co., Tokyo, Japan
Chromatographic analysis			
Methanol	67-56-1	HPLC	Fisher Scientific UK LTD
Acetonitrile	75-05-08	HPLC	J. T. Baker, Deventer, Netherlands
Formic acid	64-18-6	p.a.	Lach-Ner, Zagreb, Croatia
Nanofilm preparation			
Titanium isopropoxide	546-68-9	>97%	Sigma-Aldrich, St. Louis, USA
Acetylacetone	123-54-6	>98%	Sigma-Aldrich, St. Louis, USA
Nitric acid	7697-37-2	p.a.	Sigma-Aldrich, St. Louis, USA
Isopropanol	67-63-0	HPLC	Fisher Scientific UK LTD
Water matrix compounds			
Humic acids	1415-95-6	p.a.	Sigma-Aldrich, St. Louis, USA
Sodium nitrate	7631-99-4	p.a.	Kemika, Zagreb, Croatia
Sodium bicarbonate	144-55-8	p.a.	Kemika, Zagreb, Croatia
Scavengers			
Ammonium oxalate	6009-70-7	p.a.	Kemika, Zagreb, Croatia
Triethanolamine	102-71-6	p.a.	Carlos Erba Reagents, Milan, Italy
Isopropanol	67-63-0	HPLC	Fisher Scientific UK LTD
Toxicity analysis			
Lyophilized bacteria (LCK 484)			Hach Lange, Dusseldorf, Germany
Sodium chloride	7647-14-5	p.a.	Kemika, Zagreb, Croatia
Other			
Hydrogen peroxide	7722-84-1	p.a.	Kemika, Zagreb, Croatia
Sodium hydroxide	1310-73-2	p.a.	Kemika, Zagreb, Croatia
Hydrochloric acid	7647-01-0	>98%	Kemika, Zagreb, Croatia

3.1.2 Water matrices

The photolytic and photocatalytic degradation of the target pollutants were investigated in tap water. MQ water (pH = 5.8) was prepared by the Millipore Simplicity UV-system (Millipore Corporation, Billerica, USA). Tap water was sampled at the laboratory faucet at the Faculty of Chemical Engineering and Technology, University of Zagreb and at ICRA – Catalan Institute for Water Research, in Girona (Spain). Prior to the sampling, the faucet was turned on and left to run at a uniform rate to flush standing water from the service pipes (2 min to 3 min). Tap water was analysed for pH, total organic carbon, and inorganic ion content. **Table 3 s**hows the composition of tap water samples.

Table 3. Composition of tap water from Zagreb and Girona (both pH = 7.4)

Ions	**Zagreb (mg/L)**	**Girona (mg/L)**
HCO_3^-	400	180
Cl^-	25	28
SO_4^{2-}	21	16
Br^-	<0.020	<0.010
NO_3^-	15	0.59
NO_2^-	<0.020	<0.003
PO_4^{3-}	<0.040	<0.008
Na^+	13	21
NH_4^+	<0.042	<0.004
Mg^{2+}	21	11
Ca^{2+}	95	57
TOC	<0.5	1.5

3.2. Instruments

The following instruments were used for the experimental work:

- Analytical balances: XS204 Delta Range (Mettler Toledo 15, Greifensee, Switzerland); Kern ABJ-NM/ABS-N (Kern & Sohn, GmBH, Stuttgart, Germany)
- Millipore Simplicity UV-system (Millipore Corporation, Billerica, USA)
- Milli-Q Advantage A10 Water purification system (Merck KGaA, Darmstadt, Germany)
- pH-meters: Mettler Toledo (Greifensee, Switzerland); GLP21+ (Crison Instruments, Barcelona, Spain)
- Luminometer LUMIStox 300 (Hach-Lange, Germany)
- TOC analyzer, type TOC-VCPH, Shimadzu Co. (Kyoto, Japan)
- Ion chromatograph: ICS 3000, Dionex (Sunnyvale, California, USA); Dionex ICS5000 (Thermofisher Scientific, Waltham, Massachussets, USA)
- High performance liquid chromatograph with photo diode detector (HPLC-PDA)
- High performance liquid chromatograph with high resolution mass spectrometer Orbitrap (LC-MS)
- Photoreactor

3.2.1 Photoreactor design

Two identical cylindrical quartz lab-scale reaction vessels with an inner diameter of 37 mm, length = 150 mm and wall thickness = 1.5 mm were adopted. In one of them, nanostructured TiO_2 film was immobilized on its inner side wall by sol-gel method and dip-coating technique [108, 187]. A schematic drawing of the experimental set-up is shown in **figure 27**.

Sections of the UV-LED strip were attached as vertical columns on cylindrical supports of diameter = 60 mm and 70 mm. Each column had 125 mm of height. UV-A LED columns contained 15 LED sources, spaced vertically by 8.3 mm, while each UV-C LED column contained 8 LED sources, spaced vertically by 16.6 mm (see **table 4**). Each column could be

easily (dis)attached to the system, so at any moment it is possible to decide how many UV-C and UV-A strips are illuminating the reaction solution. Four cylindrical LED supports were made, two of which had 6 LED columns (#LED = 6) and the other two with #LED = 4. The light sources were all facing towards the cylinder's central axis and their distribution was radially symmetric, with intervals of 60° and 90° for structures with #LED = 6 and 4, respectively. For degradation tests, each photoreactor (with or without the TiO_2 nanofilm) was placed concentrically with the LEDs support. Distance between the photoreactor's wall and LEDs (D_w) varied (10 or 15 mm) according to the diameter of the support. The output power of the system was measured by the + UT230B power meter by UNI-Trend Technology (Dongguan, China).

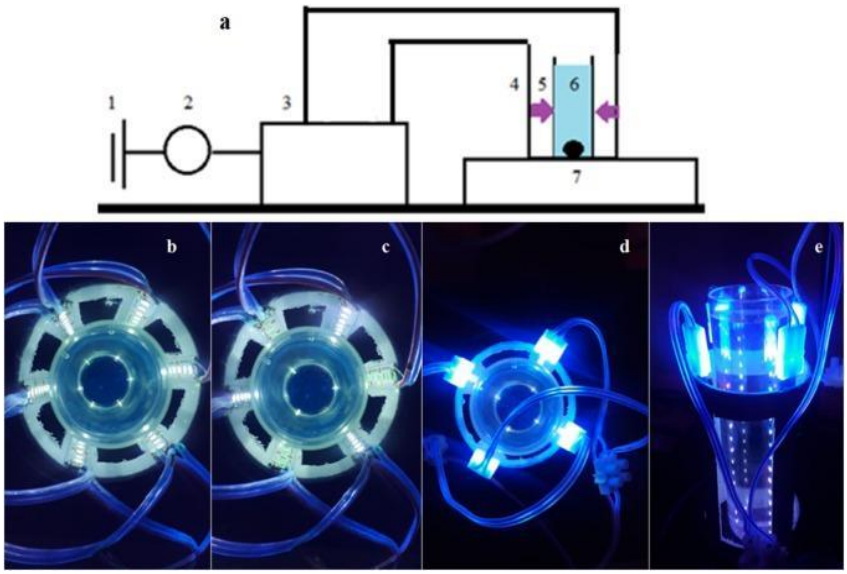

Figure 27. Experimental setup. (a) 1 - energy source, 2 - power meter, 3 - LED control board, 4 - LED columns, 5 - UV rays reaching the reactor, 6 – reactor, and 7 - magnetic stirrer. Below, upview of (b) arrays #LED = 6, D_W = 15 mm; (c) #LED = 3, D_W = 15 mm, (d) #LED = 4, D_W = 10 mm; (e) side view of #LED = 4, D_W = 10 mm [166]

Commercially available UV-LED strips in the UV-A range (365 nm) and UV-C range (272 nm) were provided by Waveform Lighting (Vancouver, USA). Photometric specifications, emission spectrum, dimensions, and other data are available in the product's specification datasheet [188–190], and summarized in **Table 4. Figure 28** shows LED strips in detail.

Table 4. UV-LED strips specifications [189, 189]

LED specification	Values	
	UV-A	UV-C
UV output per lamp	20 mW	2.5 mW
Emission angle	120°	120°
Input voltage	12 V	12 V
LED spacing	8.3 mm	16.6 mm
Wavelength	365 nm	272 nm
Spectrum FWHM	10 nm	10 nm
LED sources per strip	15	8

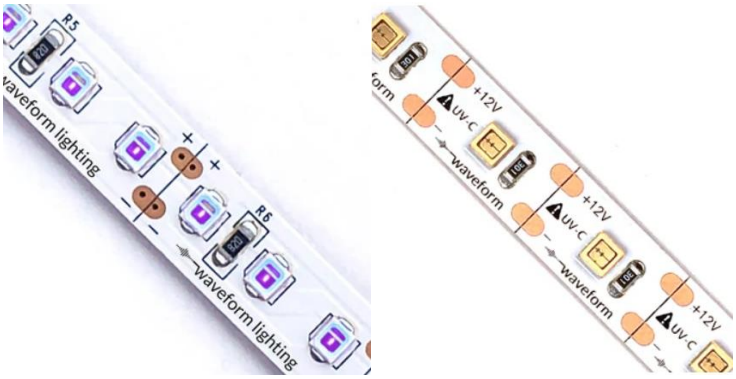

Figure 28. UV-LED strips in detail (left, UV-A; right: UV-C) [187, 188]

The LED strips were connected to an Arduino Pro Mini microcontroller coupled with IRFZ44 N MOS- FETs, shown in **figure 29**. Arduino's Pulse Width Modulation frequency is 490 Hz [191]. The ARDUINO control board enables to turn on all LED columns simultaneously or half of them, as shown in **figure 27 b–e**. Using pulse-width modulation (PWM) script on the Arduino it was possible to control the DCy of the LEDs.

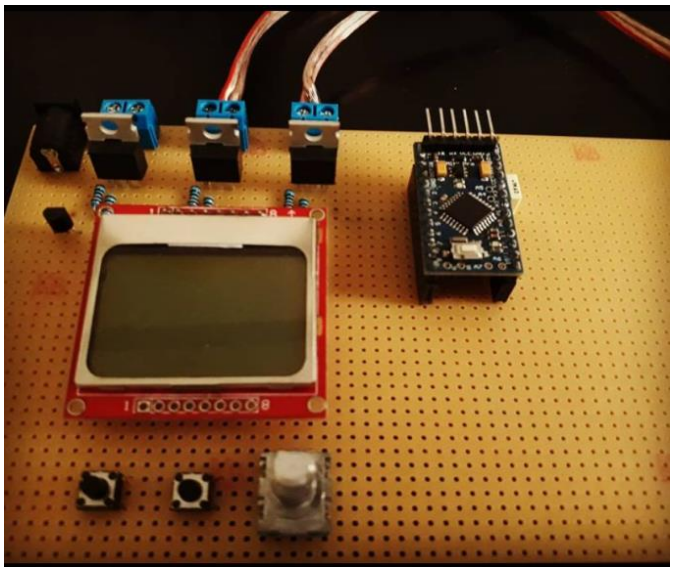

Figure 29. ARDUINO control board

3.2.2. Determination of target pollutants via HPLC

Samples were directly analyzed by HPLC-PDA shown on **figure 30** (Waters 2795 Alliance HPLC System with 2996 PDA-Detector, Waters, Milford, Massachusetts). The instrument consists of a photo diode array detector, a vacuum degasser, a quaternary pump and a thermostated chromatographic column unit. The separation was carried out on the Kinetex C18 column (150 mm x 4.6 mm, 5 μm, 100 Å, Phenomenex).

Figure 30. Waters 2795 Alliance HPLC system with 2996 PDA detector

3.2.3. High resolution mass spectrometer - Orbitrap

Samples were directly analyzed by LC-MS Orbitrap shown on **figure 31** (Orbitrap Exploris 120, Thermo Fisher Scientific, Massachusetts, USA). The instrument consists of a quadrupole-orbitrap analyser with a Q-trap for high-resolution accurate mass capability. The ion source is heated-electrospray ionization. The separation was carried out on the Hypersil gold column (50 mm x 2 mm, particle size 1.9 μm, Thermo Scientific).

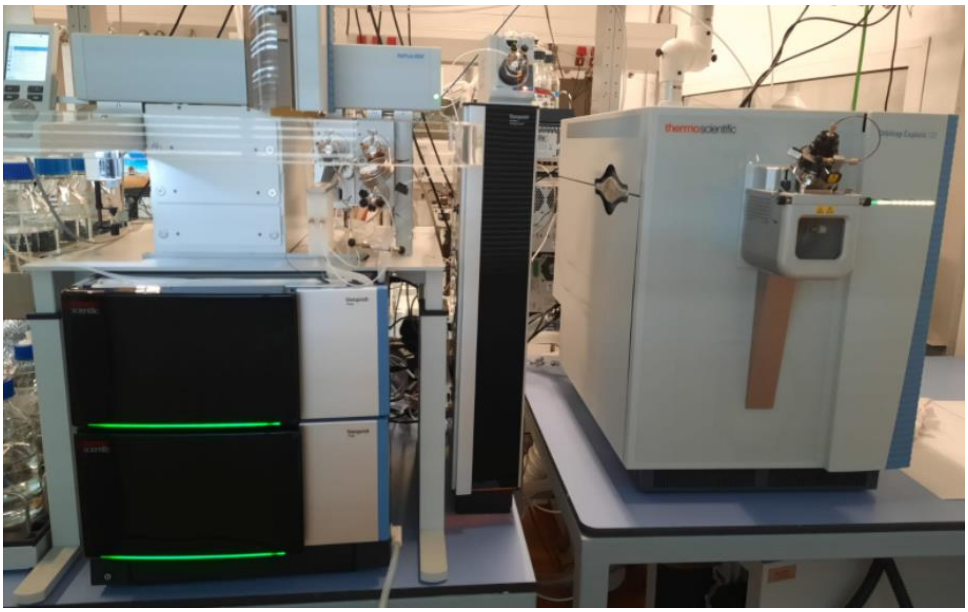

Figure 31. LC-MS Orbitrap Exploris 120

3.2.4. Luminometer

Vibrio Fischeri bioluminescence measurements were performed on a LUMIStox 300 Hach Lange instrument (Dusseldorf, Germany) with a thermostated LUMIStherm block for incubation of bacteria. All measurements were performed at a temperature of (15 ± 1) °C.

3.2.5 Softwares

The simulation of light behaviour inside the photoreactor was performed with the professional version of the OpticStudio® - an optic, laser and illumination design software provided by Zemax (Seattle, USA). The software is capable of simulating all relevant light phenomena like absorption, reflection and refraction in the media of air, quartz glass and water.

The design of experiments analysis was performed by the software Design Expert 12, provided by StatEase® (Minneapolis, USA). The software is capable of performing multiple types of DoE, providing ANOVA analysis and surface graphs.

The softwares Masslynx 4.1 (Waters, MA, USA) and Compound Discoverer 3.3 (Thermo Fisher, MA, USA) were used for HPLC-PDA and LC-MS data analysis, respectively.

3.3 Methods

3.3.1. Preparation of standard solutions

The CIP solution had a γ_0 of 10 mg/L and was freshly prepared in MQ water prior to each experiment. The compound was weighted on an analytical balance. The solution was sonicated for 45 minutes until complete dilution. The same procedure was followed to prepare the pharmaceutical mix solution, which had a γ_0 of 2 mg/L for each one of the 5 target compounds (CIP, SMX, TMP, VEN and DV). The pharmaceutical mix solution was prepared both in MQ and tap water from Zagreb. For TP analysis, individual solutions for all 5 OMPs of γ_0 of 10 mg/L were prepared in MQ and tap water from Girona.

Sodium bicarbonate ($NaHCO_3$), sodium nitrate ($NaNO_3$) and/or humic acids (HA) were added to the pharmaceutical mix solution to investigate the effects of these compounds on OMPs degradation. After their addition, the solution was kept in the dark under constant magnetic stirring for 30 minutes until complete dilution of the added compounds prior to the start of the degradation experiments.

The impact of initial pH on the simultaneous degradation of the 5 target pharmaceuticals in MQ water (γ_0 of each = 2 mg/L) by UV-A photocatalysis was investigated in MQ water. Initial pH values of 5.0, 7.0 and 9.0 were obtained by drops of NaOH or HCl added to the initial solution and measured by the pH-meter.

To investigate the degradation mechanisms by UV-A photocatalysis, 3 experiments with different radical scavengers were performed in MQ water. Isopropanol (ISOP), triethanolamine (TEA), and ammonium oxalate (AOX) were adopted as scavengers of hydroxyl radicals ($^{\bullet}OH$), superoxide radicals ($^{\bullet}O_2^-$), and positive holes (h^+), respectively [50, 192, 193]. Each of the 3 experiments were performed with a scavenger/total pharmaceuticals mass ratio of 100/1 (γ_0 of each scavenger = 1 g/L).

3.3.2. Preparation and immobilization of TiO_2 film

A colloidal TiO_2 solution (sol) was prepared by dissolving titanium isopropoxide (TIP) in isopropanol. A magnetic stirrer was used to continuously stir the liquid. Then, acetylacetone and nitric acid were added successively. The solution was stirred vigorously for 2 h and after that it was sonicated for 30 min. The molar ratio of these reactants was: TIP:PrOH:AcAc:HN = 1:35:0.63:0.015. The solution was poured into the cylindrical reactor, kept there for 10 min, and slowly poured out of them. The film was dried at 100 ℃ for 1 h prior to the deposition of the next layer. After the deposition of three layers, the films were annealed at 550 ℃ for 4 h. This nanofilm and its characterization were obtained following the method developed and described in detail by [10, 187].

3.3.3 HPLC methods

For the quantitative determination of the target pollutants in the solutions after photolytic and photocatalytic experiments, chromatographic methods were developed using high-performance liquid chromatography coupled to photodiode array detection (HPLC-PDA)**.** The mobile phase was composed of 0.1% formic acid in MQ water (A) and 0.1% formic acid in acetonitrile (B). The flow rate was 1.0 mL min^{-1}. The column temperature was 20 °C. The injection volume for each sample was 20 μL.

For the solutions containing only CIP as target pollutant, the elution method was isocratic (method 1) with a volume proportion A:B = 87:13. The retention time t_r for CIP was 7 minutes. The total elution time of the method was 8.5 minute. CIP peak was detected at the wavelength of 278.8 nm.

For the solutions containing the pharmaceuticals mixture (CIP, SMX, TMP, VEN and DV), a method with gradient elution was developed (method 2). The initial volume proportion of eluents A:B was 89:11 (v/v) until t = 13.5 min. From that point until t = 15.0, linear gradient elution was applied and the proportion of A:B = 83:17 (v/v) was achieved, which was kept

constant until t = 25 min. At this point, the mobile phase composition had a step change back to the initial one (11% B) until the end of elution, at t = 28 min. CIP, TMP, SMX, VEN, and DV peaks were detected at the wavelength of 278.8 nm, 273.8 nm, 269.8 nm, 274.8 nm, and 274.8 nm, respectively. The retention time of each compound (in minutes) was 11.3 (CIP), 6.3 (TMP), 19.4 (SMX), 23.0 (VEN), and 9.6 (DV).

To determine the concentration of each compound during degradation, linear calibration curves were obtained with $R^2 > 0.995$ between 10 mg/L and 1 mg/L for method 1 and between 2 mg/L and 0.2 mg/L for method 2. The Mass Lynx software provides the peak area A for each target pollutant at its chosen wavelength, so the relative concentration γ/γ_0 at a time of reaction t can be obtained according to equation 31:

$$\frac{\gamma}{\gamma_{0_{(t)}}} = \frac{A_{(t)}}{A_{t=0}} \tag{31}$$

3.3.4. Transformation product analysis

TP analysis for degradation of individual OMP solutions (see **section 3.3.1**) was carried out. UV-C photolysis in MQ water and UV-A photocatalysis in both MQ and tap water from Girona (**table 3**) were investigated. Experiments lasted between 210 and 360 minutes, depending on the target pollutant. Samples were analysed by the LC-MS Orbitrap. A gradient chromatographic method using MQ water (A) in methanol (B) was developed. Initially, the volume proportion of A:B was 98:2 until t = 4.75 min, when a linear gradient elution was applied. The proportion 2:98 was obtained at t = 6 minutes and kept constant until t = 9 minutes. At this point, the composition had a step change back to the initial one (2% B) until the end of elution (t = 12 min). Prior to analysis, samples were diluted 50x in MQ water and filtered with a PVDF syringe filter 0.22 μm.

The Compound Discovery Software was used in both full-scan mode with an *m/z* range from 100 to 1000 and selected-ion monitoring in the positive polarity. The Orbitrap resolution was 6000 for MS and 15000 for MS^2. Besides that, a literature review on the topic was made to list the most common previously-obtained TPs for all the target pollutants in both photolytic and

photocatalytic routes [33, 35, 49, 54, 107, 186, 194–200]. According to the scheme proposed by [201], the structures of possible TPs were suggested. If the software was able to identify a compound based on its database in full-scan mode (comparing MS^2 data), the TP was considered a "probable structure" (**figure 32**).

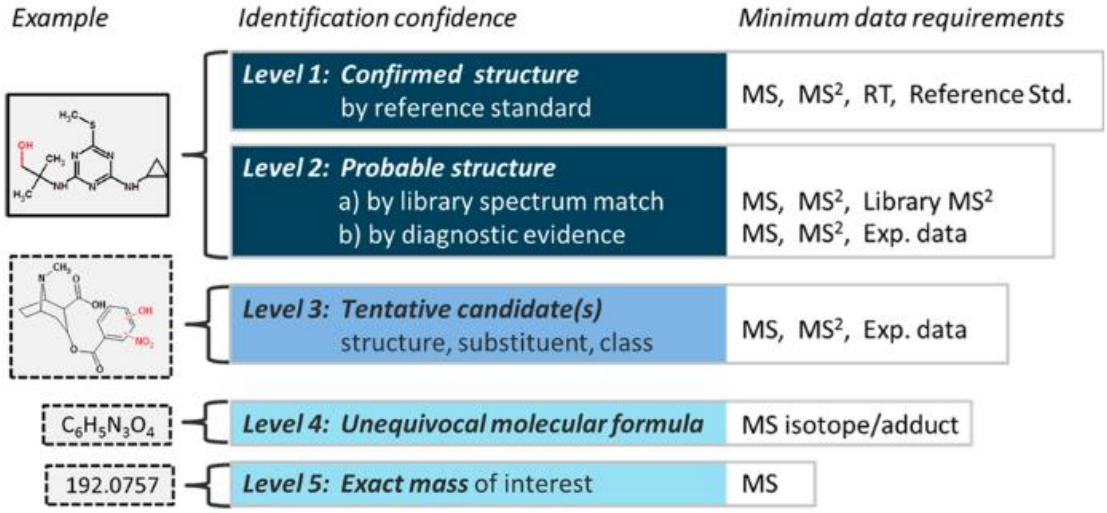

Figure 32. Proposed identification confidence levels in high resolution mass spectrometric analysis. Reprinted from [201]. Copyright 2022, with permission from the American Chemistry Society.

If the software could not find any correspondent structure in its database to a molecular formula which was previously obtained in the literature and detected in the samples in the ion-selected mode, the TP was considered a "tentative candidate". The level of confidence of the first type is higher than the latter.

3.3.5 Toxicity and total organic carbon analysis

Toxicity and TOC analysis were performed for initial solutions containing target pollutants and after degradation experiments were finalised. An attempt of correlation between proposed TPs and the solution's toxicity, matrix and treatment was also made.

TOC analysis was performed using a TOC analyzer, type TOC-VCPH, Shimadzu Co. The equipment performs a wet chemical oxidation, which uses a combination of UV irradiation and

persulfate for oxidation. All carbon in the sample is oxidized to CO_2, which is then measured by a non-dispersive infra-red detector.

Toxicity tests were performed according to standard bioluminescent method described in ISO 11348-3:2007 standard with fresh *Vibrio fischeri* bacteria. A culture of fresh bacterium was prepared from the lyophilized bacteria on a microbial growth medium, which was then used for further measurements. Luminescence was monitored initially and after 30 min as a parameter indicating toxicity or inhibition. The percentage of inhibition was determined by comparing the luminescence of the pure bacterial inoculum with the luminescence of the bacterial inoculum after 30 min of incubation from the addition of the sample. All measurements were performed at an instrument operating temperature of 15 ± 1 °C. The pH-value of the resuspension solution and 2% NaCl solution used was adjusted to 7.0 ± 0.2 to avoid a negative effect of pH on bacterial luminescence. The adjustment was made by adding sodium hydroxide or hydrochloric acid and measuring the pH-value with the pH meter. The geometric sequence with 2% NaCl solution was used to prepare the dilutions and measurements.

3.3.6. Photoreactor design: light profile simulation

The simulation of light behaviour inside the photoreactor was performed with the professional version of the OpticStudio® software. Each LED was configured following the specifications in the UV-LED strip datasheet (**table 4**) and considered as a point-source. Simulations using UV-C rays were not possible because the software did not have absorption spectrum information for lower wavelengths in its library. The side and up views of the simulation of one LED strip with its rays passing through the photoreactor is shown on **figure 33**.

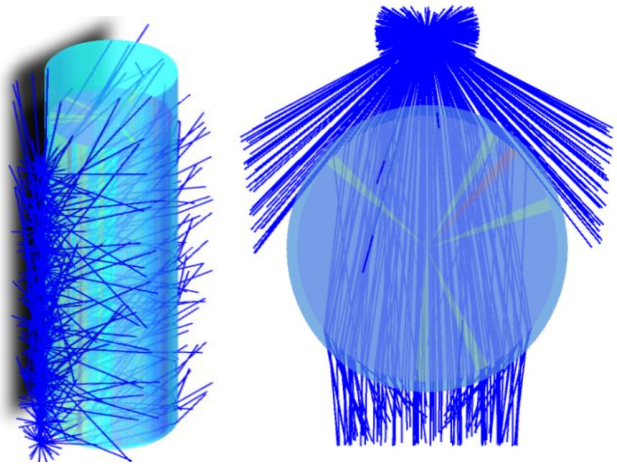

Figure 33. Side and up views of the simulation of one LED strip with its rays passing through the photoreactor

The eight different UV-LED arrays analysed are shown in **figure 34**. For the material inside the reactor, the properties of seawater were chosen in the software library as the one that approached the target-pollutants solution the most.

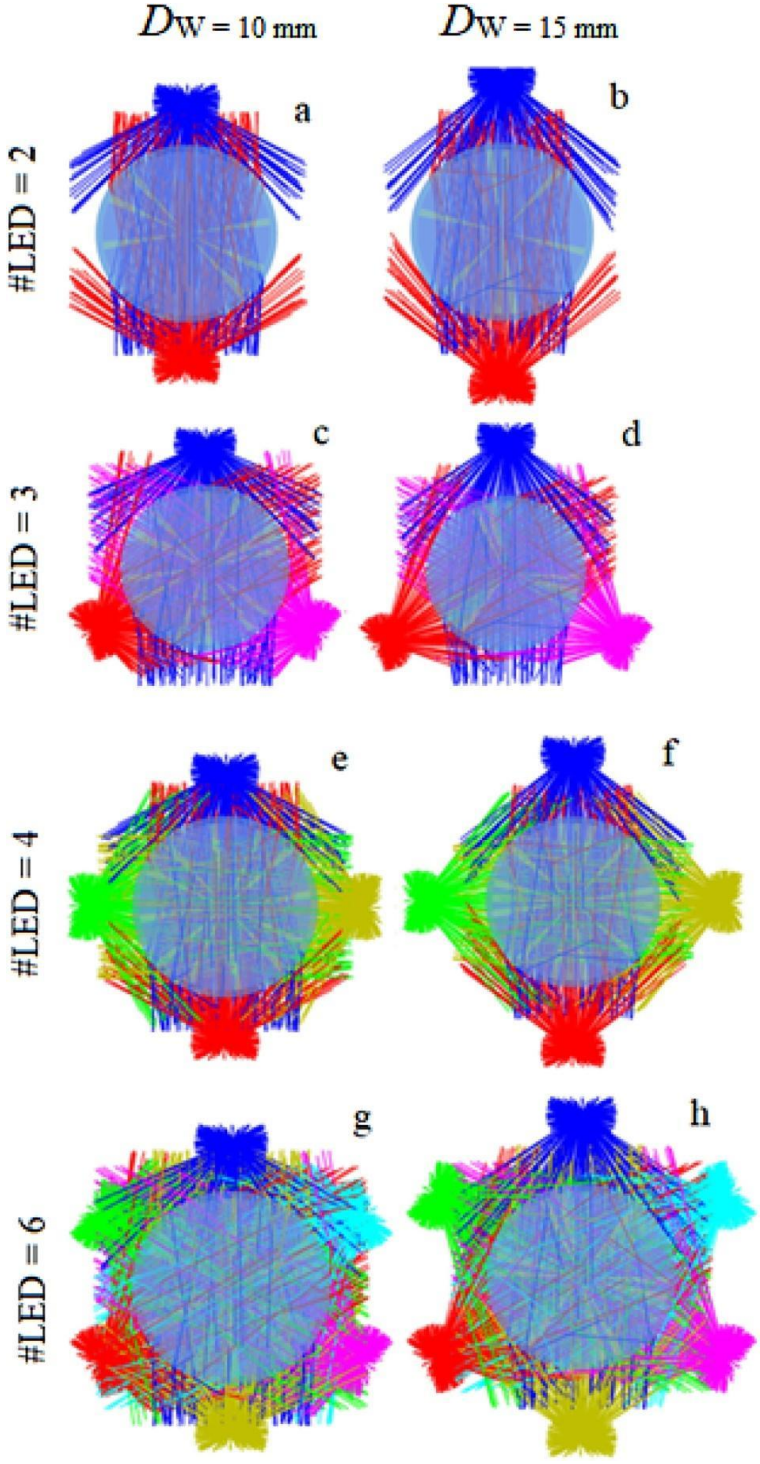

Figure 34. Photoreactor arrays tested, viewed from above [166]

In the simulation, each point-source emitted 10^6 rays for analysis. For irradiance evaluation, the software tool "detector" was used to put 2D rectangular invisible detectors on the

reactor's wall (positioned between the quartz glass and the water media) with the same height as the average water level during the experiments (13 cm) and with an insignificant width (0.1 mm). The first detector was positioned tangent to the circumference of the reactor, facing a LED column directly. Other detectors were put at intervals of 15°, always tangent to the reactor's circumference, until completing it. Each detector provided 200 pixels irradiance data along the cylinder's height. Planar projections of the photoreactor's irradiance behaviour were created by transferring the data of each one of the 24 detectors (example on **figure 35**) to Microsoft's Excel and formatting cell's values with colour scales. For radiant flux evaluation, the integrity of the photoreactor was put inside an invisible cuboid detector which gave the light profile of the reactor's cross sections. As object of analysis, the cross section was placed at height of 6.5cm (approximated as "middle cross section"). Both X and Y axis of the detector's image provided by the software had 250 pixels of radiant flux data, each.

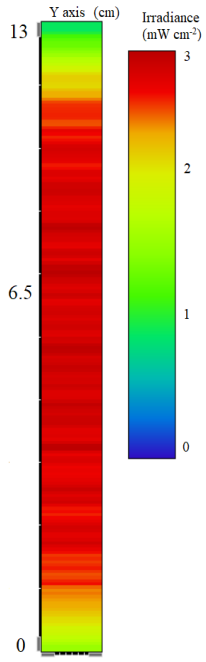

Figure 35. Example of irradiance detector output given by the OpticStudio software

3.3.7. Photolytic and photocatalytic degradation of pharmaceuticals

All experiments were performed in a dark room. Initial volume of the reaction solution was 150 mL for all the experiments. The total illumination time for each degradation test was 60 min, and 1 mL samples to HPLC-PDA analysis were collected in duplicate at fixed intervals of 0, 7, 15, 25, 35, 45 and 60 min of illumination time. When the DCy of the experiments was different from 1.00, the total experiment duration and the sampling interval were adjusted accordingly to maintain the same illumination time for each sample point. Experiments using DCy = 0.50 lasted for 120 min while those using DCy = 0.75 lasted 80 min. Only UV-A LED strips were used for this kind of experiments.

In order to investigate the effects of different variables and their significance on the pharmaceuticals degradation, three designs of experiments were prepared and analysed:

1. DoE #1 - a full-factorial categorical design with 2 levels (representing the number of points evaluated inside the tested range. For 2 levels, experiments were performed only for minimum and maximum value of the selected range) investigating the impact of 4 different variables (presence of catalyst; use of CPI; number of LED columns around the reactor and their distance to the reactor walls) on the degradation of CIP
2. DoE #2 – a full-factorial categorical design with 2 levels investigating the impact of 4 different variables on the simultaneous degradation of CIP, SMX, TMP, VEN and DV
3. DoE #3 - a randomized response-surface Box-Benhken design with 3 independent variables on 3 levels to investigate the effect of matrix components on the simultaneous degradation of CIP, SMX, TMP, VEN and DV.

For DoE #2 and #3, the array c from **figure 34** was the selected photoreactor design. The experiments were performed using reactors with and without TiO_2 and both UV-A or UV-C LEDs used alternately. **Table 5** shows the acronyms applied in each of the processes.

Table 5. Applied acronym: P, A = photolysis, UV-A; P, C = photolysis, UV-C; PC, A = photocatalysis, UV-A; PC, C= photocatalysis, UV-C.

LED wavelength	TiO_2 nanofilm	
	NO	YES
UV-A	P, A	PC, A
UV-C	P, C	PC, C

To evaluate the influence of H_2O_2 addition in the simultaneous degradation of target pollutants, the 4 processes from **table 5** were repeated using the initial solution containing all OMPs, and the addition of H_2O_2 (0.1 mM).

To evaluate the formation of TPs under different circumstances, the array c was used for both UV-C photolysis and UV-A photocatalysis. Exceptionally, reaction time for these cases was longer than 60 minutes (see **section 3.3.4**).

3.3.7.1. Preliminary tests, assumptions, calculations and approximations

a) Hydrolysis, reactivity with peroxide and adsorption

Preliminary experiments were performed to check the degradation of all the target pollutants by hydrolysis, hydrogen peroxide and losses due to adsorption on TiO_2 under the experimental conditions. For the hydrolytic degradation test, solutions of an initial analytes' concentrations (γ_0 = 2 mg/L) were collected in duplicate daily for a week while being kept in a dark room at room temperature. For the peroxide experiments, 0.1 mM of H_2O_2 was added to the same mixture solution at the same initial concentration (γ_0 = 2 mg/L) and kept it under dark conditions for 3 h. For the adsorption experiments, the same solution was placed in the photoreactors with and without TiO_2 nanofilm during 2 h and further analysed by HPLC. No decrease in analytes concentrations was observed during any of the experiments.

b) Temperature

The initial temperature of the solution in the reactor was 21 °C for all the experiments. In UV-A LEDs experiments only, a small table-fan was added to the experimental set up (**figure 27**) and placed to reduce the solution temperature increase that was between 1.5 and 2.5 °C by the end of the experiments. Although it is well known that temperature affects reaction kinetics [173, 202], this interval was assumed to be small for practical purposes and further calculations and analysis assumed process conditions as isothermal. Works investigating the temperature impact on photocatalytic performance generally work with a minimum 10 °C of difference between experiments [165, 203, 204] and are not the focus of this study. For experiments performed with UV-C LEDs, it was necessary to add the small table-fan to keep the temperature constant, since it is known that LEDs of lower wavelengths are more prone to cause overheat [7].

c) Reaction rate constants calculation

When photolysis and photocatalysis are the only source of degradation of a target pollutant, its concentration (γ) can be determined by the mass balance of equation 32:

$$-\frac{\mathrm{d}\gamma}{\mathrm{dt}} = k_p \cdot \gamma + k_{pc} \cdot \gamma \tag{32}$$

In which k_p and k_{pc} are the degradation rate constants for photolysis and photocatalysis, respectively. By integrating this equation in time, we obtain equation 33.

$$-\mathrm{Ln}\frac{\gamma_{(t)}}{\gamma_0} = \left(k_\mathrm{p} + k_\mathrm{pc}\right) \cdot t \tag{33}$$

The sum of k_p and k_{pc} is defined as the apparent degradation rate constant k_{app} (equation 34)

$$k_p + k_{pc} = k_{app} \tag{34}$$

Being so, the total reaction can be described by the first order equation 35. k_{app} (in min^{-1}) is the slope of the plot of $-Ln\frac{\gamma_{(t)}}{\gamma_0}$ vs t (in minutes).

$$-\mathrm{Ln}\frac{\gamma_{(t)}}{\gamma_0} = k_{app} \cdot t \quad (35)$$

For the photoreactor without the TiO_2 naofilm, it is assumed that all degradation is caused by photolysis (k_{pc} = 0, so k_p = k_{app}). The slope of the plot of $-Ln\frac{\gamma_{(t)}}{\gamma_0}$ vs t for experiments performed without TiO_2 results in the k_p value. The error of the constants can be obtained by using the function LINEST in Microsoft excel, while individual error bars of each point in degradation curves was calculated as standard error.

d) Electrical energy per order (E_{EO}) calculation

E_{EO} can be obtained (in kWh m^{-3}) for each OMP via equation 36 [205], in which t is the amount of time (min) required to reach 90% of degradation of a target pollutant, P is the electrical power (W) required by the system and V is the reaction volume (L) of the system.

$$E_{EO} = \frac{P \cdot t}{V \cdot 60} \quad (36)$$

The time to reach the aforementioned degradation can be obtained by isolating t in equation 35 for $\frac{\gamma_{(t)}}{\gamma_0}$ = 0.1, according to equation 37. For that, it is necessary to assume that the kinetic rate $\underline{k}_{app}$ is constant until 90% of degradation is reached.

$$E_{EO}(\mathrm{kWh\ m^{-3}})_{\mathrm{OMP}} = \frac{-\ln 0.1}{k_{app}\ (\mathrm{min^{-1}})_{\mathrm{OMP}}} \cdot \frac{\mathrm{P\ (W)_{Lights}}}{\mathrm{V_{Reactor}}\ (L) \cdot 60} \quad (37)$$

3.3.7.2. Simultaneous wavelength experiments

The use of simultaneous wavelength on the degradation of the 5 target pollutants and its impact on k_{app} and E_{EO} values was also investigated. LED arrays c and g (**figure 34**) were tested, with alternating UV-A and UV-C LED strips for both reactors with and without the TiO_2

nanofilm. The acronyms for the tested process are shown on **table 6**. The experiments were performed in MQ water using DCy of 1.00 and 0.50, as well as in tap water (continuous lighting). γ_0 of each pollutant was 2 mg/L.

Table 6. List of acronyms for experiments using simultaneous wavelengths

TiO_2 nanofilm	LED strips	Applied acronym
No	1 UV-A, 2 UV-C	**P, SW3**
Yes	1 UV-A, 2 UV-C	**PC, SW3**
No	3 UV-A, 3 UV-C	**P, SW6**
Yes	3 UV-A, 3 UV-C	**PC, SW6**

4. RESULTS AND DISCUSSION

4.1 Photoreactor design and light profile simulation

Figure 36 shows the photoreactor's middle cross section radiant flux (mW) profile for all the 8 UV-A-LED arrays from **figure 34**, as provided by the OpticStudio software. It is possible to visualize that the arrays that had the LEDs closer to reactor walls (D_W = 10 mm, on **figure 34's** left side) obtained higher radiant fluxes in comparison with the ones of D_W = 15 mm and the same number of LEDs. Increasing the number of LEDs also resulted in higher radiant fluxes, as expected. In arrays containing less LEDs, the presence of "dark zones" can be noted (arrays a and b), while intense light peaks are observed in the centre when the maximum number of LEDs are used (arrays g and h). The degradation constant rate of photolysis can be related with the radiant flux, because the first law of photochemistry states that light has to be absorbed to cause a photochemical reaction [206]. Among other variables, this absorption depends on the incident radiant flux [207].

Using the average value and standard deviation of all pixels of **figure 36**, it is possible to obtain a quantitative relation between photoreactor design, light intensity and homogeneity in the middle cross section. **Figure 37** shows the average value of the radiant fluxes inside the photoreactor and their respective standard deviation for each array. A linear correlation (R^2 > 0.96) between #LED and average radiant flux was obtained for both cases (D_W = 10 mm and D_W = 15 mm). The standard deviation value represents the homogeneity of the system, with smaller values for more homogenous designs. **Figure 37** shows that arrays with shorter distances between LEDs and reactor walls had a slightly less homogenous design, since light produces a conical pathway with its intensity proportional to the square value of distance [208]; so the closer the source-point is from the reactor, more concentrated the flux will be. A previous study by [170] performed for planar geometries obtained similar results, increasing light homogeneity when LEDs are positioned further away from the reactor. However, in their study it was showed that a large number of LEDs increases the system's homogeneity. For our cylindrical case, it can be observed in **figure 38** that homogeneity remained unchanged for #LED 2, 3 and 4 – and then increases for #LED =6. This can be explained by the fact that all LEDs in our experiments are facing towards the photoreactor's middle axis. This cause light to concentrate in the middle point of the cross section, creating a light peak that reduces homogeneity. For [170], the additional

LEDs were never facing each other, with each point facing a different correspondent perpendicular point in the illuminated plane surface. Therefore, different geometries will have different correlations between their light profiles and LED arrays.

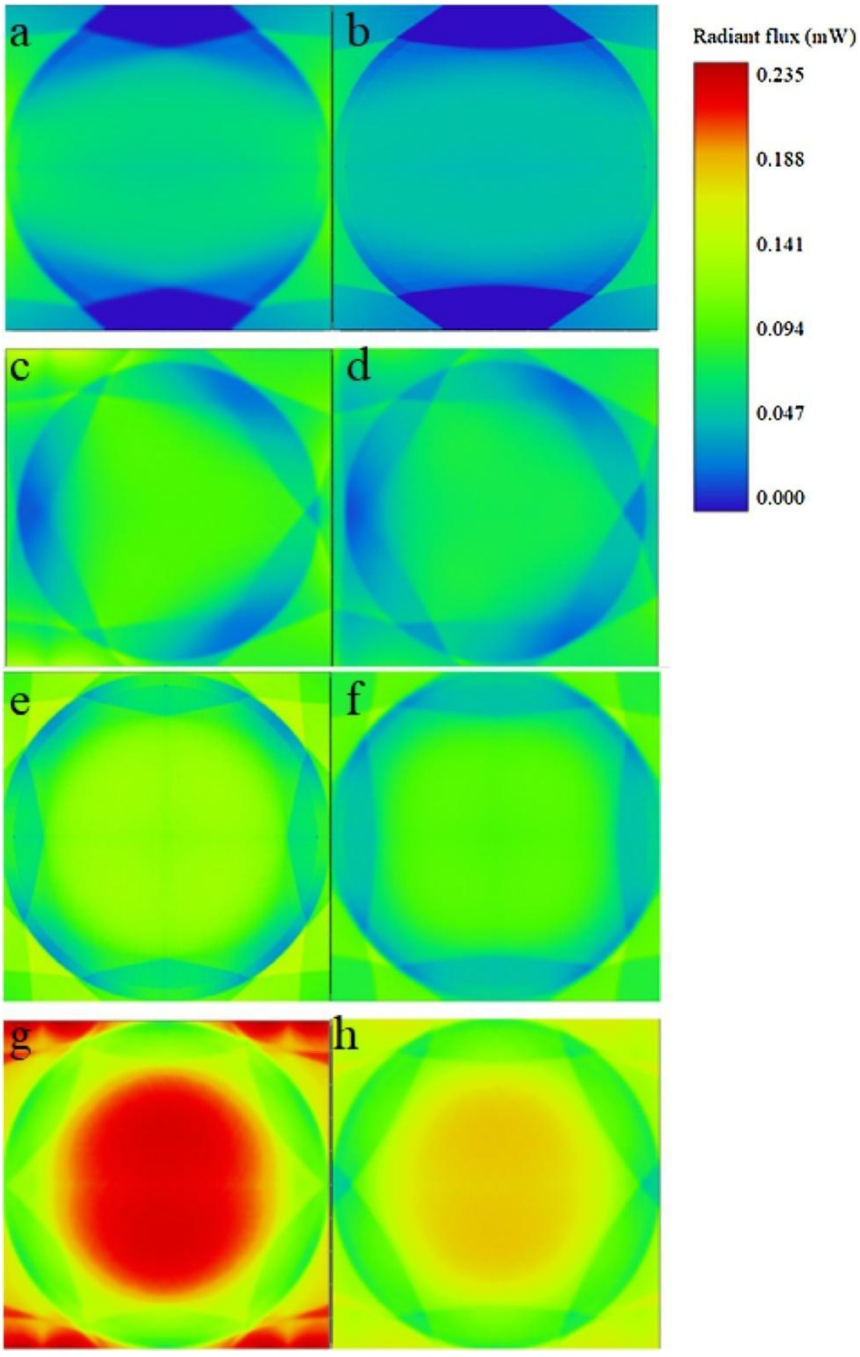

Figure 36. Middle cross section radiant flux profiles for all arrays provided by OpticStudio. Arrays a-h are in accordance to **figure 34** [166]

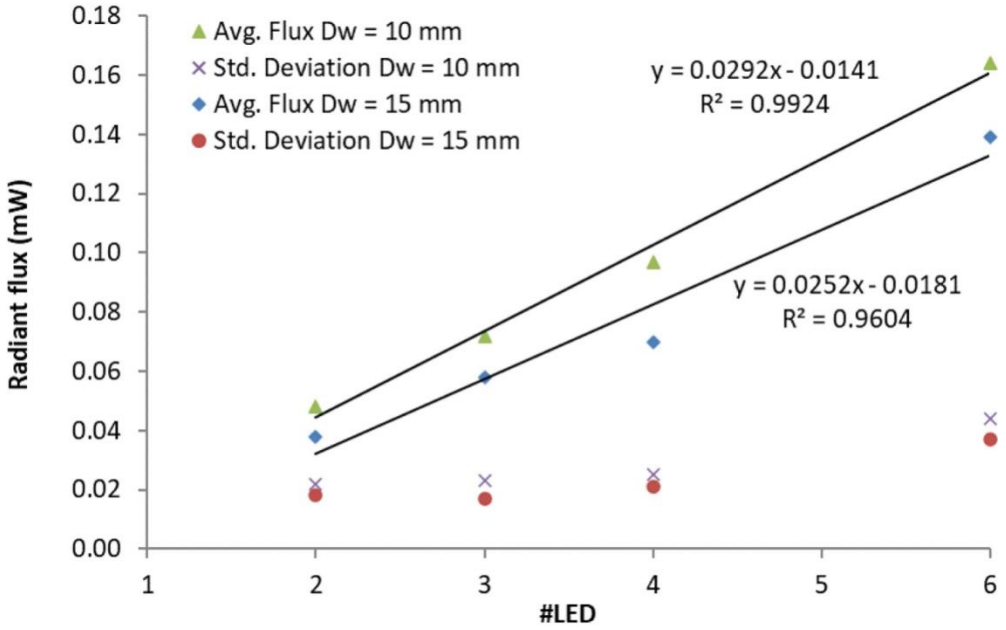

Figure 37. Average radiant fluxes and standard deviations for arrays from **figure 35** and their relation to #LED and D_W [166]

The behaviour of irradiance flux and its correlations with #LED and D_W leads to a similar analysis. **Figure 38** shows the planar projection of the simulated values of irradiance (mW cm^{-2}) at the reactor's side wall. Since the TiO_2 nanofilm was embedded on this region, its irradiance values should impact on photocatalytic rates [172, 209]. Analogously with the cross-section analysis, a larger #LED resulted in larger irradiance values, while lower #LED resulted in "dark zones". Also as before, shorter D_W resulted in higher irradiance values. **Figure 39** shows the average value and standard deviation of all pixels of **figure 38**, again obtaining a linear correlation (R^2> 0.97) between average irradiance and #LED for both tested D_W. Light homogeneity was slightly higher when longer D_W was used, but the standard deviation reached its lower levels for #LED = 3. This happens because the design with 3 LED strips is the only one that does not have any strip facing each other directly. When strips face each other, light is concentrated in the same area and homogeneity falls. The design with #LED =2 had the smaller homogeneity because it combines 2 LED strips facing each other (concentrating light in the same spot) and the lack of other light sources, creating dark zones.

The analysis of light intensity and homogeneity of a photoreactor is paramount to the understanding and optimization of UV-based processes, since both dark zones and excessive light areas hinder the process performance [87].

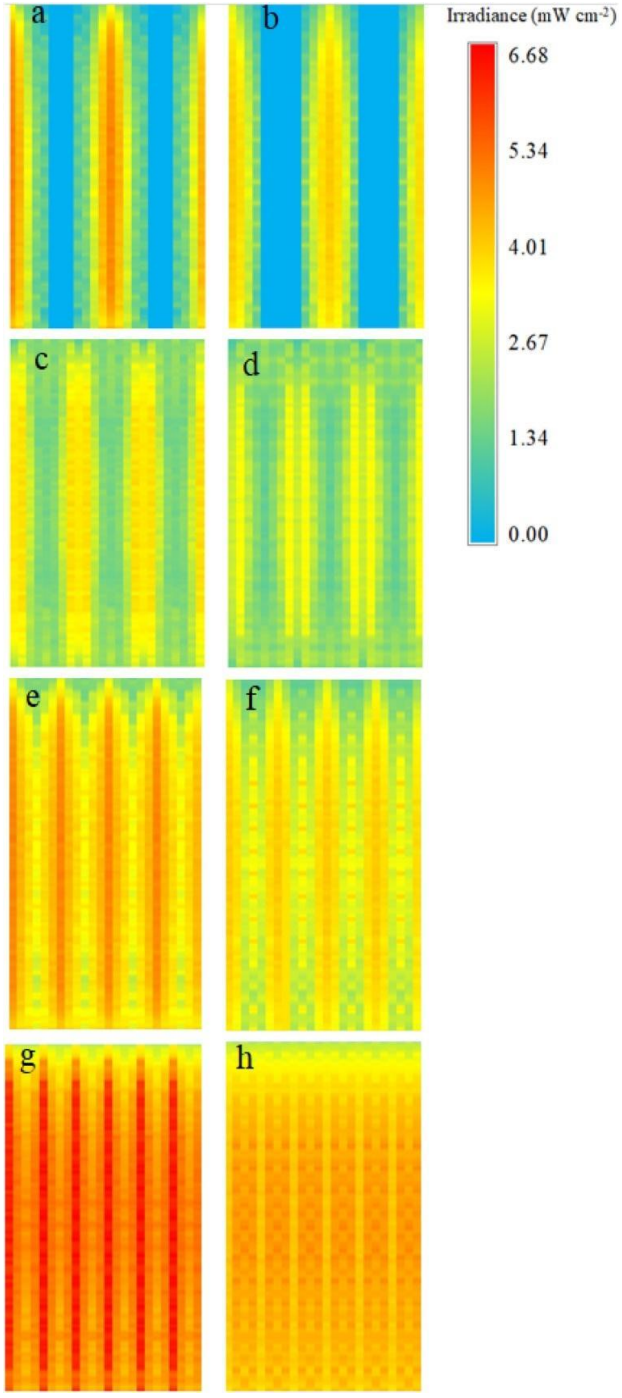

Figure 38. Planar projection of simulated irradiance values for all arrays provided by OpticStudio. Arrays a-h are in accordance to **figure 35** [166]

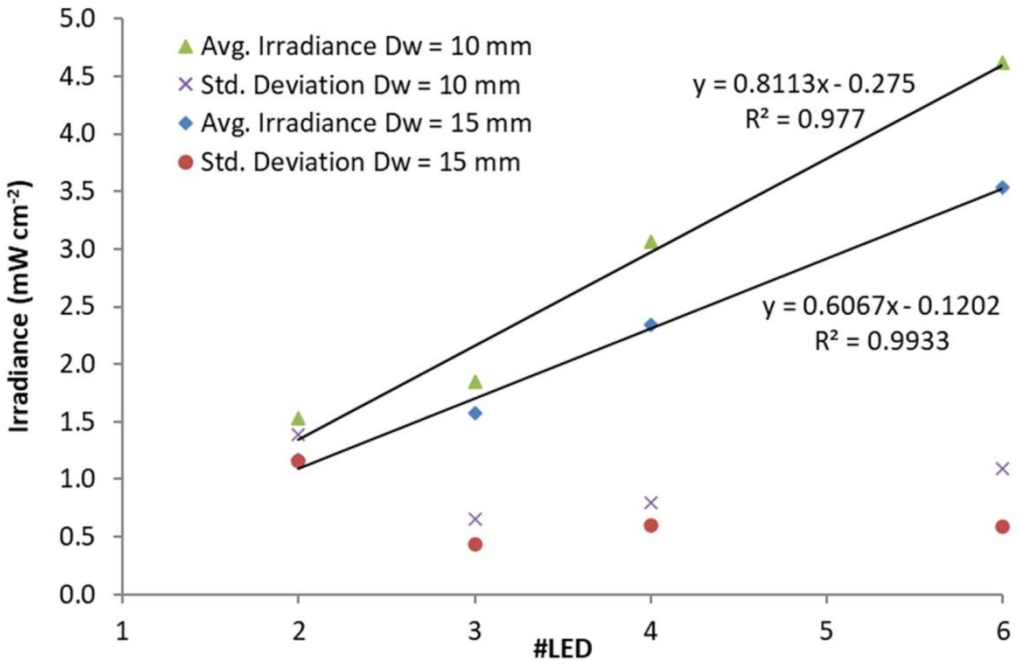

Figure 39. Average irradiance and standard deviation for arrays from **figure 35** and their relation to #LED and D_W [166]

4.2 Degradation of ciprofloxacin

4.2.1 Impact of photoreactor design on kinetic rates and electrical energy per order consumption

A full-factorial categorical design of 2 levels investigating the impact of 4 different variables on the degradation of CIP (k_{app} and E_{EO} values as dependent variables) was performed using the Design Expert 12 software. **Table 7** shows the independent variables, their tested range and coded values. A total of 2^4 = 16 experiments were necessary, with all possible different combinations of independent variables at coded levels -1 and +1. The list of these experiments can be found on **table 8**. Additional 16 experiments (**table 9**) were performed using other possible photoreactor arrays (among the ones in **figure 34**) and DCy combinations to verify the validity of the method for code values between -1 and 1 for #LED and DCy. The resulting linear equations were compared with the totality of the experimental data to verify their validity for the interval studied. The software provided the ANOVA analysis to evaluate the significance of each

factor. Lastly, k_p and k_{pc} were compared and their dependence on the average radiant flux and irradiance for each array was evaluated. **Figures 40-41** shows the degradation vs time plots for all 32 performed experiments.

Table 7. Variables and their ranges for DoE #1

Independent variable	Abbreviation	Lower level	Higher level
Number of LED columns around the reactor	**#LED (A)**	2	6
Distance between columns and reactor walls (mm)	***D*w (B)**	10	15
Duty cycle	**DCy (C)**	0.50	1.00
Presence of TiO_2 catalyst	**Ti (D)**	NO	YES
Code		**-1**	**1**

Table 8. Experiments performed for the full factorial design (DoE #1)

Array	DCy	TiO_2
a	1.00	YES
a	1.00	NO
a	0.50	YES
a	0.50	NO
b	1.00	YES
b	1.00	NO
b	0.50	YES
b	0.50	NO
g	1.00	YES
g	1.00	NO
g	0.50	YES
g	0.50	NO
h	1.00	YES
h	1.00	NO
h	0.50	YES
h	0.50	NO

Table 9. Additional experiments for model validation

Array	DCy	TiO_2
c	1.00	NO
e	1.00	NO
d	1.00	NO
f	1.00	NO
c	1.00	YES
e	1.00	YES
d	1.00	YES
f	1.00	YES
c	0.75	NO
c	0.50	NO
c	0.75	YES
c	0.50	YES
d	0.75	NO
d	0.50	NO
d	0.75	YES
d	0.50	YES

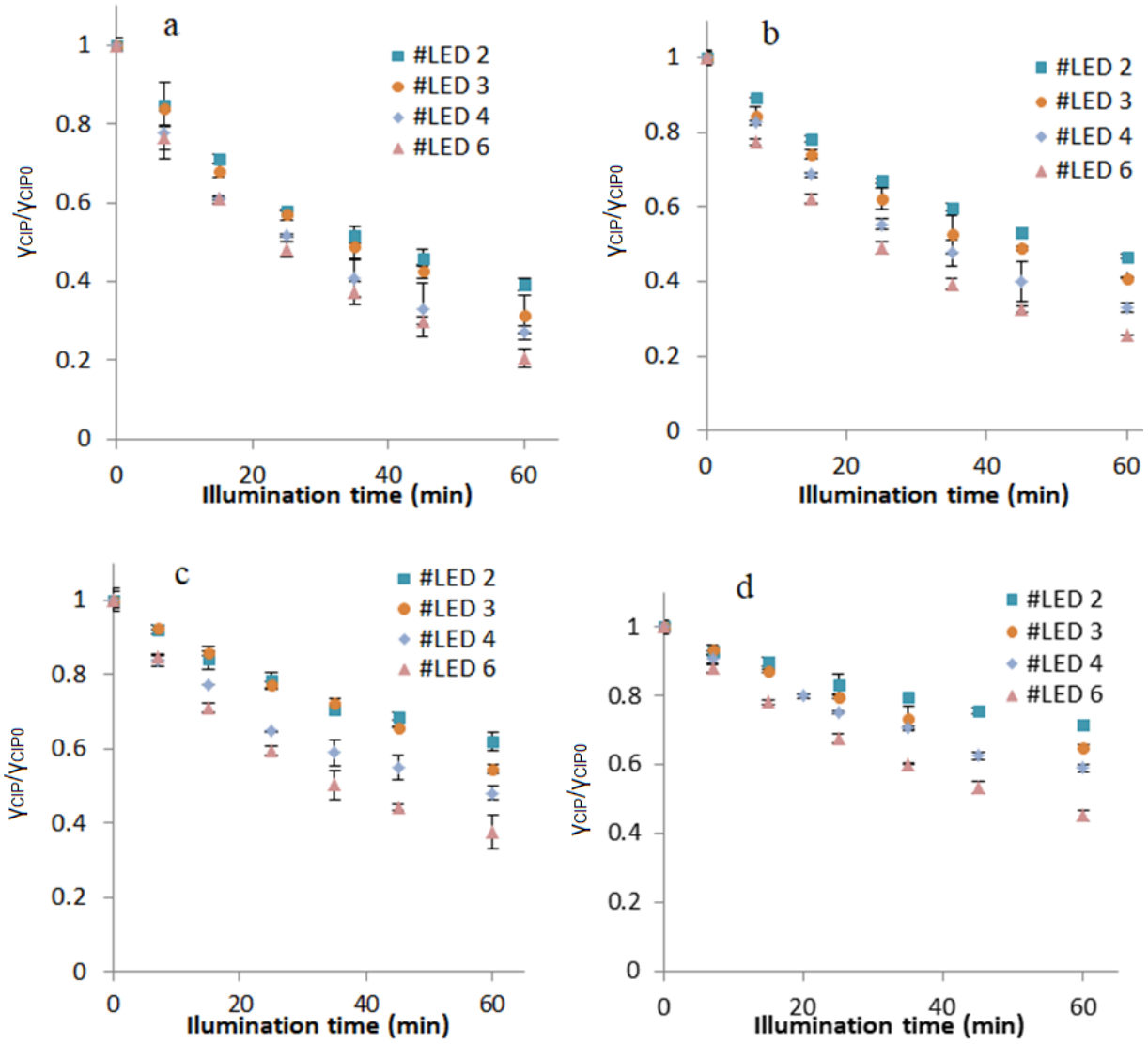

Figure 40. CIP degradation vs time plots for all DoE n#1 experiments with error bars representing standard error.

a) *D*w = 10 mm, DCy = 1.00, photocatalysis (#LED – in legend)
b) *D*w = 15 mm, DCy = 1.00, photocatalysis (#LED – in legend)
c) *D*w = 10 mm, DCy = 1.00, photolysis (#LED – in legend)
d) *D*w = 15 mm, DCy = 1.00, photolysis (#LED – in legend) [166]

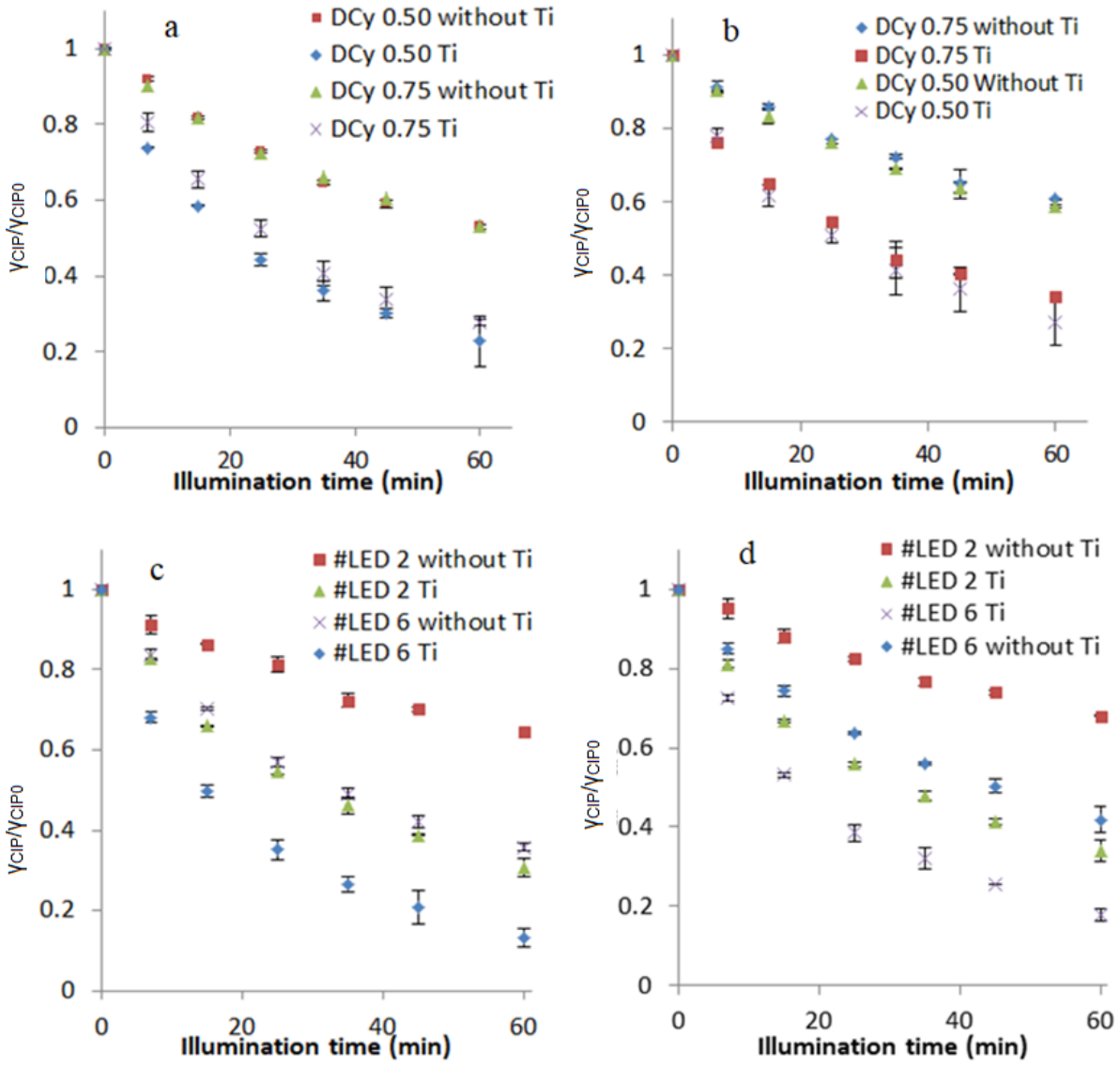

Figure 41. (Continuation**)** CIP degradation vs time plots for all DoE n#1 experiments with error bars representing standard error.

a) #LED = 3, *D*w = 10 mm (DCy, photolysis/photocatalysis – in legend)
b) #LED = 3, *D*w = 15 mm (DCy, photolysis/photocatalysis – in legend)
c) DCy = 0.50 (Dw = 10 mm (#LED, photolysis/photocatalysis – in legend)
d) DCy = 0.50 Dw = 15 mm (Dw, #LED, photolysis/photocatalysis – in legend) [166]

The half normal plot of all effects for k_{app} and E_{EO} provided by the Design Expert software are shown in **figure S1**. The intensity of each individual and combined effect is shown by the Pareto chart in **figure 42**. It is possible to graphically visualize which effects are the most significant. Effects above the *t*-value line were considered significant at a level of 95 %, while effects above the Bonferroni limit were of even higher significance [210]. **Figure 43** shows the

correlation between predicted and experimental values for DoE #1. The selection of significant effects was made by choosing the minimum number of effects (respecting the hierarchy) that would keep the correlations on **figure 43** at a $R^2 > 0.96$ – since it shows the plots of experimental vs predicted k_{app} (a) and E_{EO} (b). Equations 38 and 39 show the obtained model (using coded independent variables) for the prediction of k_{app} and E_{EO}, respectively.

$$k_{app}(\text{min}^{-1}) = 0.0163 + 0.0048 \cdot \#LED - 0.0014 \cdot D_W - 0.0015 \cdot DCy + 0.0054 \cdot Ti - 0.0012 \cdot DCy \cdot Ti \quad (38)$$

$$E_{EO}(\text{kWh m}^{-3}) = 213.3 + 6.1 \cdot \#LED + 19.8 \cdot D_W - 3.7 \cdot DCy - 73.1 \cdot Ti + 11.8 \cdot \#LED \cdot DCy + 12.0 \cdot \#LED \cdot Ti - 10.9 \cdot D_W \cdot Ti + 10.1 \cdot DCy \cdot Ti \quad (39)$$

The considerable agreement between the predicted and experimental data shown on **figure 43** indicates that the equations 38 and 39 are excellent predictors inside the tested range.

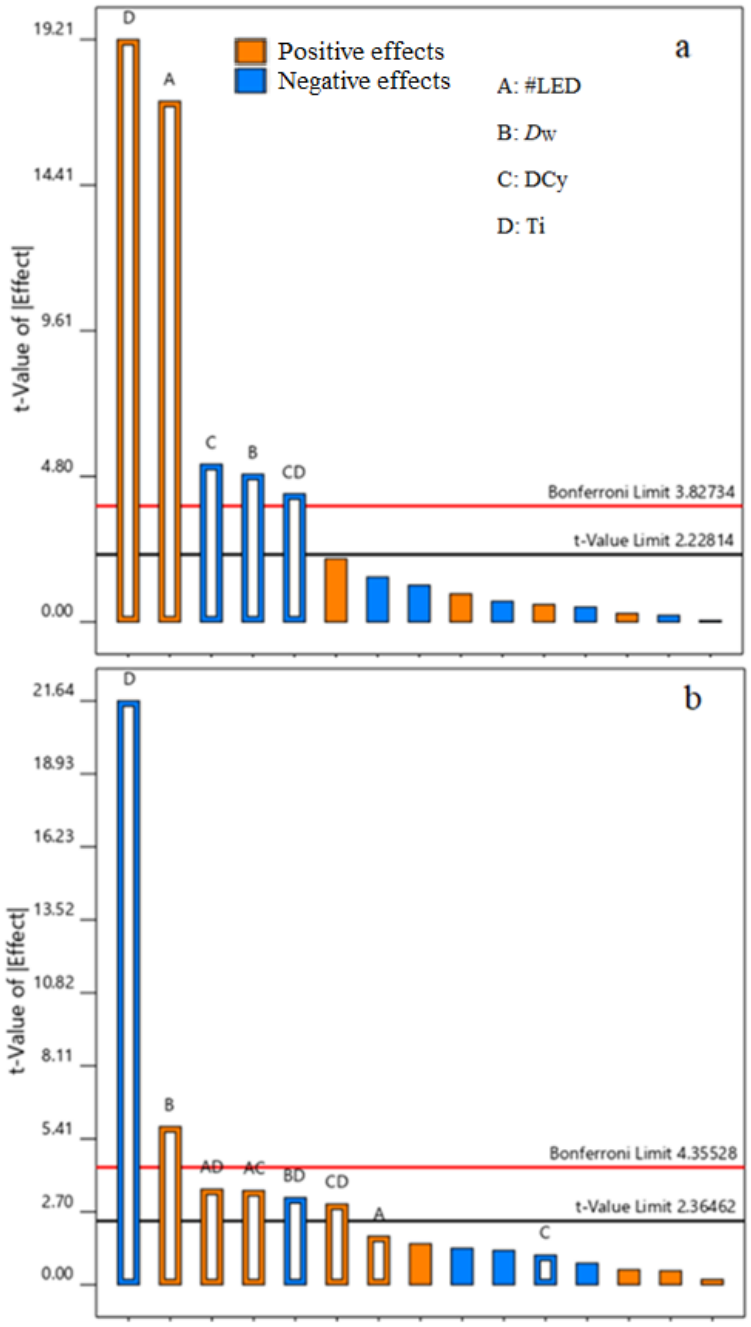

Figure 42. Pareto charts and significant effects (signalled with a white bar) for k_{app} (a) and E_{EO} (b) for DOE #1[166]

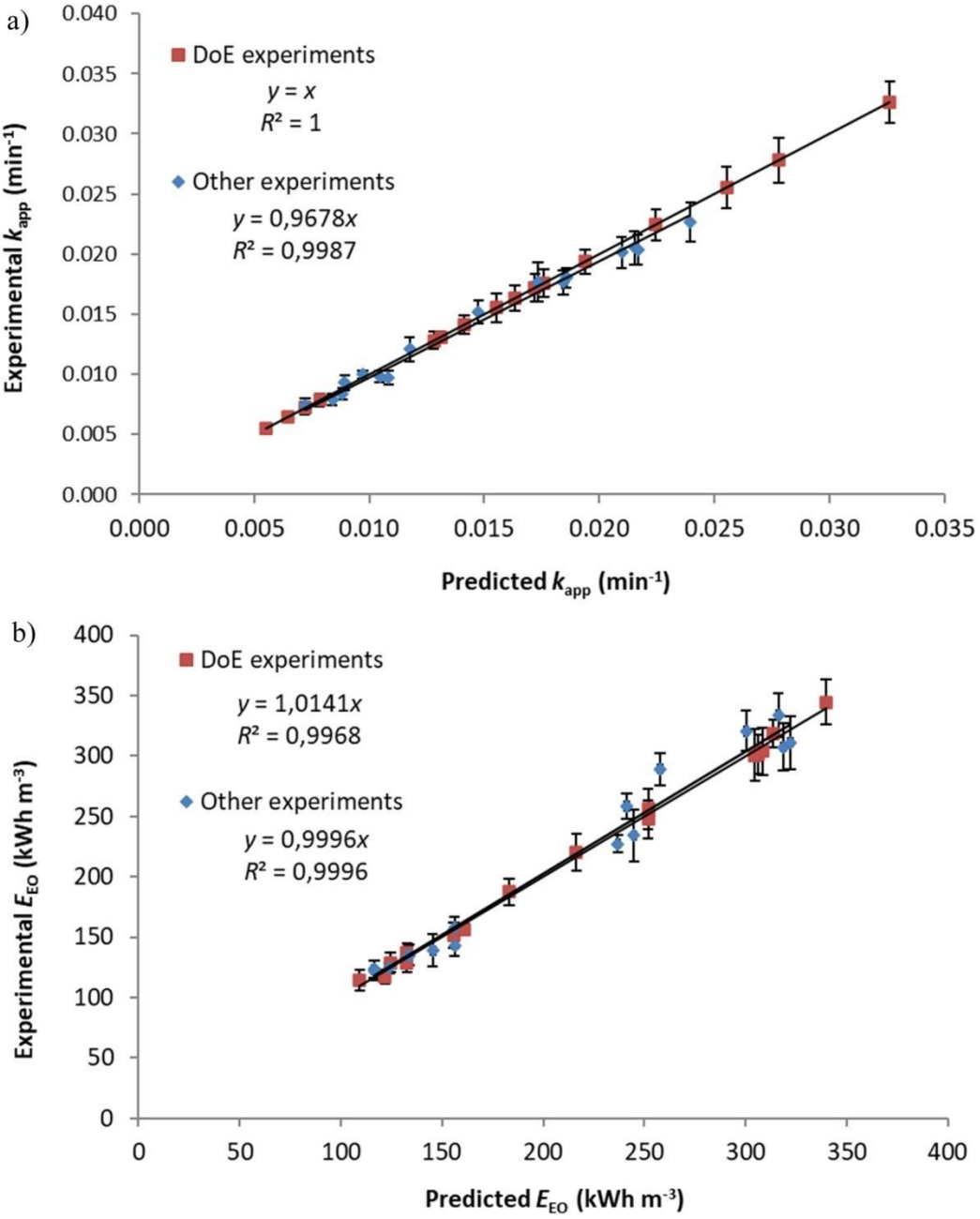

Figure 43. Models' verification: experimental vs predicted values for k_{app} (a) and E_{EO} (b) for DoE #1[166]

Tables 10 and 11 show the results of analysis of variance (ANOVA) provided by the Design Expert software for k_{app} and E_{EO}, respectively. The results confirm that the obtained models were significant.

Table 10. ANOVA analysis for DoE n#1 (k_{app})

Source	Sum of Squares	df	Mean Square	F-value	p-value	k_{app}
Model	0.0009	5	0.0002	146.53	< 0.0001	significant
A-#LED	0.0004	1	0.0004	294.96	< 0.0001	
B-Dw	0.0000	1	0.0000	23.72	0.0007	
C-DCy	0.0000	1	0.0000	27.04	0.0004	
D-Ti	0.0005	1	0.0005	369.09	< 0.0001	
CD	0.0000	1	0.0000	17.83	0.0018	
Residual	0.0000	10	1.3×10^{-6}			
Cor Total	0.0009	15				

Table 11. ANOVA analysis for DoE n#1 (E_{EO})

Source	Sum of Squares	df	Mean Square	F-value	p-value	E_{EO}
Model	1×10^5	8	12578.31	68.89	< 0.0001	significant
A-#LED	590.3	1	590.30	3.23	0.1152	
B-Dw	6265.4	1	6265.44	34.31	0.0006	
C-DCy	218.7	1	218.71	1.20	0.3100	
D-Ti	85505.8	1	85505.80	468.29	< 0.0001	
AC	2225.0	1	2225.02	12.19	0.0101	
AD	2289.2	1	2289.16	12.54	0.0095	
BD	1899.4	1	1899.36	10.40	0.0145	
CD	1632.7	1	1632.68	8.94	0.0202	
Residual	1278.1	7	182.59			
Cor Total	1.02×10^5	15				

Regarding k_{app} values, higher #LED (effect A; positive) and lower D_W (effect B; negative) resulted in higher kinetic rate constants, since the light intensity reaching the photoreactor is higher (see **section 4.1**). On top of that, the most significant effect to increase k_{app} was the presence of the catalyst (effect D; positive). The presence of the TiO_2 nanofilm allows

photocatalytic reactions to take place (see equations 16-21), in addition to photolytic ones. The effect of duty cycle was also highly significant (C; negative) demonstrating that the use of lower duty cycles and controlled periodic illumination enhances photocatalytic degradation. Interestingly, the combined effect CD (catalyst presence and duty cycle; negative) was also above the Bonferroni limit and, thus, highly significant. The contribution of controlled periodic illumination and lower duty cycles can only be recognized when the TiO_2 nanofilm is present, since without it only photolytic reactions happen [121]. As it was mentioned in **section 2.9**, once radicals are generated by the photocatalytic mechanism, light is not necessary to the next steps of the reaction. However, for photolysis, when lights are off no reaction takes place. Being so, controlled periodic illumination can only benefit processes containing the TiO_2 nanofilm. When no catalyst is present (−) and lower duty cycles are used (−), the effect CD remains negative, annulling the performance increase brought by effect C. This results in photolytic degradation rates which are independent of duty cycle values. When the catalyst is present (+) and a lower duty cycle is used (−), CD effect becomes positive, and its contribution is added to the effect C, increasing k_{app} values.

Regarding E_{EO} values, the only largely relevant negative effect is the TiO_2 presence, with D_w being of positive relevancy. This means that the presence of the catalyst greatly reduced energy expenses, due to the fastest degradation by ROS species [211]. The higher light intensity brought by shorter D_W also contributed to reducing energy expenses. Four other small effects between the Bonferroni and *t*-value limits were included in the E_{EO} final model (equation 39), as well as two nonsignificant effects due to hierarchy. It is remarkable that neither #LED nor DCy had a significant impact on E_{EO} values. For #LED, this can be explained by the fact that, although additional light sources increase k_{app} values, they also increase energy consumption. Analysing the results, it can be concluded that the benefit brought by additional light sources around the reactor is negatively compensated by additional energy consumption. For controlled periodic illumination, the attachment of the ARDUINO control board results in additional energy costs for the system [166]. **Table 12** shows the power required for each combination of #LED and DCy tested, as measure by the multimeter. It can be seen that when a duty cycle of 0.50 is adopted, power demands are not exactly 50% of the continuous value, but higher than that. This means that additional energy is required, and just like for the #LED case, the benefit brought by DCy for degradation is neutralized by this additional demand. Possibly, a larger-scale scenario would be

less affected by this disadvantage, since the amount of power necessary to feed the control board compared to the larger LED array (1.8 W) becomes negligible.

Table 12. Power (W) required for each combination of #LED and DCy tested for DoE #1

# LED	DCy	*P* (W)
0	-	1.8
2	1.00	6.2
3	1.00	8.4
4	1.00	10.5
6	1.00	15.0
2	0.50	4.0
3	0.50	5.1
3	0.75	6.9
6	0.50	7.9

Figure 44 shows all obtained k_{app} and E_{EO} values for this section. Should be noted that arrays with the higher reaction rates were not the most energy-efficient ones. Aiming to obtain the best photoreactor design among all the tested ones, the lowest E_{EO} value should be sought. The array **a** (#LED = 2 with TiO_2) had the lowest experimental value of 113 kWh m^{-3}. However, the array **c** (#LED = 3 with TiO_2) had a similar E_{EO} value (116 kWh m^{-3}) and a k_{app} 25% higher than the first array. Furthermore, in **section 4.1** it was established that light distribution along the catalyst surface is more homogenous for array **c (figure 34)**. Consequently, this array is chosen as the optimal one for the continuation of this study.

Although it was possible to reduce E_{EO} values by 67% (comparison between highest and lowest E_{EO} obtained) by changing the photoreactor design, values above 100 kWh m^{-3} are considered economically unfeasible for practical purposes [5, 6]. The difficulty in obtaining lower E_{EO} values comes mainly from the intrinsic low photonic performance of photocatalysis itself [5] as explained in **section 2.9**. Nevertheless, the recent technological improvements of UV-LEDs wall-plug efficiencies could greatly contribute to reducing energy expenses 10 to 20 times in the next 5 years [87,173].

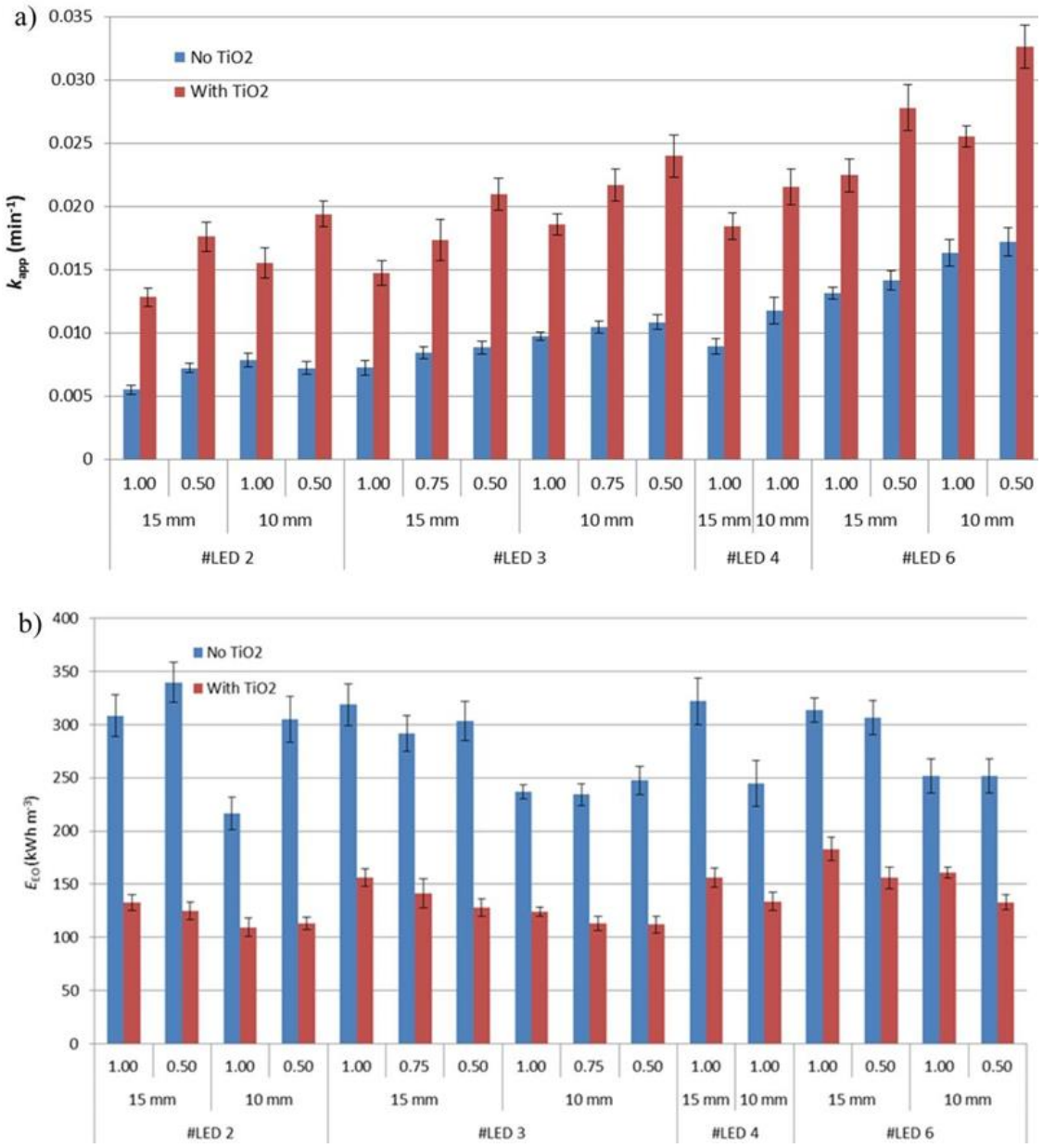

Figure 44. k_{app} (a) and E_{EO} (b) values for all experiments as a function of the DCy, Ti, D_w and #LED [166]

4.2.2. Impact of controlled periodic illumination on photolytic and photocatalytic rate constant

The observed photolytic kineti rate constant k_p of CIP was plotted as a function of the average radiant flux in the photoreactor's middle cross section (obtained in **section 4.1**) in **figure 45**. A good linear correlation can be found with R^2 = 0.95, demonstrating that an increase in the light intensity results in a proportional increase in the k_p of CIP. Controlled periodic illumination (DCy = 0.50) did not affect k_p values, as expected by the discussion done on **section 4.2**. Photolytic reactions depend on photons emission and the absorption of the latter with target molecules, a contact which does not happen if the light is turned off.

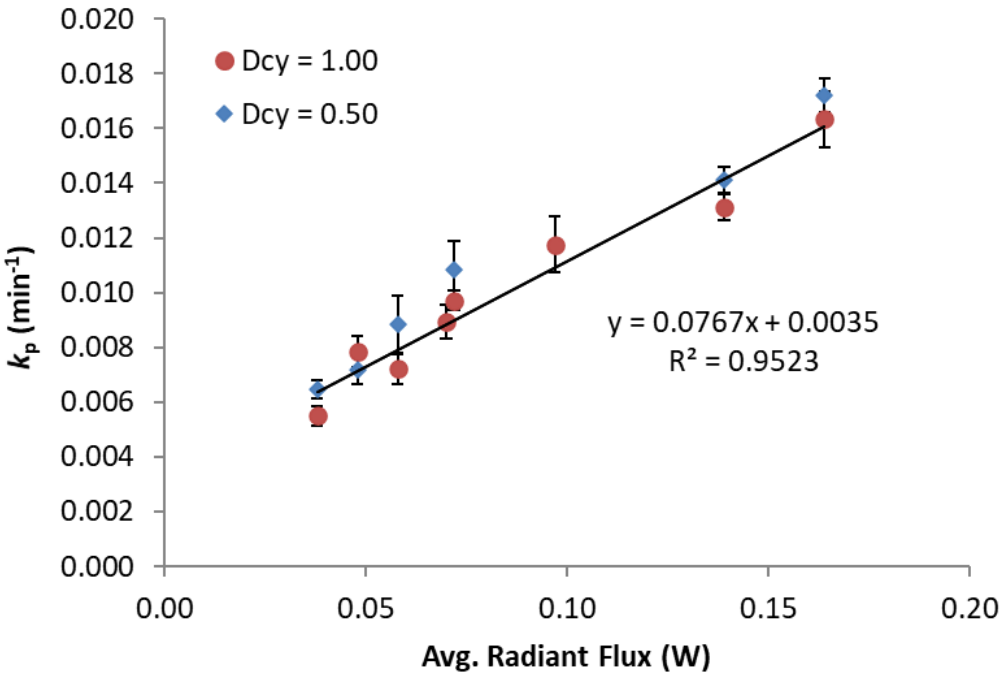

Figure 45. Photolytic degradation rate constant k_p of CIP vs average radiant flux [166]

Figure 46 shows the photocatalytic constant k_{pc} as a function of the average light irradiance obtained in **section 4.1.** It can be observed that, for the same DCy, increasing the light intensity only improves k_{pc} until a limit value. After that, k_{pc} reaches a plateau. This means that, when more LEDs are used, the proportion of CIP being degraded by photocatalysis decreases. It is possible that the excess of light promotes the recombination of the electron/hole pair, reducing

radical production [127, 185]. The adoption of lower DCy allows k_{pc} values to exceed this plateau, due to the reduction of this recombination [161]. By adopting CPI and allowing more radical-based reactions to happen when the lights are off, the photonic efficiency of the system is increased.

It is important to highlight that the benefit brought by CPI will depend on the different reaction pathways of each substance [212] and that the current analysis is only valid for the target pollutant CIP. For substances that are promptly photolyzed by wavelengths in the LED's working spectrum, increasing the photocatalytic route might not improve overall degradation considerably. Other important variables that should be analysed are the LED's wavelength and the system's matrix, with a large potential to affect degradation rates [213] (see **section 4.3.2**).

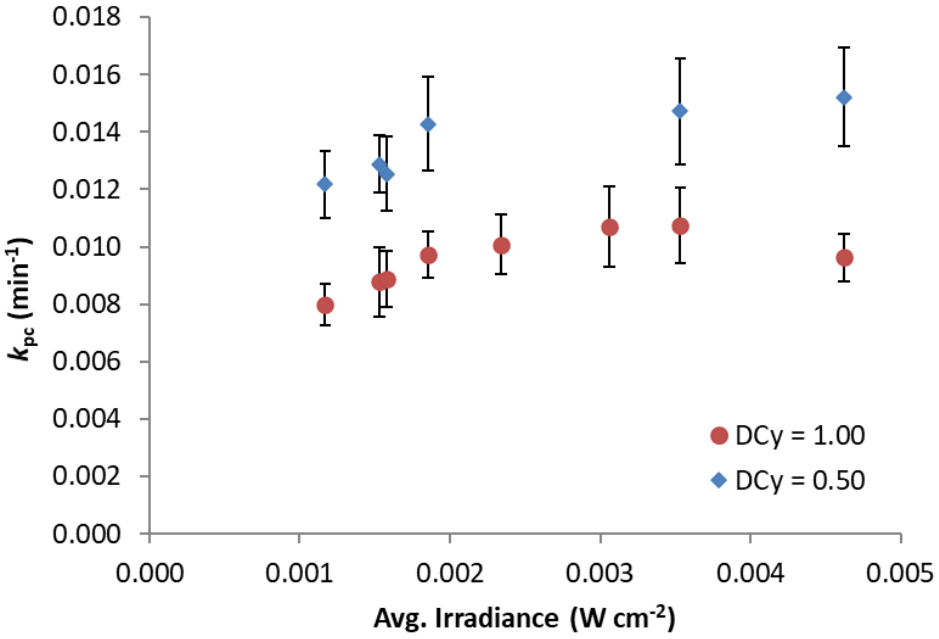

Figure 46. Photocatalytic degradation rate constant k_{pc} of CIP vs average irradiance [166]

4.3. Simultaneous degradation of target pharmaceuticals

The degradation of the 5 contaminants of emerging concern (CIP, SMX, TMP, VEN and DV) in ultrapure water was investigated for the different treatments according to **table 5** in **section 3.3.7. Table S1** shows the data of all the experiments performed during this section.

Figure 47 shows the k_{app} values for all target pollutants individually (Ind.) and in a mixture (Mix.) at γ_0 = 2 mg/L for each substance. It is noticeable how each compound reacts differently to each treatment. CIP was the only compound degraded by UV-A photolysis. TMP was completely impervious to both UV-A and UV-C photolysis. TMP, VEN and DV had the lowest degradation rates overall. SMX had the fastest degradation (0.36 min^{-1}) for UV-C photolysis, being the only compound that degraded faster without the presence of the catalyst nanofilm (comparing under the same wavelength). A hypothesis for this is that the presence of the catalyst creates a "screening effect" that hinders the contact between the photons and the target pollutant. The ROS species generated during this process (by the contact between the photons and the catalyst) do not compensate for the losses in available photons for the direct faster photolysis degradation route, and k_{app} decreases [119, 172, 214]. The screening effect is more common for lower wavelengths, since their respective photons are more easily absorbed [129].

The degradation of pollutants will depend on [212]: (1) the types and amount of available ROS; (2) the pollutants respective reactivity with each of the generated ROS and photons [215]; (3) the interaction between the pollutant and the catalyst surface [163]; (4) the ionic state of each pollutant in solution (there might be distinct reactivity for the same parent compound for both photolytic and photocatalytic routes); (5) the pollutant's absorption spectrum and quantum yield for a given wavelength (specific for photolysis) [216, 217]. Most of these points depend, directly or indirectly, on the matrix composition and pH [50].

It is apparent on **figure 47** that most pollutants had their degradation hindered by the presence of other substances for all treatments. SMX, TMP, VEN and DV had their k_{app} values reduced by an average of approximately 50% when in mixture. This decrease was expected, given that a higher number of substances reduces the availability of catalytic sites and photons [47, 121]. Another reason is that the presence of multiple TPs might negatively affect degradation routes of target pollutants [166]. However, CIP presented a 40% increase of k_{app} during UV-A photocatalysis while constants for its other processes remained stable. A possible explanation for that lies in the initial pH (**Table S1**) of the mixture of target pollutants (6.7) - which was higher than the initial pH of the solution containing only CIP (6.0). CIP's p*K*a is 6.1 [47]. It has been reported [47] that the predominant ionic form below this value (cationic) has lower photolytic and

photocatalytic degradation rates than the one above it (zwitterionic) due to changes in its surface affinity with TiO_2 and reactivity with photons. It is possible that the ionization of other pollutants in mixture increases the pH of solution to the point that the zwitterionic species of CIP becomes the predominant one, thus resulting in its faster degradation routes. This does not mean that the reduction of available catalytic sites and inhibitions brought by other substances does not negatively affect CIP degradation, but, instead, indicates that the fastest reactivity of the zwitterionic species is capable to overcome these hurdles. The different reactivity of ionic states helps to explain why the degradation of SMX was so fast for the individual case. It is reported [50] that its cationic state, predominant at pH < 5.6, has the fastest degradation rates. The solution containing only SMX starts its reaction approximately at this pH-value (decreasing it even further by the end of the experiment), contributing to the quick reaction (**Table S1**).

.

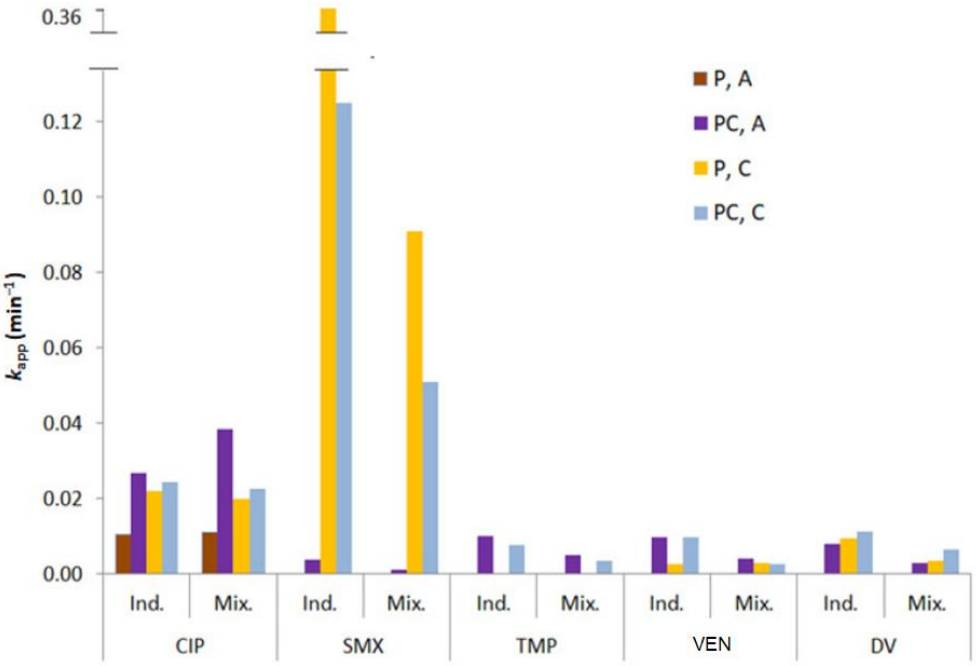

Figure 47. k_{app} values for individual (Ind.) and simultaneous (Mix.) degradation of target pollutants in MQ water [212]

4.3.1 Impact of H_2O_2 addition

The 4 experiments performed with the mixture of all 5 target pollutants at γ_0 = 2 mg/L (P, A; PC, A; P, C; PC, C) was repeated with the addition of hydrogen peroxide (0.1 mM, a value commonly found in literature [218, 219]). **Figure 48** shows the k_{app} values of these experiments. Averagely, the addition of peroxide resulted in constant rates 10 times higher than before (compared to **figure 47**). As explained in **section 2.5**, in the presence of peroxide equation 4 generates more hydroxyl radicals to both photolytic and photocatalytic systems, allowing a much faster degradation in most cases. Among all tested pollutants, only SMX did not present a significant degradation improvement. As it was explained in **section 4.3**, this is due to the already very high reactivity of this molecule with UV-C rays.

When comparing with the same emission wavelength, most substances had faster degradation without the presence of the catalyst nanofilm than with it. Again, this can be explained by the screening effect. Equation 4 happens without the catalyst and can take place during both photolytic and photocatalytic cases. However, when the catalyst is present less photons are available for this reaction. Although the catalyst allows equation 17 to happen, the photonic efficiency of this process can be decreased by charge carrier recombination (see **section 2.5.1**). Thus, when peroxide is present in the system it is probable that the addition of TiO_2 would hinder the overall performance and ROS production. Nevertheless, each case-scenario should be evaluated with its particularities.

Evidently, the performance improvement brought by H_2O_2 should not be underestimated. However, additional process costs due to this chemical should be carefully considered [220]. Another is that, as it happens with TiO_2 in slurry form, the literature [121] shows that peroxide increases reaction rates until a maximum concentration value (which will vary depending on the characteristics of each process), acting as a radical scavenger and hindering pollutant degradation after this point [94].

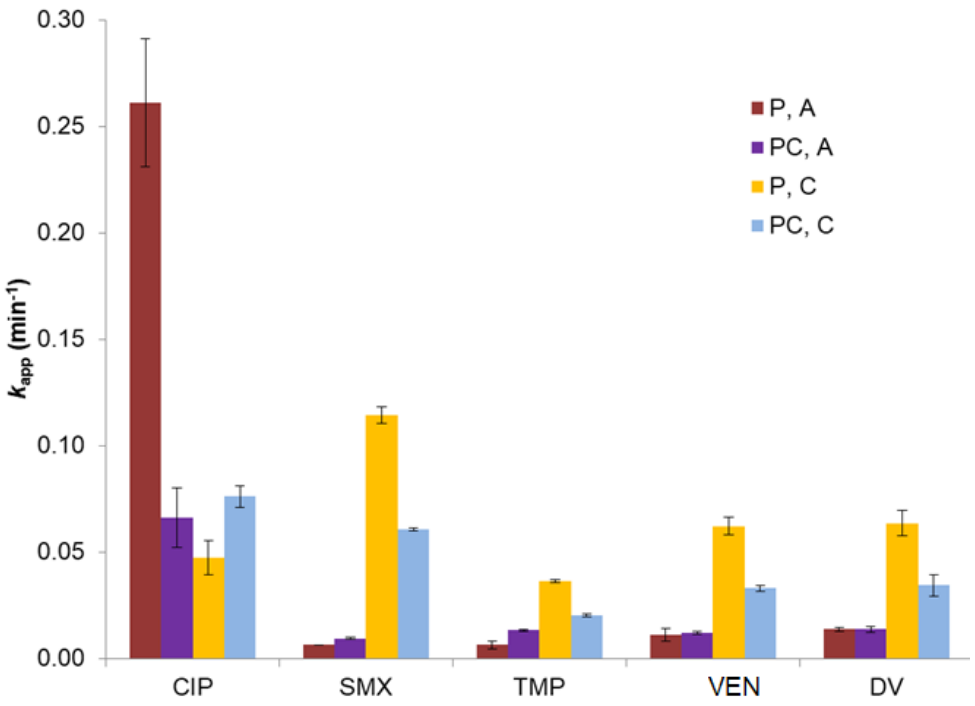

Figure 48. k_{app} values for simultaneous degradation of target pollutants in MQ water with $[H_2O_2]_0$ = 0.1 mM

4.3.2. Impact of process variables and matrix on kinetic rates, total organic carbon abatement and toxicity

Once the optimal UV-LED array was determined in **section 4.2.1**, a second full-factorial categorical design of 2 levels investigating the impact of 4 different variables on the simultaneous degradation of CIP, SMX, TMP, VEN and DV (in terms of individual k_{app} values, %TOC decrease and the difference between final and initial toxicity of the effluent as dependent variables) was performed using the Design Expert 12 software. **Table 13** shows the independent variables, their tested ranges and coded values.

Table 13. Variables and their ranges for DoE #2

Independent variable	Lower level	Higher level
Matrix (A)	MQ water	Tap water
LEDs wavelength (B)	272 nm (UV-C)	365 nm (UV-A)
Presence of TiO_2 catalyst (C)	NO	YES
Duty Cycle (D)	0.5	1.0 (continuous)
Coded value	**-1**	**1**

Again, a total of 16 experiments with all possible combinations of the 4 variables at coded values -1 and +1 were made (**table 14**).

Table 14. Experiments performed for full factorial design (DoE #2)

Run	Coded variables			
	A	B	C	D
1	1	1	1	1
2	1	1	1	-1
3	1	1	-1	1
4	1	1	-1	-1
5	1	-1	1	1
6	1	-1	1	-1
7	1	-1	-1	1
8	1	-1	-1	-1
9	-1	1	1	1
10	-1	1	1	-1
11	-1	1	-1	1
12	-1	1	-1	-1
13	-1	-1	1	1
14	-1	-1	1	-1
15	-1	-1	-1	1
16	-1	-1	-1	-1

4.3.2.1 Kinetic analysis

All kinetic results are shown in **table S1** (experiments 24-39). The half-normal plots of k_{app} pointing out significant effects for all the 5 target pollutants are shown in **figure S2**. Equations 40-44 represent the prediction models using coded dependent variables for all OMPs' k_{app} values, including the significant effects and those necessary by hierarchy. A Box-Cox transformation was used when its respective model had a higher fit than the linear one.

$$k_{\mathrm{app}_{(\mathrm{CIP})}} = 0.0317 + 0.0046\mathrm{A} - 0.0020\mathrm{B} + 0.0041\mathrm{C} - 0.0033\mathrm{D} - 0.0044\mathrm{AB} - 0.0053\mathrm{AC} + 0.0086\mathrm{BC} - 0.0020\mathrm{CD} \quad (40)$$

$$k_{\mathrm{app}_{(\mathrm{SMX})}} = 0.0225 - 0.0122\mathrm{A} - 0.0182\mathrm{B} - 0.0034\mathrm{C} + 0.0159\mathrm{AB} + 0.0053\mathrm{AC} + 0.0077\mathrm{BC} \quad (41)$$

$$k_{\mathrm{app}_{(\mathrm{TMP})}} = 0.0013 - 0.0008\mathrm{A} + 0.0004\mathrm{B} + 0.0010\mathrm{C} + 0.0002\mathrm{AB} - 0.0005\mathrm{AC} + 0.0007\mathrm{BC} \quad (42)$$

$$\sqrt{k_{\mathrm{app}_{(\mathrm{VEN})}}} = 0.0368 - 0.0097\mathrm{A} - 0.0060\mathrm{B} + 0.0235\mathrm{C} + 0.0059\mathrm{AB} + 0.0036\mathrm{AC} + 0.0074\mathrm{BC} + -0.0076\mathrm{BC} \quad (43)$$

$$\sqrt{k_{\mathrm{app}_{(\mathrm{DV})}}} = 0.0408 - 0.0111\mathrm{A} - 0.0202\mathrm{B} + 0.01157\mathrm{C} - 0.0100\mathrm{AC} + 0.0091\mathrm{BC} \quad (44)$$

By analysing the Pareto charts for all compounds (**figure 49**) together with equations 40-44 it is noticeable that each OMP reacted very differently to each scenario, as it was discussed in **section 4.3**. In spite of that, it is possible to find effects which were highly significant for all cases. The effect BC (combination of wavelength with presence of catalyst) was considerably significant and positive for every substance. Highest k_{app} values were generally obtained for UV-A photocatalysis and UV-C photolysis. This is in agreement with results from **figure 49**, since UV-A photolysis is incapable of degrading any of the tested OMPs except CIP and UV-C rays are more prone to suffer screening effects in the presence of the catalyst [212], thus hindering direct photolytic degradation. The additional ROS species generated by the presence of the catalyst did not compensate for the photo-absorption losses of the system when UV-C was used. In the presence of the catalyst (+), longer wavelengths (+) will result in a positive impact on k_{app} values. On the contrary, the absence of the catalyst (−) and shorter wavelengths (−) will result in a positive impact as well.

Also, as expected, the effect of the matrix (A) was significant for all cases. Photocatalytic processes are highly sensitive to changes in the matrix [221] (see **section 2.5.1.2).** It is well known that tap water contains many substances which may affect ROS formation [114, 212], as well as change the predominant ionic species of each target pollutant based on its pH-values. As it can be seen on **table 3**, tap water from Zagreb contains a large amount of bicarbonates, which

are known radical scavengers (see equation 1) capable of reducing the availability of hydroxyl radicals. However, the presence of bicarbonates increases the pH of the matrix, which may lead to faster degradation for some substances [83, 161]. For all substances, the tested degradation was faster in MQ water. The only exception was CIP, which had the A effect positive. The explanation for that revolves around the fact that the neutral state of CIP, predominant at pH > 6.1 is more reactive than its negative state, which tends to be the predominant species during MQ water experiments. As it was mentioned in **section 2.9**, there is a considerable lack of data regarding degradation of OMPs in real matrices, such as tap water. It is fundamental to evaluate photocatalysis under such scenarios due to its potential as a final-step (point-of-use) polishing treatment [5, 121].

The effect of the duty cycle (D) was only significant for CIP degradation. **Figure 47** shows that CIP is the substance which had the largest k_{app} increase when the TiO_2 nanofilm is used in UV-A based processes, meaning that this compound is highly reactive towards ROS species generated during photocatalysis. Since lower duty cycles increase the generation of these species, controlled periodic illumination should favour CIP degradation. Parallel to the discussion from **section 4.2.2**, the benefit brought by lower duty cycles can only be effective when the catalyst is present [166], hence the high significance of the effect CD for CIP.

TMP, VEN and DV had low k_{app} values overall. The change in the matrix from MQ to tap water made the ROS species capable of their degradation unavailable and considerably hindered the degradation. Since TMP and VEN were impervious to photolysis, the presence of the catalyst (C) was their most significant positive effect. Moreover, this effect was positive and significant for every compound except SMX. As explained in **section 4.3**, the fast degradation rate of this pollutant by UV-C photolysis makes the addition of the catalyst acting as a “screening”, hindering the process and lowering the degradation rates. Due to that, the most significant effect for SMX was wavelength (B). The presence of the matrix (effects A and AB) was also highly significant for this compound, given that UV-C rays are more easily absorbed by tap water before reaching the target pollutant [212].

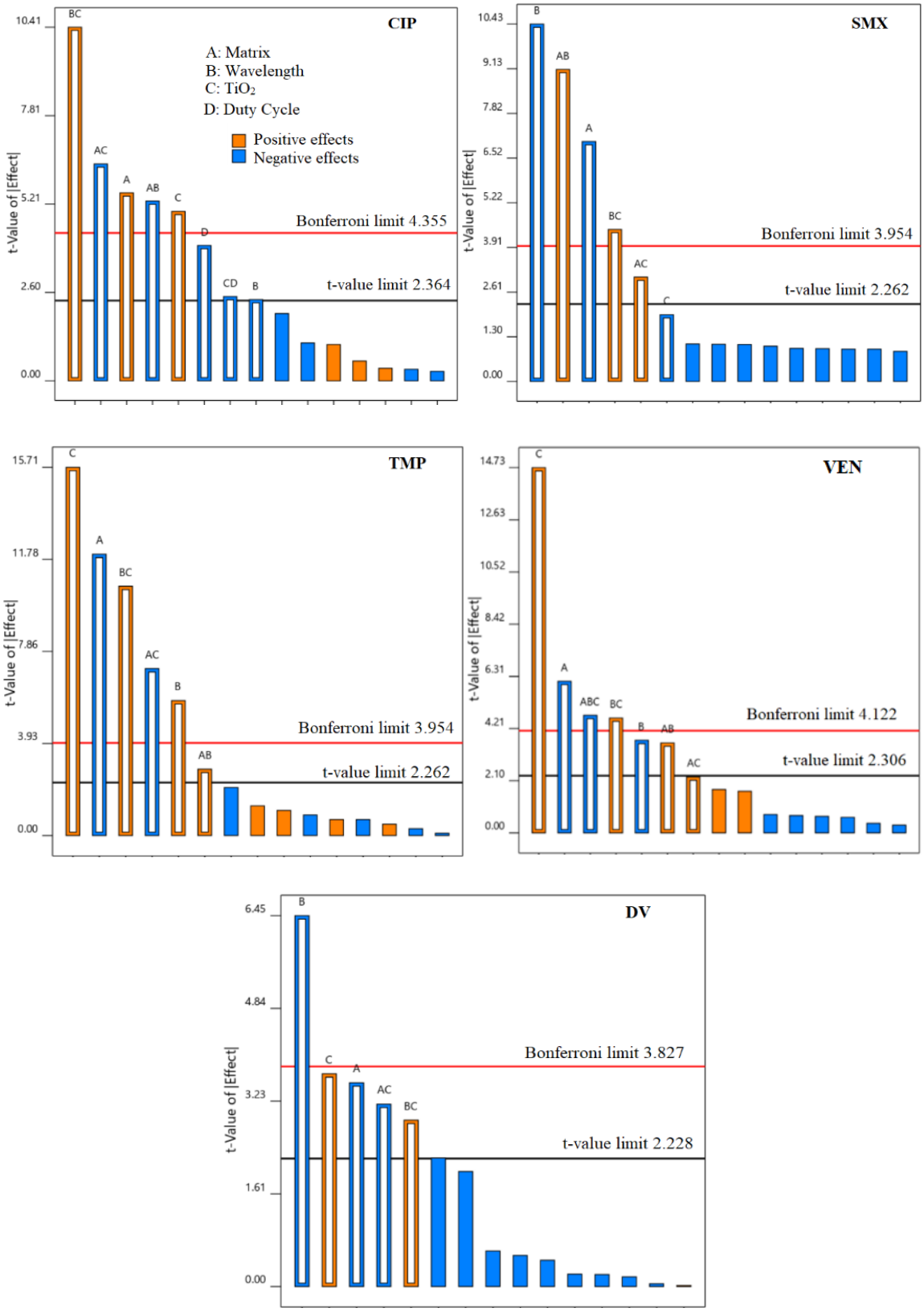

Figure 49. Pareto charts for the 5 target pollutants (DoE #2). Significant effects signalled with a white bar [212]

The plots comparing the predicted k_{app} values obtained by equations 40-44 with the experimental ones are shown in **figure 50**. It can be observed that VEN and DV did not have a correlation model as good as the other target pollutants. This might have happened due to the influence of other factors of high significance in the degradation of these compounds which were not considered in this design of experiments - such as the impact of countless TPs and the matrix's pH. The ANOVA data (**table 15**) for all OMPs, provided by the Design Expert software, show that the models were significant.

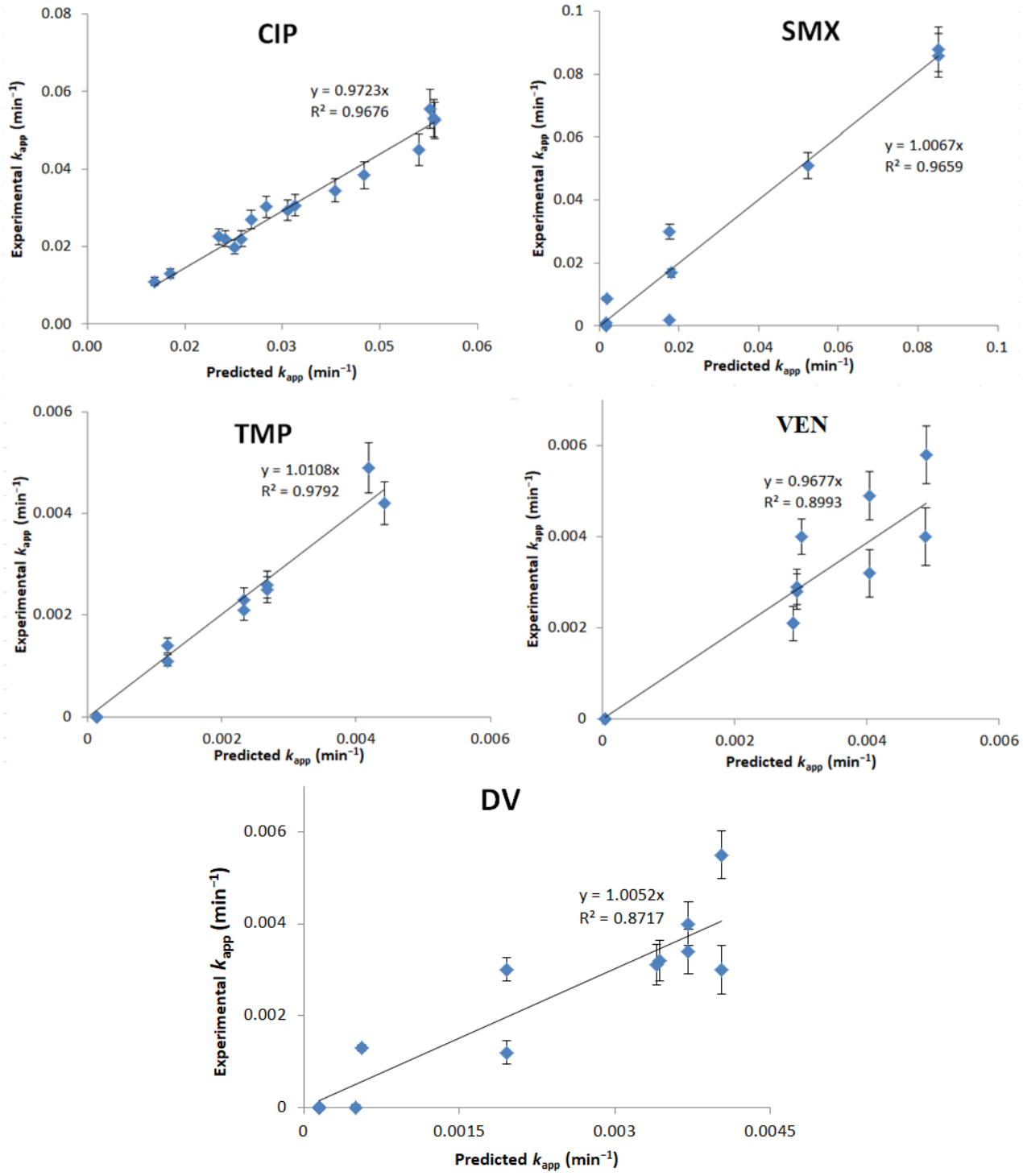

Figure 50. Predicted vs experimental k_{app} values for DoE #2 [212]

Table 15. ANOVA data for k_{app} values (DOE #2) [212]

Source	Sum of Squares	df	Mean Square	F-value	p-value	CIP
Model	0.0028	8	0.0004	32.58	< 0.0001	significant
A-Matrix	0.0003	1	0.0003	30.66	0.0009	
B-Wavelength	0.0001	1	0.0001	5.72	0.0480	
C-TiO_2	0.0003	1	0.0003	24.90	0.0016	
D-Duty Cycle	0.0002	1	0.0002	15.90	0.0053	
AB	0.0003	1	0.0003	28.03	0.0011	
AC	0.0004	1	0.0004	40.80	0.0004	
BC	0.0012	1	0.0012	108.44	< 0.0001	
CD	0.0001	1	0.0001	6.17	0.0420	
Residual	0.0001	7	0.0000			
Cor Total	0.0029	15				

Source	Sum of Squares	df	Mean Square	F-value	p-value	VEN
Model	0.0135	7	0.0019	47.20	< 0.0001	significant
A-Matrix	0.0015	1	0.0015	37.34	0.0003	
B-Wavelength	0.0006	1	0.0006	13.94	0.0058	
C-TiO_2	0.0088	1	0.0088	216.99	< 0.0001	
AB	0.0005	1	0.0005	13.15	0.0067	
AC	0.0002	1	0.0002	5.09	0.0541	
BC	0.0009	1	0.0009	21.46	0.0017	
ABC	0.0009	1	0.0009	22.46	0.0015	
Residual	0.0003	8	0.0000			
Cor Total	0.0138	15				

Source	Sum of Squares	df	Mean Square	F-value	p-value	SMX
Model	0.0133	6	0.0022	45.59	< 0.0001	significant
A-Matrix	0.0024	1	0.0024	49.05	< 0.0001	
B-Wavelength	0.0053	1	0.0053	108.83	< 0.0001	
C-TiO2	0.0002	1	0.0002	3.79	0.0833	
AB	0.0040	1	0.0040	82.91	< 0.0001	
AC	0.0005	1	0.0005	9.27	0.0139	
BC	0.0010	1	0.0010	19.68	0.0016	
Residual	0.0004	9	0.0000			
Cor Total	0.0137	15				

Source	Sum of Squares	df	Mean Square	F-value	p-value	TMP
Model	0.0000	6	6.5×10^{-6}	99.34	< 0.0001	significant
A-Matrix	9.4×10^{-6}	1	9.5×10^{-6}	144.09	< 0.0001	
B-Wavelength	2.2×10^{-6}	1	2.2×10^{-6}	33.15	0.0003	
C-TiO_2	0.0000	1	0.0000	246.87	< 0.0001	
AB	5.3×10^{-7}	1	5.3×10^{-7}	8.01	0.0197	
AC	3.3×10^{-6}	1	3.3×10^{-6}	50.75	< 0.0001	
BC	7.4×10^{-6}	1	7.4×10^{-6}	113.15	< 0.0001	
Residual	5.9×10^{-7}	9	6.6×10^{-8}			
Cor Total	0.0000	15				

Source	Sum of Squares	df	Mean Square	F-value	p-value	DV
Model	0.0135	5	0.0027	17.26	0.0001	significant
A-Matrix	0.0020	1	0.0020	12.56	0.0053	
B-Wavelength	0.0065	1	0.0065	41.61	< 0.0001	
C-TiO_2	0.0021	1	0.0021	13.69	0.0041	
AC	0.0016	1	0.0016	10.06	0.0100	
BC	0.0013	1	0.0013	8.38	0.0160	
Residual	0.0016	10	0.0002			
Cor Total	0.0151	15				

4.3.2.2 Total organic carbon and toxicity analysis

As it was explained throughout all **section 4.3,** the reactivity of each OMP can greatly vary one from the other, under the same treatment conditions. Furthermore, the removal of a target compound does not often result in its complete mineralization [222]. An overall analysis of the effluent total organic carbon percentage decrease (%TOC decrease) helps towards a better understanding of the general efficiency of each treatment. Equation 45 shows the obtained model for the %TOC decrease obtained from the DoE #2. Its half-normal plot is shown on **figure S3**. Its Pareto chart is shown on **figure 51**.

$$\%\text{TOC decrease} = 11.1187 - 6.1812A - 1.0437B + 2.4312C + 2.0313AB - 1.0688AC + 4.2438BC - 3.2813ABC \quad (45)$$

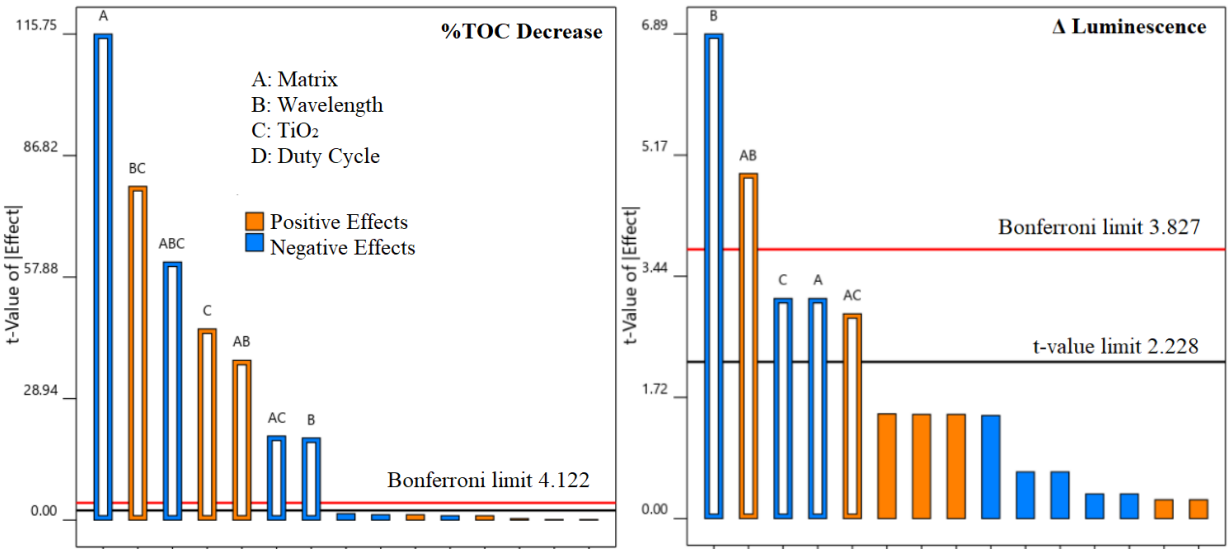

Figure 51. Pareto charts of %TOC decrease and Δ luminescence for DoE #2 [210]

The Pareto chart shows that the most significant effect for %TOC decrease was the matrix (A, negative), followed by the combined effect of wavelength and catalyst presence (BC, positive). These results reinforce the discussion of **section 4.3.2.1**, indicating that the performance of photocatalysis can be considerably hindered in real matrices such as tap water. Additionally, better degradation results were obtained either by UV-A photocatalyis or UV-C photolysis. **Figure 52** shows the plot comparing the predicted %TOC decrease values obtained from equation 45 and the real experimental values. Averagely, a mineralization of only 5% of TOC was achieved in the experiments performed in tap water, and of about 25% in the experiments performed in MQ water. The initial TOC value of tap water without OMP spiking was already very small (< 0.5 mg/L, **table 3**). This demonstrates how sensitive photocatalysis can be to the presence of organic matter and how its adoption for OMP removal in real wastewaters can result in little to no mineralization [92]. Both ANOVA data (**table 16**) and the excellent correlation of **figure 52** indicate that the prediction model of equation 45 for %TOC decrease is highly accurate.

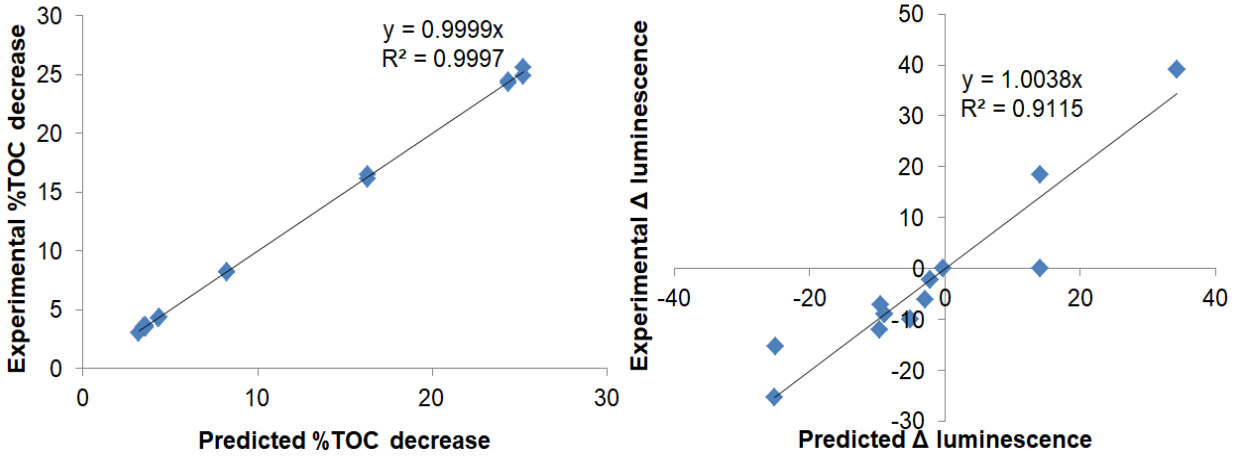

Figure 52. Predicted vs experimental %TOC decrease and Δ luminescence for DoE #2[212]

Table 16. ANOVA data for %TOC decrease and Δ luminescence in DoE #2 [212]

Source	Sum of Squares	df	Mean Square	F-value	p-value	%TOC decrease
Model	1268.04	7	181.15	3970.38	< 0.0001	significant
A-Matrix	611.33	1	611.33	13398.92	< 0.0001	
B-Wavelength	17.43	1	17.43	382.04	< 0.0001	
C-TiO_2	94.58	1	94.58	2072.89	< 0.0001	
AB	66.02	1	66.02	1446.92	< 0.0001	
AC	18.28	1	18.28	400.56	< 0.0001	
BC	288.15	1	288.15	6315.63	< 0.0001	
ABC	172.27	1	172.27	3775.68	< 0.0001	
Residual	0.3650	8	0.0456			
Cor Total	1268.40	15				

Source	Sum of Squares	df	Mean Square	F-value	p-value	Δ Luminescence
Model	4433.49	5	886.70	19.91	< 0.0001	Significant
A-Matrix	435.77	1	435.77	9.78	0.0107	
B-Wavelength	2113.70	1	2113.70	47.46	< 0.0001	
C-TiO_2	435.77	1	435.77	9.78	0.0107	
AB	1070.93	1	1070.93	24.05	0.0006	
AC	377.33	1	377.33	8.47	0.0155	
Residual	445.36	10	44.54			
Cor Total	4878.85	15				

The analysis of the variation in the bioluminescence of *Vibrio fischeri* provides an estimation of the changes in the effluent's toxicity after each one of the 16 experiments

performed during DoE #2. Equation 46 shows the obtained model for Δ luminescence. Its half-normal plot is shown on **figure S3** and its Pareto chart is shown on **figure 51**.

$$\Delta\,\text{Luminescence} = -0.6938 - 5.2188A - 11.4938B - 5.2188C + 8.1812AB + 4.8562AC \quad (46)$$

The results show that the most significant effect for Δ luminescence was the chosen wavelength. Applying lower values (UV-C) helped reducing the effluent's overall toxicity, while UV-A had the opposite effect, increasing it. The importance of evaluating the toxicity of the effluent prior and after an AOP treatment is of the highest priority, given that the formation of more toxic TPs would be completely against the main goal of water treatment itself. It has been reported by the literature that photolytic and/or photocatalytic degradation of CIP and SMX may result in more toxic by-products [33, 198]; often, degradation of TMP results in by-products as toxic as the main compound, even though TMP is considered toxic only in combination with other antibiotics due to synergistic effects [35, 194, 200]. In the first phases of the treatment steps, the degradation of VEN may produce more toxic compounds, followed by a toxicity decrease [186]. The toxicity of the effluent is subject to synergistic and antagonistic effects due to the mixtures of a multitude of compounds, being hard to be predicted [26, 42]. However, under the limited tested range of the DoE, it was possible to obtain a good prediction model using equation 46, considered significant by the ANOVA (**table 16**). The high significance of effects A (matrix, negative) and AB (matrix and wavelength, positive) indicates that cleaner matrices were able to attain lower final toxicity levels because they may allow a faster/higher degradation not only of the target compounds but also of the degradation by-products, as demonstrated by the highest mineralization (%TOC decrease) rates in MQ water.

4.3.3 Effect of initial pH on UV-A photocatalysis

As it was mentioned in **sections 4.3 and 4.3.2**, the changes in the matrix composition will affect the effluent's pH – which, on its turn, will influence the amount of ROS produced and affect OMPs' degradation rates. To further elucidate the impact of initial pH on k_{app} during UV-A photocatalysis, its value was adjusted with a few drops of NaOH or HCl to the solutions containing each of the 5 target pollutants (γ_0= 2 mg/L) in MQ water. UV-A photocatalysis was the chosen process due to its overall best results in **section 4.3.2.**

Figure 53 shows the obtained k_{app} values. All substances except SMX presented a degradation increase at higher pH, partially due to the effect of the terms represented in equation 19. As pH increases, more hydroxyl radicals are generated in detriment of positive holes h^+ (see **section 4.3.3** for a study of the reactivity of each one of the target pollutants to hydroxyl and superoxide radicals and h^+). The combination of the changes in the availability of the reactive species with the alterations in the dominant ionic species of each target pollutant (as presented in **section 4.3**) explains the variations in k_{app} of all the substances: while both CIP and TMP had more reactive species at pH >7, SMX presented the opposite behaviour. Since the pK_a of both VEN and DV are above 9, no considerable changes in their dominant ionic form took place and the difference in the reaction rates are due to the additional hydroxyl radical generated by the terms of equation 19 [223]. At initial pH = 5, the degradation of DV was completely inhibited.

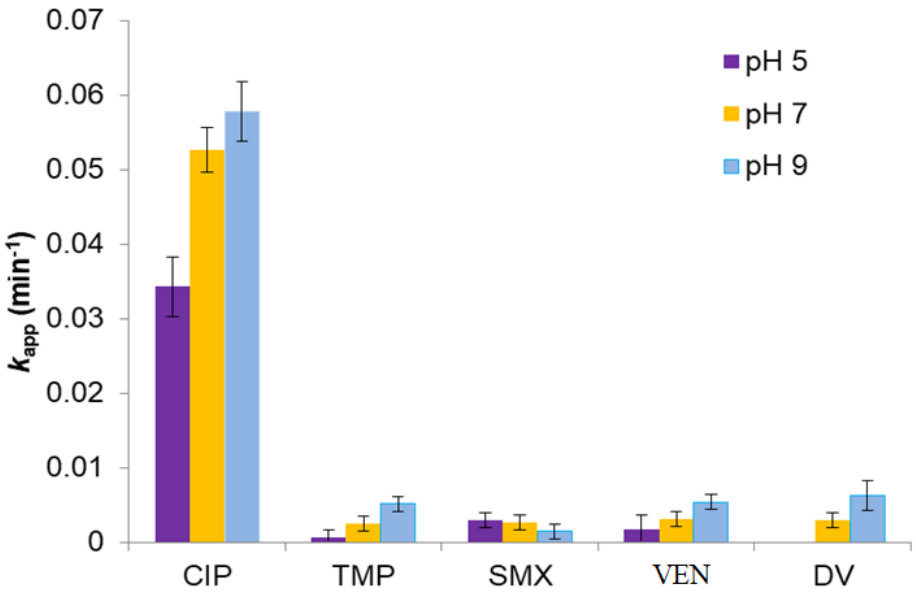

Figure 53. k_{app} values for different initial pH during UV-A photocatalysis in ultra-pure water [212]

4.3.4. Mechanisms of degradation for UV-A photocatalysis

Equations 20-22 and **figure 10** show possible reaction routes for target pollutants during photocatalysis. By adding scavengers which are known to be highly reactive to each one of these species, it is possible to estimate OMPs' reactivity and which reaction mechanisms take place. **Figure 54** shows the degradation plots of UV-A photocatalysis in MQ water for solutions, with a 100:1 (mass ratio) excess of scavengers of hydroxyl radical, superoxide radical and positive holes (and at γ_0 = 2 mg/L of each one of the 5 target pollutants). Their respective scavengers were isopropanol, triethanolamine and ammonium oxalate [82, 192, 224]. **Figure 55** shows the relative decrease in % of k_{app} in comparison with the experiments performed without the corresponding scavenger (**section 4.3**).

Analysing both **figures 54 and 55** it is evident that isopropanol completely inhibited the degradation of 4 of the target pollutants and decreased the k_{app} value of CIP about 50%. This demonstrates that the hydroxyl radical is the main contributor to the degradation during the photocatalysis. It is well established that the reaction constant rates of this ROS are generally higher than all the others. CIP and TMP showed a decrease of about 75% and 50% in their

degradation rates in the presence of triethanolamine, showing that these substances are reactive towards the superoxide radical. SMX, TMP and DV k_{app} values decreased approximately 35%, 15% and 25% (respectively) due to the presence of ammonium oxalate – indicating that positive holes h^+ also contribute to their degradation.

Although this analysis helps in elucidating the OMPs' reactivity and the chosen pathways, the results should be taken carefully. As an example, SMX's degradation was 100% inhibited by isopropanol; however, this does not mean that SMX is highly reactive towards hydroxyl radicals. It could mean that the hydroxyl radicals are the only substances in the system reacting with SMX, albeit slowly. By looking at **figure 54**, only 7% of SMX degradation was reached after 1 hour of reaction without any scavenger – which means that SMX generally resist considerably against this treatment. Moreover, the addition of scavengers may affect the matrix's pH, so it can be difficult to differentiate the effects caused by the pH from the ones caused by the scavengers [224].

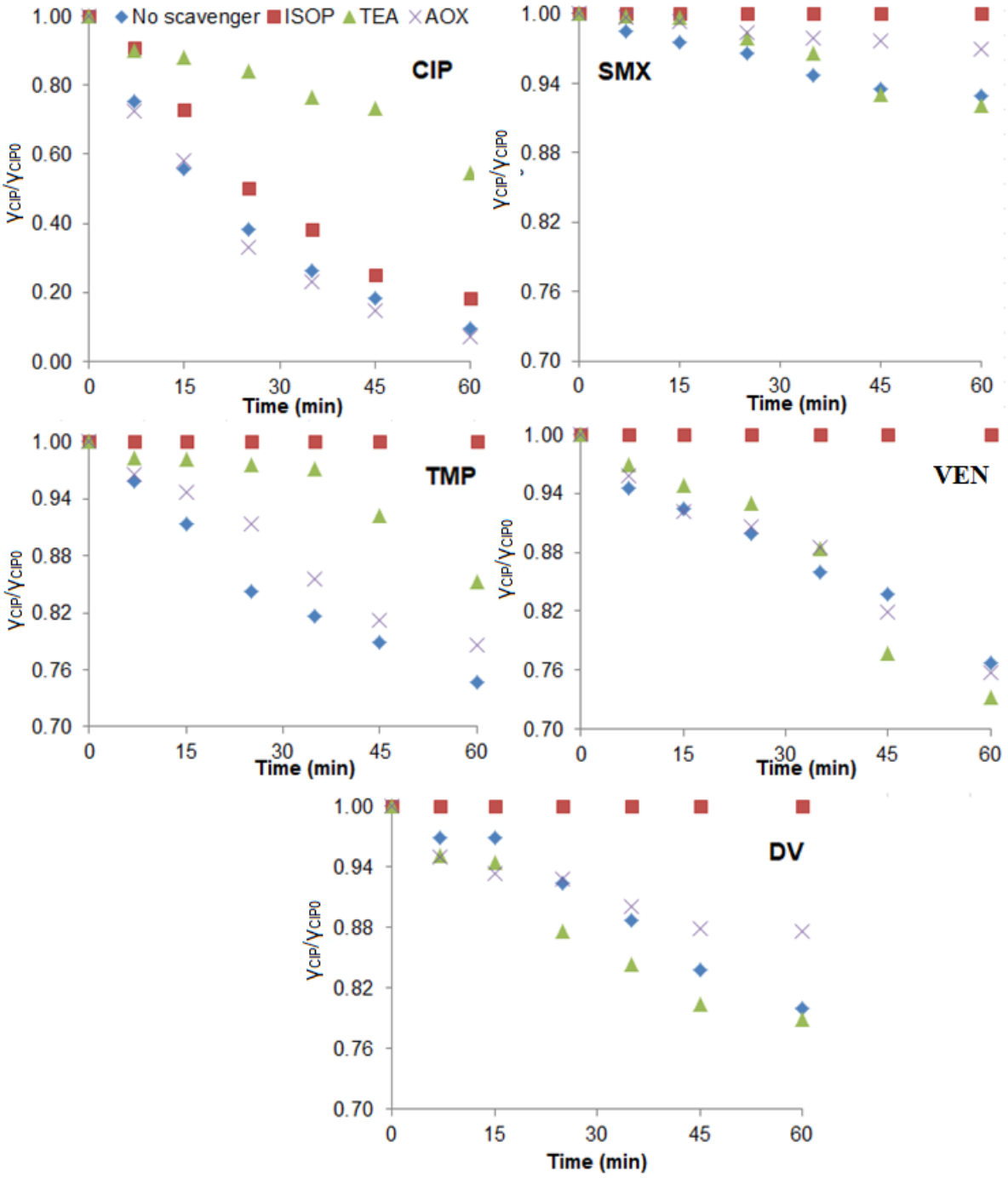

Figure 54. Degradation of target pollutants in the presence of scavengers for UV-A photocatalysis in MQ water (different scale for CIP) [212]

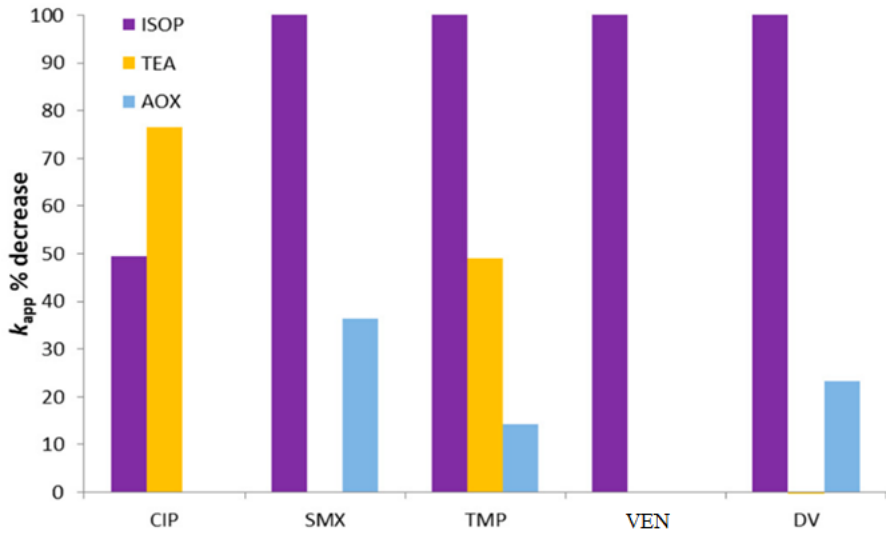

Figure 55. k_{app} % decrease in the experiments with the scavengers related to the experiments without them (UV-A photocatalysis in MQ water) [212]

4.3.5. Impact of bicarbonates, nitrates and humic acids on kinetic rates of UV-A photocatalysis

A third DoE was performed to investigate the effect of matrix components on the simultaneous degradation of CIP, SMX, TMP, VEN and DV (individual k_{app} values as the studied dependent variables) by UV-A photocatalysis using the LED array c (**figure 34**). A randomized response-surface Box-Benhken design with 16 runs was made with 3 independent variables on 3 levels. **Table 17** shows the chosen variables, their tested range and coded values. The list of necessary experiments performed provided by the Design Expert software can be found in **table 18**. Mathematical models for k_{app} prediction, ANOVA analysis and surface-response graphs were obtained by the software. Choices of square root transformations and different fits (linear or quadratic) were made to increase the adjusted and predicted R^2 values. As it was observed in **sections 4.3.2.1 and 4.3.3**, the matrix plays a significant role in photocatalytic degradation of OMPs.

The constituents of the matrix will influence the amount of light being absorbed by the system, the availability of ROS and the ionic state of each target pollutant (varying its reactivity) [121]. The choice of bicarbonates (HCO_3^-), nitrates (NO_3^-) and humic acids (HA) was made

because they are commonly found in water bodies (HA, specifically, in river and/or lake water [37]), so that the performance of UV-A photocatalysis is tested in a more real-like scenario. The tested range of **table 17** was loosely based on values of HCO_3^- and NO_3^- commonly found in tap water, as well as their regulations limits (50 mg/L for NO_3^-) [59, 225]. The tested range of HA was arbitrarily set to simulate the presence of organic matter in the matrix. The Box-Benhken design was chosen because it provides surface-response graphs which fit the continuous character of the independent variables for this section. Unlike the previous categorical designs described in **sections 4.2.1 and 4.3.2**, the mathematical models obtained in this section are not valid only at the limits of our coded tested range but throughout the whole interval of the range for all studied 3 variables. Kinetic results can be found in **table S1**.

Table 17. Variables and their ranges for DoE #3

Independent variable	**Lower level**	**Mid level (mg/L)**	**Higher level (mg/L)**
Bicarbonates (A)	0	200	400
Nitrates (B)	0	15	30
Humic acids (C)	0	1.5	3
Coded values	**-1**	**0**	**1**

Table 18. List of required experiments for DoE #3

Run	Coded variables		
	A	B	C
1	-1	-1	-1
2	0	-1	-1
3	-1	1	-1
4	-1	-1	1
5	1	-1	-1
6	0	-1	1
7	-1	0	-1
8	0	0	0
9	-1	-1	0
10	-1	0	1
11	-1	1	0
12	1	-1	0
13	1	0	-1
14	1	1	0
15	1	0	1
16	0	1	-1

Equations 47-50 show the obtained models for prediction of k_{app} values for 4 of the target pollutants.

$$\sqrt{k_{\mathrm{app}_{(\mathrm{CIP})}}} = 0.1940 - 0.0253\mathrm{A} - 0.0008\mathrm{B} + 0.0027\mathrm{C} - 0.0006\mathrm{AB} - 0.0023\mathrm{AC} - 0.0131\mathrm{BC} \quad (47)$$

$$\sqrt{k_{\mathrm{app}_{(\mathrm{SMX})}}} = 0.0340 - 0.007\mathrm{A} - 0.0015\mathrm{B} + 0.0043\mathrm{C} - 0.0053\mathrm{AB} - 0.0017\mathrm{AC} - 0.0006\mathrm{BC} + 0.0062\mathrm{A}^2 - 0.002\mathrm{B}^2 - 0.0027\mathrm{C}^2 \quad (48)$$

$$k_{\mathrm{app}_{(\mathrm{VEN})}} = 0.012 + 0.004\mathrm{A} - 0.0005\mathrm{B} - 0.0005\mathrm{C} + 0.00005\mathrm{AB} - 0.0004\mathrm{AC} + 0.0007\mathrm{BC} - 0.0059\mathrm{A}^2 - 0.0002\mathrm{B}^2 - 0.00017\mathrm{C}^2 \quad (49)$$

$$\sqrt{k_{\mathrm{app}_{(\mathrm{DV})}}} = 0.1154 + 0.0445\mathrm{A} + 0.0048\mathrm{B} + 0.0063\mathrm{C} - 0.0022\mathrm{AB} - 0.0032\mathrm{AC} - 0.0072\mathrm{BC} - 0.0447\mathrm{A}^2 - 0.009\mathrm{B}^2 + 0.0053\mathrm{C}^2 \quad (50)$$

Table 19 shows ANOVA data for all 5 target pollutants provided by the Design Expert software. An accurate model for TMP could not be obtained. A few hypotheses for that can be raised. First, under the tested range, an overall very low reactivity of TMP with all the agents present in the photocatalytic system. Perhaps a different range, shorter or larger, would result in a more accurate prediction. Secondly, the impact of other factors which were not accounted for in the DoE could be highly significant (e.g., initial pH, different TMP reactivity for different ionization states, and influence of multiple TPs). Finally, it is possible that none of these variables influence k_{app} values of TMP, or that their opposite effects cancel each other out.

Table 19. ANOVA data for DoE #3 [212]

Source	Sum of Squares	df	Mean Square	F-value	p-value	CIP
Model	0.0116	6	0.0019	21.37	< 0.0001	significant
A-Bicarbonates	0.0070	1	0.0070	76.67	< 0.0001	
B-Nitrates	5.9×10^{-6}	1	5.9×10^{-6}	0.0647	0.8049	
C-Humic acid	0.0001	1	0.0001	0.7926	0.3965	
AB	2.8×10^{-6}	1	2.8×10^{-6}	0.0309	0.8645	
AC	0.0000	1	0.0000	0.4399	0.5238	
BC	0.0011	1	0.0011	11.66	0.0077	
Residual	0.0008	9	0.0001			
Cor Total	0.0125	15				

Source	Sum of Squares	df	Mean Square	F-value	p-value	TMP
Model	3.2×10^{-6}	6	5.3×10^{-7}	1.65	0.2394	not significant
A-Bicarbonates	1.2×10^{-9}	1	1.2×10^{-9}	0.0037	0.9530	
B-Nitrates	2.0×10^{-8}	1	2.0×10^{-8}	0.06	0.8059	
C-Humic acid	3.4×10^{-7}	1	3.4×10^{-7}	1.07	0.3279	
AB	5.7×10^{-7}	1	5.7×10^{-7}	1.80	0.2128	
AC	5.9×10^{-7}	1	5.9×10^{-7}	1.84	0.2083	
BC	6.9×10^{-7}	1	6.9×10^{-7}	2.15	0.1768	
Residual	2.9×10^{-6}	9	3.2×10^{-7}			
Cor Total	6.0×10^{-6}	15				

Source	Sum of Squares	df	Mean Square	F-value	p-value	SMX
Model	0.0010	9	0.0001	21.96	0.0006	significant
A-Bicarbonates	0.0005	1	0.0005	90.20	< 0.0001	
B-Nitrates	0.0000	1	0.0000	3.40	0.1148	
C-Humic acid	0.0001	1	0.0001	23.13	0.0030	
AB	0.0002	1	0.0002	36.62	0.0009	
AC	0.0000	1	0.0000	2.77	0.1473	
BC	2.2×10^{-6}	1	2.2×10^{-6}	0.4350	0.5340	
A^2	0.0001	1	0.0001	18.56	0.0050	
B^2	0.0000	1	0.0000	1.98	0.2095	
C^2	0.0000	1	0.0000	4.55	0.0768	
Residual	0.0000	6	5.0×10^{-6}			
Cor Total	0.0010	15				

Source	Sum of Squares	df	Mean Square	F-value	p-value	VX
Model	0.0003	9	0.0000	22.63	0.0006	significant
A-Bicarbonates	0.0002	1	0.0002	111.08	< 0.0001	
B-Nitrates	1.6×10^{-6}	1	1.6×10^{-6}	1.05	0.3460	
C-Humic acid	2.5×10^{-6}	1	2.5×10^{-6}	1.64	0.2475	
AB	1.6×10^{-6}	1	1.6×10^{-6}	1.07	0.3403	
AC	1.2×10^{-6}	1	1.2×10^{-6}	0.77	0.4149	
BC	2.9×10^{-6}	1	2.9×10^{-6}	1.93	0.2146	
A^2	0.0001	1	0.0001	48.33	0.0004	
B^2	1.5×10^{-6}	1	1.5×10^{-6}	0.0978	0.7651	
C^2	6.2×10^{-6}	1	6.2×10^{-6}	0.0412	0.8459	
Residual	9.0×10^{-6}	6	1.5×10^{-6}			
Cor Total	0.0003	15				

Source	Sum of Squares	df	Mean Square	F-value	p-value	DV
Model	0.0279	9	0.0031	21.90	0.0006	significant
A-Bicarbonates	0.0187	1	0.0187	131.81	< 0.0001	
B-Nitrates	0.0002	1	0.0002	1.30	0.2984	
C-Humic acid	0.0003	1	0.0003	2.25	0.1841	
AB	0.0000	1	0.0000	0.23	0.6518	
AC	0.0001	1	0.0001	0.45	0.5261	
BC	0.0003	1	0.0003	1.78	0.2310	
A^2	0.0053	1	0.0053	37.67	0.0009	
B^2	0.0003	1	0.0003	1.87	0.2202	
C^2	0.0001	1	0.0001	0.64	0.4550	
Residual	0.0008	6	0.0001			
Cor Total	0.0288	15				

Figure 56 shows the plots of predicted vs experimental values of k_{app} using the four models from equations 47-50. Good fits, higher than 0.93, were obtained.

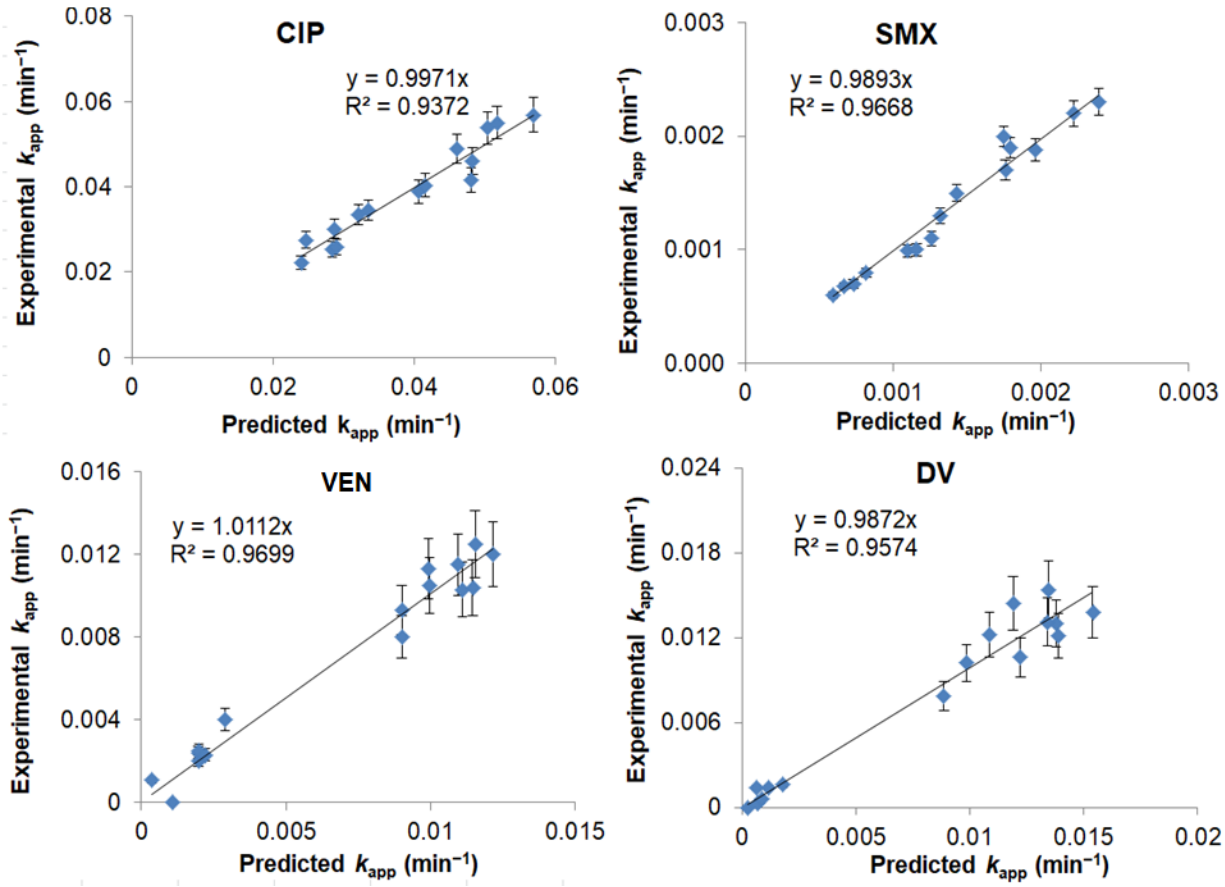

Figure 56. Predicted vs experimental values of k_{app} for DoE #3 [212]

The surface graphs obtained by the software applying the equations 47-50 are shown on **figure 57**. By analysing them together with the ANOVA data, it is possible to confirm the high significance of the presence of bicarbonates given the high F-values of A and A^2 (when the quadratic model is applied) effects for all OMPs. Interestingly, the presence of bicarbonate had a positive impact for the degradation of VEN and DV, whilst a negative impact for CIP and SMX. According to equation 1, bicarbonates act as radical scavengers of hydroxyl radicals, hindering their reaction with target pollutants. However, the presence of bicarbonates increases the pH of the matrix [226], which could be beneficial for photocatalytic degradation in some cases. By looking at **table S1**, the initial pH-value of the investigated water sample was higher in the experiments involving bicarbonates, which has been shown in **section 4.3.3** to decrease SMX and increase VEN and DV k_{app} values. Although it has been shown that the k_{app} of CIP should increase under higher pH, the presence of the same scavenger which causes this pH increase ends

up hindering the degradation. This is possibly due to the high reactivity of CIP to hydroxyl radicals. Being so, the benefit brought by a higher pH-value is not sufficient to increase (or even maintain) the ROS availability and CIP k_{app} goes down. Although it is not possible to differentiate the scavenging effect of bicarbonate from the effect of the modification of the pH in the matrix, it is possible to estimate, by observing the change in the k_{app} values, if this variable has an overall positive or negative effect on the degradation of each target pollutant.

The presence of nitrates and humic acids in the matrix may cause positive and negative effects on the degradation, with every target compound responding differently to specific process conditions. Humic acids may cause screening effects and divert radicals from the target compounds and lower their availability (negative effect) or they can generate new radicals via photosensitization under UV light (positive effect) [37, 121, 227]. Nitrates can act as electron aceptors on the catalyst valence band, hampering ROS production (negative effect), or undergo photolysis under UV light, creating more radicals (positive effect) [37, 228]. Additionally, the possible reaction pathways of humic acids and nitrates with a multitude of TPs may cause all sorts of unpredicted inhibition or promotion effects. In **figure 57** it is possible to see that the presence of nitrates and humic acids was not highly significant for VEN and DV. For CIP, a higher degradation was obtained for the matrices combining higher concentrations of humic acids and lower ones of nitrates, or vice versa (BC effect). The presence or the absence of both of them at the same time led to lower degradation rates. For SMX, the addition of humic acid had an overall positive effect, and the presence of nitrates was beneficial as long as the bicarbonates were low (AB effect).

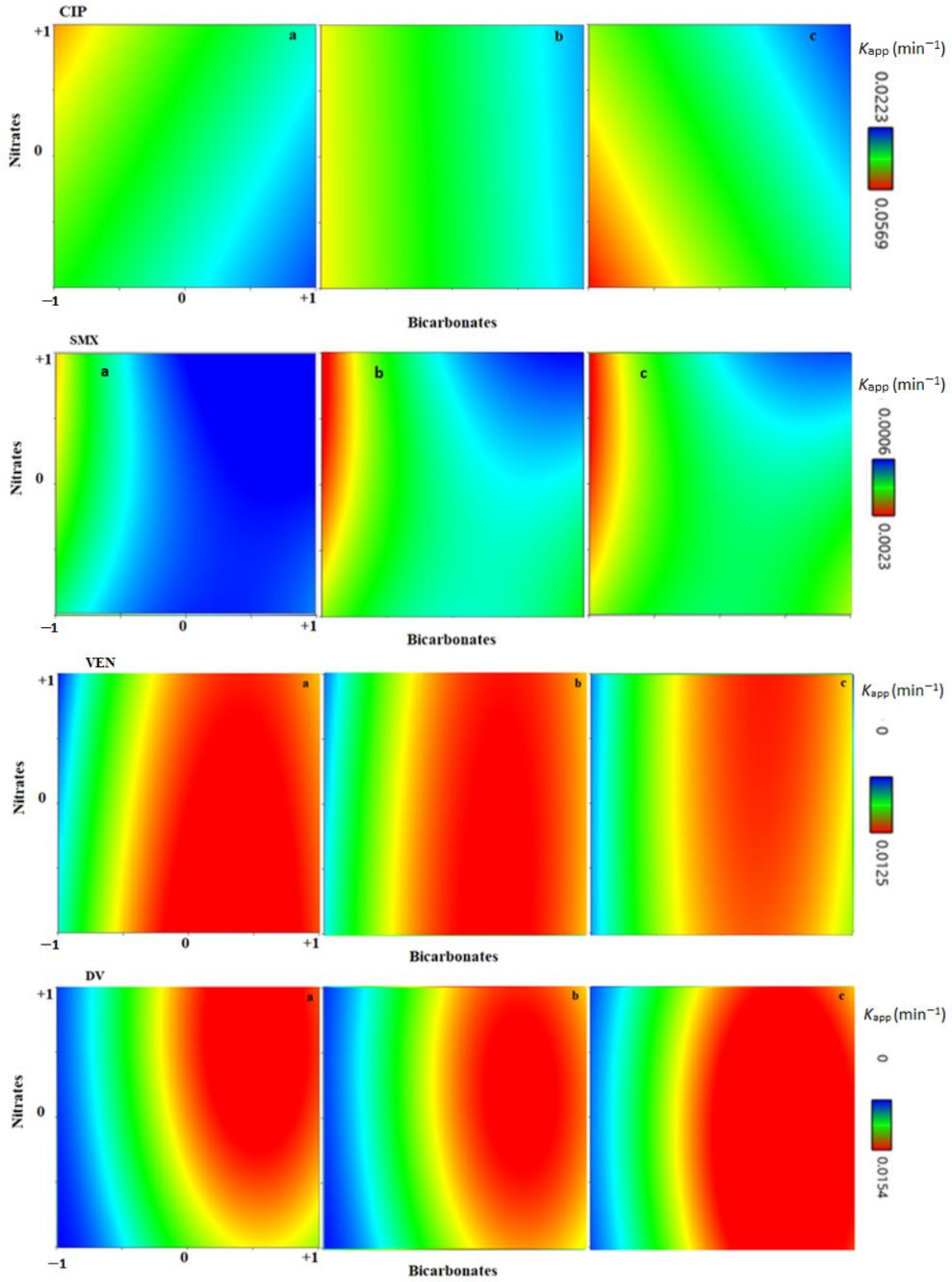

Figure 57. Surface graphs of k_{app} for CIP, SMX, VEN, and DV. X-axis: coded bicarbonates; Y-axis: coded nitrates; a, b, and c of each row represents humic acids coded values of −1, 0, and +1, respectively [212]

4.3.6 Simultaneous wavelength and E_{EO} analysis

The inclusion of E_{EO} analysis as a dependent variable for DoEs #2 and #3 could not be done due to the fact that, for some experiments, experimental k_{app} was equal to zero. Replacing this value on equation 37 results in E_{EO} tending to infinity (∞) and valid equation models would not be obtained. However, it is of paramount importance to evaluate E_{EO} values for the different scenarios discussed so far. **Figure 58** shows E_{EO} values obtained for all 5 target pollutants during their simultaneous degradation under different conditions. The standard performances in MQ water were compared with cases using duty cycle and two simultaneous wavelength (SW) variants. In the first one (P or PC, SW3 LEDs), two strips of UV-A LED and one of UV-C LED were used. In the second one (P or PC, SW6 LEDs), three strips of both UV-A and UV-C LEDs were used simultaneously (see **table 6**). The obtained kinetic results are shown in **table S1**.

Figure 58 helps to analyse the possible benefits brought by additional light sources and controlled periodic illumination (as it was made in **section 4.2.2**, but now including UV-C sources). The impact of simultaneous wavelength and the use of a real water matrix (tap water) on E_{EO} performance were also evaluated.

Although controlled periodic illumination has shown potential to reduce energy expenses [121, 163], the results show that lowering duty cycle led to contrasting results. UV-A photocatalysis had a reduction on E_{EO} values for most target compounds (except TMP), but UV-C photocatalysis did not show any considerable improvement. This is possibly due to the fact that, when UV-C light is used, photolytic rates can be responsible for a larger proportion of OMP degradation due to their higher energy levels. As it was explained in **section 4.2.1**, controlled periodic illumination can only benefit photocatalytic rates, not photolytic ones [166].

The use of simultaneous wavelength did not present any significant gain in E_{EO} compared to the standard photoreactor design. As explained in **section 2.9**, the effect of wavelength coupling could benefit both photolysis and photocatalysis, but when light sources with too far away wavelengths (like the present case, UV-C and UV-A) are used simultaneously, no wave interference takes place [212]. Moreover, adding more light sources generally led to an increase in E_{EO} values in most cases. This is in agreement with the results of **section 4.2.1**, in which the kinetic benefit brought by additional light sources did not compensate the supplementary required

energy. The results in tap water were also diverse, with CIP obtaining lower E_{EO} values, while other compounds demanded more energy to be degraded, or even becoming completely impervious to degradation in some cases. As it was explained in **section 4.3.2**, tap water contains substances which may benefit or hinder the degradation, depending on the target pollutant.

E_{EO} values in **figure 58** range approximately between 100 and 1000 kWh m^{-3}, as expected by recent literature reviews on this topic, still being considered unfeasible for practical purposes [6, 121]. The low photonic efficiency is an intrinsic problem of photocatalysis that can be reduced, but (so far) not completely overcome by new advances in UV-LED technology. Moreover, E_{EO} values greatly vary depending on the target pollutant and the treatment of choice. Each pollutant can respond differently depending on the emitted wavelength. Nevertheless, both UV-A and UV-C E_{EO} magnitudes are on the same average level, which represents an important advance in this technology. A non-significant difference was observed between UV-A and UV-C LEDs. Until a few years ago, a main concern regarding UV-LEDs was that the UV-C range was exceedingly energy-demanding when compared to longer wavelengths [7]. As it was seen throughout this work, UV-C can greatly contribute to the degradation of compounds highly reactive to it, even if its combination with TiO_2 is not recommended.

The recent advances in the UV-LED technology have been exponentially increasing its wall-plug efficiency and, as mentioned in **section 2.9**, this has a direct impact on the feasibility and affordability of the process. The foreseen improvements of 10 to 20 times in E_{EO} values in the next 4 years [173] will not be enough to make this technology as sustainable as one would like, but will certainly represent a significant advance.

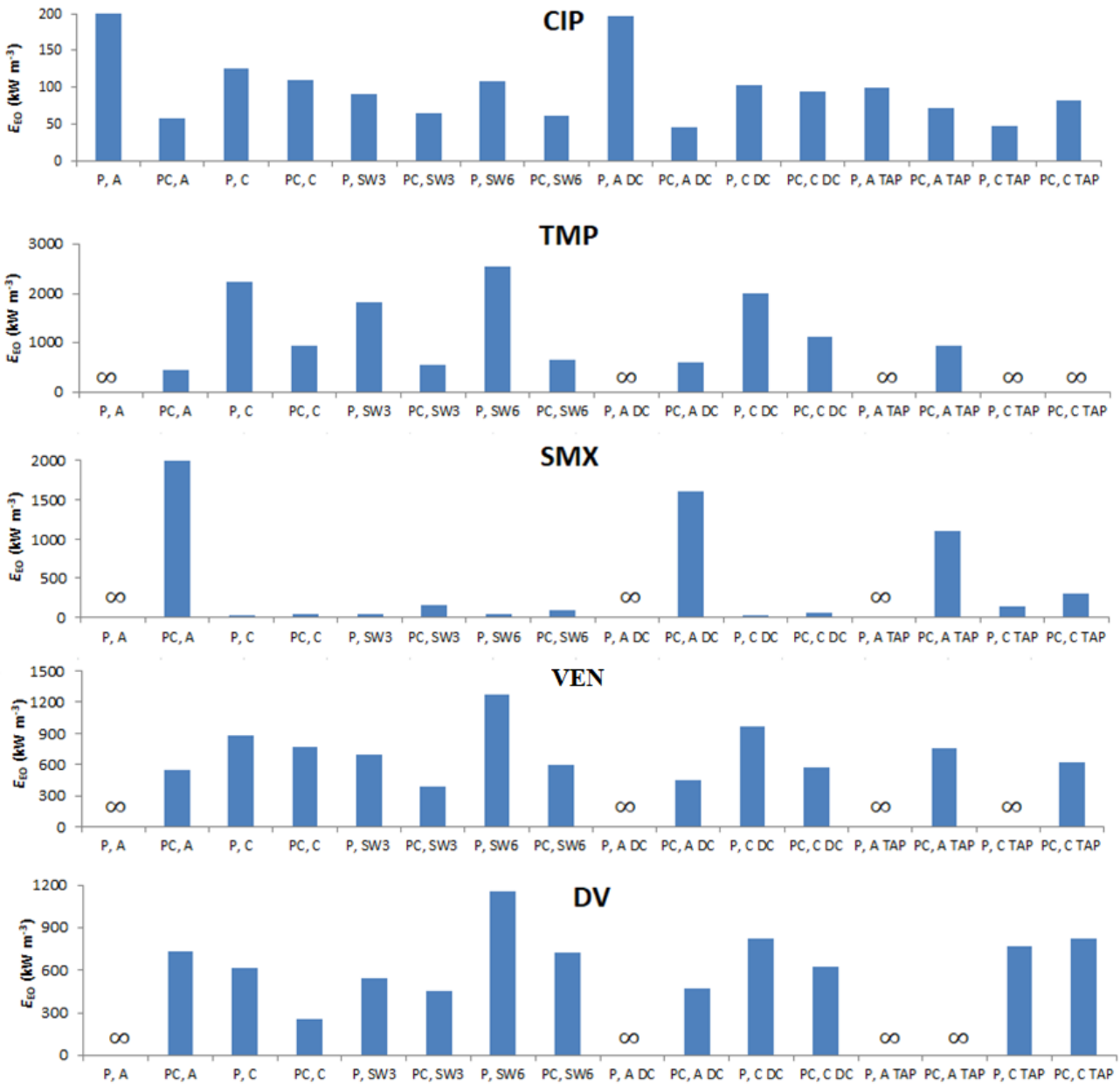

Figure 58. E_{EO} values for the 5 target pollutants under different scenarios. Experiments performed in MQ water, except the ones labelled with "TAP" (tap water). Experiments performed under continuous illumination, except the ones labelled with "DC" (duty cycle = 0.50) [212]

4.4. Investigation of transformation products

4.4.1 Correlation between transformation products and toxicity for UV-A photocatalysis

Figure 59 shows the degradation plots during UV-A photocatalysis for solutions containing the target pollutants individually (γ_0 = 10 mg/L) in MQ water. In the same graphs, the inhibition of *Vibrio fischeri* was monitored as representative of the solution's toxicity. Experiments ran until the complete degradation of the parent compound or until a maximum of 6 hours. The results show that the toxicity of all the solutions varied with time due to the degradation of parent compounds and, likely, due to the formation (and abatement) of TPs. Different behaviours, however, were observed. CIP had a peak with the highest toxicity value (100% of inhibition at 2 h) and even after its complete degradation (3.5 h) the solution presented 22% of inhibition. SMX had an initial decrease in the toxicity, reaching only 10% of inhibition after 2 h, only to increase steadily again up to 56% of inhibition after 6 h of reaction. In the solution containing TMP, the inhibition was always low, but after its complete degradation, the solution still presented an inhibition of about 8%. VEN had a toxicity peak in the first minutes of degradation, which was further reduced only to increase again up to 53% after 6 hours of reaction. Finally, DV's solution presented a slow but steady increase of toxicity with time, showing 50% of inhibition even after almost 80% of the parent compound degradation. The toxicity levels were always higher at the end than at the beginning of the reaction, indicating the formation of TPs more harmful to *Vibrio fischeri* than the parent compounds. Similar results are ubiquitous in the literature [33, 35, 54, 196, 229].

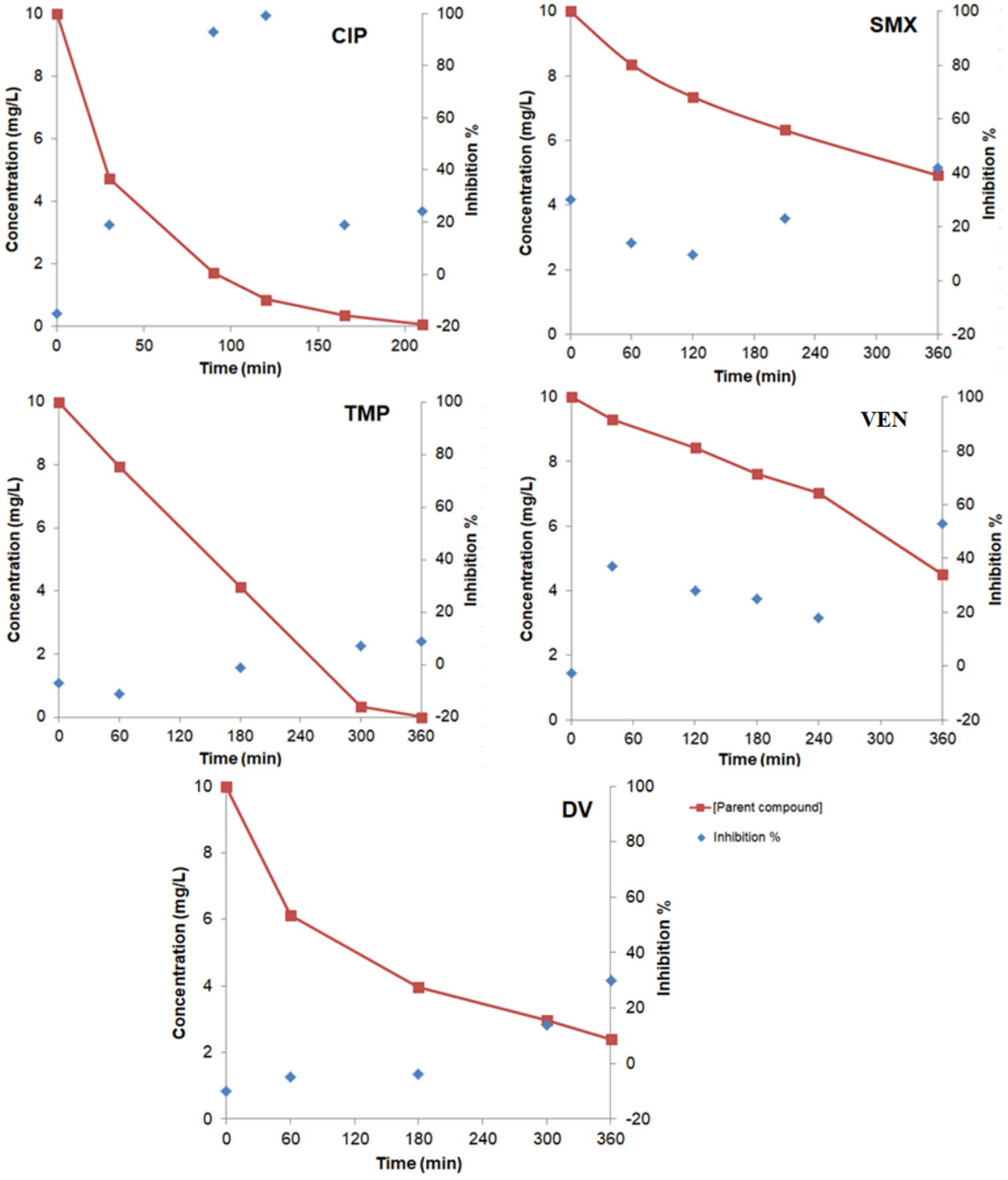

Figure 59. Curves of *Vibrio fischeri* bacteria luminescence inhibition during UV-A photocatalysis of solutions containing the target pollutants individually

Preliminary TP monitoring (as newly formed peaks) performed using the HPLC-PDA for the same experiments from **figure 59** is shown in **figure 60**. Initially, these TPs were not properly identified, so they are generically called TP-A, TP-B (etc) in respect to each parent compound in **figure 60**. Once the TP is identified, it is assigned by the parent compound followed by a number (e.g. DV-2). It was not possible to detect any TP for VEN. A common problem which increases the complexity of the system is the possibility of synergistic toxic effects of different compounds in the mixture. Toxicity synergy occurs when the health effect caused by the exposure to multiple chemicals at the same time is greater than the sum of the effects of the individual chemicals [42]. Synergy can be observed when analysing **figures 59 and 60** since changes in *Vibrio fischeri* inhibition cannot be directly attributed to the formation of the detected TPs or to the degradation of the parent compound. Nonetheless, some preliminary hypotheses of possible correlation between the toxicity and the detected compounds can be made. Four different TPs were observed for CIP, and the peak area of TP-B corresponds to the maximum *Vibrio fischeri* inhibition value observed, suggesting that the increase in the toxicity can be, at least partially, related to this compound. For CIP at t = 90 minutes, CIP, TP-A, TP-C and TP-D were abated while TP-B increased, jointly to a toxicity increase. For SMX, an increase in the toxicity was observed with a decrease of the parent component and an increase of the detected TP. No direct relation between the concentration of the detected TP of DV and the toxicity could be found, but it is apparent that the toxicity of the solution increased (initially slowly and faster after t = 180 min) when the parent compound was degraded. For TMP, there was no significant increase in the toxicity, regardless of the complete degradation of the parent compound and the formation of at least two TP.

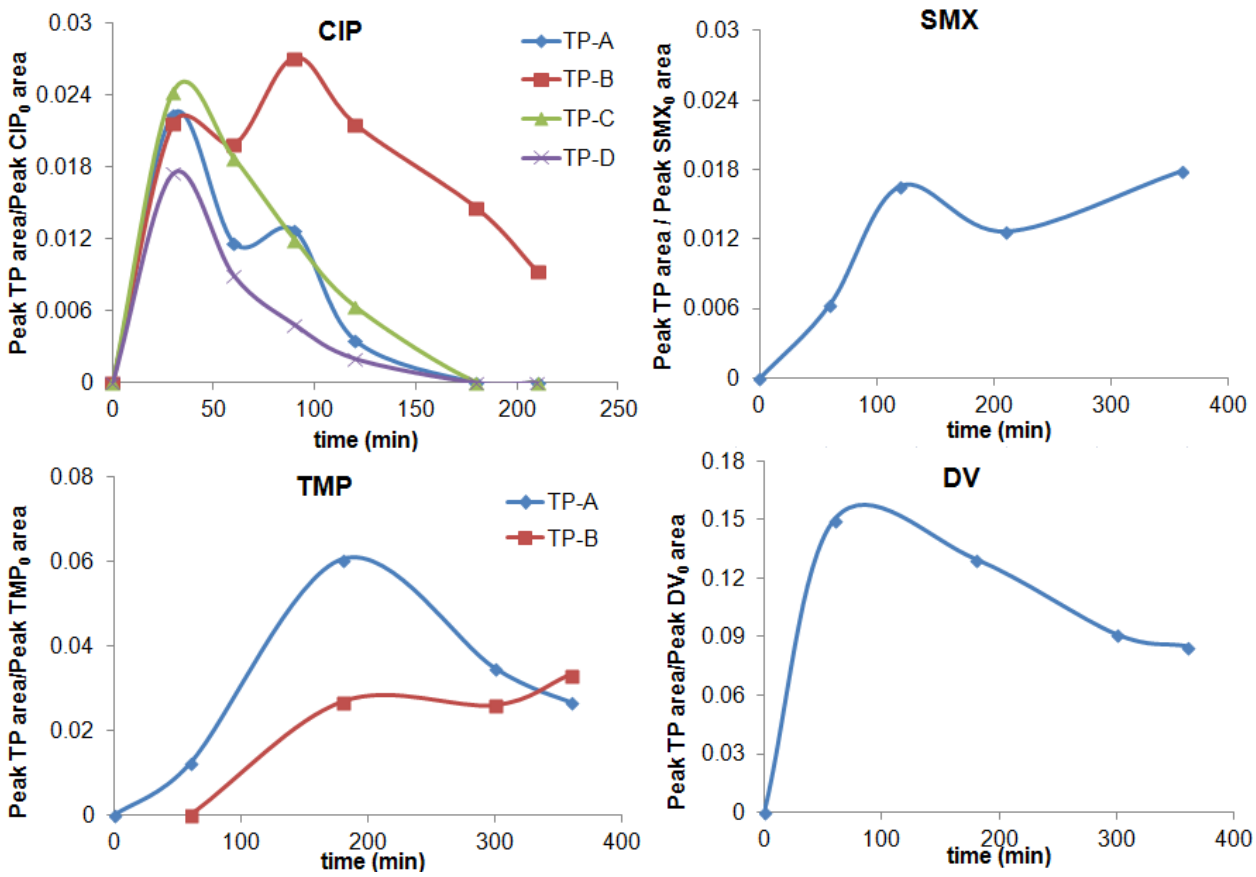

Figure 60. Preliminary TPs monitoring by HPLC-PDA for the experiments of **figure 60**

The LC-MS Orbitrap analysis was able to identify, with different levels of confidence [201], the list of TPs on **table S2** for UV-A photocatalysis in MQ water of initial solutions of TMP, VEN and DV. The analysis of CIP and SMX could not properly identify any TP previously found in the literature or new ones with an acceptable level of confidence. Possible reasons for that are: 1) hydrolysis of TPs; 2) an inadequate chromatographic method; 3) contamination of samples before, during or after the experiment; 4) inadequate ionization method, collision energy levels or other MS configuration parameters. The literature regarding the TPs of CIP suggests that the initial reaction is the defluorination (favored at high pH) [107], followed by the oxidation and opening of the piperazine ring [32, 40]. For SMX, the literature suggests that under the photolytic and photocatalytic routes the molecule undergoes a cleavage forming smaller TPs, like sulfanilic acid and 4-amino-N-(5-methyloxazol-2-yl) benzenesulfonamide [35, 198, 230].

Figures S4-S8 shows the MS^2 spectra of the detected TPs. **Figure 61** shows the TPs' peaks over time and **figures 62-64** show the proposed TPs.

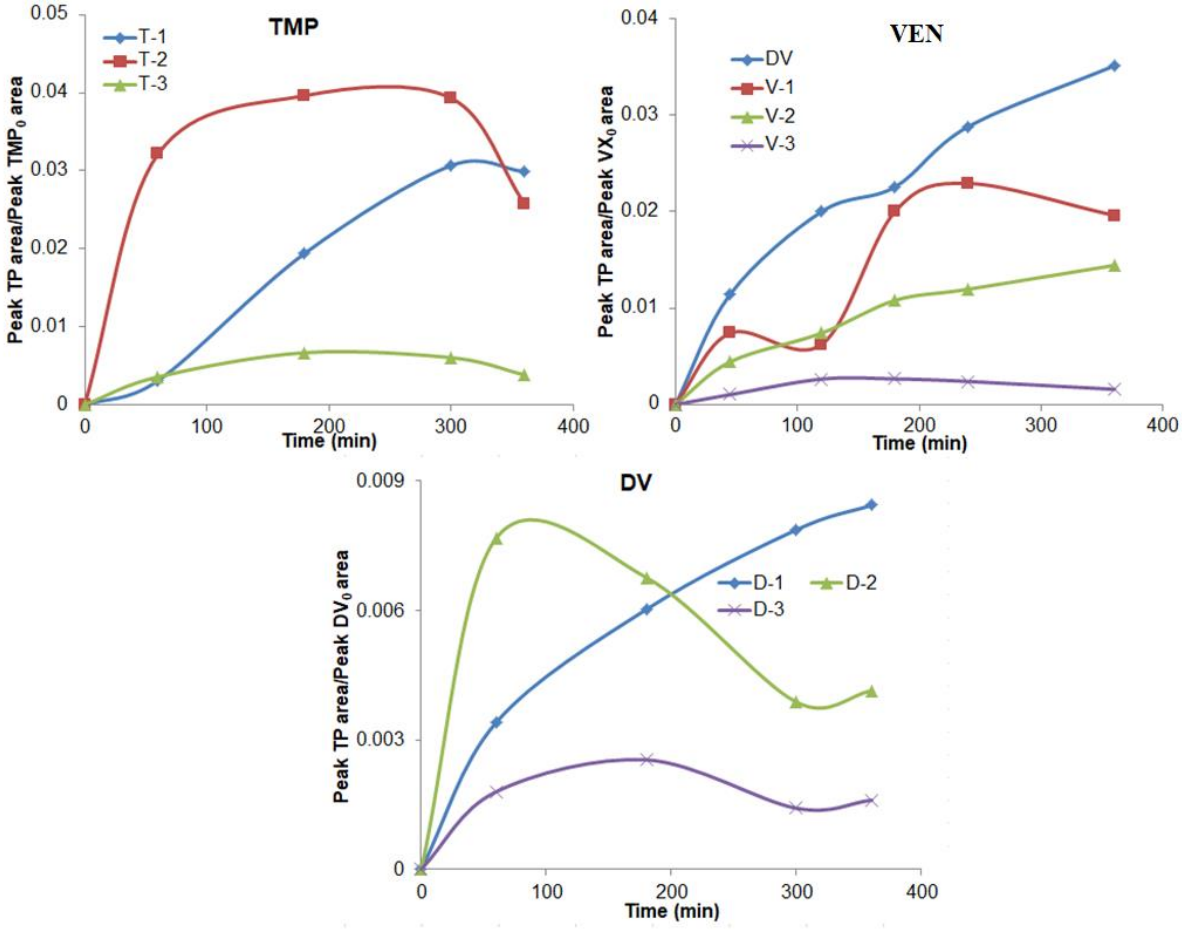

Figure 61 LC-MS monitoring of TPs over time during the experiments of **figure 59.**

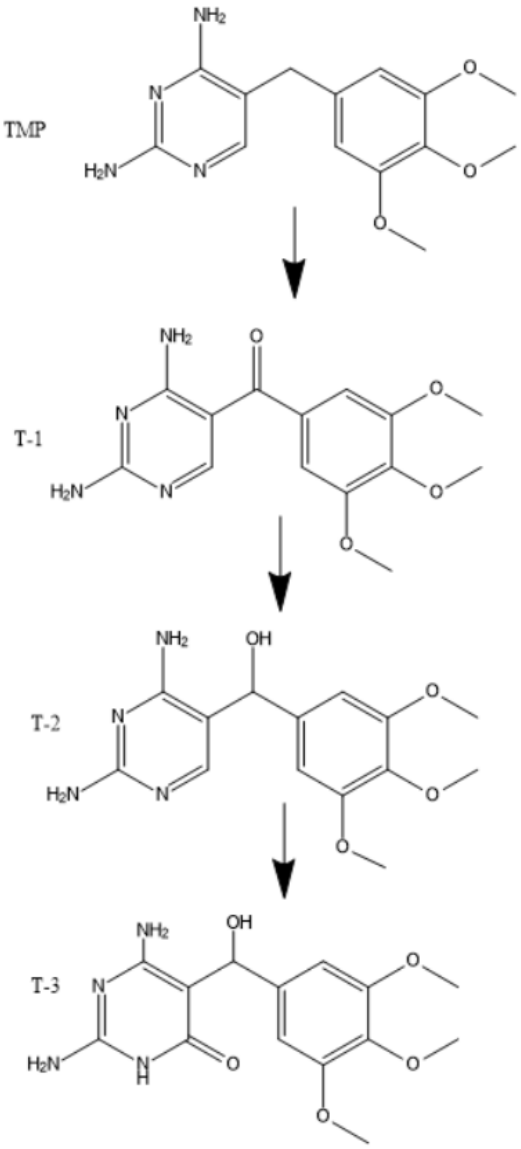

Figure 62. Proposed TPs for TMP during UV-A photocatalysis

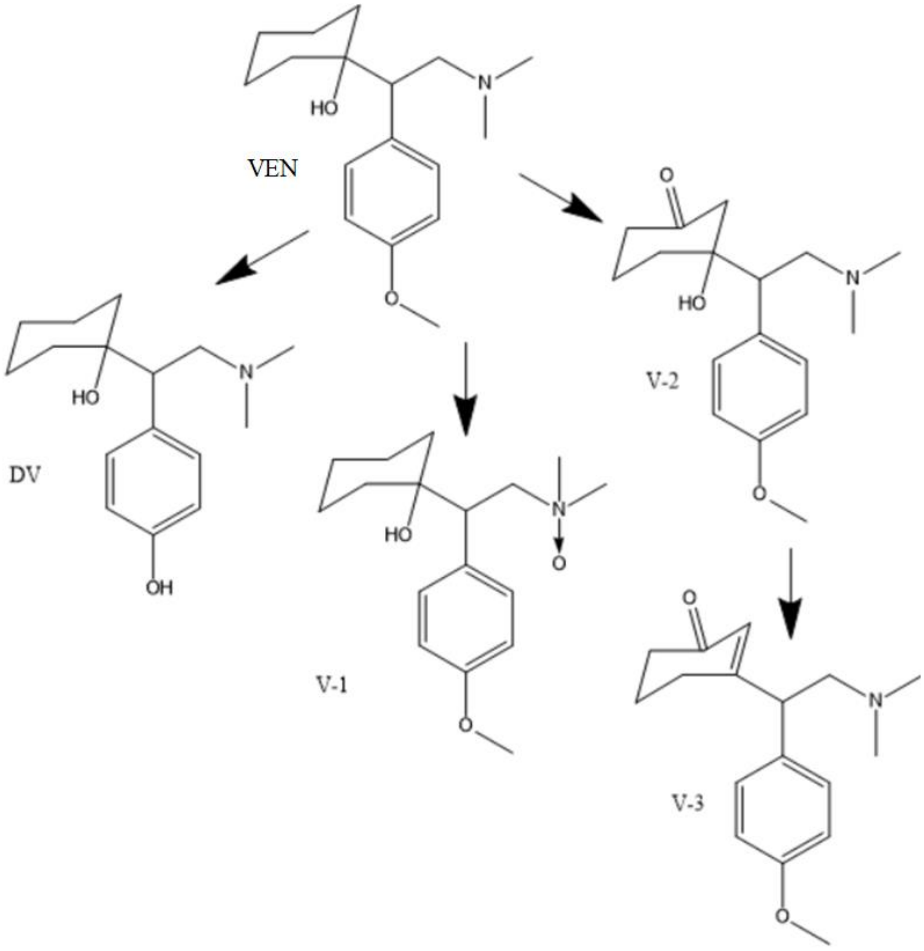

Figure 63. Proposed TPs for VEN during UV-A photocatalysis

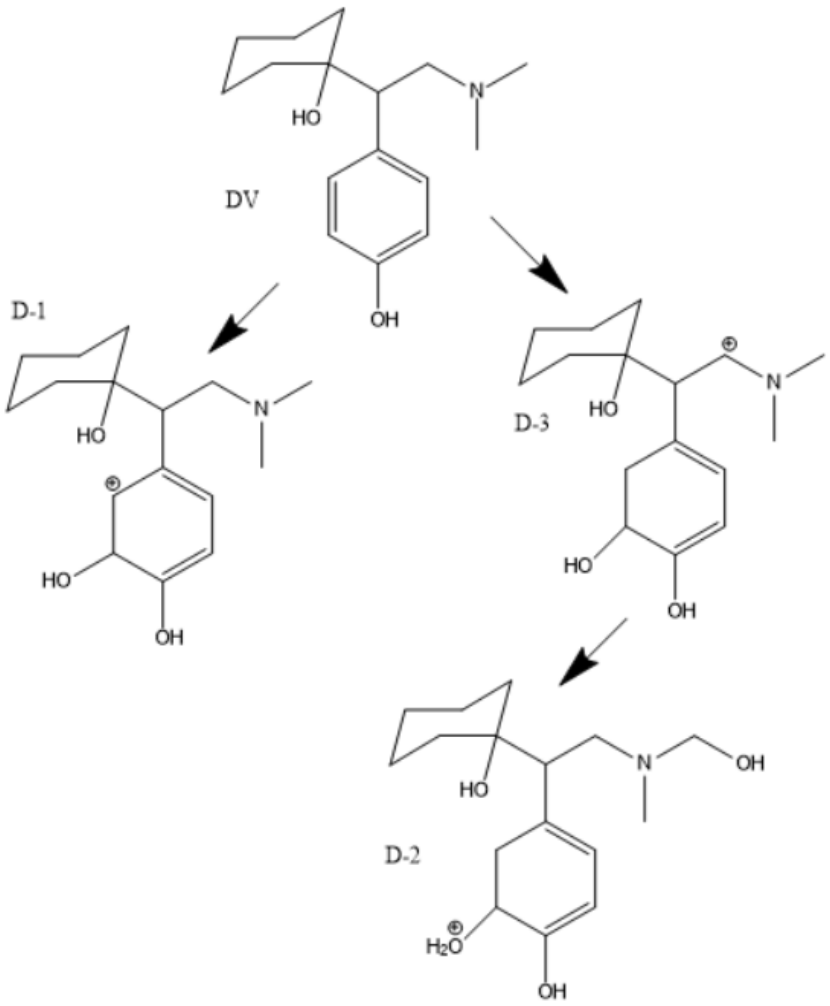

Figure 64. Proposed TPs for DV during UV-A photocatalysis

Analysing the TPs of TMP, the formation of T-1 and T-2 (**figure 62**) comes from the oxidation of the bridging methyl group between the two rings. Similar results were obtained elsewhere [35, 113, 194]. By comparing TMP data on **figure 60 and 61**, TP-A and TP-B might be associated with T-2 and T-1, respectively, since their concentration vs time plots were similar. The formation of T-3, in smaller concentrations, was detected by the Orbitrap. This compound comes from the oxidation of the pyrimidine 2,4-diamine ring [200]. Regardless of the parent compound being completely removed after 6 hours of treatment, smaller TPs could not be found.

Regarding VEN, the most common TP found, and the only one that could be completely confirmed by direct MS^2 comparison with the standard, was DV. The compound is formed by

demethylation. The other TPs in **figure 63** are related to an oxidation at different points of the molecule [186]. The compound V-1 was newly identified by the software as a probable structure. A relation between VEN's TPs and the toxicity suggests that the compounds formed during the photocatalysis are more toxic than the parent compound, since the inhibition of *Vibrio fischeri* increased with time (**figure 59**). However, this increase could not be directly related to any TP in particular.

As for DV (**figure 64**), the degradation pathways followed the hydroxylation of the aromatic ring, as previously described in [195]. It is possible that the TP found in the preliminary analysis (**figure 60**) is D-2 due to their similar concentration vs time plots. There might be a correlation between the increase in the toxicity and the increase of TP D-1, since *Vibrio fischeri* inhibition increased when more of this compound was detected.

Toxicity could be related to TPs that were not detected by the Orbitrap, possibly due to their smaller size and/or possibly short lives. Another important point to consider this analysis solely an initial approximation is the fact that, although performed under the same conditions, samples for the *Vibrio fischeri* experiments and the preliminary TP analysis were taken from an experiment in Zagreb while the Orbitrap analysis was performed using samples from a replicate experiment done months later in Girona. Further experiments and more solid methodologies are necessary for a more accurate analysis.

4.4.2 Correlation between transformation products and matrix for UV-A photocatalysis

The same TPs for TMP, VEN and DV from the previous section (**table S2**) were observed when UV-A photocatalysis was performed in tap water. Nevertheless, their concentration changed. **Figure 65** shows the monitoring of the TPs over time for UV-A photocatalysis in tap water. As it was previously mentioned (**section 4.3.2**) changes in the matrix affect the availability of the radicals and, consequently, the pollutants' degradation rates. It can be observed in **figure 64** that T-1 was much more recalcitrant in tap water than in MQ. It is possible that the decrease in available radicals in tap water make the second reaction step of **figure 62** slower. Compared to **section 4.4.1,** the TPs of VEN and DV were detected at smaller amounts.

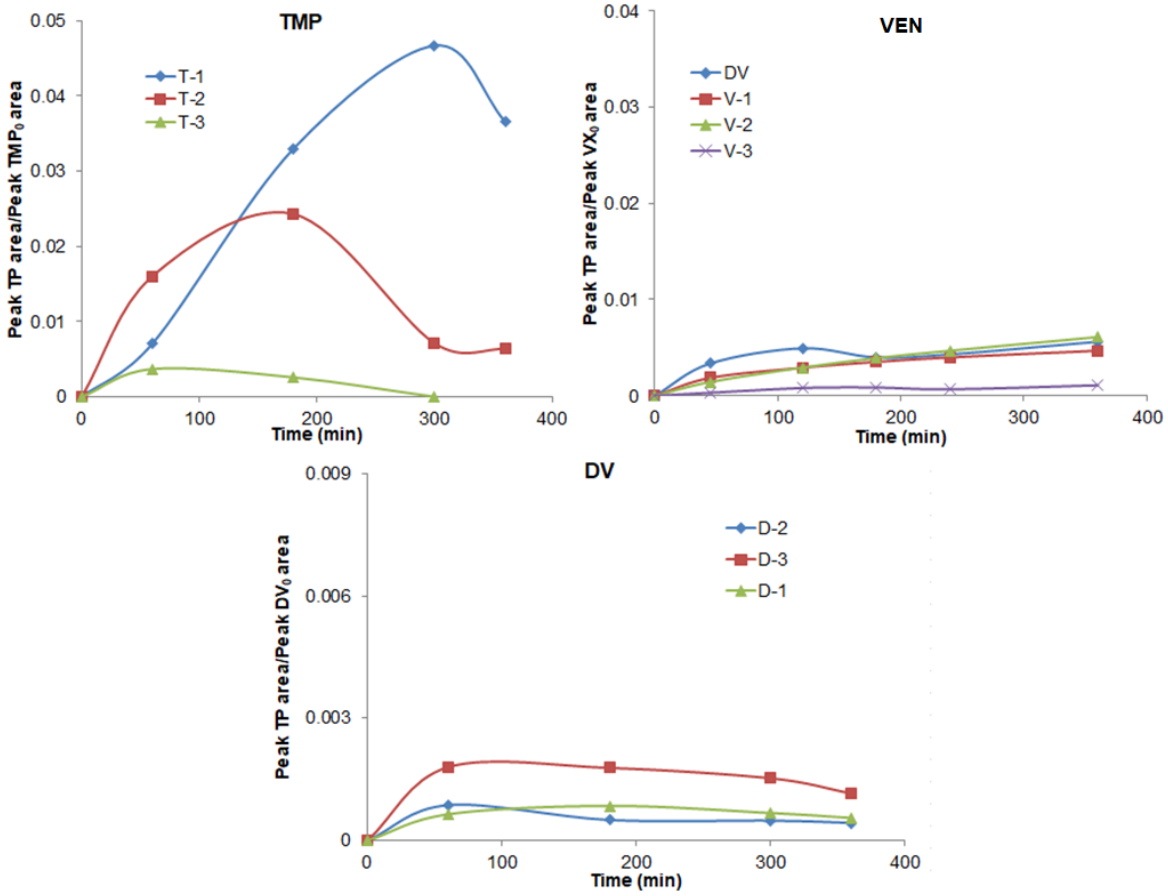

Figure 65. LC-MS monitoring of TPs over time during UV-A photocatalysis experiments in tap water

4.4.3 Correlation between transformation products and treatment method

The searching for TPs was carried also under UV-C photolysis. As it was shown **in section 4.3**, TMP could not be degraded by this method, and no TPs could be detected. The LC-MS monitoring of VEN and DV's TPs over time is shown in **figure 66**. Different TPs were observed for both compounds (**table S3, figures S5-S8**), suggesting different reaction routes for UV-C photolysis and UV-A photocatalysis. **Figures 67 and 68** show the proposed TPs formed during UV-C photolysis for these 2 target pollutants.

Analysing the degradation of VEN, it is possible to see that, additionally to DV, its isomer n-desmethylvenlafaxine (V-4) was detected by the software as a probable structure (**figure 67**). V-5 and V-6 are the result of hydroxylation and oxidation steps caused by the UV-C rays [186].

The amount of DV formed compared to UV-A photocatalysis was smaller. **Figure 47** showed that DV is degraded faster by UV-C photolysis than UV-A photocatalysis, so it is probable that this compound was further broken into smaller pieces and do not accumulate in the system.

On the other hand, the analysis of DV on **figure 66** shows a larger formation of the TP D-1 for UV-C photolysis in comparison to UV-A photocatalysis (**figure 61**)**.** The formation of D-4 indicates that UV-C photolysis was able to break the cyclohexane ring of DV (**figure 68**), which was not detected during UV-A photocatalysis.

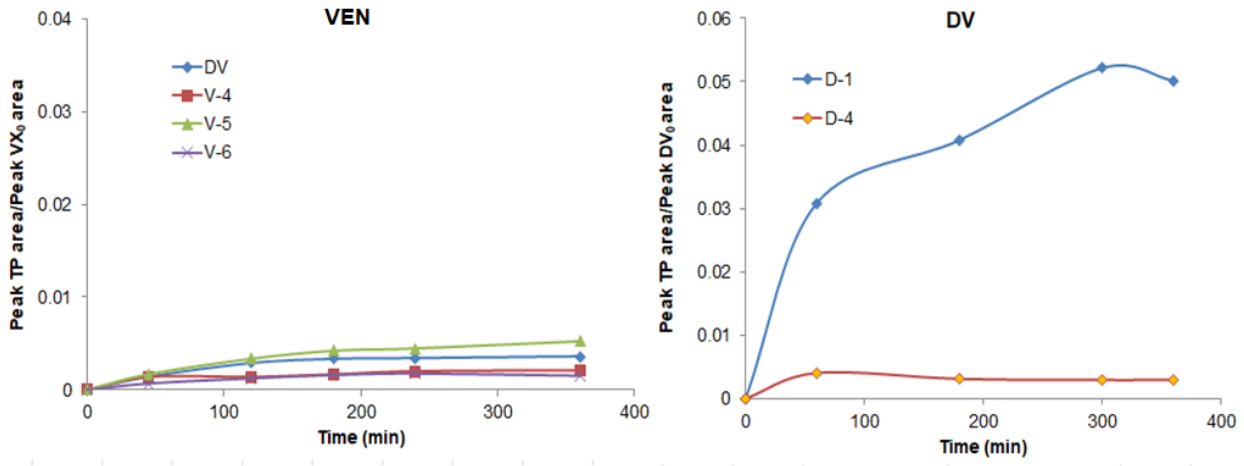

Figure 66. LC-MS monitoring of TPs over time for UV-C photolysis of VEN and DV

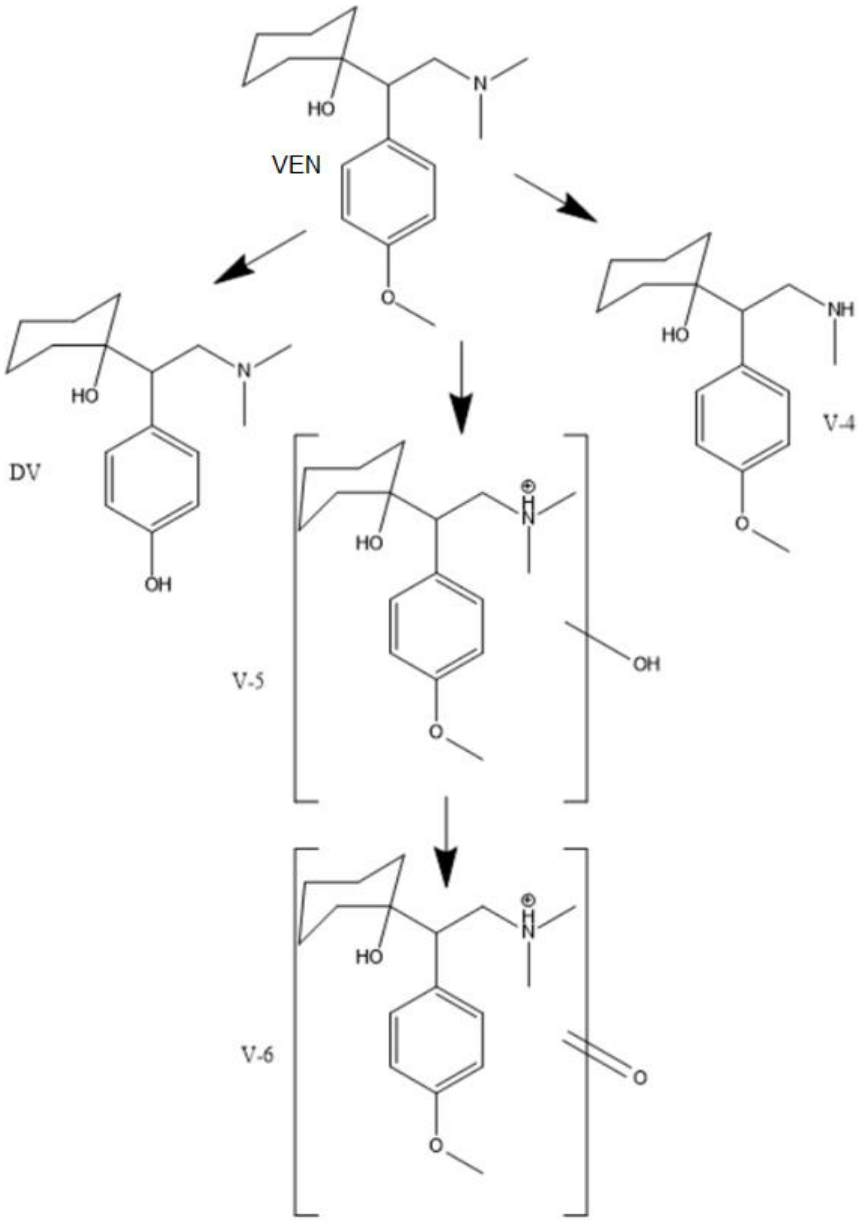

Figure 67. Proposed TPs for VEN by UV-C photolysis

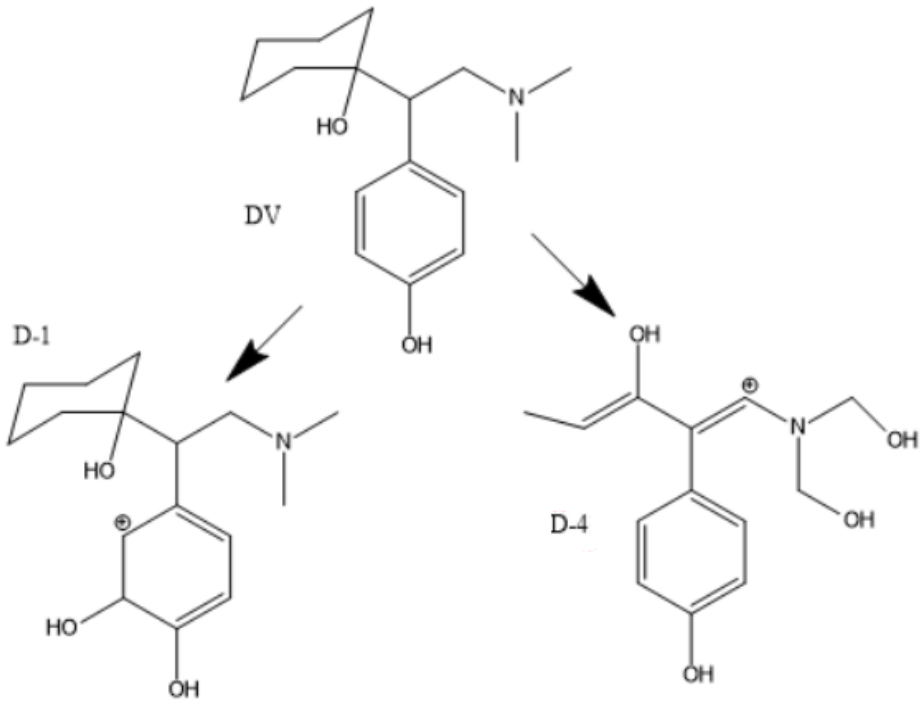

Figure 68. Proposed TPs for DV by UV-C photolysis

4.4.4 Interpretation

It is noticeable on **table S2** that all the TPs found had higher or similar molecular masses in comparison to their parent compounds. To attain mineralization, it is expected that molecules are broken into smaller pieces. ROS species (such as the •OH radical) can break up molecules but they can as well add moieties (e.g. -OH) to them, via hydroxylation [115, 113, 200]. The lack of smaller molecules may explain the increase in toxicity and puts in evidence the recalcitrant character of the tested OMPs and the difficulties in reaching their complete mineralization via AOPs.

It is important to investigate the TPs formed during photolytic and photocatalytic processes due to their potentially more toxic features compared to their respective parent compounds. Part of the EU Watch List's goal is to gather information not only about CECs but also about their respective TPs and how they affect the environment. However, given the synergistic character of how toxicity manifests itself in water and the uncountable amount of

substances in real matrices, to establish clear correlations between TPs and toxicity can be quite elusive. The analysis of **section 4.4** showed that making this correlation can be very complicate even in an ideal scenario with one target pollutant at a time in solution.

A more realistic approach should compare toxicity indicators prior and after the treatment. If toxicity levels of the effluent increase, measures can be taken to change that: altering process variables or to consider additional pre or post-treatment steps are common options. Performing a strenuous MS analysis, aiming at finding which molecules might be responsible for the toxic properties of an effluent and come up with strategies to specifically degrade them, is highly unpractical. Nonetheless, the compounds which have been routinely signalled as precursors of highly toxic TPs should be properly identified, monitored and handled. Whenever possible, their use should be limited and less harmful compounds replacements should be sought.

5. CONCLUSIONS

After a comprehensive literature review of the state-of-the-art of photocatalysis, it was shown that this technology, albeit receiving considerable scientific attention in the past decades, still ranks among the most energy-demanding processes. Among the causes, the most significant is its low photonic efficiency. This results in a lack of real applications of this technology. Nevertheless, the quick development of UV-LEDs has the potential to open up new horizons for the photocatalysis due to their unique features. In a scenario of phasing-out of UV mercury lamps, further studies exploring UV-LEDs for water treatment are fundamental for an efficient technological transition.

The flexibility allowed by the point-source character of UV-LEDs was explored with the simulation of different lab-scale cylindrical photoreactor designs. The optimal LED array of choice was the one that combined high light intensity with homogeneity, avoiding dark or overlit zones. The impact of photoreactor design on the degradation of ciprofloxacin, an antibiotic currently in the EU Watch List of Contaminants of Emerging Concern (2020), was investigated. A full-factorial design of experiments approach was used. The results showed that, while the adoption of more LEDs and controlled periodic illumination increased the degradation rates (k_{app}), the energetic trade-off was not statistically sufficient to turn this gain into lower electrical energy per order consumption (E_{EO}). Only the presence of a TiO_2 nanofilm on the inner walls of the reactor and a reduction of the distance between the LEDs and the reactor walls could reduce the energy consumption. It was demonstrated that controlled periodic illumination can only be effective in the presence of a catalyst, not contributing to photolysis.

The investigation was carried on further by an exhaustive study of the degradation of 5 target pollutants (all in the EU Watch List) under vastly different scenarios. The performances of UV-A and UV-C photolytic and photocatalytic processes were evaluated for solutions containing the pollutants individually and in mixture. The pollutants reacted differently to each treatment, which evidences the complexity of dealing with these systems. The fastest degradation performances were achieved by UV-A photocatalysis and/or UV-C photolysis. Due to the higher absorptivity of UV-C rays, their combination with TiO_2 resulted in screening effects that hindered direct photolysis. A second full-factorial design of experiments investigating the impact of different variables provided an in-depth quantitative confirmation for this analysis. Besides that,

the influence of the matrix was the key aspect in reducing the effluent's total organic carbon, highlighting the importance of pre-treatments for photocatalysis. A study of toxicity, measuring the inhibition of *Vibrio fischeri*'s bioluminescence, showed the potential for the formation of transformation products more toxic than the parent compounds during the treatment.

The addition of 0.1 mM of hydrogen peroxide to the system increased all the degradation rates, generating more radicals than the presence of TiO_2. The impact of initial pH for UV-A photocatalysis was investigated, as well as the reactivity of each one of the 5 target pollutants to possible photocatalytic reaction routes. A third design of experiments was made using Box-Behnken surface-response graphs investigating the impact of commonly found substances in water matrices on the degradation rates by means of UV-A photocatalysis. Again, the responses varied drastically depending on the pollutant and matrix composition.

High resolution LC-MS Obitrap was applied to identify the transformation products of individual solutions of 3 target compounds (trimethoprim, venlafaxine and o-desmethylvenlafaxine) for UV-A photocatalyis and UV-C photolysis. Different transformation products were obtained for each treatment, but correlations between these substances and the effluents' toxicity levels were not conclusive due to a multitude of possible synergistic effects. For UV-A photocatalysis the use of both MQ and tap water resulted in the same transformation products for all the target compounds, but different concentrations were obtained as a consequence of the different availability of radicals caused by the changes in the matrix.

The evaluation of E_{EO} under different scenarios suggests that UV-LED photocatalysis remains unfeasible for real applications. However, values for both UV-A and UV-C LEDs are now in the same range of traditional mercury lamps, which was not the case just a few years ago. The exponential improvement of UV-LEDs' wall plug efficiency can have a direct impact on energy demands, which will certainly reduce its process costs in the near future. Although the intrinsic hurdles of photocatalysis remain unsolved - such as issues like light permeability or radical transport when larger reactor diameters are used, the formation of toxic transformation products and the low photonic efficiency – this technology can find its niche in point-of-use small scale applications such as a final polishing step for specific uses that demand an effluent of superior quality.

6. REFERENCES

[1] M. T. H. van Vliet, E. R. Jones, M. Florke, W. H. P. Franssen, N. Hanasaki, Y. Wada, J. R. Yearsley, Global water scarcity including surface water and expansions of clean water technologies, Environ. Res. Lett. 16 (2021) 024020.

[2] J. Wilkinson, P. S. Hooda, J. Barker, S. Barton, J. Swinden, Occurrence, fate and transformation of emerging contaminants in water: An overarching review of the field, Environ. Pollut. 231 (2017) 954–970.

[3] A. C. Chávez-Mejía, I. Navarro-González, R. Magaña-López, D. Uscanga-Roldán, P. I. Zaragoza-Sánchez, B. E. Jiménez-Cisneros, Presence and natural treatment of organic micropollutants and their risks after 100 years of incidental water reuse in agricultural irrigation, Water (Switzerland) 11 (2019) 2148.

[4] M. Jiménez-Tototzintle, I. J. Ferreira, S. S. Duque, P. R. G. Barrocas, E. M. Saggioro, Removal of contaminants of emerging concern (CECs) and antibiotic resistant bacteria in urban wastewater using UVA/TiO_2/H_2O_2 photocatalysis, Chemosphere 210 (2018) 449–457.

[5] S. K. Loeb, P. J. Alvarez, J. A. Brame, E. L. Cates, W. Choi, J. Crittenden, D. D. Dionysiou, Q. Li, G. Li-Puma, X. Quan, D. L. Sedlak, T. Waite, P. Westerhoff, J. Kim, The Technology Horizon for Photocatalytic Water Treatment: Sunrise or Sunset?, Environ. Sci. and Technol. 53 (2019) 2937–2947.

[6] D. B. Miklos, C. Remy, M. Jekel, K. G. Linden, J. E. Drewes, U. Hübner, Evaluation of advanced oxidation processes for water and wastewater treatment – A critical review, Water Res. 139 (2018) 118–131.

[7] J. Chen, S. K. Loeb, J. Kim, LED revolution: Fundamentals and prospects for UV disinfection applications, Environ. Sci.: Water Res. and Technol. 3 (2017) 188–202.

[8] L. Yin, B. Wang, H. Yuan, S. Deng, J. Huang, Y. Wang, G. Yu, Pay special attention to the transformation products of PPCPs in environment, Emerging Contaminants. 3 (2017) 69–75.

[9] European Commission, Commission Implementing decision 2020/1161 establishing a

watch list of substances for Union-wide monitoring in the field of water policy pursuant to Directive 2008/105/EC of the European Parliament and of the Council. Official J. of the EU 257 (2020) 32–35.

[10] K. Robert, E. Rik, J. Marion, G. Christian, J. Hollender, Assessment of Micropollutants from Municipal Wastewater- Combination of Exposure and Ecotoxicological Effect Data for Switzerland, WasteWater - Evaluation and Management (2011) 31.

[11] S. A. Fast, V. G. Gude, D. D. Truax, J. Martin, B. S. Magbanua, A Critical Evaluation of Advanced Oxidation Processes for Emerging Contaminants Removal, Environ. Processes 4 (2017) 283–302.

[12] N. A. Sabri, H. Schmitt, B. Van Der Zaan, H. W. Gerritsen, T. Zuidema, H. H. M. Rijnaarts, A. A. M. Langenhoff, Prevalence of antibiotics and antibiotic resistance genes in a wastewater effluent-receiving river in the Netherlands, J. of Environ. Chem. Eng. 8 (2020) 102245.

[13] A. Lempart, E. Kudlek, M. Dudziak, Determination of micropollutants in water samples from swimming pool systems, Water (Switzerland). 10 (2018) 1083.

[14] J. Rogowska, M. Cieszynska-Semenowicz, W. Ratajczyk, L. Wolska, Micropollutants in treated wastewater, Ambio 49 (2019) 487.

[15] V. Leendert, H. Van Langenhove, K. Demeestere, Trends in liquid chromatography coupled to high-resolution mass spectrometry for multi-residue analysis of organic micropollutants in aquatic environments, TrAC - Trends in Anal. Chem. 67 (2015) 192–208.

[16] F. Bonvin, J. Omlin, R. Rutler, W. B. Schweizer, P. J. Alaimo, T. J. Strathmann, K. McNeill, T. Kohn, Direct photolysis of human metabolites of the antibiotic sulfamethoxazole: Evidence for abiotic back-transformation, Environ. Sci. and Technol. 47 (2013) 6746–6755.

[17] Y. Luo, W. Guo, H. H. Ngo, L. D. Nghiem, F. I. Hai, J. Zhang, S. Liang, X. C. Wang, A review on the occurrence of micropollutants in the aquatic environment and their fate and

removal during wastewater treatment, Sci. of the Total Environ. 473–474 (2014) 619–641.

[18] S. B. Guerreiro, R. J. Dawson, C. Kilsby, E. Lewis, A. Ford, Future heat-waves, droughts and floods in 571 European cities, Environ. Res. Lett. 13 (2018) 034009.

[19] M. G. Grillakis, Increase in severe and extreme soil moisture droughts for Europe under climate change, Sci. of the Total Environ. 660 (2019) 1245–1255.

[20] S. M. Elliott, M. L. Erickson, A. L. Krall, B. A. Adams, Concentrations of pharmaceuticals and other micropollutants in groundwater downgradient from large on-site wastewater discharges, PLoS ONE. 13 (2018) 1–17.

[21] A. Cruz-Alcalde, C. Sans, S. Esplugas, Priority pesticides abatement by advanced water technologies: The case of acetamiprid removal by ozonation, Sci. of the Total Environ. 599–600 (2017) 1454–1461.

[22] J. Liu, J. Ye, H. Ou, J. Lin, Effectiveness and intermediates of microcystin-LR degradation by UV/H_2O_2 via 265 nm ultraviolet light-emitting diodes, Environ. Sci. and Pollut. Res. 24 (2017) 4676–4684.

[23] Y. Shao, Z. Chen, H. Hollert, S. Zhou, B. Deutschmann, T.B. Seiler, Toxicity of 10 organic micropollutants and their mixture: Implications for aquatic risk assessment, Sci. of the Total Environ. 666 (2019) 1273–1282.

[24] L. Jacquin, Q. Petijean, J Cote, P. Laffaille, S. Jean, Effects of Pollution on Fish Behavior, Personality, and Cognition: Some Research Perspectives, Front. Ecol. Evol. 8 (2020) 86

[25] P. He, D. S. Aga, Comparison of GC-MS/MS and LC-MS/MS for the analysis of hormones and pesticides in surface waters: Advantages and pitfalls, Anal. Methods 11 (2019) 1436–1448.

[26] S. M. Yashas, B. R. Murthy, Synergistic Impact of Endocrine Disrupting Compounds (EDCs) On Environmental Facilities: A Mini Review, Int. J. of Eng. Trends and Technol. 52 (2017) 17–21.

[27] S. Das, S. Ghosh, A. Misra, A. J. Tamhankar, A. J. Mishra, C. S. Lundborg, S. K. Tripathy, Sunlight assisted photocatalytic degradation of ciprofloxacin in water using fe doped zno nanoparticles for potential public health applications, Int. J. of Environ. Res. and Public Health 15 (2018) 1–11.

[28] M. Z. Akbari, Y. Xu, Z. Lu, L. Peng, Review of antibiotics treatment by advance oxidation processes, Environ. Advances 5 (2021) 100111.

[29] L. Kotthoff, J. Keller, D. Lörchner, T. F. Mekonnen, M. Koch, Transformation products of organic contaminants and residues—overview of current simulation methods, Molecules 24 (2019) 1–23.

[30] X. Hu, X. Hu, Q. Peng, L. Zhou, X. Tan, L. Jiang, C. Tang, H. Wang, S. Liu, Y. Wang, Z. Ning, Mechanisms underlying the photocatalytic degradation pathway of ciprofloxacin with heterogeneous TiO_2, Chem. Eng. J. 380 (2020) 122366.

[31] S. I. Polianciuc, A. E. Gurzau, B. Kiss, M. G Stefan, F. Loghin, Antibiotics in the environment: causes and consequences, Med. Pharm. Rep. 93 (2020) 231.

[32] I. H. Acir, K. Guenther, Endocrine-disrupting metabolites of alkylphenol ethoxylates – A critical review of analytical methods, environmental occurrences, toxicity, and regulation, Sci. of the Total Environ. 635 (2018) 1530–1546.

[33] A. B. Siddique, S. M. Harrison, F. J. Monahan, E. Cummins, N. P. Brunton, Bisphenol A and metabolites in meat and meat products: Occurrence, toxicity, and recent development in analytical methods, Foods 10 (2021) 714.

[34] S. Hussain, C. Ramnarayanan, T. S. Roopashree, K. Anwer, N. Sreeharsha, A. B. Nair, Rapid , precise and affordable estimation of venlafaxine and its metabolites in highly polluted effluent waters: proof-of-concept for methodology, Molecules 25 (2020) 4793.

[35] C. Zwiener, Occurrence and analysis of pharmaceuticals and their transformation products in drinking water treatment, Anal. and Bioanal. Chem. 387 (2007) 1159–1162.

[36] C. Chu, P. R. Erickson, R. A. Lundeen, D. Stamatelatos, P. J. Alaimo, D. E. Latch, K. McNeill, Photochemical and Nonphotochemical Transformations of Cysteine with

Dissolved Organic Matter, Environ. Sci. and Technol. 50 (2016) 6363–6373.

[37] D. Dabić, S. Babić, I. Škorić, The role of photodegradation in the environmental fate of hydroxychloroquine, Chemosphere 230 (2019) 268–277.

[38] T. Ahamad, M. Naushad, S. M. Alshehri, Analysis of degradation pathways and intermediates products for ciprofloxacin using a highly porous photocatalyst, Chem. Eng. J. (2020) 127969.

[39] A. R. Silva, P. M. Martins, S. A. C. Teixeira, S. Carabinero, K. Kuehn, M. M. Alves, S. Lanceros-Mendez, L. Pereira, Ciprofloxacin wastewater treated by UVA photocatalysis: Contribution of irradiated TiO_2 and ZnO nanoparticles on the final toxicity as assessed by *Vibrio fischeri*, RSC Advances 98 (2016).

[40] A. Cruz-Alcalde, C. Sans, S. Esplugas, Exploring ozonation as treatment alternative for methiocarb and formed transformation products abatement, Chemosphere 186 (2017) 725–732.

[41] S. K. Alharbi, J. Kang, L. D. Nghiem, J. P. van de Merwe, F. D. L. Leusch, W. E. Price, Photolysis and UV/H_2O_2 of diclofenac, sulfamethoxazole, carbamazepine, and trimethoprim: Identification of their major degradation products by ESI–LC–MS and assessment of the toxicity of reaction mixtures, Process Safety and Environ. Protection 112 (2017) 222–234.

[42] Q. Cai, J. Hu, Decomposition of sulfamethoxazole and trimethoprim by continuous UVA/LED/TiO_2 photocatalysis: Decomposition pathways, residual antibacterial activity and toxicity, J. of Hazardous Mat. 323 (2017) 527–536.

[43] P. Paíga, M. Correia, M. J. Fernandes, A. Silva, M. Carvalho, J. Vieira, S. Jorge, J. G. Silva, C. Freire, C. Delerue-Matos, Assessment of 83 pharmaceuticals in WWTP influent and effluent samples by UHPLC-MS/MS: Hourly variation, Sci. of the Total Environ. 648 (2019) 582–600.

[44] T. Thay, B. Salisbury, P Zito, Ciprofloxacin, Statpearls Publishing, 2021.

[45] URL: https://www.norman-network.com/nds/ecotox/lowestPnecsIndex.php (accessed on

25th June 2022)

[46] S. Li, J. Hu, Transformation products formation of ciprofloxacin in UVA/LED and UVA/LED/TiO_2 systems: Impact of natural organic matter characteristics, Water Res. 132 (2018) 320–330.

[47] M. Zrnčic, S. Babić, D. Mutavdžic Pavlović, Determination of thermodynamic pKa values of pharmaceuticals from five different groups using capillary electrophoresis, J. of Sep. Sci. 38 (2015) 1232–1239.

[48] H. B. Park, Z. Wei, J. Oh, H. Xu, C. S. Kim, R. Wang, T. P. Wyche, G. Piizzi, R. A. Flavell, J. M. Crawford, Sulfamethoxazole drug stress upregulates antioxidant immunomodulatory metabolites in Escherichia coli, Nature Microbiol. 5 (2020) 1319–1329.

[49] S. Willach, H. V. Lutze, K. Eckey, K. Löppenberg, M. Lüling, J. B. Wolbert, D. M. Kujawinski, M. A. Jochmann, U. Karst, T. C. Schmidt, Direct Photolysis of Sulfamethoxazole Using Various Irradiation Sources and Wavelength Ranges - Insights from Degradation Product Analysis and Compound-Specific Stable Isotope Analysis, Environ. Sci. and Technol. 52 (2018) 1225–1233.

[50] R. Yuan, Y. Zhu, B. Zhou, J. Hu, Photocatalytic oxidation of sulfamethoxazole in the presence of TiO_2: Effect of matrix in aqueous solution on decomposition mechanisms, Chem. Eng. J. 359 (2019) 1527–1536.

[51] E. D. Barnett, D. W. Teele, J. O. Klein, H. J. Cabral, S. J. Kharasch, Comparison of ceftriaxone and trimethoprim-sulfamethoxazole for acute otitis media, Pediatrics 99 (1997) 23–28.

[52] E. C. Tucker, M. B. Roberts, D. L. Gordon, Miscellaneous antibacterial drugs, Side effects of drugs annual 39 (2017) 229.

[53] D. Veltishchev, Efficacy of Venlafaxine in the Treatment of Depression: Results of Recent Trials, Neurosci. and Behav. Physiol. 45 (2015) 576–578.

[54] S. Giannakis, I. Hendaoui, M. Jovic, D. Grandjean, L. F. De Alencastro, H. Girault, C.

Pulgarin, Solar photo-Fenton and UV/H_2O_2 processes against the antidepressant Venlafaxine in urban wastewaters and human urine. Intermediates formation and biodegradability assessment, Chem. Eng. J. 308 (2017) 492–504.

[55] European Medicines Agency, Withdrawal assesment report for Ellefore, London, 2009, 1-28

[56] A. Lajeunesse, S. A. Smyth, K. Barclay, S. Sauvé, C. Gagnon, Distribution of antidepressant residues in wastewater and biosolids following different treatment processes by municipal wastewater treatment plants in Canada, Water Res. 46 (2012) 5600–5612.

[57] Council of the European Union, Council Directive 2000/60/EC establishing a framework for community action in the field of water policy, Official J. of the European Communities L327 (2002) 1.

[58] Council of the European Union, Council Directive 2008/105/EC on environmental quality standards in the field of water policy, Official J. of the EU L348 (2008) 84.

[59] Council of the European Union. Council Directive 98/83/EC on the Quality of water intended for human consumption, Official J. of the European Comminities L330 (1998) 32.

[60] Council of the European Union, Directive 2010/75/EU Industrial Emissions, Official J. of the EU L334 (2010) 17.

[61] European Commission, Implementing decision EU 2015/495 establishing a watch list of substances for Union-wide monitoring in the field of water policy pursuant to Directive 2008/105/EC of the European Parliament and of the Council, Official J. of the EU L78 (2015) 40.

[62] European commission, Implementing decision EU 2018/840 establishing a watch list of substances for Union-wide monitoring in the field of water policy, Official J. of the EU L141 (2018) 9–12.

[63] R. Tröger, P. Klöckner, L. Ahrens, K. Wiberg, Micropollutants in drinking water from

source to tap - Method development and application of a multiresidue screening method, Sci. of the Total Environ. 627 (2018) 1404–1432.

[64] R. Díaz, M. Ibáñez, J. V. Sancho, F. Hernández, Target and non-target screening strategies for organic contaminants, residues and illicit substances in food, environmental and human biological samples by UHPLC-QTOF-MS, Anal. Methods 4 (2012) 196–209.

[65] L. Diep, F. P. Martins, L. C. Campos, P. Hofmann, J. Tomei, M. Lakhanpaul, P. Parikh, Linkages between sanitation and the sustainable development goals: A case study of Brazil, Sustainable Development 29 (2021) 339–352.

[66] F. J. R. Paumgartten, Pesticides and public health in Brazil, Current Opinion in Toxicol. 22 (2020) 7–11.

[67] S. S. Caldas, J. L. O. Arias, C. Rombaldi, L. L. Mello, M. B. R. Cerqueira, A. F. Martins, E. G. Primel, Occurrence of pesticides and PPCPs in surface and drinking water in southern Brazil: Data on 4-year monitoring, J. of the Brazilian Chem. Soc. 30 (2019) 71–80.

[68] G. Fernandes, V. C. Aparicio, M. C. Bastos, E. De Gerónimo, J. Labanowski, O. D. Prestes, R. Zanella, D. R. dos Santos, Indiscriminate use of glyphosate impregnates river epilithic biofilms in southern Brazil, Sci. of the Total Environ. 651 (2019) 1377–1387.

[69] A. N. Ortega, R. B. Neves, Legal aspects of urban water and sanitation regulatory services: An analysis of how the spanish experience positively would contribute to the brazilian new regulation, Water (Switzerland) 13 (2021) 1023.

[70] URL: https://www.who.int/news/item/18-06-2019-1-in-3-people-globally-do-not-have-access-to-safe-drinking-water-unicef-who (acessed on 30th September 2021)

[71] G. Lofrano, J. Brown, Wastewater management through the ages: A history of mankind, Sci. of the Total Environ. 408 (2010) 5254–5264.

[72] L. Rizzo, S. Malato, D. Antakyali, V. G. Beretsou, M. B. Đolić, W. Gernjak, E. Heath, I. I. Ivancev-Tumbas, P. Karaolia, A. R. Lado Ribeiro, G. Mascolo, C. S. McArdell, H. Schaar, A. M. T. Silva, D. Fatta-Kassinos, Consolidated vs new advanced treatment

methods for the removal of contaminants of emerging concern from urban wastewater, Sci. of the Total Environ. 655 (2019) 986–1008.

[73] URL: https://pixabay.com/fr/photos/cleaning-station-de-traitement-des-eaux--2826988/ (accessed on 30th September 2021)

[74] H. A. Hasan, M. H. Muhammad, N. I. Ismail, A review of biological drinking water treatment technologies for contaminants removal from polluted water resources, J. of Water Process Eng. 33 (2020) 101035.

[75] H. Shen, H. Fan, N. Wu, J. Hu, A comparison of removal efficiencies of conventional drinking water treatment and advanced treatment equipped with ozone-biological activated carbon process, Environ. Technol. (UK) 42 (2021) 4079–4089.

[76] C. Teodosiu, A. F. Gilca, G. Barjoveanu, S. Fiore, Emerging pollutants removal through advanced drinking water treatment: A review on processes and environmental performances assessment, J. of Cleaner Production 197 (2018) 1210–1221.

[77] Y. Deng, R. Zhao, Advanced Oxidation Processes (AOPs) in Wastewater Treatment, Current Pollut. Reports 1 (2015) 167–176.

[78] E. Cako, K. D. Gunasekaran, R. D. C. Cheshmeh Soltani, G. Boczkaj, Ultrafast degradation of brilliant cresyl blue under hydrodynamic cavitation based advanced oxidation processes (AOPs), Water Resources and Industry 24 (2020) 100134.

[79] J. M. Poyatos, M. M. Muñio, M. C. Almecija, J. C. Torres, E. Hontoria, F. Osorio, Advanced oxidation processes for wastewater treatment: state of the art, Water, Air, and Soil Pollut. 205 (2010) 187–204. https://doi.org/10.1007/s11270-009-0065-1.

[80] J. R. Bolton, K. G. Bircher, W. Tumas, C. A. Tolman, Figures-of-merit for the technical development and application of advanced oxidation technologies for both electric and solar-driven systems, Pure and App. Chem. 73 (2001) 627–637.

[81] D. Awfa, M. Ateia, M. Fujii, C. Yoshimura, Photocatalytic degradation of organic micropollutants: Inhibition mechanisms by different fractions of natural organic matter, Water Res. 174 (2020) 115643.

[82] T. Liu, K. Yin, C. Liu, J. Luo, J. Crittenden, W. Zhang, S. Luo, Q. He, Y. Deng, H. Liu, D. Zhang, The role of reactive oxygen species and carbonate radical in oxcarbazepine degradation via UV, UV/H_2O_2: Kinetics, mechanisms and toxicity evaluation, Water Res. 147 (2018) 204–213.

[83] Y. Ye, H. Bruning, W. Liu, H. Rijnaarts, D. Yntema, Effect of dissolved natural organic matter on the photocatalytic micropollutant removal performance of TiO_2 nanotube array, J. of Photochem. and Photobiol. A: Chem. 371 (2019) 216–222.

[84] S. Verma, S. Nakamura, M. Sillanpää, Application of UV-C LED activated PMS for the degradation of anatoxin-a, Chem. Eng. J. 284 (2016) 122–129.

[85] L. Santos-Juanes, M. M. B. Martin, E. Ortega-Gomez, A.C Reina, I. M. Roman-Sanchez, J. L. C. Lopez, J. A. S. Perez, Economic evaluation of the photo-Fenton process. Mineralization level and reaction time: The keys for increasing plant efficiency, J. of Hazardous. Mat. 186 (2011) 1924.

[86] K. Pazdzior, L. Bilinska, S. Ledakowicz, A review of the existing and emerging technologies in the combination of AOPs and biological processes in industrial textile wastewater treatment, Chem.Eng. J. 376 (2019) 120597.

[87] G. Matafonova, V. Batoev, Recent advances in application of UV light-emitting diodes for degrading organic pollutants in water through advanced oxidation processes: A review, Water Res. 132 (2018) 177–189.

[88] F. S. Souza, V. V. da Silva, C. K. Rosin, L. H. Hainzenreder, A. Arenzon, L. A. Féris, Comparison of different advanced oxidation processes for the removal of amoxicillin in aqueous solution, Environ. Technol. (UK) 39 (2018) 549–557.

[89] E. Chatzisymeon, S. Foteinis, D. Mantzavinos, T. Tsoutsos, Life cycle assessment of advanced oxidation processes for olive mill wastewater treatment, J. of Cleaner Production 54 (2013) 229–234.

[90] S. Arzate, S. Pfister, C. Oberschelp, J. A. Sánchez-Pérez, Environmental impacts of an advanced oxidation process as tertiary treatment in a wastewater treatment plant, Sci. of

The Total Environ. 694 (2019) 133572.

[91] K. Londhe, C. Lee, Y. Zhang, S. Grdanovska, T. Kroc, C. A. Cooper, A K. Venkatesan, Energy Evaluation of Electron Beam Treatment of Perfluoroalkyl Substances in Water: A Critical Review, ACS EST Eng. 5 (2021) 827.

[92] D. Bertagna Silva, A. Cruz-Alcalde, C. Sans, J. Giménez, S. Esplugas, Performance and kinetic modelling of photolytic and photocatalytic ozonation for enhanced micropollutants removal in municipal wastewaters, App. Catal. B: Environ. (2019) 211–217.

[93] M. E. H. Bergmann, J. Rollin, Product and by-product formation in laboratory studies on disinfection electrolysis of water using boron-doped diamond anodes, Catal. Today 124 (2007) 198–203.

[94] J. K. Im, I. H. Cho, S. K. Kim, Q. D. Zoh, Optimization of carbamazepine removal in O_3/UV/H_2O_2 system using a response surface methodology with central composite design, Desalination 285 (2012) 306.

[95] S. Guittonneau, J.P. Duguet, C. Bonnel, J. De Laat, M. Doré, Oxidation Of Parachloronitrobenzene In Dilute Aqueous Solution by O_3 + UV And H_2O_2 + UV: A Comparative Study, Ozone: Sci. and Eng. 12 (1990) 73–94.

[96] L. Clarizia, D. Russo, I. Di Somma, R. Marotta, R. Andreozzi, Homogeneous photo-Fenton processes at near neutral pH: A review, App. Catal. B: Environ. 209 (2017) 358–371,

[97] L. Gao, Y. Cao, L. Wang, S. Li, A review on sustainable reuse applications of Fenton sludge during wastewater treatment, Frontiers of Environ. Sci. and Eng. 16 (2022).

[98] J. M. Coronado, F. Fresno, M. D. Hernández-Alonso, R. Portela, Design of advanced photocatalytic materials for energy and environmental applications, Springer, London 2013, 1-100.

[99] A. Fujishima, K. Honda, Electrochemical photolysis of water at a semiconductor electrode Nature 238 (1972) 37-38.

[100] Y. Abdel-Maksoud, E. Imam, A. Ramadan, TiO_2 solar photocatalytic reactor systems: Selection of reactor design for scale-up and commercialization—analytical review, Catal. 6 (2016) 138.

[101] K. Hashimoto, H. Irie, A. Fujishima, TiO_2 photocatalysis: A historical overview and future prospects, Jap. J. of App. Phys. Part 1: Regular Papers and Short Notes and Review Papers. 44 (2005) 8269–8285.

[102] K. Perović, F. M. de la Rosa, M. Kovačić, U. L. Štangar, F. Fresno, D. D. Dionysiou, A. L. Bozić, Recent achievements in development of TiO_2 -based composite photocatalytic materials for solar driven water purification and water splitting, Mat. 13 (2020) 1338.

[103] M. Khairy, W. Zakaria, Effect of metal-doping of TiO_2 nanoparticles on their photocatalytic activities toward removal of organic dyes, Egyptian J. of Petrol. 23 (2014) 419–426.

[104] C. Kittel, Introduction to solid state physics, 8th edition, John Wiley and Sons, Hoboken, 2005, 187-217.

[105] R. Daghrir, P. Drogui, D. Robert, Modified TiO_2 for environmental photocatalytic applications: A review, Ind. and Eng. Chem. Res. 52 (2013) 3581–3599.

[106] B. K. Zaveri, N. G. De Souza, A. C. Parenky, H. Choi, LED-Based Ultraviolet Oxidation of Pharmaceuticals: Effects of Wavelength and Intensity, pH, and TiO_2 Loading, Water Environ. Res. 90 (2018) 790–799.

[107] A. Salma, S. Thoröe-Boveleth, T. C. Schmidt, J. Tuerk, Dependence of transformation product formation on pH during photolytic and photocatalytic degradation of ciprofloxacin, J. of Hazardous Mat. 313 (2016) 49–59.

[108] M. Čizmić, D. Ljubas, M. Rožman, D. Ašperger, L. Ćurković, S. Babíc, Photocatalytic degradation of azithromycin by nanostructured TiO_2 film: Kinetics, degradation products, and toxicity, Mat. 12 (2019) 873.

[109] K. Natarajan, T. S. Natarajan, H. C. Bajaj, R. J. Tayade, Photocatalytic reactor based on UV-LED/TiO_2 coated quartz tube for degradation of dyes, Chem. Eng. J. 178 (2011) 40–

49.

[110] C. B. Oskal, S. Meric, A Comparative Heterogeneous Photocatalytic Removal Study on Amoxicillin and Clarithyromicin Antibiotics in Aqueous Solutions, J. of Water technol. and Treatment methods 1:4 (2018) 116.

[111] B. Yang, H. D. Park, S. W. Hong, S. H. Lee, J. A. Park, J. W. Choi, Photocatalytic degradation of microcystin-LR and anatoxin-a with presence of natural organic matter using UV-light emitting diodes / TiO_2 process, J. of Water Process Eng. 34 (2020) 101163.

[112] F. Azeez, E. Al-Hetlani, M. Arafa, Y. Abdelmonem, A. A. Nazeer, M. O. Amin, M. Madkour, The effect of surface charge on photocatalytic degradation of methylene blue dye using chargeable titania nanoparticles, Sci. Reports 8 (2018) 1–9.

[113] C. Sirtori, A. Agüera, W. Gernjak, S. Malato, Effect of water-matrix composition on Trimethoprim solar photodegradation kinetics and pathways, Water Res. 44 (2010) 2735–2744.

[114] Y. Ye, Y. Feng, H. Bruning, D. Yntema, H. H. M. Rijnaarts, Photocatalytic degradation of metoprolol by TiO_2 nanotube arrays and UV-LED: Effects of catalyst properties, operational parameters, commonly present water constituents, and photo-induced reactive species, App. Catal. B: Environ. 220 (2018) 171–181.

[115] H. C. Yılmaz, E. Akgeyik, S. Bougarrani, M. El Azzouzi, S. Erdemoğlu, Photocatalytic degradation of amoxicillin using Co-doped TiO_2 synthesized by reflux method and monitoring of degradation products by LC–MS/MS, J. of Dispersion Sci. and Technol. 41 (2019) 412-425.

[116] L. Zhang, C. Moralejo, W. A. Anderson, A review of the influence of humidity on photocatalytic decomposition of gaseous pollutants on TiO_2-based catalysts, The Canadian J. of Chem. Eng. 98 (2020) 263.

[117] M. S. F. A. Zamri, N. Sapawe, Kinetic Study on Photocatalytic Degradation of Phenol Using Green Electrosynthesized TiO_2 Nanoparticles, Mat. Today: Proceedings 19 (2019)

1261.

[118] M. E. Leblebici, J. Rongé, J. A. Martens, G. D. Stefanidis, T. Van Gerven, Computational modelling of a photocatalytic UV-LED reactor with internal mass and photon transfer consideration, Chem. Eng. J. 264 (2015) 962–970.

[119] A. Manassero, M. L. Satuf, O. M. Alfano, Photocatalytic reactors with suspended and immobilized TiO_2: Comparative efficiency evaluation, Chem. Eng. J. 326 (2017) 29–36.

[120] P. J. Valadés-Pelayo, F. Guayaquil Sosa, B. Serrano, H. de Lasa, Eight-lamp externally irradiated bench-scale photocatalytic reactor: Scale-up and performance prediction, Chem. Eng. J. 282 (2015) 142–151.

[121] D. Bertagna Silva, G. Buttiglieri, S. Babić, State-of-the-art and current challenges for TiO_2/UV-LED photocatalytic degradation of emerging organic micropollutants, Environ. Sci. and Pollut. Res. 28 (2021) 103-120.

[122] M. R. Eskandarian, M. Fazli, M. H. Rasoulifard, H. Choi, Decomposition of organic chemicals by zeolite-TiO_2 nanocomposite supported onto low density polyethylene film under UV-LED powered by solar radiation, App. Catal. B: Environ. 183 (2016) 407–416.

[123] J. P. Ghosh, G. Achari, C. H. Langford, Design and evaluation of a UV LED Photocatalytic Reactor Using Anodized TiO_2 Nanotubes, Water Environ. Res. 88 (2015) 785–791.

[124] D. Ljubas, G. Smoljanić, H. Juretić, Degradation of Methyl Orange and Congo Red dyes by using TiO2 nanoparticles activated by the solar and the solar-like radiation, J. of Environ. Manag, 161 (2015) 83-91.

[125] Y. Boyjoo, M. Ang, V. Pareek, Light intensity distribution in multi-lamp photocatalytic reactors, Chem. Eng. Sci. 93 (2013) 11–21.

[126] J. Z. Bloh, A holistic approach to model the kinetics of photocatalytic reactions, Frontiers in Chem. 7 (2019) 1–13.

[127] M. Martín-Sómer, C. Pablos, R. van Grieken, J. Marugán, Influence of light distribution

on the performance of photocatalytic reactors: LED vs mercury lamps, App. Catal. B: Environ. 215 (2017) 1–7.

[128] C. J. Escudero, O. Iglesias, S. Dominguez, M. J. Rivero, I. Ortiz, Performance of electrochemical oxidation and photocatalysis in terms of kinetics and energy consumption. New insights into the p-cresol degradation, J. of Environ. Manag. 195 (2017) 117–124.

[129] Z. Ran, Y. Fang, J. Sun, C. Ma, S. Li, Photocatalytic oxidative degradation of carbamazepine by TiO_2 irradiated by UV light emitting diode, Catal. 10 (2020) 1–13.

[130] J. D. Mason, M. T. Cone, E. S. Fry, Ultraviolet (250–550 nm) absorption spectrum of pure water, App. Optics 55 (2016) 7163.

[131] L. V. M. de Assis, P. N. Tonolli, M. N. Moraes, M. S. Baptista, A. M. L. Castrucci, How does the skin sense sunlight? An integrative view of light sensing molecules, J. of Photochem. and Photobiol. C: Photochem. Reviews 47 (2021) 100403.

[132] E. Maverakis, Y. Miyamura, M. P. Bowen, G. Correa, Y. Ono, H. Goodarzi, Light, including ultraviolet, J. of Autoimmunity 34 (2010) 247–257.

[133] L. A. Walsh, M. L. Stock, L. M. Peterson, M. Gerrard, Women's sun protection cognitions in response to UV photography: The role of age, cognition, and affect, J. of Behav. Med. 37 (2014) 553–563.

[134] S. Mimasaka, T. Oshima, M. Ohtani, Visualization of old bruises in children: Use of violet light to record long-term bruises, Forensic Sci. Int. 282 (2018) 74–78.

[135] B. A. Lyon, A. D. Dotson, K. G. Linden, H. S. Weinberg, The effect of inorganic precursors on disinfection byproduct formation during UV-chlorine/chloramine drinking water treatment, Water Res. 46 (2012) 4653–4664.

[136] Z. C. Gao, Y L.. Lin, B. Xu, Y. Xia, C. Y. Hu, T.C. Cao, X.Y. Zou, N.Y. Gao, Evaluating iopamidol degradation performance and potential dual-wavelength synergy by UV-LED irradiation and UV-LED/chlorine treatment, Chem. Eng. J. 360 (2019) 806–816.

[137] H. H. Eriksen, F. X. Perrez, The Minamata Convention: A Comprehensive Response to a Global Problem, Review of European, Comparative and Int. Environ. Law 23 (2014) 195–210.

[138] C. M. Bourget, An Introduction to Light-emitting Diodes, Hortscience 43 (2008) 1944–1946.

[139] H. Amano, R. Collazo, C. De Santi, S. Einfeldt, M. Funato, J. Glaab, S. Hagedorn, A. Hirano, H. Hirayama, R. Ishii, Y. Kashima, Y. Kawakami, R. Kirste, M. Kneissl, R. Martin, F. Mehnke, M. Meneghini, A. Ougazzaden, P.J. Parbrook, S. Rajan, P. Reddy, F. Römer, J. Ruschel, B. Sarkar, F. Scholz, L.J. Schowalter, P. Shields, Z. Sitar, L. Sulmoni, T. Wang, T. Wernicke, M. Weyers, B. Witzigmann, Y.R. Wu, T. Wunderer, Y. Zhang, The 2020 UV emitter roadmap, J. of Phys. D: App. Phys. 53 (2020) 503001.

[140] G. D. Christian, P. K. Dasgupta, K. A. Schug, Analytical Chemistry, 9th Edition, Wiley, New Jersey, 2014, 596-616; 649-701; 735-764.

[141] M. Petrović, M, D. Hermando, S. Diaz-Cruz, D. Barcelo, Liquid Chromatography–Tandem Mass Spectrometry for the Analysis of Pharmaceutical Residues in Environmental Samples: A Review, J. of Chromatography A 1067 (2005) 1-14

[142] J. Kool, W. M. A. Niessen, Analyzing Biomolecular Interactions by Mass Spectrometry, Wiley-VCH, Weinheim, 2015, 1-43

[143] A. Cappielo, G. Famiglini, P. Palma, Electron Ionization for LC/MS, Anal. Chem. 75 (2003) 497.

[144] J. Solstwisch, T. W. Jaskolla, F. Hillenkamp, M. Karas, K. Dreisewerd, Ion Yields in UV-MALDI Mass Spectrometry As a Function of Excitation Laser Wavelength and Optical and Physico-Chemical Properties of Classical and Halogen-Substituted MALDI Matrixes, Anal. Chem. 84 (2012) 6567.

[145] A. K. Jarmusch, A. M, Musso, T. Shymanovich, S. A. Jarmusch, M. J. Weavil, M. E. Lovin, B. M. Ehrmann, S. Saari, D. E. Nichols, S. H. Faeth, N. B. Cech, Comparison of electrospray ionization and atmospheric pressure photoionization liquid chromatography

mass spectrometry methods for analysis of ergot alkaloids from endophyte-infected sleepygrass (Achnatherum robustum), J. of Pharm. and Biomed. Analysis 117 (2016) 11–17.

[146] S. Banerjee, S. Mazumdar, Electrospray Ionization Mass Spectrometry: A Technique to Access the Information beyond the Molecular Weight of the Analyte, Int. J. of Anal. Chem. 2012 (2012) 1–40. https://doi.org/10.1155/2012/282574.

[147] B. Grund, L. Marvin, B. Rochat, Quantitative performance of a quadrupole-orbitrap-MS in targeted LC-MS determinations of small molecules, J. of Pharm. and Biomed. Analysis 124 (2016) 48–56.

[148] M. Beccaria, D. Cabooter, Current developments in LC-MS for pharmaceutical analysis, Analyst 145 (2020) 1129–1157.

[149] A. A. Bletsou, J. Jeon, J. Hollender, E. Archontaki, N. S. Thomaidis, Targeted and non-targeted liquid chromatography-mass spectrometric workflows for identification of transformation products of emerging pollutants in the aquatic environment, TrAC Trends in Anal. Chem. 66 (2015) 32-44.

[150] URL: https://www.shimadzu.com/an/lcms/support/fundamental/mass_analyzers.html (accessed September 30th, 2021).

[151] A. Makarov, D. Grinfeld, K. Ayzikov, Fundamentals of Orbitrap analyzer, Elsevier, Amsterdam, 2019, 37-61.

[152] G. C. McAllister, D. H. Phanstiel, J. Brumbaugh, M. S. Westphall, J. J. Coon, Higher-energy Collision-activated Dissociation Without a Dedicated Collision Cell, Mol. and Cel. Proteomics 10 (2011) 0111-009465

[153] URL: https://www.thermofisher.com/es/es/home/industrial/mass-spectrometry/mass-spectrometry-learning-center/mass-spectrometry-technology-overview/mass-analyzer-technology-overview.html (acessed on September 30th 2021)

[154] Y. P. Lin, M. Mehrvar, Photocatalytic treatment of an actual confectionery wastewater using $Ag/TiO_2/Fe_2O_3$: Optimization of photocatalytic reactions using surface response

methodology, Catal. 8 (2018) 1–17.

[155] M. M. Abdulredha, S. A. Hussain, L. C. Abdullah, Optimization of the demulsification of water in oil emulsion via non-ionic surfactant by the response surface methods, J. of Petrol. Sci. and Eng. 184 (2020) 106463.

[156] S. L. C. Ferreira, R. E. Bruns, H. S. Ferreira, G. D. Matos, J. M. David, G. C. Brandão, E. G. P. da Silva, L. A. Portugal, P.S. dos Reis, A. S. Souza, W. N. L. dos Santos, Box-Behnken design: An alternative for the optimization of analytical methods, Analytica Chimica Acta 597 (2007) 179–186.

[157] J. S. G. Neto, S. Satyro, E. M. Saggioro, M. Dezotti, Investigation of mechanism and kinetics in the TiO_2 photocatalytic degradation of Indigo Carmine dye using radical scavengers, Int. J. of Environ. Sci. and Technol. 18 (2021) 163–172.

[158] Y. Picó, D. Barceló, Transformation products of emerging contaminants in the environment and high-resolution mass spectrometry: A new horizon, Anal. and bioanal. Chem. 407 (2015) 6257–6273.

[159] S. Saito-Shida, T. Hamasaka, S. Nemoto, H. Akiyama, Multiresidue determination of pesticides in tea by liquid chromatography-high-resolution mass spectrometry: Comparison between Orbitrap and time-of-flight mass analyzers, Food Chem. 256 (2018) 140–148.

[160] G. Q. Li, W. L. Wang, Z. Y. Huo, Y. Lu, H. Y. Hu, Comparison of UV-LED and low pressure UV for water disinfection: Photoreactivation and dark repair of Escherichia coli, Water Res. 126 (2017) 134–143.

[161] P. Xiong, J. Hu, Decomposition of acetaminophen (Ace) using TiO_2/UVA/LED system, Catal. Today 282 (2016) 1-9.

[162] V. Vaiano, O. Sacco, D. Sannino, G. Di Capua, N. Femia, Enhanced performances of a photocatalytic reactor for wastewater treatment using controlled modulation of LEDs light, Chem. Eng. Transactions 57 (2017) 553–558.

[163] O. Tokode, R. Prabhu, L. A. Lawton, P. K. J. Robertson, Effect of controlled periodic-

based illumination on the photonic efficiency of photocatalytic degradation of methyl orange, J. of Catal. 290 (2012) 138–142.

[164] R. Liang, J. C. Van Leuwen, L. M. Bragg, M. J, Arlos, L. C. M. L. C. Fong, O. M. Schneider, I. Jaciw-Zurakowsky, A. Fattahi, S. Rathod, P. Peng, M. R. Servos, Y. N. Zhou, Utilizing UV-LED pulse width modulation on TiO_2 advanced oxidation processes to enhance the decomposition efficiency of pharmaceutical micropollutants, Chem. Eng. J. 361 (2019) 439–449.

[165] O. M. Schneider, R. Liang, L. Bragg, I. Jaciw-Zurakowsky, A. Fattahi, S. Rathod, P. Peng, M. R. Servos, Y. N. Zhou, Photocatalytic degradation of microcystins by TiO_2 using UV-LED controlled periodic illumination, Catal. 9 (2019) 1–10.

[166] D. Bertagna Silva, G. Buttiglieri, T. Babić, L. Ćurković, S. Babić, Impact of UV-LED photoreactor design on the degradation of contaminants of emerging concern, Process Safety and Environ. Protection 153 (2021) 94–106.

[167] Sutisna, M. Rokhmat, E. Wibowo, Khairurrijal, M. Abdullah, Prototype of a flat-panel photoreactor using TiO_2 nanoparticles coated on transparent granules for the degradation of Methylene Blue under solar illumination, Sustainable Environ. Res. 27 (2017) 172–180.

[168] L. Yu, G. Achari, C. H. Langford, Design and Evaluation of a Novel Light-Emitting Diode Photocatalytic Reactor for Water Treatment, J. of Environ. Eng. (US) 144 (2018) 1–9.

[169] C. Casado, J. Marugán, R. Timmers, M. Muñoz, R. van Grieken, Comprehensive multiphysics modeling of photocatalytic processes by computational fluid dynamics based on intrinsic kinetic parameters determined in a differential photoreactor, Chem. Eng. J. 310 (2017) 368–380.

[170] C. Casado, R. Timmers, A. Sergejevs, C. Clarke, D. Allsopp, C. Bowen, R. van Grieken, J. Marugán, Design and validation of a LED-based high intensity photocatalytic reactor for quantifying activity measurements, Chem. Eng. J. 327 (2017) 1043–1055.

[171] M. Nakahashi, K. Mawatari, A. Hirata, M. Maetani, T. Shimohata, T. Uebanso, Y. Hamada, M. Akutagawa, Y. Kinouchi, A. Takahashi, Simultaneous irradiation with different wavelengths of ultraviolet light has synergistic bactericidal effect on vibrio parahaemolyticus, Photochem. and Photobiol. 90 (2014) 1397–1403.

[172] P. O. Nyangaresi, Y. Qin, G. Chen, B. Zhang, Y. Lu, L. Shen, Comparison of UV-LED photolytic and UV-LED/TiO_2 photocatalytic disinfection for Escherichia coli in water, Catal. Today 335 (2019) 200–207.

[173] M. Kneissl, T. Y. Seong, J. Han, H. Amano, The emergence and prospects of deep-ultraviolet light-emitting diode technologies, Nature Photonics 13 (2019) 233–244.

[174] V. A. Sakkas, M. Islam, C. Stalikas, T. A. Albanis, Photocatalytic degradation using design of experiments: A review and example of the Congo red degradation, J. of Hazardous Mat. 175 (2010) 33–44.

[175] S. Mortazavian, A. Saber, D. E. James, Optimization of photocatalytic degradation of acid blue 113 and acid red 88 textile dyes in a uv-c/tio 2 suspension system: Application of response surface methodology (rsm), Catal. 9 (2019) 360.

[176] L. Lin, W. Jiang, M. Bechelany, M. Nasr, J. Jarvis, T. Schaub, R. R. Sapkota, P. Miele, H. Wang, P. Xu, Adsorption and photocatalytic oxidation of ibuprofen using nanocomposites of TiO_2 nanofibers combined with BN nanosheets: Degradation products and mechanisms, Chemosphere 220 (2019) 921–929.

[177] S. Wu, F. Wang, Q. Li, J. Wang, Y. Zhou, N. Duan, S. Niazi, Z. Wang, Photocatalysis and degradation products identification of deoxynivalenol in wheat using upconversion nanoparticles@TiO_2 composite, Food Chem. 323 (2020) 126823.

[178] F. Chen, Q. Yang, D. Wang, F. Yao, Y. Ma, X. Li, J. Wang, L. Jiang, L. Wang, H. Yu, Highly-efficient degradation of amiloride by sulfate radicals-based photocatalytic processes: Reactive kinetics, degradation products and mechanism, Chem. Eng. J. 354 (2018) 983–994.

[179] M. Jiménez-Salcedo, M. Monge, M. T. Tena, Photocatalytic degradation of ibuprofen in

water using TiO_2/UV and g-C3N4/visible light: Study of intermediate degradation products by liquid chromatography coupled to high-resolution mass spectrometry, Chemosphere 215 (2018) 605.

[180] D. Krakkó, E. Gombos, V. Licul-Kucera, S. Dóbé, V. G. Mihucz, G. Záray, Enhanced photolytic and photooxidative treatments for removal of selected pharmaceutical ingredients and their degradation products in water matrices, Microchem. J. 150 (2019) 104136.

[181] D. A. da Silva, R. P. Cavalcante, R. F. Cunha, A. Machulek Junior, S. C. Oliveira, Optimization of nimesulide oxidation via a UV-ABC/H_2O_2 treatment process: Degradation products, ecotoxicological effects, and their dependence on the water matrix, Chemosphere 207 (2018) 457–468.

[182] C. Solá-Gutiérrez, S. Schröder, M. F. San-Román, I. Ortiz, Critical review on the mechanistic photolytic and photocatalytic degradation of triclosan, J. of Environ. Management 260 (2020) 110101.

[183] W. L. Wang, Q. Y. Wu, N. H. Huang, Z. B. Xu, M. Y. Lee, H. Y, Hu, Potential risks from UV/H_2O_2 oxidation and UV photocatalysis: A review of toxic, assimilable, and sensory-unpleasant transformation products, Water Res. 141 (2018) 109–125.

[184] Y. Wang, C. Chen, D. Zhou, H. Xiong, Y. Zhou, S. Dong, B. E. Rittmann, Eliminating partial-transformation products and mitigating residual toxicity of amoxicillin through intimately coupled photocatalysis and biodegradation, Chemosphere 237 (2019) 124491

[185] J. J. Rueda-Marquez, I. Levchuk, P. F. Ibañez, M. Sillanpää, A critical review on application of photocatalysis for toxicity reduction of real wastewaters, J. of Cleaner Production 258 (2020) 120694.

[186] D. Lambropoulou, E. Evgenidou, V. Saliverou, C. I. Kosma, I. Konstantinou, Degradation of venlafaxine using TiO_2/UV process: Kinetic studies, RSM optimization, identification of transformation products and toxicity evaluation, J. of Hazardous Mat. 323 (2017) 513–526.

[187] L. Ćurković, D. Ljubas, S. Šegota, I. Bačić, Photocatalytic degradation of Lissamine Green B dye by using nanostructured sol-gel TiO_2 films, J. of Alloys and Compounds 604 (2014) 309–316.

[188] URL: https://www.waveformlighting.com/photometrics/TR_7021.65LR.pdf (acessed on 30th September 2021)

[189] URL: https://store.waveformlighting.com/collections/led-strips/products/real-uv-led-strip-lights?variant=12527605252198 (acessed on 30th September 2021)

[190] URL: https://www.waveformlighting.com/datasheets/CS_7026.pdf (accessed on 30th September 2021).

[191] URL: https://www.arduino.cc/en/tutorial/PWM. (accessed on 30th September 2021).

[192] M. Sarafraz, M. Sadeghi, A. Yazdanbakhsh, M. Amini, M. M. Sadani, A. Eslami, Enhanced photocatalytic degradation of ciprofloxacin by black Ti^{3+}/N-TiO_2 under visible LED light irradiation: Kinetic, energy consumption, degradation pathway, and toxicity assessment, Process Safety and Environ. Protection 137 (2020) 261–272.

[193] Q. Wang, S. Yu, W. Qin, X. Wu, Isopropanol-assisted synthesis of highly stable MAPbBr3/p-g-C_3N_4 intergrowth composite photocatalysts and their interfacial charge carrier dynamics, Nanoscale Advances 2 (2020) 274–285.

[194] J. I. Martínez-Costa, J. Rivera-Utrilla, R. Leyva-Ramos, M. Sánchez-Polo, I. Velo-Gala, A. J. Mota, Individual and simultaneous degradation of the antibiotics sulfamethoxazole and trimethoprim in aqueous solutions by Fenton, Fenton-like and photo-Fenton processes using solar and UV radiations, J. of Photochem. and Photobiol. A: Chem. 360 (2018) 95–108.

[195] J. García-Galán, A. Anfruns, R. Gonzalez-Olmos, S. Rodríguez-Mozaz, J. Comas, UV/$H2O_2$ degradation of the antidepressants venlafaxine and O-desmethylvenlafaxine: Elucidation of their transformation pathway and environmental fate, J. of Hazardous Mat. 311 (2016) 70–80.

[196] M. Samy, M. G. Ibrahim, M. G. Alalm, M. Fujii, S. Ookawara, T. Ohno, Photocatalytic

degradation of trimethoprim using S-TiO_2 and Ru/WO_3/ZrO_2 immobilized on reusable fixed plates, J. of Water Process Eng. 33 (2020) 3–10.

[197] R. A. Osawa, B. T. Barrocas, O. Monteiro, M. C. Oliveira, M. H. Florêncio, Photocatalytic degradation of amitriptyline, trazodone and venlafaxine using modified cobalt-titanate nanowires under UV–Vis radiation: Transformation products and in silico toxicity, Chem. Eng. J. 373 (2019) 1338–1347.

[198] A. G. Trovó, R. F. P. Nogueira, A. Agüera, C. Sirtori, A. R. Fernández-Alba, Photodegradation of sulfamethoxazole in various aqueous media: Persistence, toxicity and photoproducts assessment, Chemosphere 77 (2009) 1292–1298.

[199] M. Gmurek, H. Horn, M. Majewsky, Phototransformation of sulfamethoxazole under simulated sunlight: Transformation products and their antibacterial activity toward Vibrio fischeri, Sci. of the Total Environ. 538 (2015) 58–63.

[200] J. Yang, G. Lv, C. Zhang, Z. Wang, X. Sun, Indirect photodegradation of sulfamethoxazole and trimethoprim by hydroxyl radicals in aquatic environment: Mechanisms, transformation products and eco-toxicity evaluation, Int. J. of Mol. Sci. 21 (2020) 1–14.

[201] E. L. Schymanski, J. Jeon, R. Gulde, K. Fenner, M. Ruff, H. P. Singer, J. Hollender, Identifying small molecules via high resolution mass spectrometry: Communicating confidence, Environ. Sci. and Technol. 48 (2014) 2097–2098.

[202] H. Zeghioud, N. Khellaf, H. Djelal, A. Amrane, M. Bouhelassa, Photocatalytic Reactors Dedicated to the Degradation of Hazardous Organic Pollutants: Kinetics, Mechanistic Aspects, and Design – A Review, Chem. Eng. Communications 203 (2016) 1415–1431.

[203] I. García-Fernández, I. Fernández-Calderero, M. I. Polo-López, P. Fernández-Ibáñez, Disinfection of urban effluents using solar TiO_2 photocatalysis: A study of significance of dissolved oxygen, temperature, type of microorganism and water matrix, Catal. Today 240 (2015) 30–38.

[204] N. Yuangpho, D. T. T. Trinh, D. Channei, W. Khanitchaidecha, A. Nakaruk, The

influence of experimental conditions on photocatalytic degradation of methylene blue using titanium dioxide particle, J. of the Australian of Ceramic Soc. 54 (2018) 557–564.

[205] K. Davididou, R. Nelson, J. M. Monteagudo, A. Durán, A. J. Expósito, E. Chatzisymeon, Photocatalytic degradation of bisphenol-A under UV-LED, blacklight and solar irradiation, J. of Cleaner Production 203 (2018) 13–21.

[206] A. Albini, Some remarks on the first law of photochemistry, Photochem. and Photobiol. Sci. 15 (2016) 319–324.

[207] T. Oppenlander, Photochemical Purification of Water and Air, Wiley VCH, Veinheim, 2003, 320-338.

[208] N. Voudoukis, S. Oikonomidis, Inverse square law for light and radiation: A unifying educational approach, European J. of Eng. Res. and Sci. 2 (2017) 23.

[209] A. Kheyrandish, F. Taghipour, M. Mohseni, UV-LED radiation modeling and its applications in UV dose determination for water treatment, J. of Photochem and Photobiol. A: Chem. 352 (2018) 113–121.

[210] C. L. Har, S. L. Hii, C. K. Yong, S. P. Siew, Statistical Screening of Factors Affecting Production of Fermentable Sugars from Sugarcane Bagasse under Solid-state Conditions, BioResources 8 (2013) 4546–4562.

[211] P. Magalhães, L. Andrade, O. C. Nunes, A. Mendes, Titanium dioxide photocatalysis: Fundamentals and application on photoinactivation, Reviews on Advanced Mat. Sci. 51 (2017) 91–129.

[212] D. Bertagna Silva, G. Buttiglieri, B. Babić, D. Ašperger, S. Babić, Performance of TiO_2/ UV-LED-Based Processes for Degradation of Pharmaceuticals : Effect of Matrix Composition and Process Variables, Nanomat. 12 (2022) 295.

[213] J. Jeong, K. Sekiguchi, K. Sakamoto, Photochemical and photocatalytic degradation of gaseous toluene using short-wavelength UV irradiation with TiO_2 catalyst: Comparison of three UV sources, Chemosphere 57 (2004) 663–671.

[214] D. Nasuhoglu, V. Yargeau, D. Berk, Photo-removal of sulfamethoxazole (SMX) by photolytic and photocatalytic processes in a batch reactor under UV-C radiation (λmax=254nm), J. of Hazardous Mat. 186 (2011) 67–75..

[215] X. Yu, J. Liu, Prediction of reaction rate constants of hydroxyl radical with chemicals in water, Water Environ. Res. 93 (2020). 934

[216] A. Bianco, M. Passananti, H. Perroux, G. Voyard, C. Mouchel-Vallon, N. Chaumerliac, G. Mailhot, L. Deguillaume, M. Brigante, A better understanding of hydroxyl radical photochemical sources in cloud waters collected at the puy de Dôme station - Experimental versus modelled formation rates, Atmos. Chem. and Phys. 15 (2015) 9191–9202.

[217] H. Y. Kim, T. H. Kim, S. Yu, Photolytic degradation of sulfamethoxazole and trimethoprim using UV-A, UV-C and vacuum-UV (VUV), J. of Environ. Sci. and Health - Part A Toxic/Hazardous Substances and Environ. Eng. 50 (2015) 292–300.

[218] P. Cheng, Y. Wang, M. Sarakha, G. Mailhot, Enhancement of the photocatalytic activity of decatungstate, $W_{10}O_{32}^{4-}$, for the oxidation of sulfasalazine/sulfapyridine in the presence of hydrogen peroxide, J. Photochem. And Photobiol. A: Chem. 404 (2021) 112890.

[219] J. Trawinski, R. Skibinski, P. Szymanski, Investigation of the photolysis and TiO_2, $SrTiO_3$, H_2O_2-mediated photocatalysis of an antipsychotic drug loxapine – Evaluation of kinetics, identification of photoproducts, and in silico estimation of properties, Chemosphere 204 (2018) 1-10.

[220] D. B. Miklos, R. Hartl, P. Michel, K. G. Linden, J. Drewes, U. Hübner, UV/H_2O_2 process stability and pilot-scale validation for trace organic chemical removal from wastewater treatment plant effluents, Water Res. 136 (2018) 169–179.

[221] C. U. Demirel, N. C. Birben, M. Bekbolet, Elucidation of background organic matter matrix effect on photocatalytic treatment of contaminants using TiO_2: A review, Catal. Today 284 (2017) 202–214.

[222] M. Yang, H. K. Liberatore, X. Zhang, Current methods for analyzing drinking water disinfection byproducts, Current Opinion in Environ. Sci. and Health 7 (2019) 98–107.

[223] M. Alhaji, K. Sanaullah, A. Khan, A. Hamza, A. Muhammad, M. Ishola, A. Rigit, S. Bhawani, Recent developments in immobilizing titanium dioxide on supports for degradation of organic pollutants in wastewater- A review, Int. J. of Environ. Sci. and Technol. 14 (2017) 2039–2052.

[224] M. Sayed, L. A. Shah, J. A. Khan, N. S. Shah, H. M. Khan, R. A. Khan, A. R. Khan, A. M. Khan, Hydroxyl radical based degradation of ciprofloxacin in aqueous solution, J. of the Chilean Chem. Soc. 61 (2016) 2949.

[225] URL:https://health.state.mn.us/communities/environment/water/contaminants/nitrate.html (accessed on 30th September 2021)

[226] N. Negishi, Y. Miyazaki, S. Kato, Y. Yang, Effect of HCO_3^- concentration in groundwater on TiO_2 photocatalytic water purification, App. Catal. B: Environ. 242 (2019) 449–459.

[227] M. Verma, A. K. Haritash, Photocatalytic degradation of Amoxicillin in pharmaceutical wastewater: A potential tool to manage residual antibiotics, Environ. Technol. and Innovation 20 (2020) 101072.

[228] S. L. Vinge, S. W. Shaheen, C. M. Sharpless, K. G. Linden, Nitrate with benefits: Optimizing radical production during UV water treatment, Environmental Science: Water Res. and Technol. 6 (2020) 1163–1175.

[229] S. Navalon, M. Alvaro, H. Garcia, Analysis of organic compounds in an urban wastewater treatment plant effluent, Environ. Technol. 32 (2011) 295-306.

[230] M. Periša, S. Babić, I. Škorić, T. Frömel, T. P. Knepper, Photodegradation of sulfonamides and their N4-acetylated metabolites in water by simulated sunlight irradiation: Kinetics and identification of photoproducts, Environ. Sci. and Pollut. Res. 20 (2013) 8934–8946.

7. APPENDIX

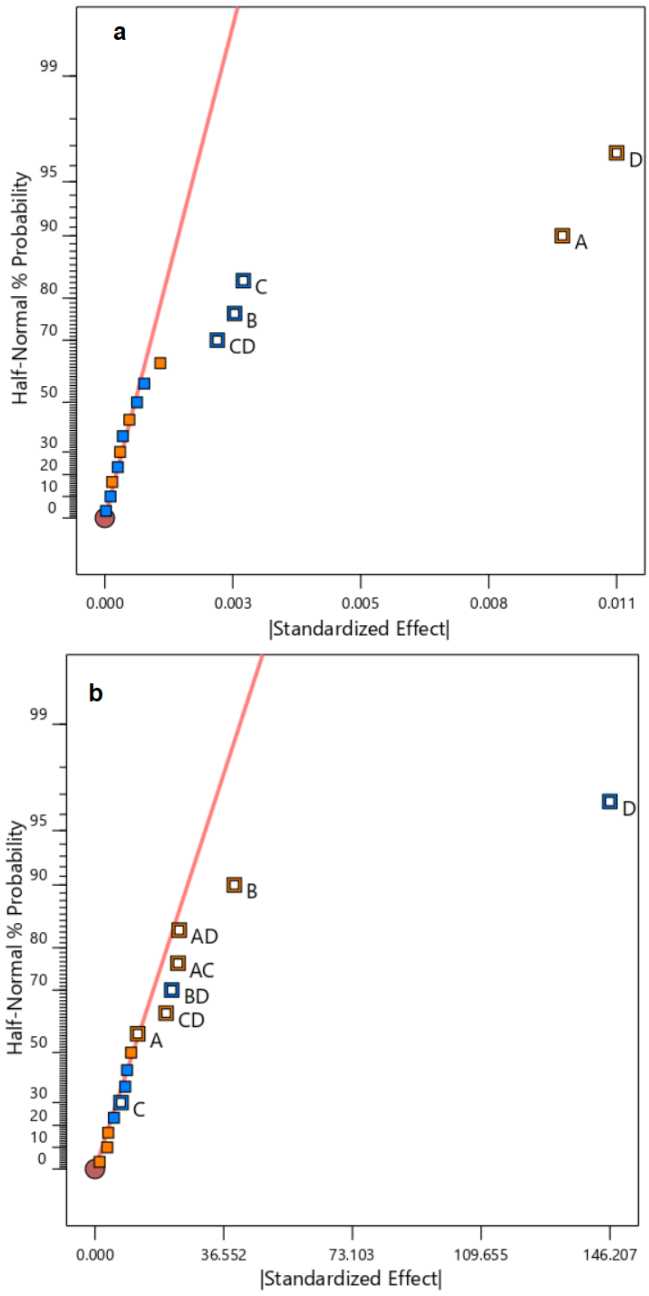

Figure S1. Half-normal plot for (a) k_{app} and (b) E_{EO} for DoE #1. Positive effects in orange, negative in blue. Significant effects signalled [166]

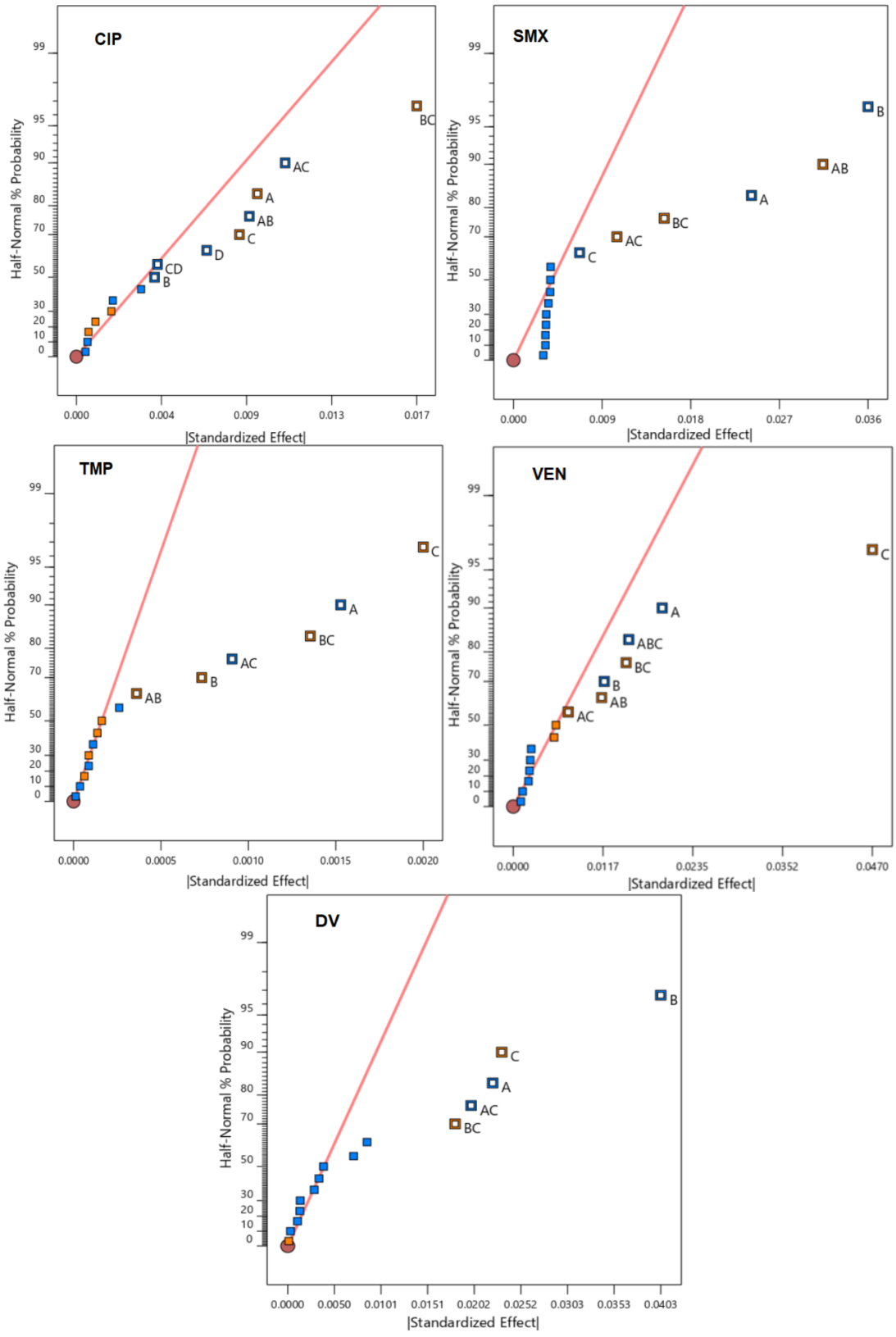

Figure S2. Half-normal plots for k_{app} all 5 target pollutants (DoE #2). Positive effects in orange, negative in blue. Significant effects signalled [212]

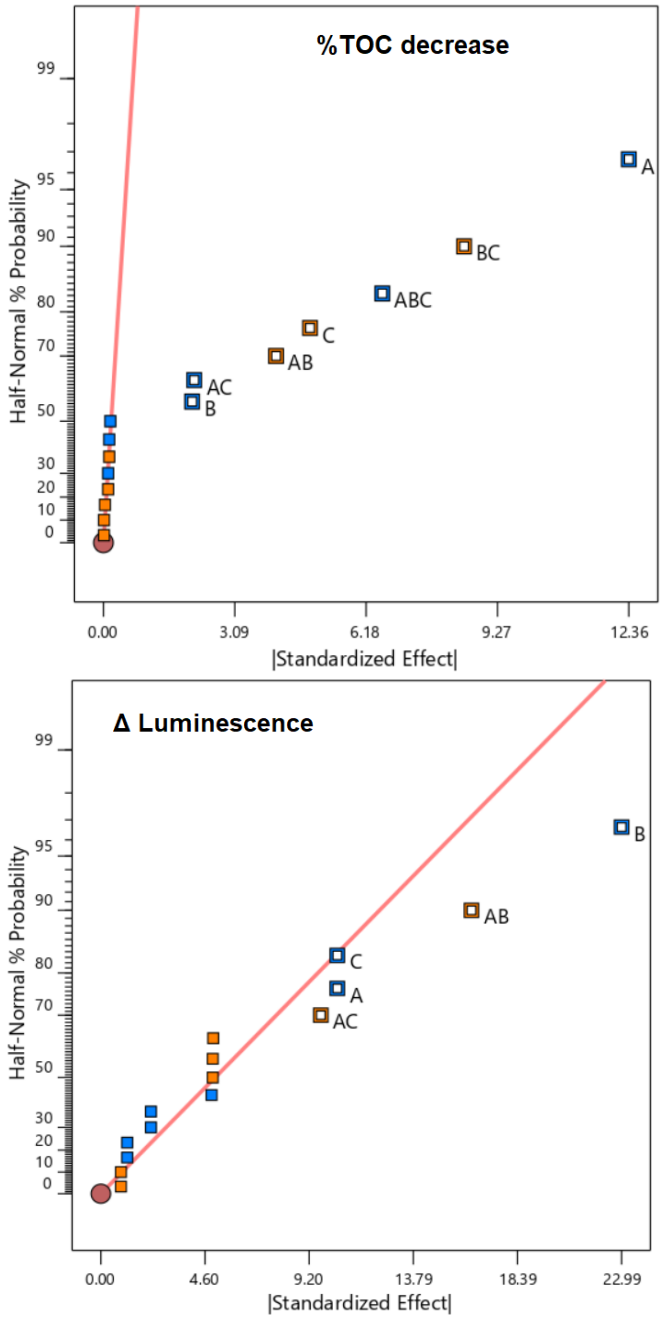

Figure S3. Half-normal plots for %TOC decrease and Δ luminescence for DoE #2. Positive effects in orange, negative in blue. Significant effects signalled [212]

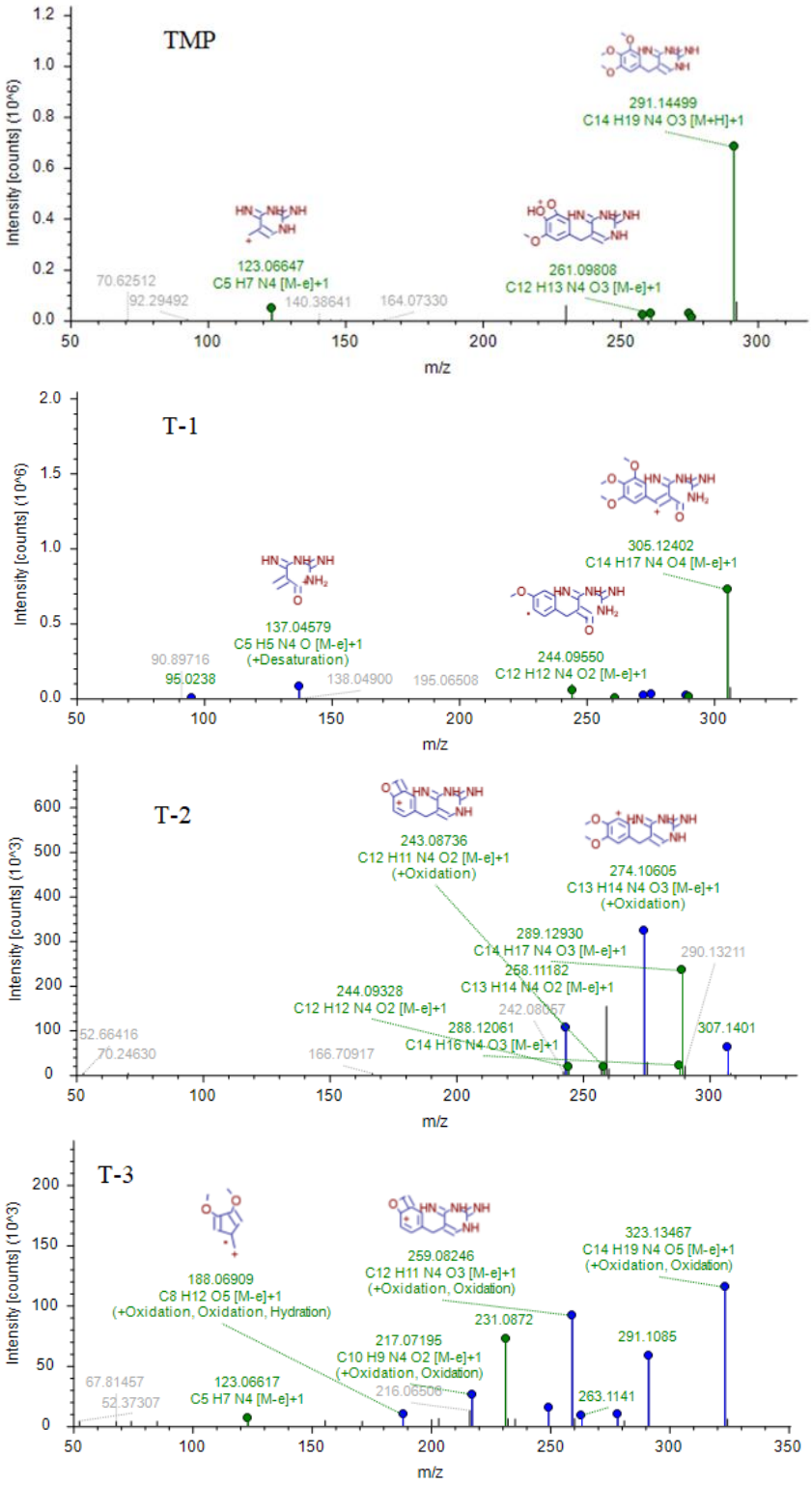

Figure S4. MS^2 of TMP and its transformation products

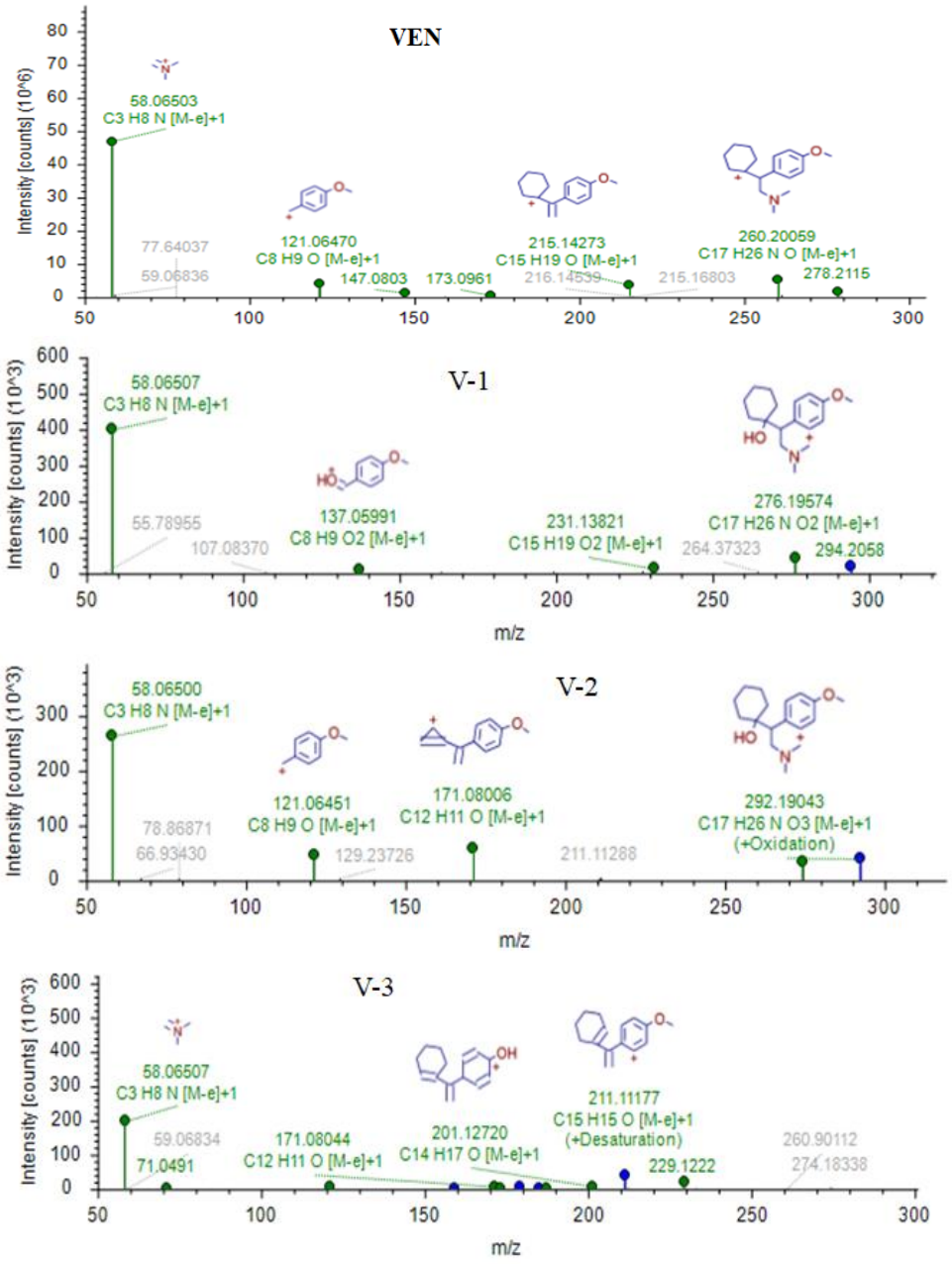

Figure S5. MS^2 of VEN and its transformation products

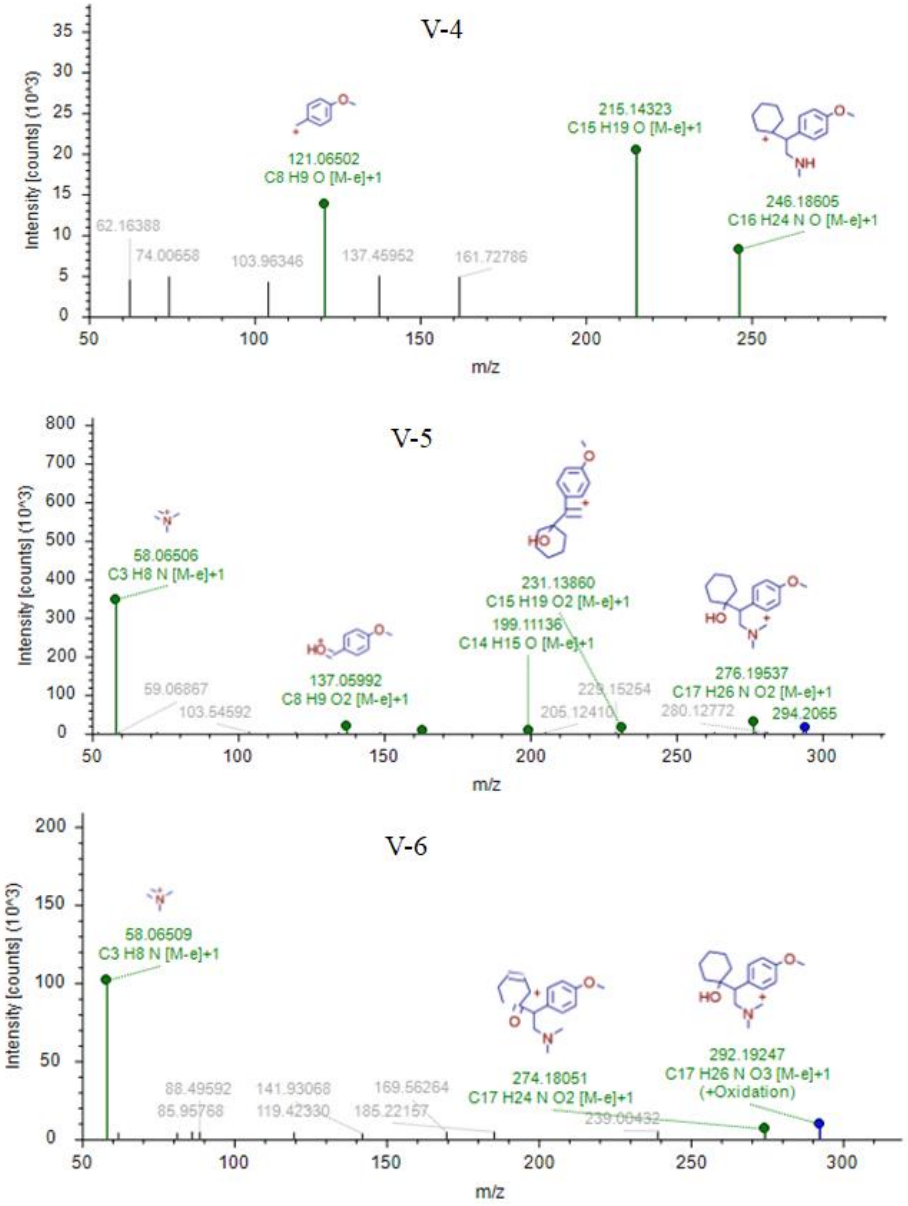

Figure S6. MS^2 of VEN and its transformation products (continuation)

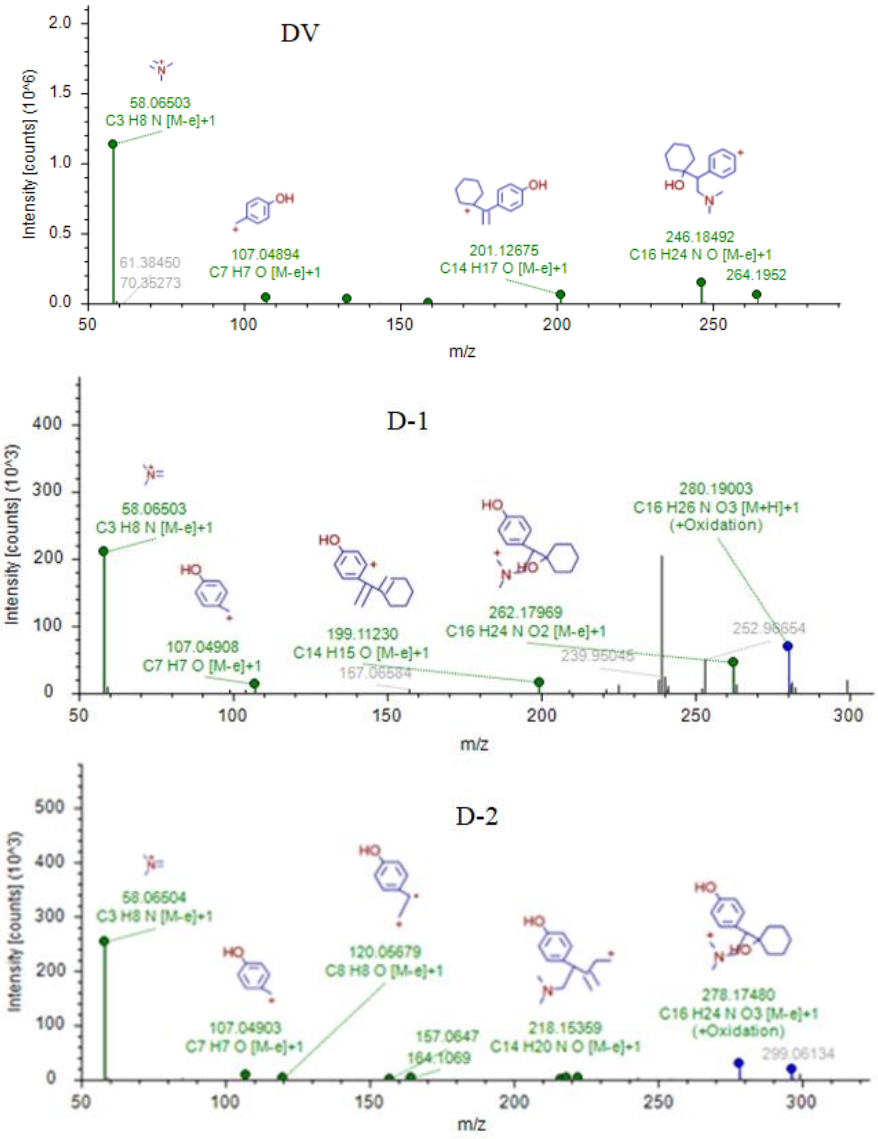

Figure S7. MS^2 of DV and its transformation products

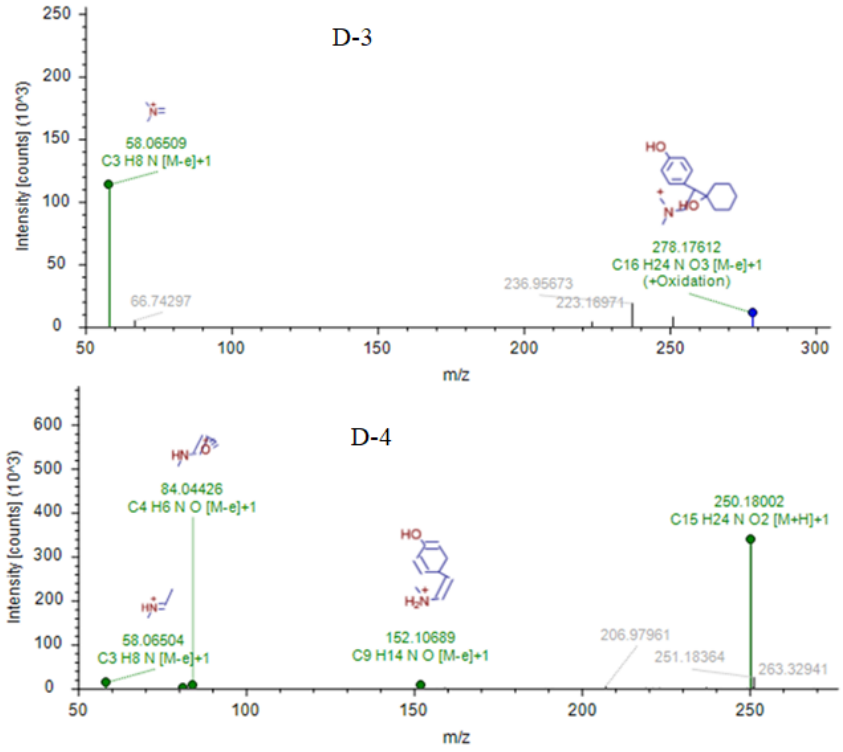

Figure S8. MS^2 of DV and its transformation products (continuation)

Table S1. Experiments performed for section 4.4 (experiments 1-20: individual degradation; exp 21-23: initial pH investigation; 24-39: DoE #2; exp 40-56: DoE #3); exp 57-60: simultaneous wavelength) [212]

	Initial concentration (mg/L)							Added (mg/L)						k_{app} (min^{-1})				
Exp №	**CIP**	**SMX**	**TMP**	**VEN**	**DV**	**Treatment**	**Matrix**	**HCO_3^-**	**NO_3^-**	**Humic acids**	**Duty Cycle**	**Initial pH**	**Final pH**	**CIP**	**SMX**	**TMP**	**VEN**	**DV**
1	2	0	0	0	0	P,A	MQ	0	0	0	1	6.0	5.4	0.0105				
2	0	2	0	0	0	P,A	MQ	0	0	0	1	5.7	5.7		0.0000			
3	0	0	2	0	0	P,A	MQ	0	0	0	1	6.4	6.3			0.0000		
4	0	0	0	2	0	P,A	MQ	0	0	0	1	5.8	5.7				0.0000	
5	0	0	0	0	2	P,A	MQ	0	0	0	1	7.0	6.7					0.0000
6	2	0	0	0	0	PC, A	MQ	0	0	0	1	6.0	4.8	0.0268				
7	0	2	0	0	0	PC, A	MQ	0	0	0	1	5.7	4.8		0.0038			
8	0	0	2	0	0	PC, A	MQ	0	0	0	1	6.4	5.6			0.0100		
9	0	0	0	2	0	PC, A	MQ	0	0	0	1	5.8	5.3				0.0097	
10	0	0	0	0	2	PC, A	MQ	0	0	0	1	7.0	5.9					0.0079
11	2	0	0	0	0	P,C	MQ	0	0	0	1	6.0	5.0	0.0220				
12	0	2	0	0	0	P,C	MQ	0	0	0	1	5.7	4.5		0.3663			
13	0	0	2	0	0	P,C	MQ	0	0	0	1	6.4	5.4			0.0000		
14	0	0	0	2	0	P,C	MQ	0	0	0	1	5.8	5.1				0.0027	
15	0	0	0	0	2	P,C	MQ	0	0	0	1	7.0	5.9					0.0094

Exp №	Initial concentration (mg/L)					Treatment	Matrix	Added (mg/L)		Humic acids	Duty Cycle	Initial pH	Final pH	k_{app} (min^{-1})				
	CIP	SMX	TMP	VEN	DV			HCO_3^-	NO_3^-					CIP	SMX	TMP	VEN	DV
16	2	0	0	0	0	PC, C	MQ	0	0	0	1	6.0	5.1	0.0244				
17	0	2	0	0	0	PC, C	MQ	0	0	0	1	5.7	4.7		0.1251			
18	0	0	2	0	0	PC, C	MQ	0	0	0	1	6.4	5.3			0.0076		
19	0	0	0	2	0	PC, C	MQ	0	0	0	1	5.8	5.1				0.0098	
20	0	0	0	0	2	PC, C	MQ	0	0	0	1	7.0	5.8					0.0112
21	2	2	2	2	2	PC,A	MQ	0	0	0	1	7.0	6.0	0.0526	0.0025	0.0026	0.0031	0.0030
22	2	2	2	2	2	PC,A	MQ	0	0	0	1	5.0	4.4	0.0343	0.0007	0.0030	0.0017	0.0000
23	2	2	2	2	2	PC,A	MQ	0	0	0	1	9.0	7.8	0.0578	0.0052	0.0015	0.0054	0.0063
24	2	2	2	2	2	P, A	MQ	0	0	0	1	6.7	6.3	0.0110	0.0000	0.0000	0.0000	0.0000
25	2	2	2	2	2	PC, A	MQ	0	0	0	1	6.7	5.8	0.0384	0.0012	0.0049	0.0040	0.0030
26	2	2	2	2	2	P, C	MQ	0	0	0	1	6.7	5.8	0.0198	0.0908	0.0000	0.0028	0.0034
27	2	2	2	2	2	PC, C	MQ	0	0	0	1	6.7	5.8	0.0226	0.0509	0.0034	0.0026	0.0064
28	2	2	2	2	2	P,A	MQ	0	0	0	0.5	6.7	6.3	0.0131	0.0000	0.0000	0.0000	0.0000
29	2	2	2	2	2	PC,A	MQ	0	0	0	0.5	6.7	5.7	0.0555	0.0016	0.0042	0.0058	0.0055
30	2	2	2	2	2	P,C	MQ	0	0	0	0.5	6.7	5.8	0.0271	0.0859	0.0014	0.0029	0.0034
31	2	2	2	2	2	PC,C	MQ	0	0	0	0.5	6.7	5.8	0.0294	0.0505	0.0025	0.0049	0.0045

	Initial concentration (mg/L)							Added (mg/L)						k_{app} (min^{-1})				
Exp №	**CIP**	**SMX**	**TMP**	**VEN**	**DV**	**Treatment**	**Matrix**	**HCO_3^-**	**NO_3^-**	**Humic acids**	**Duty Cycle**	**Initial pH**	**Final pH**	**CIP**	**SMX**	**TMP**	**VEN**	**DV**
32	2	2	2	2	2	P,A	TAP	0	0	0	1	7.7	7.6	0.0220	0.0000	0.0000	0.0000	0.0000
33	2	2	2	2	2	PC,A	TAP	0	0	0	1	7.7	7.6	0.0306	0.0020	0.0023	0.0029	0.0000
34	2	2	2	2	2	P,C	TAP	0	0	0	1	7.7	7.4	0.0525	0.0167	0.0000	0.0000	0.0032
35	2	2	2	2	2	PC,C	TAP	0	0	0	1	7.7	7.4	0.0302	0.0082	0.0000	0.0040	0.0030
36	2	2	2	2	2	P,A	TAP	0	0	0	0.5	7.7	7.6	0.0210	0.0000	0.0000	0.0000	0.0000
37	2	2	2	2	2	PC,A	TAP	0	0	0	0.5	7.7	7.6	0.0450	0.0024	0.0021	0.0029	0.0013
38	2	2	2	2	2	P,C	TAP	0	0	0	0.5	7.7	7.4	0.0530	0.0170	0.0000	0.0040	0.0030
39	2	2	2	2	2	PC,C	TAP	0	0	0	0.5	7.7	7.4	0.0345	0.0087	0.0000	0.0021	0.0012
40	2	2	2	2	2	PC,A	MQ	200	0	0	1	9.0	8.8	0.0335	0.0019	0.0007	0.0071	0.0079
41	2	2	2	2	2	PC,A	MQ	0	30	0	1	6.8	5.7	0.0550	0.0017	0.0019	0.0011	0.0006
42	2	2	2	2	2	PC,A	MQ	0	0	3	1	6.6	5.8	0.0569	0.0037	0.0017	0.0020	0.0014
43	2	2	2	2	2	PC,A	MQ	400	0	0	1	9.1	8.9	0.0275	0.0012	0.0008	0.0104	0.0102
44	2	2	2	2	2	PC,A	MQ	200	30	3	1	9,1	9.0	0.0223	0.0016	0.0007	0.0093	0.0106
45	2	2	2	2	2	PC,A	MQ	0	15	0	1	6.7	5.8	0.0490	0.0022	0.0020	0.0025	0.0014
46	2	2	2	2	2	PC,A	MQ	200	15	1.5	1	9.1	8.9	0.0302	0.0023	0.0010	0.0120	0.0131
47	2	2	2	2	2	PC,A	MQ	0	0	1.5	1	5.7	5.8	0.0461	0.0019	0.0019	0.0023	0.0000

	Initial concentration (mg/L)						Added (mg/L)						k_{app} (min^{-1})				
Exp №	**CIP**	**SMX**	**TMP**	**VEN**	**DV**	**Treatment**	**Matrix**	**HCO_3^-**	**NO_3^-**	**Humic acids**	**Duty Cycle**	**Initial pH**	**Final pH**	**CIP**	**SMX**	**TMP**	**VEN**	**DV**
48	2	2	2	2	2	PC,A	MQ	0	15	3	1	6.7	5.7	0.0538	0.0025	0.0022	0.0024	0.0016
49	2	2	2	2	2	PC,A	MQ	0	30	1.5	1	6.8	5.7	0.0417	0.0025	0.0023	0.0000	0.0003
50	2	2	2	2	2	PC,A	MQ	400	0	1.5	1	9.1	8.9	0.0259	0.0022	0.0015	0.0113	0.0122
51	2	2	2	2	2	PC,A	MQ	200	30	3	1	9.0	8.8	0.0345	0.0027	0.0011	0.0125	0.0154
52	2	2	2	2	2	PC,A	MQ	400	30	1.5	1	9.0	8.8	0.0304	0.0030	0.0006	0.0105	0.0144
53	2	2	2	2	2	PC,A	MQ	400	15	3	1	9.0	8.8	0.0302	0.0029	0.0013	0.0080	0.0138
54	2	2	2	2	2	PC,A	MQ	200	30	0	1	9.0	8.8	0.0404	0.0021	0.0006	0.0103	0.0130
55	2	2	2	2	2	PC,A	MQ	400	15	0	1	9.1	8.8	0.0254	0.0032	0.0019	0.0115	0.0121
56	2	2	2	2	2	PC,A	MQ	200	0	3	1	9.0	8.8	0.0371	0.0025	0.0010	0.0122	0.0147
57	2	2	2	2	2	P, SW3	MQ	0	0	0	1	6.7	6.0	0.0259	0.0589	0.0013	0.0034	0.0043
58	2	2	2	2	2	PC, SW3	MQ	0	0	0	1	6.7	5.6	0.0368	0.0157	0.0042	0.0061	0.0052
59	2	2	2	2	2	P, SW6	MQ	0	0	0	1	6.7	4.8	0.0373	0.0876	0.0016	0.0032	0.0035
60	2	2	2	2	2	PC, SW6	MQ	0	0	0	1	6.7	4.5	0.0659	0.0431	0.0063	0.0068	0.0056

Table S2. TPs found for UV-A photocatalysis (both MQ and tap water)

TP	Parent compound	*m/z* ($M+H^+$)	RT (min)	Chemical formulae	Mass error (ppm)	Reaction	Identification confidence	Ref.
T-1	TMP	305.104	2.095	$C_{14}H_{16}N_4O_4$	-1.23	Oxidation	Probable structure	[113, 196]
T-2	TMP	307.139	1.584	$C_{14}H_18N_4O_4$	-1.35	Hydroxylation	Probable structure	[41, 113]
T-3	TMP	323.134	1.781	$C_{15}H_{18}N_4O_5$	-1.34	Hydroxylation, oxidation	Tentative candidate	[200]
DV	VEN	264.195	2.091	$C_{16}H_{25}NO_2$	-1.25	Demethylization	Confirmed structure	[54, 186]
V-1	VEN	294.206	2.242	$C_{17}H_{27}NO_3$	-1.27	Oxidation	Probable structure	New
V-2	VEN	292.190	1.617	$C_{17}H_{25}NO_3$	-1.10	Desaturation, oxidation	Tentative candidate	[54, 197]
V-3	VEN	274.179	2.141	$C_{17}H_{23}NO_2$	-0.87	Dehydration	Tentative candidate	[194]
D-1	DV	280.190	1.434	$C_{16}H_{25}NO_3$	-1.22	Oxidation	Tentative candidate	[195]
D-2	DV	296.185	1.147	$C_{16}H_{25}NO_4$	-1.47	Oxidation	Tentative candidate	[195]
D-3	DV	278.174	1.940	$C_{16}H_{23}NO_3$	-1.59	Desaturation, oxidation	Tentative candidate	[195]

Table S3. TPs found for UV-C photolysis in MQ water

TP	Parent compound	*m/z* ($M+H^+$)	RT (min)	Chemical formulae	Mass error (ppm)	Reaction	Identification confidence	Ref.
DV	VEN	264.195	2.081	$C_{16}H_{25}NO_2$	-1.13	Demethylization	Confirmed structure	[56, 197]
V-4	VEN	264.195	2.607	$C_{16}H_{25}NO_2$	-1.25	Demethylization	Probable structure	[197]
V-5	VEN	294.206	2,261	$C_{17}H_{27}NO_3$	-1.10	Hydroxylation	Tentative candidate	[197]
V-6	VEN	292.190	2.488	$C_{17}H_{25}NO_2$	-1.24	Oxidation	Tentative candidate	[197]
D-1	DV	280.019	1.674	$C_{16}H_{25}NO_3$	-1.22	Oxidation	Tentative candidate	[195]
D-4	DV	250.180	1.306	$C_{15}H_{23}NO_3$	-1.12	Demethylization	Tentative candidate	[195]

Author's biography

Danilo Bertagna Silva [redacted] He graduated in Chemical Engineering from the State University of Campinas in 2015 then continued his studies for a brief period at the Federal University of Rio de Janeiro, where his interest in wastewater treatment started. During his undergraduate period, he spent a year at the University of Hull (UK) where he also worked on the obtainment of biofuels using solar energy and vegetable oils.

He holds his M.Sc. degree from the Erasmus Mundus joint program "Chemical Innovation and Regulation" after taking modules in the University of Algarve (Portugal) and writing his thesis "UV Light-Assisted Ozonation For Micropollutant Removal in Domestic Wastewaters" in the University of Barcelona (Spain). He had professional internship experiences in the Membrane Innovation Centre (Czech Republic) as a laboratory assistant and as a wine-making apprentice engineer at the Guaspari winery (Brazil).

Danilo was hired in 2019 as an early stage researcher by the NOWELTIES project, an Innovative Training Network part of the framework of EU Horizon 2020's Marie Skłodowska-Curie Actions. His research focuses on the development, evaluation and optimization of UV-LED based technologies for the removal of contaminants of emerging concern from water. During the project, he spent two and a half years in the Faculty of Chemical Engineering and Technology, University of Zagreb (Croatia) and 6 months in the Catalan Institute for Water Research (Girona, Spain).

Author's published works

D. Bertagna Silva, G. Buttiglieri, B. Babić, D. Ašperger, S. Babić, Performance of TiO_2/ UV-LED-Based Processes for Degradation of Pharmaceuticals : Effect of Matrix Composition and Process Variables, Nanomat. 12 (2022) 295.

D. Bertagna Silva, G. Buttiglieri, T. Babić, L. Ćurković, S. Babić, Impact of UV-LED photoreactor design on the degradation of contaminants of emerging concern, Process Safety and Environ. Protection. 153 (2021) 94–106.

D. Bertagna Silva, G. Buttiglieri, S. Babić, State-of-the-art and current challenges for TiO_2/UV-LED photocatalytic degradation of emerging organic micropollutants, Environ. Sci. and Pollut. Res. 28 (2021) 103-120.

D. Bertagna Silva, A. Cruz-Alcalde, C. Sans, J. Giménez, S. Esplugas, Performance and kinetic modelling of photolytic and photocatalytic ozonation for enhanced micropollutants removal in municipal wastewaters, App. Catal. B: Environ. (2019) 211–217.